LIMITATIONS IN THERMAL SIMILITUDE

D2-121352-1

FINAL REPORT
CONTRACT NAS8-21422
December 1969

Prepared by
THE BOEING COMPANY
Aerospace Systems Division
Seattle, Washington

Prepared for
NATIONAL AERONAUTICS AND SPACE ADMINISTRATION
George C. Marshall Space Flight Center
Huntsville, Alabama

LIMITATIONS
IN
THERMAL SIMILITUDE

by

Robert K. MacGregor

Final Report
Contract NAS8-21422

December 1969

Prepared by

THE BOEING COMPANY
Aerospace Systems Division
Seattle, Washington

Prepared for

NATIONAL AERONAUTICS AND SPACE ADMINISTRATION
George C. Marshall Space Flight Center
Marshall Space Flight Center, Alabama

TABLE OF CONTENTS

TABLE OF CONTENTS (continued)

LIST OF ILLUSTRATIONS

LIST OF ILLUSTRATIONS (continued)

LIST OF ILLUSTRATIONS (continued)

LIST OF ILLUSTRATIONS (continued)

ACKNOWLEDGEMENT

The author acknowledges V. G. Klockzien and R. L. Shannon for permission to utilize portions of their paper "Thermal Scale Modeling of Spacecraft" (SAE Paper 690196, January 1969) in the introduction to this document.

LIMITATIONS IN THERMAL SIMILITUDE

by Robert K. MacGregor

1.0 SUMMARY

The results of a research program to examine and define some of the limitations in thermal scale modeling are presented in this report. The primary objective of this program was an understanding of the errors inherent in scale modeling as a result of uncertainties in thermophysical properties, geometric dimensions, and the test environment. Secondary objectives of the program were the development of additional scaling criteria or compromise techniques which would be applicable to a number of special problem areas in scale modeling.

A statistical study of the errors inherent in scale modeling as a result of uncertainties (probable errors) in thermophysical properties, geometric dimensions, and test environment has been completed. The range of the resulting probable errors in scale modeling has been presented as a function of the overall scaling ratio. Thus, a limitation on the lower bound of the scaling ratio is seen to be a function of the probable error that the modeler is willing to accept. In general, scale ratios below one-tenth result in excessive errors in the modeling techniques.

A study to develop scaling criteria for selected scale modeling problem areas and to examine the errors resulting from scale modeling of these areas has been completed. This study also includes the identification of techniques for compromising the scaling criteria for these problem areas. The special problem areas considered were:

1) Transient Response
2) Thermal Control Coatings
3) Multilayer Insulation
4) Thermal Gradient Effects
5) Instrumentation Effects
6) Test Environment Effects

An experimental program was conducted to support the conclusions reached in the analytic studies and the error analyses. A prototype and half scale vehicle were tested for a number of combinations of solar illumination and internal power dissipation under a simulated space environment. The random experimental errors observed showed good agreement with the probable errors predicted by the analysis.

A detailed numerical thermal analysis was conducted to support the test program. The numerical analysis showed good agreement with the results of the experiments. The numerical analysis technique was also used to correct the experimental data for compromises of the scaling criteria. This improved the agreement between the two sets of experimental data (model and prototype) by reducing the systematic differences resulting from violations of the scaling criteria.

It is concluded that:

1) multilayer insulation is the major problem area in the scale modeling of unmanned spacecraft

2) numerical analysis can be used to improve thermal scale model experimental results by correcting for known compromises of the scaling criteria

3) the probable errors in the experimental scale modeling study fall within the range predicted by the statistical analysis of errors due to uncertainties in thermophysical properties, geometric dimensions, and the test environment.

2.0 INTRODUCTION

The successful operatio of both manned and unmanned spacecraft in planetary orbits or on interplanetary missions requires that temperatures be controlled within specific ranges for spacecraft equipment, structures and atmospheres. Desired temperature ranges are determined by the performance requirements of the specific items. Most electronic, mechanical and fluid components require, for efficient operation, that temperatures be maintained within the range -30 to +130°F (240-330°K); however, certain components must be maintained well within this range. Batteries for example, are required to be maintained within the range 30-100°F (270-310°K). Structures can normally operate over a relatively wide range of temperatures. An exception to this is the optical telescope structure which, for reasons of optical quality, has severe limits on temperature gradients and temperature changes. Atmospheres inside a spacecraft cabin will generally be limited in regard to temperature and rate of temperature change, since the atmosphere must be habitable by man. The problem of temperature control is accentuated by the varying internal and external heat loads that a spacecraft can experience. Equipment and occupants of a spacecraft generally will operate according to some duty cycle which results in the internal heat load varying with time. The spacecraft itself can experience variations in external heat load due to orbiting through the earth's shadow or by changing orientation with respect to the sun.

Spacecraft temperature control is, then, a critical technical problem demanding careful design and development. Generally speaking, the development of spacecraft temperature control systems involves a combination of analyses and tests to design the system and to determine the resultant distribution of temperatures throughout the spacecraft. The analyses are normally accomplished with the aid of digital computers, for reasons of speed of solution and their ability to handle large problems. Thermal tests are most often utilized in the system development program for establishing or verifying the design concept, or for

verifying the analytical model. These tests can also be used to establish the performance of the resultant system under space conditions. The latter use implies perfect simulation of the space environment and perfect modeling. If either of these conditions are not met, the test data must be corrected for the effects of imperfect modeling or imperfect environment simulation. Since space environment simulation is normally not perfect and thermal modeling compromises are inevitable, thermal tests are probably best used to verify an analytical model that can be used to predict the thermal performance of the system in the space environment. As spacecraft have grown in size and complexity, larger and more complex simulation facilities have been required to accomplish the necessary testing. It has been postulated that use of small scale models for thermal tests would allow the use of smaller and less expensive test facilities and would reduce test time.

Thermal scale modeling, then, is an alternative to full-scale thermal testing that becomes attractive when large spacecraft are involved in projects with short development times and limited development budgets. In addition, simplified scale models could be used early in a development program to verify a design concept and consequently have utility in any thermal control system development program.

The heat transfer mechanisms present in an unmanned spacecraft are radiation and conduction; convection being absent since these spacecraft do not normally carry atmospheres. Thermal scaling of such a spacecraft is then concerned with the thermal scaling of a radiation-conduction heat transfer system.

The basic similitude criteria for the radiation-conduction system can be developed either from dimensional analysis or from the differential equations necessary to describe the behavior of the system under consideration. The latter technique is the preferred one when such equations are available since it can give more direct insight into the physical behavior of the system.

In applying the similarity ratios thus developed to the design of thermal scale models, two techniques are generally proposed. These are referred to as temperature preservation and material preservation. The first of these techniques requires that temperatures be identical at identical locations on the scale model and on the full size prototype. This technique then allows a direct determination of prototype temperature from scale model test data. The materials preservation technique requires that materials be identical in both scale model and full size prototype, thus simplifying materials selection problems, but resulting in model temperatures which do not directly compare with prototype temperatures. Extensive studies into the derivation of the scale modeling criteria and the application of these criteria to spacecraft have been presented in References 1-42.

The heat transfer mechanisms present in manned spacecraft include convection. Thermal scaling of manned spacecraft is then concerned with thermal scaling of a radiation-conduction-convection heat transfer system. Only a limited discussion of this problem exists in the literature (References 38 and 41). A research program titled "A Thermal Scale Modeling Study for Apollo and Apollo Applications," is presently in existence (References 43-48) in which an investigation is being made of thermal scale modeling applications to radiation-conduction-convection systems.

Limitations on the use of thermal scale models will manifest themselves as a limit on the major length scaling ratio. Limitations on the maximum size, and hence the maximum scale ratio, will most often result from the size of the space chamber and the solar simulator that is to be utilized. Limits on the smallest feasible size model or scale model ratio can result from available materials, material gages, and material properties (Reference 50). However, since the major purpose of the scaled thermal model is to predict accurately the equivalent prototype spacecraft temperatures, the measure of the model effectiveness is its prediction accuracy. This is true whether the model is used to predict

spacecraft temperature performance directly, or indirectly by verification of an analytical model. The most significant limit on the smallest feasible scaling ratio, then, is the desired prediction accuracy. This desired accuracy will vary according to the program needs but probably in most cases is on the order of 1-5 percent of absolute temperature.

The accuracy of scaled model test data is determined by the errors or uncertainties associated with the design and fabrication of the model and the accuracy of the environmental simulation. The random or systematic experimental errors will manifest themselves in all thermal tests, full size or scaled; consequently, they will not influence the limiting scale ratio. The errors and uncertainties associated with the scale model design and fabrication will result from the failure of the scaled model to completely satisfy the model criteria. Factors affecting the scale model design and fabrication can be categorized as due to materials, fabrication costs, fabrication practices, and test instrumentation.

Errors in scale model temperature predictions from the materials standpoint can be caused by limitations on available materials, thermophysical properties, and uncertainties in property values. Errors resulting from fabrication result from dimensional and solid angle tolerances. Model temperature errors can also be caused by the necessity of instrumenting the model. Such items as thermocouple location accuracy, instrumentation heat leaks, and instrumentation lead geometry can all influence the resultant temperature prediction.

The objective in calling attention to the limitations of scale modeling is to better define the boundaries of the application of thermal modeling and to see how far scaling can be carried, not that it has been proven feasible in all typical cases. Such research is necessary to provide the thermal designer with information useful in making a judgment about the application of thermal scaling to a particular thermal design problem. Identification of inherent difficulties and limitations in the techniques will also serve to focus future research on the more difficult problem areas.

3.0 FUNDAMENTALS OF THERMAL SCALE MODELING

Portions of this section will briefly review the fundamental relations which guide thermal scale modeling techniques and the use of these relations to correct experimental results when compromises of the scaling criteria occur. Additionally, the probable errors inherent in scale modeling as a result of uncertainties in thermophysical properties, geometric tolerances; and environment simulation will be discussed.

3.1 Scale Modeling Criteria

General scale modeling criteria and technique oriented criteria (temperature and material preservation techniques) have been developed, presented, applied, and discussed by previous investigators (References 1-49). These general criteria are summarized in Table 1 in cartesian and cylindrical coordinate systems for both the general three dimensional and two dimensional "geometric distortion" cases. The simplified equations which form the basis of the temperature preservation technique of scale modeling are presented in Table 2. The work conducted under this study will deal only with the temperature preservation technique (as opposed to material preservation) unless otherwise specifically noted.

The equation relating the thermal conductivity of the model material to the scale ratio for the general three dimensional case

$$\frac{k_m}{k_p} = \frac{L_m}{L_p} \quad (1)$$

is quite restrictive in terms of real materials. Figure 1 shows the ranges of available thermal conductivities of the common metal alloys (References 70-75). While the high conductivity alloys are reasonably easy to scale, the low conductivity steels would present difficulties.

---

* For nomenclature, see page 17.

As spacecraft are generally fabricated from thin structural elements, the thermal gradient across the thickness of the element is negligible. Under these conditions the two dimensional (geometric distortion) scaling criteria

$$\frac{k_m}{k_p} = \frac{L_m^2}{L_p^2} \frac{d_p}{d_m} \tag{2}$$

may be applied. This technique allows the modeler to trade-off thickness vs. conductivity. If a suitable conductivity is not available, then a higher conductivity material may be used in conjunction with a thinner gage, or a lower conductivity with a thicker gage combination. Figure 2 shows this relationship between thermal conductivity ratio and thickness ratio for a number of scale ratios.

The geometric distortion technique is not without bounds however. The model gages must be stiff enough to support themselves and at the other extreme, thin enough that they do not establish the gradients within themselves that were originally assumed negligible.

One attractive possibility is the case of extreme geometric distortion. In this case the prototype material is also used for the model material. Equation (2) reduced to

$$\frac{d_m}{d_p} = \frac{L_m^2}{L_p^2} \tag{3}$$

A half scale model would require gages one quarter of their corresponding thickness in the prototype. While this does not seem unreasonable, a tenth scale model would require gages one hundredth of their original thickness. As the spacecraft is fabricated from the minimal gages required for structural reasons, it would appear that the application of extreme geometric distortion techniques is limited to larger scale models (probably one-third scale or larger).

As a current study (Reference 50) is investigating the limitations in scale modeling due to available materials and gages, the subject will not be discussed in further detail in this report.

The general equations presented in Table 1 can be formulated either by dimensional analysis or by a non-dimensionalization of the governing differential equation and its associated boundary conditions. If the differential equations and boundary conditions governing the inter-relationship between energy and temperature are expressed for a typical nodal volume and then non-dimensionalized, the coefficient of each term will be representative of an energy flow rate and each of the following forms will be represented:

1) energy emitted by the nodal surface

$$q_a = \sigma\varepsilon L^2 T^4 \tag{4}$$

2) energy conducted through the element

$$q_b = kLT \tag{5}$$

3) energy dissipated through internal generation

$$q_c = q' \tag{6}$$

4) energy absorbed due to external irradiation

$$q_d = SL^2 \tag{7}$$

5) energy conducted across a joint interface

$$q_e = hT \tag{8}$$

6) internal energy change due to thermal capacity

$$q_f = \frac{\rho c_p L^3 T}{t} \tag{9}$$

To complete the non-dimensionalization of the equations and associated boundary conditions, the coefficients are divided through by one of the coefficients.

Table 3 shows the results of dividing through by the conducted energy as opposed to the emitted energy terms. If these dimensionless parameters can be made equal for the model and the prototype, then solutions to the differential equation will hold for both the model and the prototype. Equating the terms for the model to the terms for the prototype results in the scaling ratios as presented in Table 4.

Note that either set of equations can be reduced, by substitution of other equations in its set, to the alternate formulation. However, the differences between these two sets of equations will be considered in detail in the following sections relating to the estimation of scaling errors due to compromise and uncertainties.

While the general relationships for scale modeling utilizing various techniques and compromises have been long established, little emphasis has been placed on the errors inherent in scale modeling. A distinction must be made between those errors which are introduced by reducing a real spacecraft design to a full size thermal test model as opposed to those errors introduced by testing a scale model of the thermal test model. Errors, or differences between a scale model and a prototype thermal test vehicle, occur as a result of compromises of the scaling criteria (violations of the assumptions on which the criteria are based) or uncertainties in thermophysical properties, geometric dimensions, and test environment.

3.2 Compromise of Modeling Criteria

If it is necessary to deviate from the requirements of the scaling criteria either by:

a) violation of the assumptions of preserved radiative properties or proportionality of model and prototype material thermal conductivities and/or capacitances, or

b) inability to provide an appropriate material gage, heater dissipation, or external environment

the general scaling criteria presented in Table 1 can be used to estimate corrections for the experimentally determined temperatures.

If the solution to the differential equations and their boundary conditions was available (either as a closed form or a numerical network solution) it would be of the form

$$T = f[k, \rho c_p, h, \alpha_s, \varepsilon, L, d, q', S] \tag{10}$$

The differences in temperature resulting from violations of the scaling criteria could be calculated from

$$\Delta T = f(x_i) - \bar{f}\,(x_i) \tag{11}$$

where x_i are the individual parameters of Equation (10), $\bar{f}\,(x_i)$ is evaluated for the parameters of the model as it was built (with compromises and violations of the scaling criteria) and $f\,(x_i)$ is evaluated for the parameters of the model as it should have been built (in accordance with the scaling criteria).

A closed form solution is generally not available. A numerical solution could be perturbed to obtain the correction factors as will be done in this study to adjust the model experimental results. Alternately,

the range of correction factors could be estimated from the formulations of the general scaling criteria presented in Table 4.

Consider the equations written for a solar flux input to an external skin element:

$$\frac{T_m}{T_p} = \frac{\alpha_{s_m} S_{F_m} L_m k_p}{\alpha_{S_p} S_{F_p} L_p k_m} \tag{12}$$

or

$$\frac{T_m}{T_p} = \left[\frac{\alpha_{s_m}}{\alpha_{s_p}} \frac{S_{F_m}}{S_{F_p}} \frac{\varepsilon_p}{\varepsilon_m} \right]^{1/4} \tag{13}$$

If the solar flux incident upon the model deviates from its nominal value and the magnitude of this deviation is known, Equations (12) and (13) can be linearized to provide an estimate of the temperature error resulting in the model. These linearized expressions of error finally appear in the form

$$\frac{\Delta T_m}{T_m} = \frac{\Delta S_{F_m}}{S_{F_m}} \tag{14}$$

and

$$\frac{\Delta T_m}{T_m} = \frac{1}{4} \frac{\Delta S_{F_m}}{S_{F_m}} \tag{15}$$

Thus, a two percent error in incident solar flux can result in a one-half to two percent error in temperature at that node. Consider the physical significance of these two alternative formulations. For the conduction based equations the indicated energy terms are balanced at the node by conduction. For the emission based equations the indicated energy terms are balanced at the node by emission.

For the solar irradiation example chosen, the absorbed solar flux has been conducted through the shell or radiated away by the exterior surface, respectively. When only conduction is involved, a two percent error in incident energy results in a two percent error in node temperature (assuming a fixed sink condition). If the absorbed energy is re-radiated, a one half percent error in temperature is indicated. In reality, the energy is both conducted and radiated away and the error in temperature is a function of the integrated problem.

This linearized technique utilizing appropriate alternate formulations of the generalized scaling criteria may be used to estimate the range of errors due to violations and compromises of the scaling criteria, but a perturbated numerical analysis is required to evaluate the magnitude of the actual error at each node.

3.3 Errors Inherent in Scale Modeling

There are errors inherent in scale modeling as a result of uncertainties in

1) material properties
2) geometric dimensions, and
3) test conditions.

The sources of many of these errors are listed in Table 5.

In general, these sources of error reduce to uncertainties in:

1) thermal conductivity
2) solar absorptance
3) infrared emittance
4) dimensions
5) heater dissipation
6) solar intensity
7) instrumentation lead losses

and in the case of transient calculations

8) specific heat
9) density and
10) instrumentation response time.

Scale models are usually built such that joint resistances will be negligible. Instrumentation lead losses and transient response considerations will be discussed separately in subsequent sections.

The remaining uncertainties in steady state scale modeling studies have been identified and probable errors estimated in Table 6. The probable errors estimated are based upon properties measurement and testing experience with Boeing facilities and may not be typical of the industry.

A statistical error analysis based upon probable error (References 51-54) results in the equation

$$\delta T_{pe} = \left[\sum_{i=1}^{n} \left(\frac{\partial T}{\partial x_i}\right)^2 (\delta x_i)^2_{pe} \right]^{1/2} \qquad (16)$$

where

δT_{pe} = the probable error in temperature

x_i = the independent problem parameters

$(\delta x_i)_{pe}$ = the probable errors identified for the independent parameters

The $(\partial T/\partial x_i)$ terms have been calculated using the conduction based general scaling criteria presented in Table 4. This results in the "maximum" probable error as opposed to probable errors generated by the emittance based criteria.

The probable errors calculated for several typical model nodes are presented in Figure 3.

An examination of the figures indicates that the non-uniformity of solar illumination within the chamber is the major source of probable error for scale ratios above 0.2. Below a one-tenth scale ratio the

effects of uncertainties in thermal conductivity and the effect of a constant geometric tolerance dominate the calculation of probable error.

The rapid increase of probable error below the one-tenth scale ratio indicates that only the most carefully conducted studies will obtain useful results for these small scale ratios. Accurate thermal conductivity measurements and tightening shop tolerances could result in accuracies greater than indicated by this study, but only at greatly increased cost.

TABLE 1. THERMAL SCALE MODELING CRITERIA

Cartesian Coordinates 3-dimensional	Cartesian Coordinates 2-dimensional	Cylindrical Coordinates 3-dimensional	Cylindrical Coordinates 2-dimensional
$\frac{k_m}{k_p} = \frac{L_m}{L_p} \cdot \frac{T_m^3}{T_p^3}$	$\frac{k_m}{k_p} = \frac{L_m^2}{L_p^2} \cdot \frac{d_p}{d_m} \cdot \frac{T_m^3}{T_p^3}$	$\frac{k_m}{k_p} = \frac{r_m}{r_p} \cdot \frac{T_m^3}{T_p^3}$	$\frac{k_m}{k_p} = \frac{r_m^2}{r_p^2} \cdot \frac{d_p}{d_m} \cdot \frac{T_m^3}{T_p^3}$
$\frac{t_m}{t_p} = \frac{L_m}{L_p} \cdot \frac{(\rho\, c_p)_m}{(\rho\, c_p)_p} \cdot \frac{T_p^3}{T_m^3}$	$\frac{t_m}{t_p} = \frac{d_m}{d_p} \cdot \frac{(\rho\, c_p)_m}{(\rho\, c_p)_p} \cdot \frac{T_p^3}{T_m^3}$	$\frac{t_m}{t_p} = \frac{r_m}{r_p} \cdot \frac{(\rho\, c_p)_m}{(\rho\, c_p)_p} \cdot \frac{T_p^3}{T_m^3}$	$\frac{t_m}{t_p} = \frac{d_m}{d_p} \cdot \frac{(\rho\, c_p)_m}{(\rho\, c_p)_p} \cdot \frac{T_p^3}{T_m^3}$
$\frac{q_m}{q_p} = \frac{L_p^2}{L_m^2} \cdot \frac{k_m}{k_p} \cdot \frac{T_m}{T_p}$	$\frac{q_m}{q_p} = \frac{L_p^2}{L_m^2} \cdot \frac{k_m}{k_p} \cdot \frac{T_m}{T_p}$	$\frac{q_m}{q_p} = \frac{r_p^2}{r_m^2} \cdot \frac{k_m}{k_p} \cdot \frac{T_m}{T_p}$	$\frac{q_m}{q_p} = \frac{r_p^2}{r_m^2} \cdot \frac{k_m}{k_p} \cdot \frac{T_m}{T_p}$
$\frac{q'_m}{q'_p} = \frac{L_m}{L_p} \cdot \frac{k_m}{k_p} \cdot \frac{T_m}{T_p}$	$\frac{q'_m}{q'_p} = \frac{d_m}{d_p} \cdot \frac{k_m}{k_p} \cdot \frac{T_m}{T_p}$	$\frac{q'_m}{q'_p} = \frac{r_m}{r_p} \cdot \frac{k_m}{k_p} \cdot \frac{T_m}{T_p}$	$\frac{q'_m}{q'_p} = \frac{d_m}{d_p} \cdot \frac{k_m}{k_p} \cdot \frac{T_m}{T_p}$
$\frac{S_m}{S_p} = \frac{L_p}{L_m} \cdot \frac{k_m}{k_p} \cdot \frac{T_m}{T_p}$	$\frac{S_m}{S_p} = \frac{L_p^2}{L_m^2} \cdot \frac{d_m}{d_p} \cdot \frac{k_m}{k_p} \cdot \frac{T_m}{T_p}$	$\frac{S_m}{S_p} = \frac{r_p}{r_m} \cdot \frac{k_m}{k_p} \cdot \frac{T_m}{T_p}$	$\frac{S_m}{S_p} = \frac{r_p^2}{r_m^2} \cdot \frac{d_m}{d_p} \cdot \frac{k_m}{k_p} \cdot \frac{T_m}{T_p}$

$\frac{h_m}{h_p} = \frac{L_p}{L_m} \cdot \frac{k_m}{k_p}$	$\frac{h_m}{h_p} = \frac{L_p}{L_m} \cdot \frac{k_m}{k_p}$	$\frac{h_m}{h_p} = \frac{r_p}{r_m} \cdot \frac{k_m}{k_p}$	$\frac{h_m}{h_p} = \frac{r_p}{r_m} \cdot \frac{k_m}{k_p}$
		$\frac{r_m}{r_p} = \frac{L_m}{L_p}$	$\frac{r_m}{r_p} = \frac{L_m}{L_p}$

Nomenclature

d = characteristic thickness, ft
k = thermal conductivity, Btu/hr·ft·^{o}F
L = characteristic length, ft
T = absolute temperature, ^{o}F
t = time, hr
ρ = density, lb_m/ft^3
c_p = specific heat at constant pressure, $Btu/lb_m\,^{o}F$
q = heat dissipation per unit volume, $Btu/hr\ ft^3$
q´ = heat dissipation, Btu/hr
S = heat flux per unit area, $Btu/hr\ ft^3$
h = joint conductance, $Btu/hr\ ft^2\ ^{o}F$
r = characteristic radius, ft

Subscripts

m refers to scale model
p refers to prototype

Note:

Assumes $a_m = a_p$ where $k_m = \bar{k}_m T_m^{a_m}$

$$k_p = \bar{k}_p T_p^{a_p}$$

Assumes radiative properties preserved

TABLE 2. THERMAL SCALE MODELING CRITERIA-TEMPERATURE PRESERVATION

Cartesian Coordinates 3-dimensional	Cartesian Coordinates 2-dimensional	Cylindrical Coordinates 3-dimensional	Cylindrical Coordinates 2-dimensional
$\frac{k_m}{k_p} = \frac{L_m}{L_p} = R$	$\frac{k_m}{k_p} = \frac{L_m^2}{L_p^2} \cdot \frac{d_p}{d_m}$	$\frac{k_m}{k_p} = \frac{r_m}{r_p} = R$	$\frac{k_m}{k_p} = \frac{r_m^2}{r_p^2} \cdot \frac{d_p}{d_m}$
$\frac{t_m}{t_p} = \frac{L_m}{L_p} \cdot \frac{(\rho\, c_p)_m}{(\rho\, c_p)_p}$	$\frac{t_m}{t_p} = \frac{d_m}{d_p} \cdot \frac{(\rho\, c_p)_m}{(\rho\, c_p)_p}$	$\frac{t_m}{t_p} = \frac{r_m}{r_p} \cdot \frac{(\rho\, c_p)_m}{(\rho\, c_p)_p}$	$\frac{t_m}{t_p} = \frac{d_m}{d_p} \cdot \frac{(\rho\, c_p)_m}{(\rho\, c_p)_p}$
$\frac{q_m}{q_p} = \frac{L_p}{L_m} = \frac{1}{R}$	$\frac{q_m}{q_p} = \frac{d_p}{d_m}$	$\frac{q_m}{q_p} = \frac{r_p}{r_m} = \frac{1}{R}$	$\frac{q_m}{q_p} = \frac{d_p}{d_m}$
$\frac{q'_m}{q'_p} = \frac{L_m^2}{L_p^2} = R^2$	$\frac{q'_m}{q'_p} = \frac{L_m^2}{L_p^2} = R^2$	$\frac{q'_m}{q'_p} = \frac{r_m^2}{r_p^2} = R^2$	$\frac{q'_m}{q'_p} = \frac{r_m^2}{r_p^2} = R^2$
$\frac{S_m}{S_p} = 1$	$\frac{S_m}{S_p} = 1$	$\frac{S_m}{S_p} = 1$	$\frac{S_m}{S_p} = 1$
$\frac{h_m}{h_p} = 1$	$\frac{h_m}{h_p} = \frac{L_m}{L_p} \cdot \frac{d_p}{d_m}$	$\frac{h_m}{h_p} = 1$	$\frac{h_m}{h_p} = \frac{r_m}{r_p} \cdot \frac{d_p}{d_m}$
		$\frac{r_m}{r_p} = \frac{L_m}{L_p}$	$\frac{r_m}{r_p} = \frac{L_m}{L_p}$

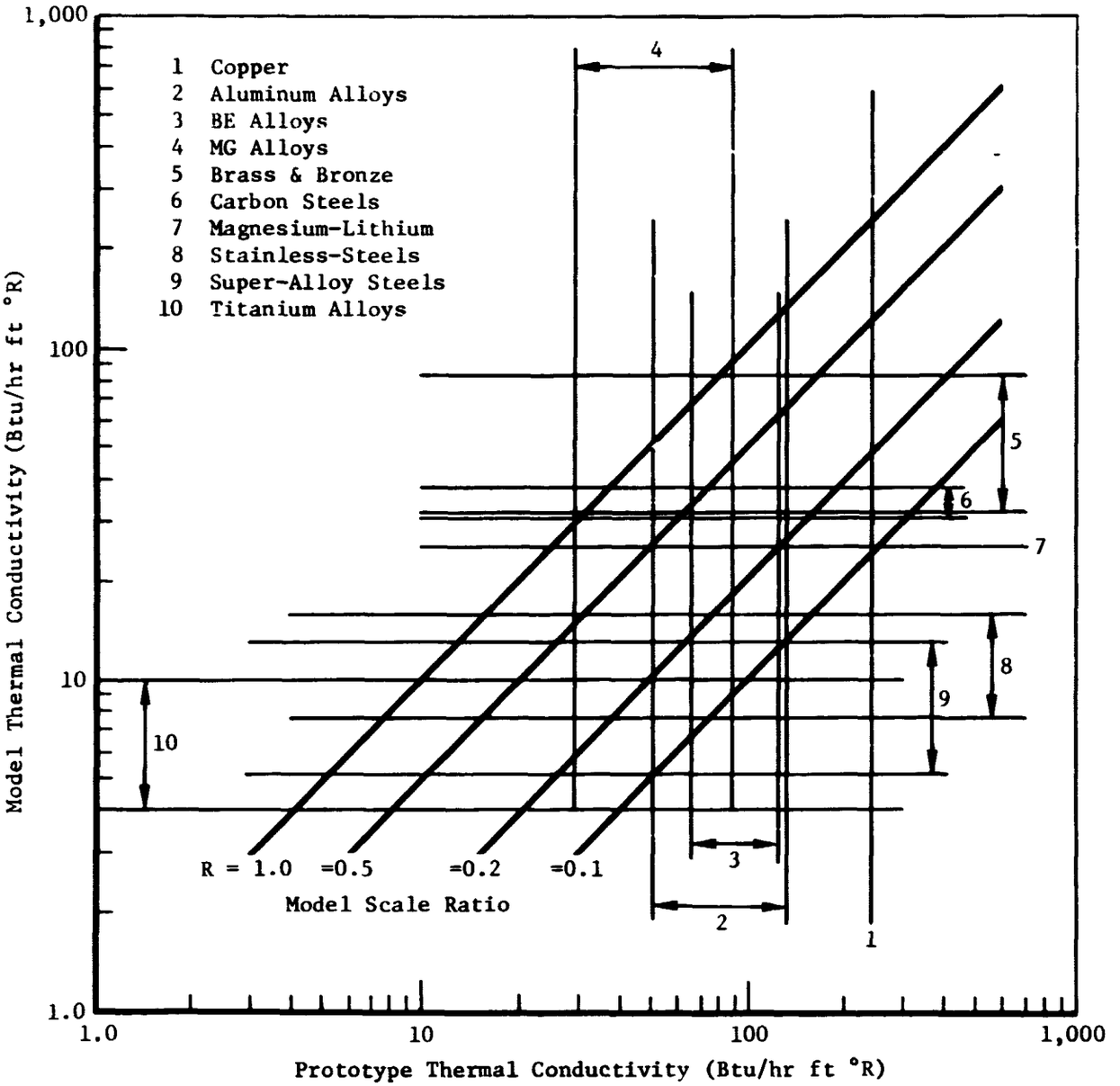

Figure 1: RANGES OF THERMAL CONDUCTIVITIES OF METALLIC MATERIALS

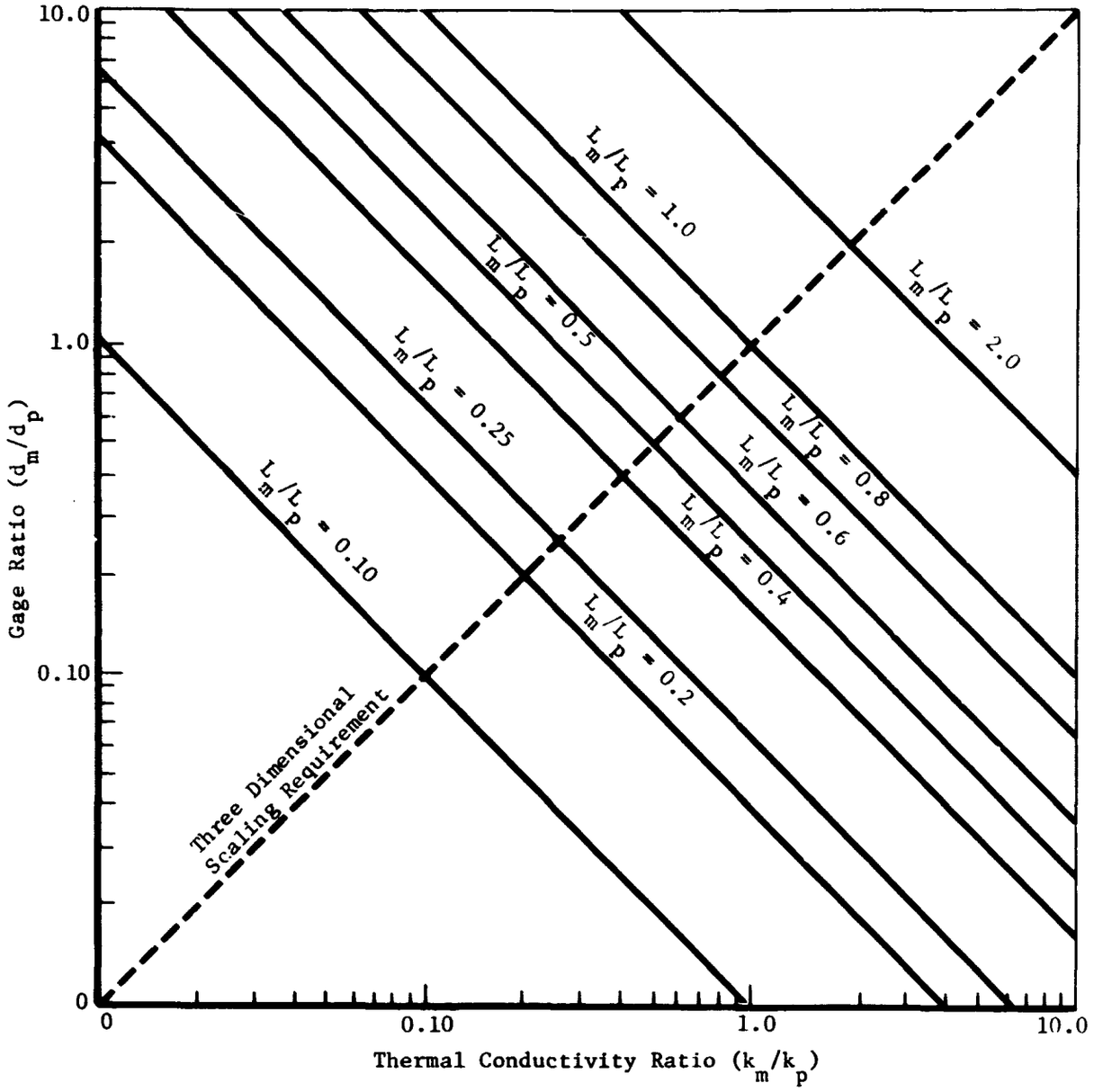

Figure 2: GEOMETRIC DISTORTION SCALING REQUIREMENTS FOR RANGES OF THERMAL CONDUCTIVITY RATIOS

TABLE 3. ALTERNATE FORMULATION OF COEFFICIENTS

Energy Term	Related by Conduction	Related by Emission
Emission	$\frac{\sigma\varepsilon\, LT^3}{k}$	1
Conduction	1	$\frac{k}{\sigma\varepsilon\, LT^3}$
Internal Generation	$\frac{q'}{kLT}$	$\frac{q'}{\sigma\varepsilon\, L^2T^4}$
Irradiation	$\frac{SL}{kT}$	$\frac{S}{\sigma\varepsilon\, T^4}$
Joint Conductance	$\frac{h}{kL}$	$\frac{h}{\sigma\varepsilon\, L^2T^3}$
Transient Relation	$\frac{\rho\, c_p L^2}{tk}$	$\frac{\rho\, c_p L}{t\sigma\varepsilon\, T^3}$

TABLE 4. ALTERNATE FORMULATION OF SCALE MODELING CRITERIA

Energy Term	Conduction Basis	Emission Basis
Emission	$\frac{T_m}{T_p} = \left[\frac{k_m}{k_p}\frac{L_p}{L_m}\frac{\varepsilon_p}{\varepsilon_m}\right]^{1/3}$	1
Conduction	1	$\frac{T_m}{T_p} = \left[\frac{k_m}{k_p}\frac{\varepsilon_p}{\varepsilon_m}\frac{L_p}{L_m}\right]^{1/3}$
Generation	$\frac{T_m}{T_p} = \frac{q'_m}{q'_p}\frac{k_p}{k_m}\frac{L_p}{L_m}$	$\frac{T_m}{T_p} = \left[\frac{q'_m}{q'_p}\frac{\varepsilon_p}{\varepsilon_m}\frac{L_p^2}{L_m^2}\right]^{1/4}$
Irradiation	$\frac{T_m}{T_p} = \frac{S_m}{S_p}\frac{L_m}{L_p}\frac{k_p}{k_m}$	$\frac{T_m}{T_p} = \left[\frac{S_m}{S_p}\frac{\varepsilon_p}{\varepsilon_m}\right]^{1/4}$
Joint Conductance	$\frac{h_m}{h_p} = \frac{k_m}{k_p}\frac{L_m}{L_p}$	$\frac{h_m}{h_p} = \frac{\varepsilon_m}{\varepsilon_p}\frac{L_m^2}{L_p^2}\frac{T_m^3}{T_p^3}$
Transient Relation	$\frac{t_m}{t_p} = \frac{(\rho c_p)_m}{(\rho c_p)_p}\frac{L_m^2}{L_p^2}\frac{k_p}{k_m}$	$\frac{t_m}{t_p} = \frac{(\rho c_p)_m}{(\rho c_p)_p}\frac{L_m}{L_p}\frac{\varepsilon_p}{\varepsilon_m}\frac{T_p^3}{T_m^3}$

TABLE 5. LIMITING FACTORS FOR MODEL SCALING RATIOS

- Materials
  - Thermal Properties
    - Thermal Conductivity, k
      - Value
      - Temperature Variation
      - Uncertainty
    - Joint Conductance, h
      - Value
      - Uncertainty
    - Specific Heat, c_p
      - Value
      - Temperature Variation
      - Uncertainty
    - Density, ρ
      - Value
      - Uncertainty
    - Coefficient of Thermal Expansion, α
      - Value
      - Uncertainty
  - Radiative Properties
    - Solar Absorptance, α_s
      - Value
      - Temperature Dependence
      - Uncertainty
    - Infrared Emittance, ϵ
      - Value
      - Temperature Dependence
      - Uncertainty
- Dimensions
  - Major Dimensions, L
    - Value
    - Tolerance
  - Minor Dimensions, d
    - Value
    - Tolerance
  - Solid Angle, ω
    - Value
    - Tolerance
- Test Environment
  - Heat Dissipation
    - Value
    - Uncertainty
    - Power Leads
  - Space Simulation
    - Background Temperature
      - Value
      - Uncertainty
    - Solar Beam
      - (Intensity, Collimation and Spectral Match)
      - Value
      - Uncertainty
- Instrumentation
  - Location
  - Tolerance
  - Response Time
  - Thermocouple Leads

TABLE 6. ESTIMATE OF ERRORS INHERENT IN SCALE MODELING

Parameter	2σ Range of Error	Probable Error
Thermal Radiation (α_s, ε)	$\pm$ 0.02	$\pm$ 0.0067
Solar Flux	$\pm$ 4.42 Btu/Hr Ft^2	$\pm$ 1.99 Btu/Hr Ft^2
Thermal Conductivity	$\pm$ 1.0 Btu/Hr Ft ^oR	$\pm$ 0.337 Btu/Hr Ft ^oR
Geometric Tolerances	$\pm$ 0.0026 Ft	$\pm$ 0.00088 Ft
Internal Dissipation	$\pm$ 0.01 Q_m	$\pm$ 0.00337 Q_m
Thermocouples	$\pm$ 3.0 ^oR	$\pm$ 1.01 ^oR

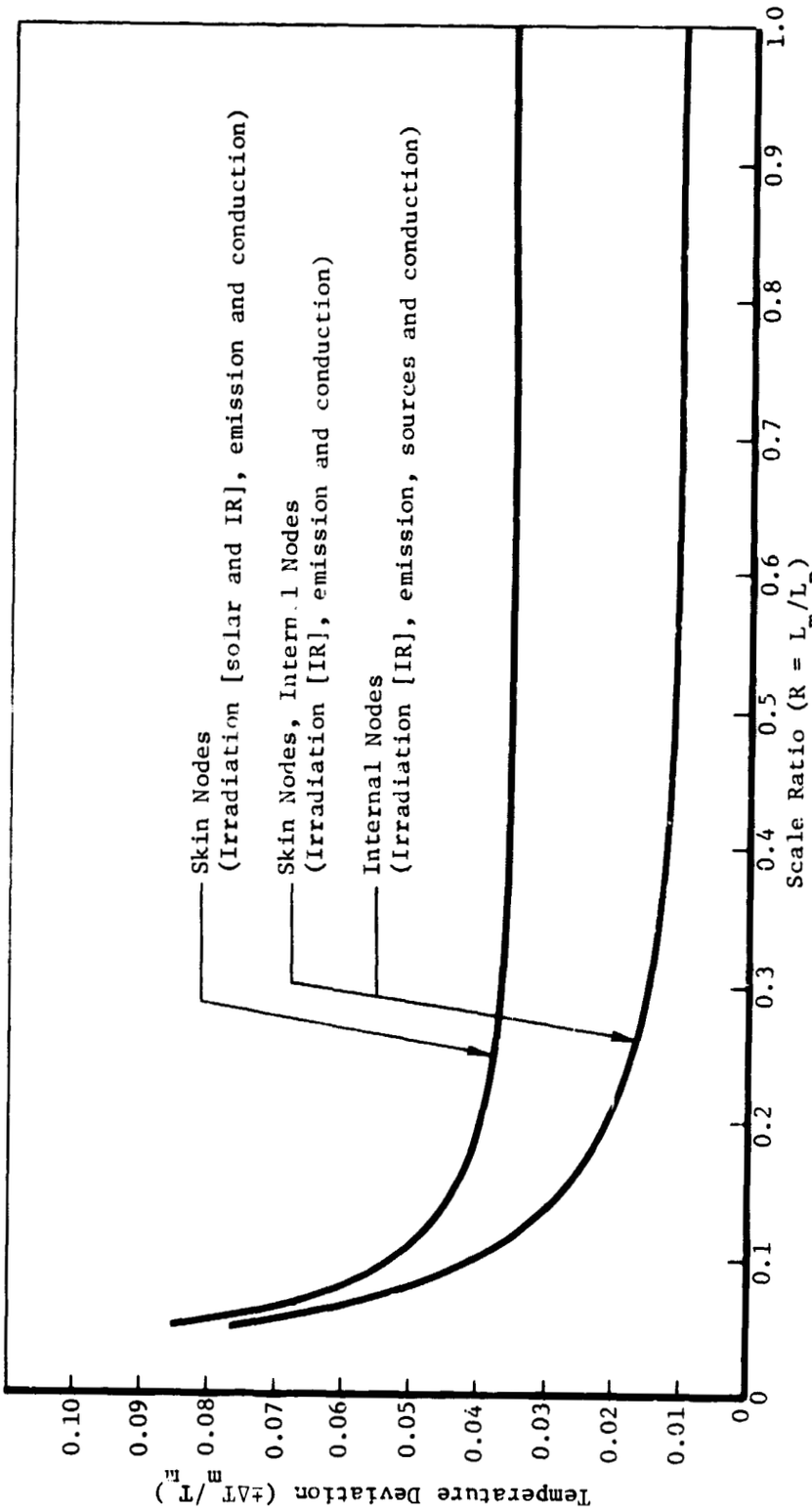

Figure 3: PROBABLE TEMPERATURE ERROR IN THERMAL SCALE MODELING AS A RESULT OF UNCERTAINTIES

PRECEDING PAGE BLANK NOT FILMED.

4.0 SELECTED PROBLEM AREAS IN SCALE MODELING

In many cases the general scaling criteria may not provide adequate guidance for understanding the effects of compromise in certain areas of model construction. Some aspects of the prototype vehicle may not be amenable to modeling within the framework of the general criteria.

As an example of this, consider a thermal control coating whose radiative properties are thickness dependent. To preserve radiative properties, the coating thickness is preserved. As its conductivity is unchanged this increases relative conduction in the paint as the scale ratio increases.

An understanding of the errors induced by compromises of the scaling criteria in selected areas and possible techniques for reducing these errors are the purpose of this section. The selected problem areas in thermal scale modeling to be discussed are:

1) Transient Response
2) Thermal Control Coatings
3) Multilayer Insulation
4) Thermal Gradient Effects
5) Instrumentation Effects
6) Test Environment

4.1 Transient Response

In scale modeling steady state conditions, the thermal conductivities and the scale model ratios are related by

$$\frac{k_m}{k_p} = \frac{L_m}{L_p} \tag{17}$$

for cases in which the gradients within the materials are three dimensional. For a multi-material spacecraft this relationship is quite restrictive.

Not only must a set of model materials be identified whose conductivities are a fixed fraction of those of the prototype materials, but sheet metal gages must also be fabricated to this ratio. The probable requirements resulting for non-standard gages substantially increase the cost of scale modeling. Fortunately, most spacecraft materials are thin members with negligible gradients in one direction. For these elements, the thermal conductivities and dimensions are related by

$$\frac{L_m^2}{L_p^2} = \frac{k_m}{k_p}\frac{d_m}{d_p} \tag{18}$$

This relationship allows standard gages to be utilized by trading thickness versus material conductivity. Even this approach however, forces compromises on the scale modeler as the number of gage-conductivity pairs is quite finite. The gages selected must be stiff enough to allow the model to support itself and yet thin enough to insure that gradients across the material will remain negligible.

Additionally, the transient response of the geometrically distorted model components is related to thickness and thermal capacity by

$$\frac{t_m}{t_p} = \frac{d_m}{d_p}\frac{(\rho\, c_p)_m}{(\rho\, c_p)_p} \tag{19}$$

It is desirable for each model-prototype material pair to have the same relative characteristic time in order for the model to have a transient response which can be related to the prototype transient response.

Substitution of Equation (18) into (19) results in the expression

$$\frac{t_m}{t_p} = \frac{L_m^2}{L_p^2}\frac{k_p}{k_m}\frac{(\rho\, c_p)_m}{(\rho\, c_p)_p} \tag{20}$$

This equation allows one to relate the characteristic response time for each material pair to the corresponding scale model ratio. Inherent in this relationship is the limitation on allowable scale model ratios if standard gages are to be utilized. This limitation was shown by Equation (18)

$$\frac{L_m}{L_p} = \left[\frac{k_m}{k_p} \frac{d_m}{d_p} \right]^{1/2} \tag{21}$$

This problem is better discussed in light of a specific example. Consider a spacecraft which is fabricated predominantly of 6061-T6 and 7075-T6 aluminums [both 0.0625 in (0.1588 cm) thickness]. It is advantageous to select the model materials from the materials listed in Table 7 due to the large selection of gages of these materials available in the company stores. This table shows the thermal conductivity and thermal capacitance for each material at room temperature. The last three columns tabulate the ratios of thermal conductance and capacitance resulting from using the material to model first the 6061-T6 and then the 7075-T6 aluminums. The results are shown, based on Equation (20), in Figure 4.

The discrete points denoted on the figure are taken from Tables 8 and 9, and represent available gages of these materials over the range required for a nominal half scale model.

A clear cut choice of material substitutions does not occur, rather a compromise is forced upon the designer.

a) If only steady state response is to be scaled then 0.010 gage (0.0254 cm) 2024-0 may be substituted for 7075-T6 and 0.020 gage (0.0508 cm) 7075-T6 may be substituted for 6061-T6 to produce, at a nominal scale ratio of 0.495, the minimum error in modeling steady state results.

b) If the transient sequence of events is important then 0.020 (0.0508 cm) 7075-T6 may be substituted for 7075-T6 and 0.020 (0.0508 cm) 6061-T4 may be substituted for 6061-T6 to produce, at a nominal scale ratio of 0.554, the minimum error in scaling the transient sequence of events.

c) If both transient and steady state results are important an additional choice is available. The 0.016 gage (0.0406 cm) 5052-0 may be substituted for 7075-T6 and 0.016 gage (0.0406 cm) 6061-T6 may be substituted for 6061-T6 to provide a compromise solution at a nominal scale ratio of 0.513. Errors here occur in both the steady state and transient response scaling but the errors are smaller than those resulting in either of the two previous choices.

In general the utilization of available materials and standard gages will force a compromise; the extent of which will be a function of the requirements of the project, and the magnitude of which will be a function of the materials and gages of the prototype which is being scaled.

In extreme cases other alternates exist for the designer.

a) Only the cost factor limits the designer to existing gages. If necessary, required gages may be machined to order.

b) The thickness of an element may be chosen on the basis of the required thermal capacitance. The conductivity may be reduced to a desired effective value by slitting or by slotting the material (References 5 and 62).

In most practical problems a compromise solution based on standard gages to scale the major portions of the spacecraft would be adopted. The remaining portions of the configuration would probably be neglected, approximated, or have special gages machined as appropriate.

While the number of suitable materials decreases as the scale model ratio decreases, limitations appear more a function of the specific materials and gages in the prototype than the general scale ratio. Due to a fortuitous combination of materials and gages on the prototype it may be easier to build a quarter scale model than a three quarter scale model if both transient and steady state scaling are required. However, in general, as the number of suitable materials decreases, so decreases the possibilities of finding suitable compromise solutions at any given scale ratio.

4.2 Thermal Control Coatings

The scaling of thermal control coatings is a potential problem area in thermal scale modeling. Coatings are applied to virtually all interior and exterior surfaces. To interior surfaces to promote radiation interchange, and to exterior surfaces to provide desired combinations of solar absorptance and infrared emission characteristics which govern the overall spacecraft temperature level.

In scale modeling the presence of coatings assists to preserve the radiative properties between model and prototype. However some coatings are applied to a thickness (10 mils) which could seriously influence the conduction balance. The coating thickness must be maintained in order to preserve the radiative properties of the surface but in the scale models this results in increased conduction through the coating.

Consider the thermal control coating shown applied to some substrate surface:

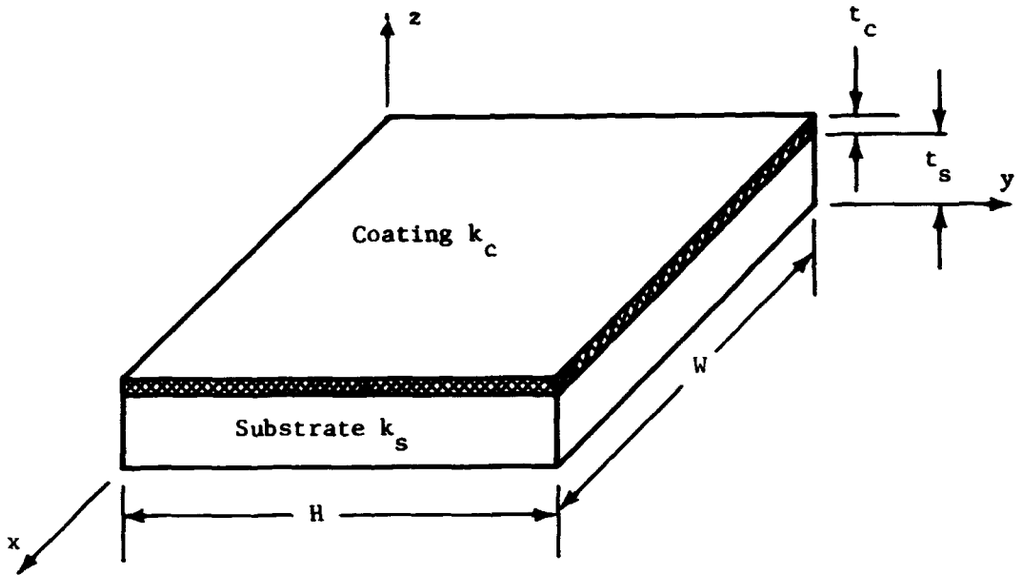

The thermal resistance for normal heat transfer through the substrate and coating may be expressed as:

$$R = \frac{1}{HW} \left[\frac{k_c t_s + k_s t_c}{t_c t_s} \right] \tag{22}$$

Ratioing the thermal resistance for a model to that of the prototype results in the equation:

$$\frac{R_m}{R_p} = \frac{H_p W_p}{H_m W_m} \left[\frac{t_{cp} t_{sp}}{t_{cm} t_{sm}} \right] \left[\frac{k_{cm} t_{sm} + k_{sm} t_{cm}}{k_{cp} t_{sp} + k_{sp} t_{cp}} \right] \tag{23}$$

If the model is constructed with rigid adherence to the three dimensional scaling criteria, where

$$\frac{H_m}{H_p} = L \qquad \frac{W_m}{W_p} = L \tag{24a}$$

$$\frac{k_{cm}}{k_{cp}} = L \qquad \frac{t_{sm}}{t_{sp}} = L \tag{24b}$$

$$\frac{k_{sm}}{k_{sp}} = L \qquad \frac{t_{cm}}{t_{cp}} = L \tag{24c}$$

then the ratio of thermal resistances reduces to:

$$\frac{R_m}{R_p} = \frac{1}{L^2} \tag{25}$$

If however the substrate is scaled and the coating conductivity and thickness are preserved, Equation (23) for the ratio of thermal resistances again reduces to

$$\frac{R_m}{R_p} = \frac{1}{L^2} \tag{26}$$

It is apparent that should normal heat transfer through the coating be the dominant conduction flux, no special considerations must be taken when the coating conductivity and thickness are preserved.

The thermal resistance for conduction heat transfer along the surface shown may be expressed as:

$$R = \frac{H}{W} \frac{1}{(k_s t_s + k_c t_c)} \tag{27}$$

The ratio of thermal resistance in the model to that in the prototype is

$$\frac{R_m}{R_p} = \frac{H_m W_p}{H_p W_m} \frac{(k_{sp} t_{sp} + k_{cp} t_{cp})}{(k_{sm} t_{sm} + k_{cm} t_{cm})} \tag{28}$$

If the model is again constructed with a rigid adherence to the three dimensional scaling criteria as presented in Table 1, the thermal resistance ratio reduces to

$$\frac{R_m}{R_p} = \frac{1}{L^2} \tag{29}$$

If the substrate is scaled while the coating thickness and conductivity are preserved, Equation (28) then reduces to

$$\frac{R_m}{R_p} = \frac{1 + [k_{cp} t_{cp} / k_{sp} t_{sp}]}{L^2 + [k_{cp} t_{cp} / k_{sp} t_{sp}]} \tag{30}$$

If it is recognized that the individual thermal resistances in the coating and substrate may be expressed as

$$R_s = \frac{H}{k_s t_s W} \tag{31a}$$

$$R_c = \frac{H}{k_c t_c W} \tag{31b}$$

and that their ratio is

$$\frac{R_s}{R_c} = \frac{k_c t_c}{k_s t_s} \tag{32}$$

Equation (30) can also be expressed as

$$\frac{R_m}{R_p} = \frac{1 + R_{sp}/R_{cp}}{L^2 + R_{sp}/R_{cp}} \tag{33}$$

The ratio of heat conduction in the model to that conducted in the prototype is

$$\frac{q_m}{q_p} = \frac{R_p}{R_m} \frac{\Delta T_m}{\Delta T_p} \tag{34}$$

but the three dimension criteria requires that the energy fluxes be scaled by the square of the scaling ratio. As strict scaling requirements have been compromised, we may use this information to calculate the temperature differences which might result, from the equation

$$\frac{\Delta T_m}{\Delta T_p} = L^2 \frac{R_m}{R_p} \tag{35}$$

which reduces, with the substitution of Equation (33), to

$$\frac{\Delta T_m}{\Delta T_p} = \frac{1 + R_{sp}/R_{cp}}{1 + (1/L^2)(R_{sp}/R_{cp})} \tag{36}$$

Figure 5 is a plot of this equation illustrating the temperature differences which might occur for several selected scaling ratios. Figure 5a illustrates the range of the abscissa over which several combinations of substrates and thermal control coatings would vary. The ranges in abscissa shown in Figure 5a are typical for 1/16 inch (0.1588 cm) skin panels with a 10 mil exterior thickness of white paint. Z-93 is a typical inorganic coating while B-1060 is a typical organic coating. Both are white, low α_s/ε coatings whose radiative properties are thickness dependent.

As most spacecraft would be fabricated from a variety of metallic materials, it is evident that models in the range of one fourth to one tenth of full size would incur considerable errors. One solution might be to overscale the substrate to compensate for the increased conduction in the coating when building a scale model.

If the model is constructed with the following scaling criteria:

$$\frac{H_m}{H_p} = L \qquad \frac{W_m}{W_p} = L \tag{37a}$$

$$\frac{k_{sm}}{k_{sp}} = L \qquad \frac{k_{cm}}{k_{cp}} = 1 \tag{37b}$$

$$\frac{t_{sm}}{t_{sp}} = B \qquad \frac{t_{cm}}{t_{sp}} = 1 \tag{37c}$$

then Equation (23) reduces to:

$$\frac{R_m}{R_p} = \frac{(k_{sp}t_{sp} + k_{cp}t_{cp})}{BL\,k_{sp}t_{sp} + k_{cp}t_{cp}} \tag{38}$$

However, if the temperature and heat transferred both through the coating and substrate are preserved, then the ratio of thermal resistances must be proportional to the inverse of the square of the scaling ratio.

Thus:

$$\frac{k_{sp}t_{sp} + k_{cp}t_{cp}}{BL\,k_{sp}t_{sp} + k_{cp}t_{cp}} = \frac{1}{L^2} \tag{39}$$

which can be rewritten as

$$\frac{B}{L} = 1 + \frac{k_{cp}t_{cp}}{k_{sp}t_{sp}}\left(1 - \frac{1}{L^2}\right) \tag{40}$$

or using the definition of individual thermal resistances as shown in Equation (31):

$$\frac{B}{L} = 1 + \frac{R_{sp}}{R_{cp}}\left(1 - \frac{1}{L^2}\right) \tag{41}$$

Figure 6 illustrates this relationship for the same range of variables as shown in Figures 5 and 5a. Here, however, a definite limitation is imposed on this method of overscaling due to the fact that eventually the coating itself conducts more energy that is permissible for the scaled coating-substrate system. At this point, compensating by this technique would have completely eliminated the substrate material. This figure indicates that only the most highly conducting substrates would allow accurate modeling below scale ratios of one-tenth.

4.3 Multilayer Insulation

The scaling of multilayer insulation is potentially the most serious problem area in thermal scale modeling. While multilayer insulation is used extensively on virtually all current spacecraft, the manufacture of multilayer blankets is essentially an art with uniformity of performance difficult to obtain (References 55-64). One of the most critical parameters in the evaluation of blanket performance is the amount of contact between layers of the blanket. Due to the free floating nature of the blankets, the variety of shapes and sizes to which they are applied, and the effects of ascent depressurization, the final blanket layer spacing and subsequent interlayer contact areas are impossible to control. This section will initially discuss some aspects of multilayer insulation performance and then examine the scaling of multilayer systems.

4.3.1 Multilayer Insulation Performance.- The performance of a multilayer system is a complex problem due to the discrete and anisotropic nature of the layers. Heat transfer through the layers is a result of radiation transport between the layers and conduction paths through and along the layers due to interlayer contact. Consider the following model of a multilayer system composed of a subsurface, (o), alternate layers of spacer and radiation shields, (n) and a cover sheet (c).

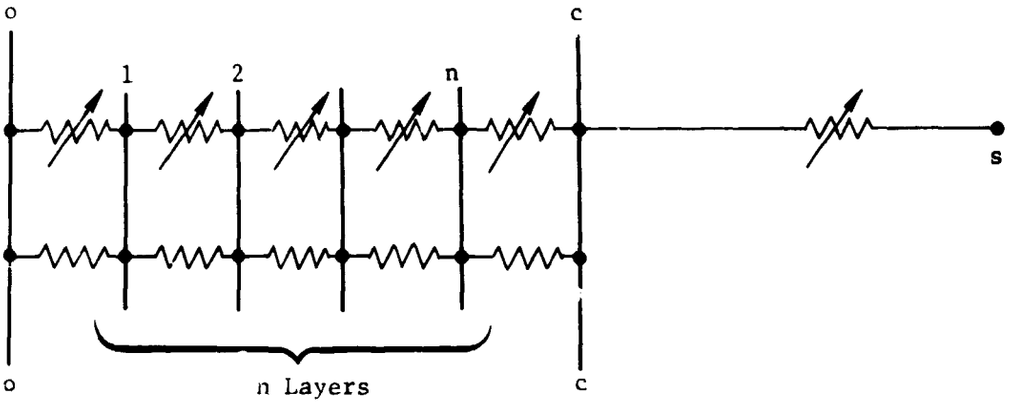

The low temperature space environment is represented by the subscript s. The resistances pictured denote the parallel radiation and conduction paths between the layers of insulation. For a typical element of cross sectional area A, γ will be the effective fractional contact area for conduction and $1-\gamma$ will be the fractional radiation area.

Utilizing the electrical analogy, the following equivalent thermal reciprocal resistances may be calculated:

1) between the subsurface and the first radiation shield

$$\frac{1}{R_a} = A\left\{\frac{\gamma k_m}{0.5\, x_m} + \frac{\gamma(1-\gamma)}{\left[\frac{1}{\varepsilon_o} + \frac{1}{\varepsilon} - 1\right]}\left[T_o^3 + T_o T_1 (T_o + T_1) + T_1^3\right]\right\} \quad (42)$$

2) between the n layers of insulation

$$\frac{1}{R_b} = A\left\{\frac{\gamma k_m}{(n-1)\, x_m} + \frac{\gamma(1-\gamma)}{(n-1)\left(\frac{2}{\varepsilon} - 1\right)}\left[T_1^3 + T_1 T_n (T_1 + T_n) + T_n^3\right]\right\} \quad (43)$$

3) between the n^{th} layer and the cover sheet

$$\frac{1}{R_c} = A \left\{ \frac{\phi k_m}{0.5(x_m+x_c)} + \frac{\sigma(1-\phi)}{[\frac{1}{\varepsilon} + \frac{1}{\varepsilon_c} -1]} [T_n^3+T_n T_c (T_n+T_c)+T_c^3] \right\} \quad (44)$$

4) between the cover sheet and space

$$\frac{1}{R_d} = A \frac{\sigma}{(1/\varepsilon_c)} T_c^3 \quad (45)$$

where

k_m = thermal conductivity across radiation shield

k_c = thermal conductivity across cover sheet

x_m = thickness of radiation shield

x_c = thickness of cover sheet

The energy transport across each of these thermal paths may be evaluated from the following expressions:

1) between the subsurface and the first radiation shield

$$(\frac{q}{A})_a = \frac{\phi k_m}{0.5\ x_m} (T_o - T_1) + \frac{\sigma(1-\phi)}{(\frac{1}{\varepsilon_o} + \frac{1}{\varepsilon} -1)} (T_o^4 - T_1^4) \quad (46)$$

2) between the n layers of insulation

$$(\frac{q}{A})_b = \frac{\phi k_m}{(n-1)\ x_m} (T_1 - T_n) + \frac{\sigma(1-\phi)}{(n-1)(\frac{2}{\varepsilon} -1)} (T_1^4 - T_n^4) \quad (47)$$

3) between the n^{th} layer and the cover sheet

$$= \frac{\phi k_i}{0.5(x_m + x_c)} (T_n - T_c) + \frac{\sigma(1-\phi)}{(\frac{1}{\epsilon_c} + \frac{1}{\epsilon} - 1)} (T_n^4 - T_c^4) \qquad (48)$$

4) between the cover sheet and the space sink

$$(\frac{q}{A})_d = \frac{\sigma}{(1/\epsilon_c)} T_c^4 \qquad (49)$$

These equations may be solved simultaneously to determine the one-dimensional energy transfer through a multilayer system as a function of its thermal properties and boundary conditions, if the effective contact area (ϕ) is known. These equations can also be used to determine sensitivity to relative contact area as shown in Figures 7 and 8.

Figures 7 and 8 show the subsurface temperatures required to drive 1.0 Btu/hr ft^2 (0.3152 Watts/m^2) and 0.1 Btu/hr ft^2 (0.03152 Watts/m^2), respectively through insulation systems where the number of layers and fractional contact areas are variable. At large values of fractional contact area the heat transfer mechanism is conduction dominant and the sub surface driving temperature increases linearly with the number of layers. At minimal values of contact area the radiation transport is dominant.

A comparison of Figures 7 and 8 indicates that:

1) very small changes in fractional contact area can radically change the dominant mode of energy transport through the insulation, and
2) as the total flux level decreases, the insulation system becomes more sensitive to the effects of fractional contact area.

The extreme dependency of one-dimensional perfor ance upon effective contact area makes calculations of performance difficult as the contact area is neither very uniform nor very controllable. Additionally two dimensional effects are present in the blankets due to the presence of seams and penetrations through the insulation. In these areas, gradients induced along the layers result in substantial parallel conduction and radiation transport (References 56 and 63).

Many current studies into the prediction of multilayer insulation performance are continuing but results to date indicate that experimental evaluations of the blanket systems are required. The question then arises, "Is it possible to scale multilayer insulation systems without a detailed understanding of performance ?"

4.3.2 Scaling Multilayer Insulation.- This section will examine the relative performance of prototype and model insulation systems to determine a set of scaling criteria which do not require a detailed understanding of performance.

The normal three dimensional criteria for the temperature preservation thermal scale modeling of spacecraft require that all dimensions and material thermal conductivities be reduced in direct proportion to the scale ratio. As the insulation blankets are normally composed of minimum gage materials (e.g. 1/4 mil mylar with a 500 Å aluminum film) and fabricated for minimum normal thermal conductivity, the application of these scaling criteria is precluded.

It is therefore necessary to examine the scaling requirements for multilayer insulation blankets in detail to see if a criteria compromise might be effected which would allow the satisfactory scale modeling of multilayer insulation blankets.

Consider the segment of a multilayer blanket shown in Figure 9. If this segment of an insulation blanket is treated as a three dimensional

solid of volume L^2B, the energy equation may be written (for a steady state case with no internal general) as

$$\frac{\partial}{\partial x}\left(k_x \frac{\partial T}{\partial x}\right) + \frac{\partial}{\partial y}\left(k_y \frac{\partial T}{\partial y}\right) + \frac{\partial}{\partial z}\left(k_z \frac{\partial T}{\partial z}\right) = 0 \tag{50}$$

The conductivities of the now anisotropic solid may be expressed as

$$k_x = k_y = k_\ell \frac{nt}{B} \tag{51}$$

$$k_z = \frac{QB}{AT} = \frac{B}{AT}\left[\frac{\sigma\varepsilon\ (1-\phi)\ A\ \Delta T^4}{n(2-\varepsilon)} + \frac{k_s \phi\ A\ \Delta T}{B}\right] \tag{52}$$

Substitution of Equations (51) and (52) into (50) with the change of variables:

$$u = x/L \qquad v = y/L \qquad w = z/B \tag{53}$$

$$\theta = T/T_o$$

results in the differential equation

$$\frac{\partial^2 \theta}{\partial u^2} + \frac{\partial^2 \theta}{\partial v^2} + \left[\frac{\sigma\varepsilon\ L^2\ (1-\phi)T^3}{n^2\ k_\ell t\ (2-\varepsilon)} + \frac{k_s \phi\ L^2}{k_\ell\ nBt}\right]\frac{\partial^2 \theta}{\partial w^2} = 0 \tag{54}$$

For the solution to Equation (54) to apply both to a prototype and model insulation system the coefficient

$$\left[\frac{\sigma\varepsilon\ L^2\ (1-\phi)\ T^3}{n^2\ k_\ell t\ (2-\varepsilon)} + \frac{k_s \phi\ L^2}{k_\ell\ nEt}\right] \tag{55}$$

must be preserved between the model and the prototype.

In regions of the blanket in which the heat transfer is only one dimensional through the blanket, Equation (54) reduces to

$$\frac{\partial^2 \theta}{\partial w^2} = 0 \tag{56}$$

For this situation, no requirement is placed upon scale modeling techniques. An identical blanket system may be used on both the prototype and the model.

In the more general cases of two dimensional heat transfer within the blanket the coefficient of Equation (54) must be preserved.

If the following restrictions are placed upon the model:

1) radiative properties are preserved,
2) temperatures are preserved, and
3) insulation material and fabrication techniques are preserved

then:

$$\begin{aligned} \epsilon_m &= \epsilon_p \\ \Delta T_m &= \Delta T_p \\ \phi_m &= \phi_p \\ k_{sm} &= k_{sp} \\ t_m &= t_p \end{aligned} \tag{57}$$

With these restrictions the coefficient of Equation (54) related for model (subscript m) and prototype (subscript p) becomes

$$\frac{n_m^2}{n_p^2} \frac{k_{\ell m}}{k_{\ell p}} = R^2 \frac{(1 + n_m/B_m)}{(1 + n_p/B_p)} \tag{58}$$

At this point a number of alternates appear.

If the thermal conductivity of the layer material is preserved and the layer packing density is preserved, then Equation (58) reduces to

$$\frac{n_m}{n_p} = R \tag{59}$$

The number of layers could be reduced proportional to the scale ratio. However, the number of layers being an integer places a severe limitation on allowable scale ratios.

Reducing the number of layers also increases the normal heat transfer through the blanket. This is allowed by the equations which assume a continuous media rather than the discretized layers actually present.

If the model blanket is constructed of the same number of layers ($n_m = n_p$) and the same packing density is maintained Equation (58) reduces to the requirement.

$$\frac{k_{\ell m}}{k_{\ell p}} = R^2 \tag{60}$$

Thus, it is shown that a multilayer insulation blanket may be modeled by an identical blanket if the conductivity along the layers can be reduced by the square of the modeling ratio.

A technique for selectively reducing the lateral conductivity of the individual material layers in the direction of the thermal flux has been suggested by Katzoff (Reference 5). This technique consists of slitting the layers in a direction normal to the local heat flux. For many situations the direction of the local heat flux will vary with the spacecraft orientation. However, in regions of seams and penetrations through the blanket, the local fluxes will be directed toward the edges of the blanket. In these regions selective slitting of the layers will aid the scale modeling of multilayer insulation blankets.

The increase in thermal resistance obtained by various slitting ratios is shown in Figure 10. The results shown are taken from a recent study (Reference 62). A further difficulty arises when effective conductivity along the layers is considered.

Several recent studies (References 56, 59 and 63) have shown that a significant amount of energy is transported along the layers by radiation. The radiation transport is even dominant in many cases without the presence of extreme temperature gradients. This means that slitting must reduce conduction heat transfer enough to scale both conduction and radiation along the layers.

This introduces a potential limitation when the removal of all conduction is not sufficient to allow adequate scaling of the radiation component alone. An understanding of performance however, would be required to determine the slitting requirements.

If the layers are considered as discrete sheets of material the energy conducted along the layers may be approximated by

$$q = -k_{\ell} A \frac{\Delta T_o}{\Delta L} \tag{61}$$

from the requirements for temperature preservation

$$\frac{q_m}{q_p} = \frac{k_{\ell_m}}{k_{\ell_p}} \frac{A_m}{A_p} \frac{\Delta T_{o_m}}{\Delta T_{op}} \frac{\Delta L_p}{\Delta L_m} = K^2 \tag{62}$$

but

$$A = ntL$$

Thus Equation (62) reduces to

$$\frac{k_{\ell_m}}{K_{\ell_p}} \frac{n_m}{n_p} \frac{t_m}{t_p} = R^2 \tag{63}$$

If the layer thickness is preserved then

$$\frac{k_{\ell_m}}{k_{\ell_p}} \frac{n_m}{n_p} = R^2 \tag{64}$$

Thus, in regions where energy transport down the layers is dominant, some combination of slitting and reduction in number of layers may be used to satisfy the scaling criteria.

One additional alternate appears feasible at this time. If the spacecraft is fabricated such that energy loss through the insulation is negligible compared to losses through penetrations, louver panels, radiator plates, etc. then scaling the insulation system could be deleted in favor of scaling the regions of dominant energy loss.

In summary, the following circumstances appear to offer some opportunity for satisfactory scale modeling of multilayer insulation:

1) If energy transport through the insulation system is negligible compared to energy losses from other portions of the vehicle, scale modeling of the insulation system may be neglected.

2) If the energy transport through the insulation is normal to the layers, no scaling is required. The prototype system can be used on the model.

3) If the energy transport along the layers is dominant, a combination of layer reduction and layer slitting may be used to satisfy scaling requirements.

4) If energy transport both through and along the layers is important, slitting the blankets may be utilized to satisfy scaling requirements. This technique is limited as the radiative transport along the layers can not be effectively scaled in this manner.

In conclusion it would appear that a great deal more effort will have to be expended on multilayer insulation technology before criteria are developed to guide scale modeling efforts over the entire spectrum of potential situations.

4.4 Instrumentation Effects

The mere presence of thermocouple instrumentation introduces a disturbing factor to the thermal balance of the structure. While this disturbance is localized it takes place at the point at which the temperature measurement is attempted. As a result, thermocouples tend to utilize the smallest wire gages available in an effort to minimize the disturbance of the thermal balance due to the presence of an additional conduction path. The fine wire gage also minimizes the thermal capacity of the thermocouple bead itself. This reduces time lags in the instrumentation by allowing the thermocouple bead to respond to transients with the same rapidity as the structure being instrumented.

Thus the testing of an appropriately instrumented prototype would involve the use of an already minimal wire gage for the thermocouples. As smaller scale models are tested it will not always be possible to appropriately scale the instrumentation. One might even reach the point where the presence of instrumentation introduces appreciable errors due to conduction along the thermocouple beads. This section will examine temperature errors which would occur for a range of cases as a result of the presence of instrumentation.

Consider the small disk of diameter D_o and thickness t shown in the following sketch:

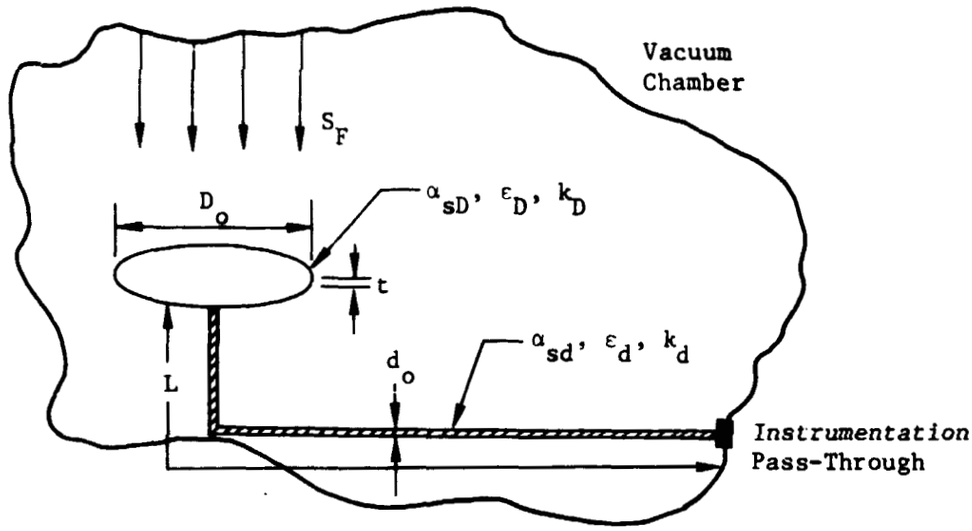

The disk is placed in a vacuum chamber [$\varepsilon_w = 0.90$, $T_w = 139^oR$ (77^oK) and illuminated by a solar simulator of intensity S_F. A thermocouple is connected to the center of the disk. The thermocouple wire is of diameter d_o, length L, and connected to an instrumentation passthrough in the chamber wall.

Performing a gross energy balance the following terms are obtained:

1) energy absorbed by disk

$$E_{(a)} = 1/4\ \alpha_{sD}\ S_F\ \pi D_o^2 \tag{65}$$

2) energy radiated from the disk

$$E_{(b)} = 2\sigma\varepsilon_D \left[\frac{\pi\ D_o^2}{4} + \pi\ D_o t \right] T^4 \tag{66}$$

3) energy absorbed by the wire

$$E_{(c)} = \alpha_{sd} S_F \pi d_o L \tag{67}$$

4) energy emitted by the wire

$$E_{(d)} = \sigma \varepsilon_d [\pi d_o L] T^4 \tag{68}$$

the gross energy balance for the system results in the equation

$$\frac{\alpha_{sD} S_F}{4\varepsilon_D} + \frac{\alpha_{sd} S_F d_o L}{\varepsilon_D D_o^2} = [1/2 + 2 \frac{t}{D_o} + \frac{\varepsilon_d}{\varepsilon_D} \frac{d_o L}{D_o^2}] \sigma T^4 \tag{69}$$

The conduction boundary condition at the interface between disk and thermocouple can be expressed as

$$-k_D A \frac{\partial T}{\partial x} \Big|_{disk} = k_d A \frac{\partial T}{\partial x} \Big|_{thermocouple} \tag{70}$$

or in non-dimensional form

$$\frac{k_D}{k_d} \frac{\partial T'}{\partial x'} \Big|_{disk} = \frac{\partial T'}{\partial x'} \Big|_{thermocouple} \tag{71}$$

Consideration of Equations 69 and 71 indicates the following dimensionless groups which govern the solution to the problem:

1) radiative properties

$$\frac{\varepsilon_d}{\varepsilon_D} ; \quad \frac{\alpha_{sD}}{\varepsilon_D} ; \quad \frac{\alpha_{sd}}{\varepsilon_d} \tag{72}$$

2) conductive interface

$$\frac{k_d}{K_D} \tag{73}$$

3) geometric properties

$$\frac{d_o}{D_o} \; ; \quad \frac{t}{D_o} \; ; \quad \frac{L}{d_o} \tag{74}$$

This problem, shown in the preceding sketch, was solved for a number of perturbations of the indicated dimensionless parameters. After a number of studies it was found that:

1) If the thermocouple wires leaving the disk were shadowed from the sun for a short distance (on the order of one foot) before being exposed to the sun, it makes no difference if the wires are totally or partially shadowed. Thus, the relationship $[\alpha_{sd}/\varepsilon_d]$ was shown to be unimportant over a reasonable range of values.

2) If the thermocouple wires were of length greater than approximately one foot, their overall length was found to be unimportant. Thus the relationship $[L/d_o]$ was also dropped from subsequent consideration.

3) The ratio of emissivities $[\varepsilon_d/\varepsilon_D]$ appeared to determine the length of thermocouple wire for the preceding effects to become negligible. Reasonable ranges of relative emissivities indicated lengths on the order of a foot or less before the preceding effects become negligible.

As the thermocouple leads from a test article in a space chamber are generally on the order of several feet these three ratios were dropped from consideration. Parametric studies were made based on the remaining four ratios. The results of these studies are presented in Figures 11 through 14.

The results of a study of relative geometric effects are shown in Figures 11 and 12. The two limiting temperatures shown in Figure 12 at large values of wire diameter are a result of the assumed passthrough

temperature. Two passthrough temperatures were utilized in the calculations. These were equal to the liquid nitrogen wall temperature [139°R (77°K)] and the external room temperature [530°R (294°K)].

The results of a study of relative conductivity are shown in Figure 13. The results of a study of the radiative properties of the target disk are shown in Figure 14.

These studies indicate that for reasonable ranges of the parameters only the effects of relative geometry are of importance. From Figure 12 it appears that negligible error will be incurred if the thermocouple wire diameter is two to three orders of magnitude small than the characteristic nodal dimension. Ranges of characteristic nodal dimension to nodal thickness appear of secondary importance.

In retrospect however, a small value of the geometric ratio (d_o/D_o) for the indicated problem really indicates that conduction losses from the thermocouple should be small relative to the input energy. As the energy input was over the face of the disk, the disk thickness was of small import. If the power input to the node had been by conduction from the adjoining structure, the disk thickness would have been significant. Our conclusions are thus limited to nodes with solar input and, for typical thermocouple gages [0.006 in. (0.0152 cm) dia.], no severe limitation is placed on thermal scale modeling.

4.5 Thermal Gradient Effects

The presence of large thermal gradients in the spacecraft structure can introduce errors when thermocouple locations are not known precisely. In a spacecraft, regions of large thermal gradients would be associated with high energy sources such as radioisotope power supplies or traveling wave tubes. Utilizing temperature preservation techniques results in gradient increases proportional to the scale model ratio. Temperature errors resulting from imprecise thermocouple placement are accentuated in the scale model.

Errors in thermocouple location can be due both to placement of the thermocouple and inability to locate the thermocouple junction with the bead itself. Consider the thermocouple shown in the following sketch:

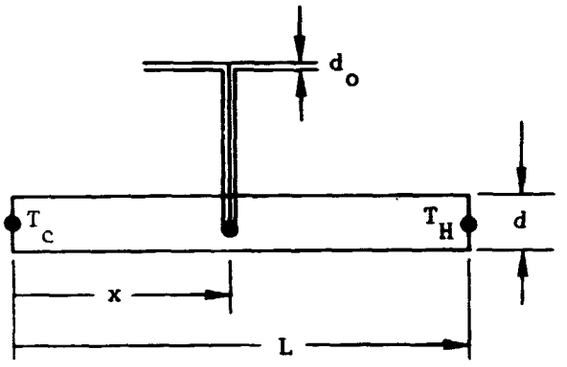

The thermocouple wires of diameter d_o are placed in a structural element of thickness d. A thermal gradient $[(T_H - T_c)/L]$ is maintained over the distance L. The thermocouple junction is located at $x \pm d_o$. It is assumed that the location can be determined within the half width of the thermocouple bead. Here the thermocouple bead is assumed to have a characteristic dimension equal to twice the wire diameter.

The temperature at the nominal thermocouple location may be expressed as

$$T_x = T_c + \frac{x}{L}(T_H - T_c) \tag{75}$$

while the temperature measured by the thermocouple may range over the following set of values

$$T_{x \pm d_o} = T_x \pm \frac{\partial T}{\partial x}\,\delta x \tag{76}$$

differentiating Equation (75) and combining equations

$$\frac{T_{x \pm d_o}}{T_x} = 1 \pm \frac{\delta x}{T_x}\,\frac{\partial T}{\partial x} \tag{77}$$

when T_x is the median temperature along the section

$$\frac{T_x \pm d_o}{T_x} = 1 \pm \frac{2\, d_o}{(T_H + T_c)} \left(\frac{\partial T}{\partial x}\right) \qquad (78)$$

This equation is shown in Figure 15 for a range of thermocouple sizes (for the larger wire sizes shown, this dimension is more characteristic of a placement error than a thermocouple wire size) and in Figure 16 for a range of mean temperature levels.

For a typical thermocouple wire size [approximately 0.001 ft. (0.03048 cm)] and temperature range, a ten thousand degree Fahrenheit per foot (182°K/cm) gradient is required to produce a 2 percent error in measured temperature.

It appears that extreme gradients are required to produce appreciable errors in temperature. Or conversely, the scale models will be extremely small before the normal range of gradients is magnified to the extreme required to produce appreciable error. As always however, it is best to select isothermal regions as thermocouple locations in order to reduce the effects of gradient induced errors.

4.6 Test Environment

The use of a vacuum chamber to simulate the space environment introduces several sources of error due to our inability to correctly simulate the space environment. These errors are a result of mismatches in the following items:

1) the solar beam
   a) intensity
   b) uniformity
   c) collimation
   d) spectral match

2) the chamber
   a) grey walls
   b) background temperature
   c) vacuum pressure.

Let us briefly examine the possible errors in temperature as a result of some of these items. Consider the simplified model shown in the following sketch:

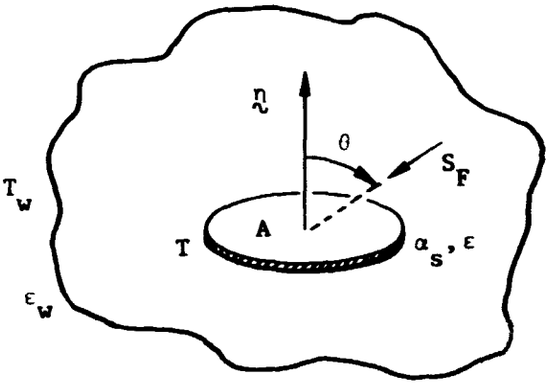

A small disk of area A and solar absorptivity α_s is exposed to a solar beam of intensity S_F at an off-solar angle θ. The disk is surrounded by an environment with an emissivity ε_w and a temperature T_w.

An energy balance on the disk with solar irradiation and emission to the surroundings provides a solution for the equilibrium temperature of the disk

$$T = \left[\left(\frac{\alpha_s}{\varepsilon}\right) \frac{S_F \cos\theta}{2\sigma} + \frac{\varepsilon_w}{\varepsilon} T_w^4\right]^{1/4} \tag{79}$$

Figure 17 examines the effects of the cold wall temperature and emissivity for a disk having the properties of a white thermal control coating and irradiated by a normal beam of one sun solar intensity. Most space simulation chambers are painted black and have

liquid nitrogen shrouds. This would result in a shroud properties on the order of a 140°R (77°K) temperature and a 0.90 emissivity. This causes temperature errors on the order of one half of one percent.

Other studies have shown that gas convection effects are negligible in the chamber after the pressure drops below the 10^{-4} to 10^{-5} torr range. Most existing chambers operate in the 10^{-8} to 10^{-11} torr range and introduce negligible errors due to gas conduction in the chamber or interior to the spacecraft.

Figure 18 examines the effect of solar intensity variations on the temperature of the disk. The local intensity in the chamber could vary as much as $\pm$ 5 percent, but in the central area of the beam a $\pm$ 2-1/2 percent variation is more characteristic of Boeing operating experience. This causes temperature errors in the + 1.0 to -0.2 percent range.

Figure 19 examines the effect of solar beam collimation angle on the temperature of the disk. Typical off collimation half angles are on the order of one to two degrees (0.0174 - 0.0348 radians) which is a negligible error. However, poor collimation would have a larger effect on nodes which should be shadowed and are not.

The spectral distribution of energy emitted by the solar simulator is not a good match with the Johnson solar curve. However, if both model and prototype use the same coatings, then the radiative properties will be preserved under the same source. This will result in slight differences between space simulator and actual space performance of the same vehicle.

In actuality, these effects are characteristic of chamber testing (References 65-69) and do not particularly relate to limitations in model size. Some effects vaguely relate to model size (usually resulting in an improvement in test results when compared with full size testing) and these are:

1) The smaller models will tend to utilize only the central portions of the solar beam which has greater uniformity than the overall beam.

2) Local penetrations in the chamber walls (instrumentation pass-throughs and viewing ports) will be more removed from the proximity of the smaller vehicles, thus reducing the chances of localized effects as a result of the penetrations.

The space simulation facility appears to provide no lower limitations on size utilizing temperature preservation techniques for scale modeling.

On the other hand the material preservation technique requires that solar irradiation be scaled by

$$\frac{S_m}{S_p} = \left(\frac{L_p}{L_m}\right)^{4/3} \tag{80}$$

As the scale ratio decreases the absorbed energy must increase out of proportion to the scale ratio as noted in the following tabulation:

L_m/L_p	S_m/S_p
0.5	2.5
0.25	6.4
0.20	8.6
0.10	21.4

Two alternates or some combination of these are available. The intensity of the solar beam can be increased and/or the solar absorptivity of the surface can be increased. For example, a surface with a white thermal control coating (α_s = 0.16; ε = 0.9) could be modeled by a black coating (α_s = 0.9; ε = 0.9) to provide an increase in absorbed solar energy by a factor of 5.6. A further model increase in solar intensity by a factor of 1.5 would allow testing of a 1/5 scale model.

However, a limitation exists here as most existing solar simulators are not capable of operation much above two solar constants. It would appear that a tenth scale model would be near the limit of the lower scaling ratio which could be tested in most existing chambers.

TABLE 7. SELECTION OF MATERIALS FOR TRANSIENT SCALING

Material	k Btu/Hr Ft ^{o}R	(ρc_p) Btu/Ft^3 ^{o}R	$\frac{k_m}{k_p}$	$\frac{(\rho c_p)_m}{(\rho c_p)_p}$	$\frac{(\rho c_p)_m}{(\rho c_p)_p}\frac{k_p}{k_m}$
6061-T6	96.6	38.6			
7075-T6	75.1	40.0			
2024-0	115.5	38.2	1.196	0.990	0.828
			1.540	0.955	0.620
7075-0	98.8	40.0	1.022	1.038	1.014
			1.318	1.0	0.760
6061-T6	96.6	38.6	1.0	1.0	1.0
			1.289	0.965	0.741
6061-T4	89.6	38.6	0.928	1.0	1.078
			1.195	0.965	0.799
5052-0	79.8	36.8	0.826	0.954	1.157
			1.062	0.920	0.865
7075-T6	75.1	40.0	0.778	1.038	1.332
			1.0	1.0	1.0
AZ-31B	43.9	26.4	0.454	0.685	1.507
			0.598	0.660	1.122
SAE 1020	37.2	55.9	0.385	1.448	3.76
			0.496	1.398	2.82
AISI 4130	22.3	54.3	0.231	1.410	6.10
			0.297	1.358	4.57
Type 304	9.77	59.8	0.101	1.550	15.36
			0.130	1.495	11.50
Type 301	7.82	55.1	0.081	1.429	17.62
			0.104	1.379	13.25

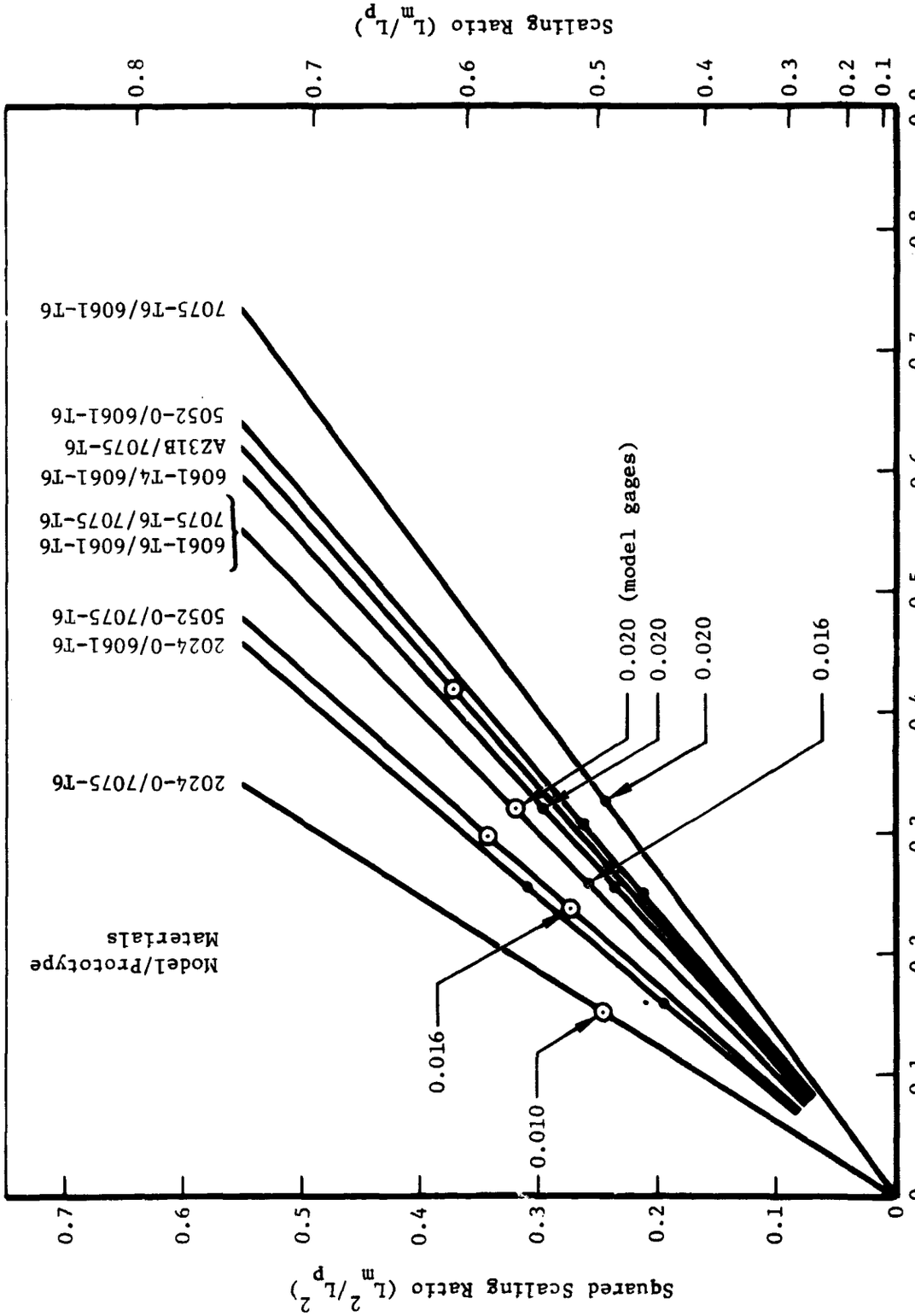

Figure 4: COMPROMISE SELECTION OF MODELING MATERIALS BASED ON AVAILABLE MATERIALS AND GAGES

TABLE 8. CANDIDATE MATERIALS FOR THERMAL SCALE MODELING
(Prototype skin made from 0.0625 inch 6061-T6 Plate - k = 96.6 Btu/Hr Ft ^{o}F)

Material	Thermal Conductivity Btu/Hr Ft ^{o}F	Nominal Half Scale Model			Nominal Quarter Scale Model		
		Required Thickness	Available Thickness	Available Scale Ratio	Required Thickness	Available Thickness	Available Scale Ratio
2024-0	115.5	0.0131	0.010 0.016	0.437 0.553	0.00327		
3003-0	101.1	0.0149	0.017	0.543	0.00374		
7075-0	98.8	0.0153	0.020	0.572	0.00383		
6061-T6	96.6	0.01563	0.016	0.506	0.00392		
6061-T4	89.6	0.0168	0.016 0.020	0.487 0.544	0.00422		
5052-0	79.8	0.0189	0.016 0.020	0.460 0.511	0.00474		
7075-T6	75.1	0.0201	0.020	0.499	0.00503		
2024-T3	69.9	0.0216	0.020 0.025	0.481 0.538	0.00541		
AZ 31B	43.9	0.0344	0.040	0.539	0.00862		
SAE 1020	37.2	0.0406	0.040 0.042	0.496 0.509	0.0102	0.018	0.333
AISI 4130	22.3	0.0678	0.063 0.071	0.482 0.512	0.0170	0.020	0.272
Type 304	9.77	0.155	0.125 0.171	0.450 0.526	0.0387	0.032 0.050	0.228 0.284
Type 301	7.82	0.193	0.125 0.190	0.402 0.496	0.0484	0.040 0.050	0.228 0.255

TABLE 9. CANDIDATE MATERIALS FOR THERMAL SCALE MODELING
(Prototype skin made from 0.0625 inch 7075-T6 Plate - k = 75.1 Btu/Hr Ft ^{o}R)

Material	Thermal Conductivity Btu/Hr Ft ^{o}F	Nominal Half Scale Model			Nominal Quarter Scale Model		
		Required Thickness	Available Thickness	Available Scale Ratio	Required Thickness	Available Thickness	Available Scale Ratio
2024-0	115.5	0.0102	0.010 0.016	0.496 0.628	0.00254		
3003-0	101.1	0.0116	0.017	0.606	0.00289		
7075-0	98.8	0.0119	0.020	0.649	0.00297		
6061-T6	96.6	0.0122	0.016	0.574	0.00304		
6061-T4	89.6	0.0131	0.010 0.016	0.437 0.553	0.00327		
5052-0	79.8	0.0147	0.016 0.020	0.522 0.584	0.00368		
7075-T6	75.1	0.0157	0.020	0.566	0.00392		
2024-T3	69.9	0.0168	0.020 0.025	0.546 0.610	0.00420		
AZ 31B	43.9	0.0268	0.040	0.612	0.0067		
SAE 1020	37.2	0.0316	0.040 0.042	0.563 0.578	0.0079	0.012	0.308
AISI 4130	22.3	0.052	0.050 0.063 0.071	0.487 0.547 0.581	0.0132	0.010 0.020	0.218 0.308
Type 304	9.77	0.120	0.100 0.125	0.456 0.510	0.030	0.02 0.032	0.204 0.258
Type 301	7.82	0.150	0.125 0.190	0.457 0.563	0.0375	0.02 0.032 0.04	0.1826 0.232 0.258

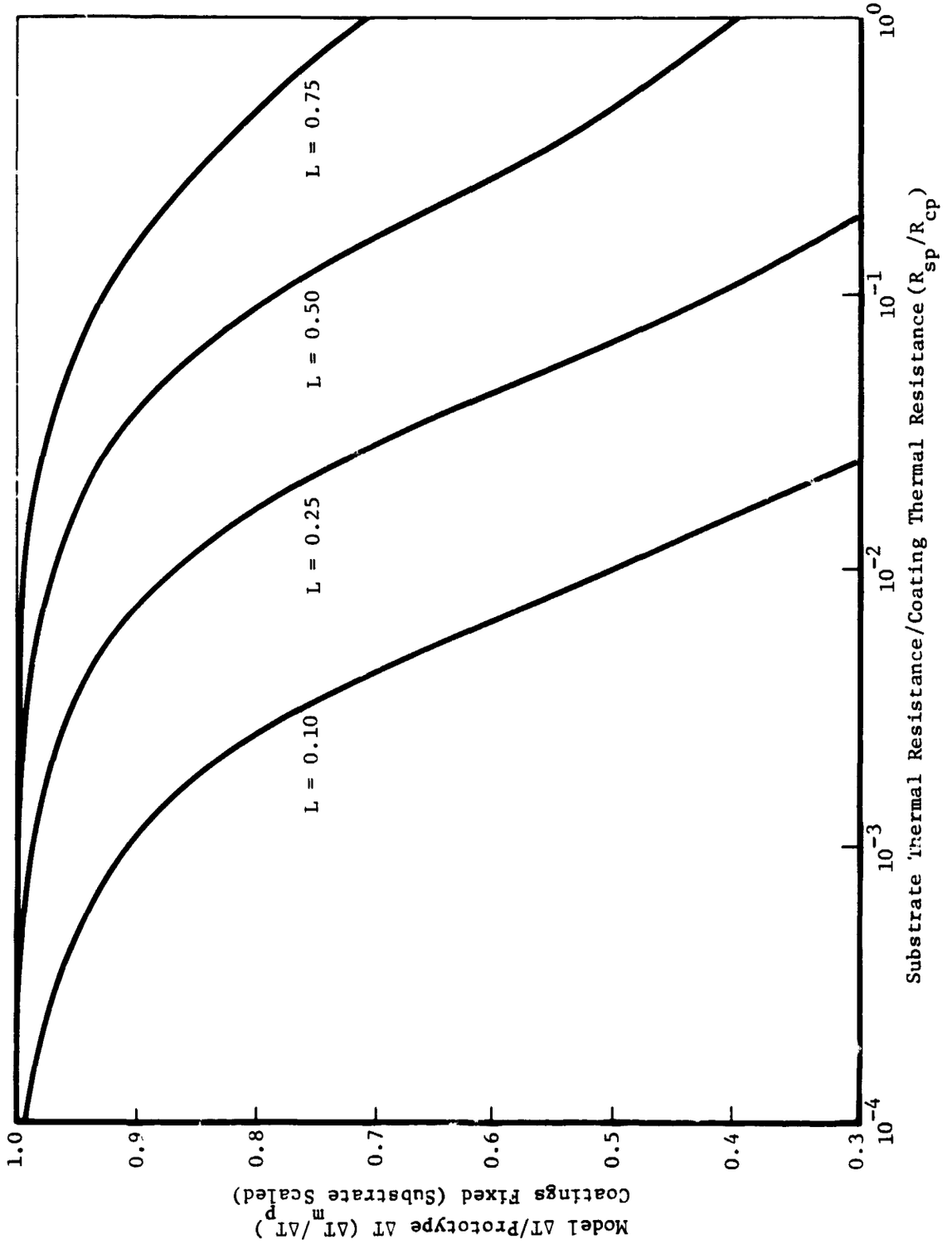

Figure 5: TEMPERATURE ERRORS RESULTING FROM FAILURE TO SCALE THERMAL CONTROL COATINGS

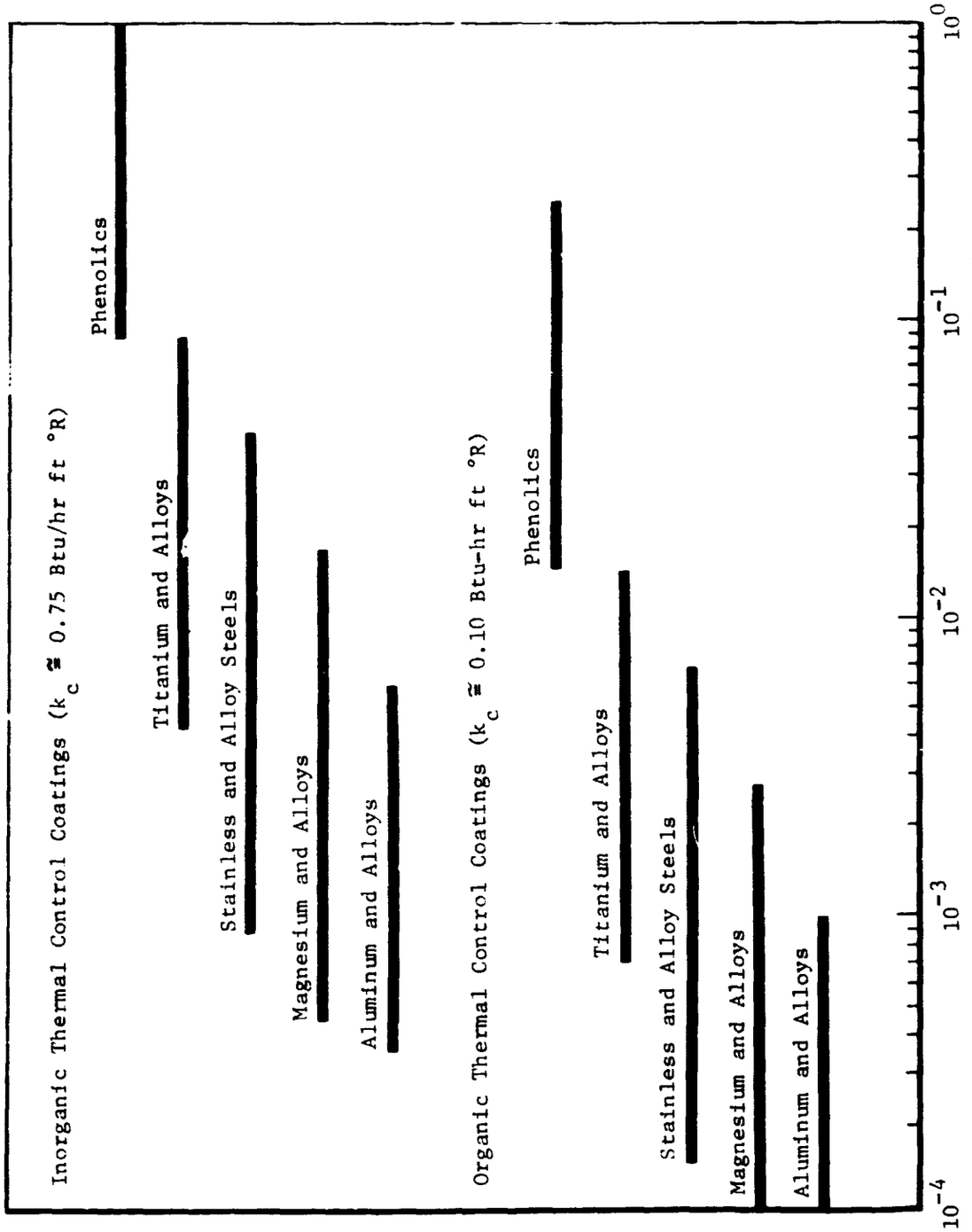

Figure 5a: RANGES OF THERMAL RESISTANCE RATIOS FOR VARIOUS MATERIALS AND THERMAL CONTROL COATINGS

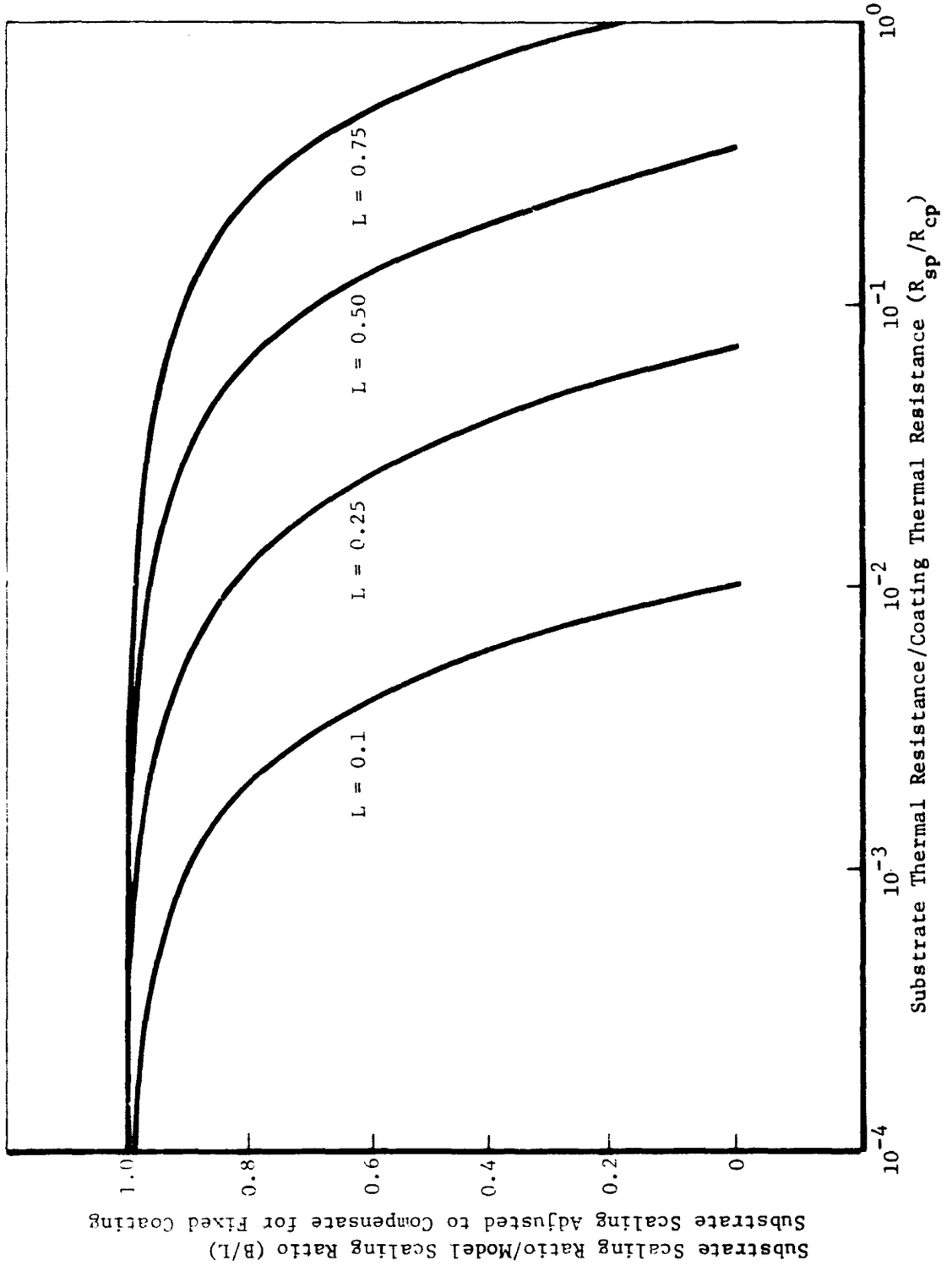

Figure 6: OVERSCALING REQUIREMENTS TO COMPENSATE FOR FAILURE TO SCALE THERMAL CONTROL COATINGS

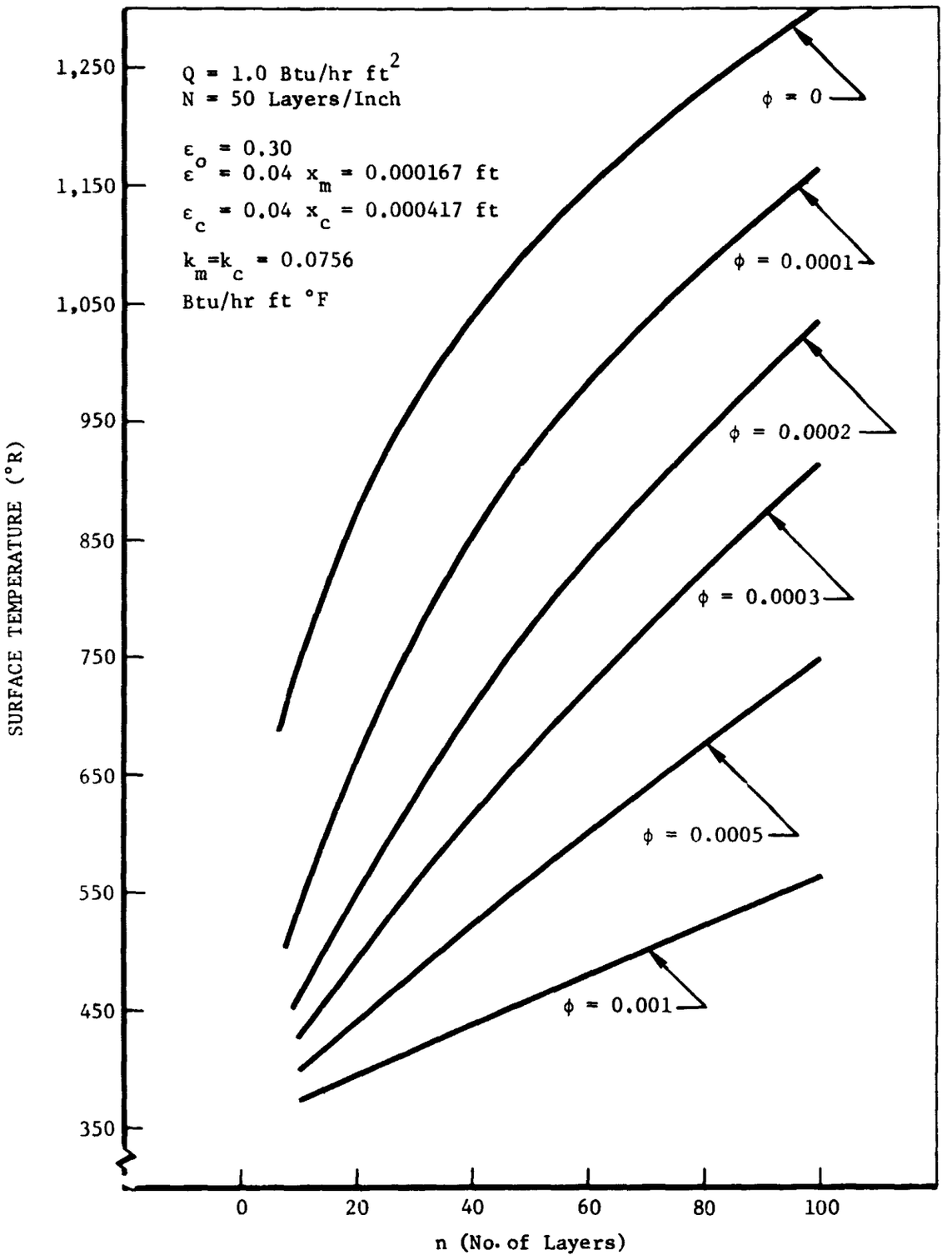

Figure 7: SENSITIVITY OF MULTILAYER INSULATION PERFORMANCE TO EFFECTIVE CONTACT AREA (Q = 1.0 Btu/hr ft^2)

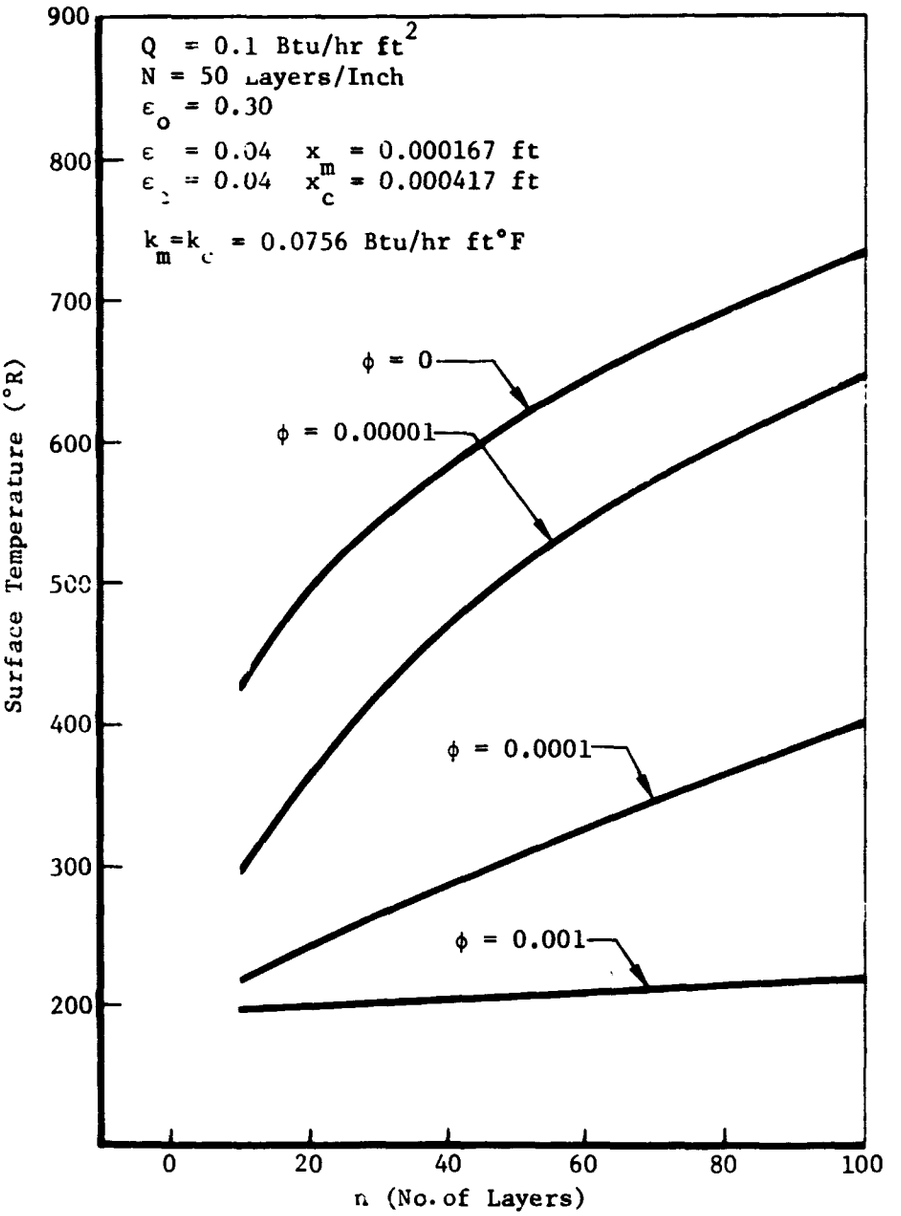

Figure 8: SENSITIVITY OF MULTILAYER INSULATION PERFORMANCE TO EFFECTIVE CONTACT AREA (Q = 0.1 Btu/hr ft^2)

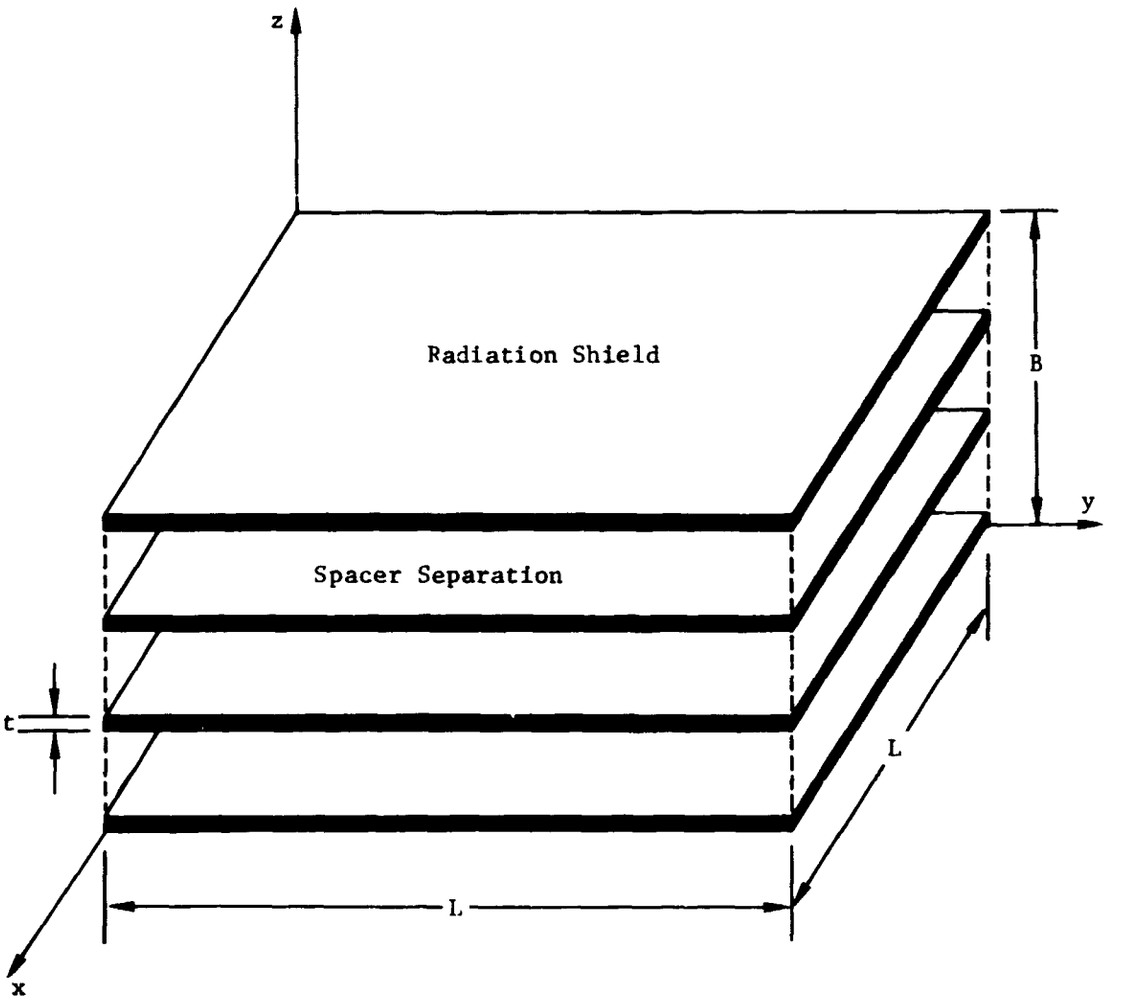

Figure 9: SCHEMATIC OF MULTILAYER INSULATION BLANKET

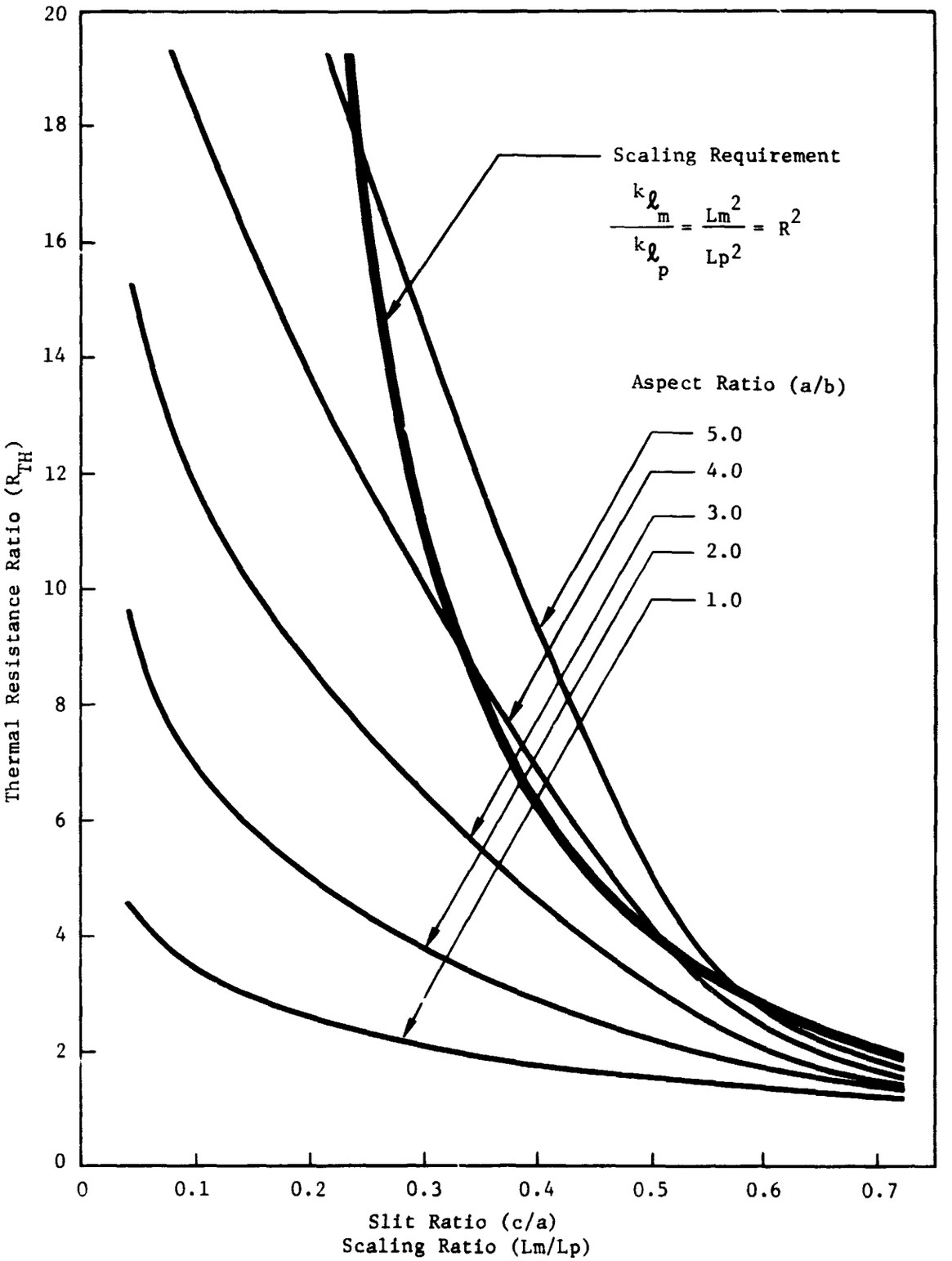

Figure 10: RELATIVE INCREASE IN THERMAL RESISTANCE DUE TO SLITTING

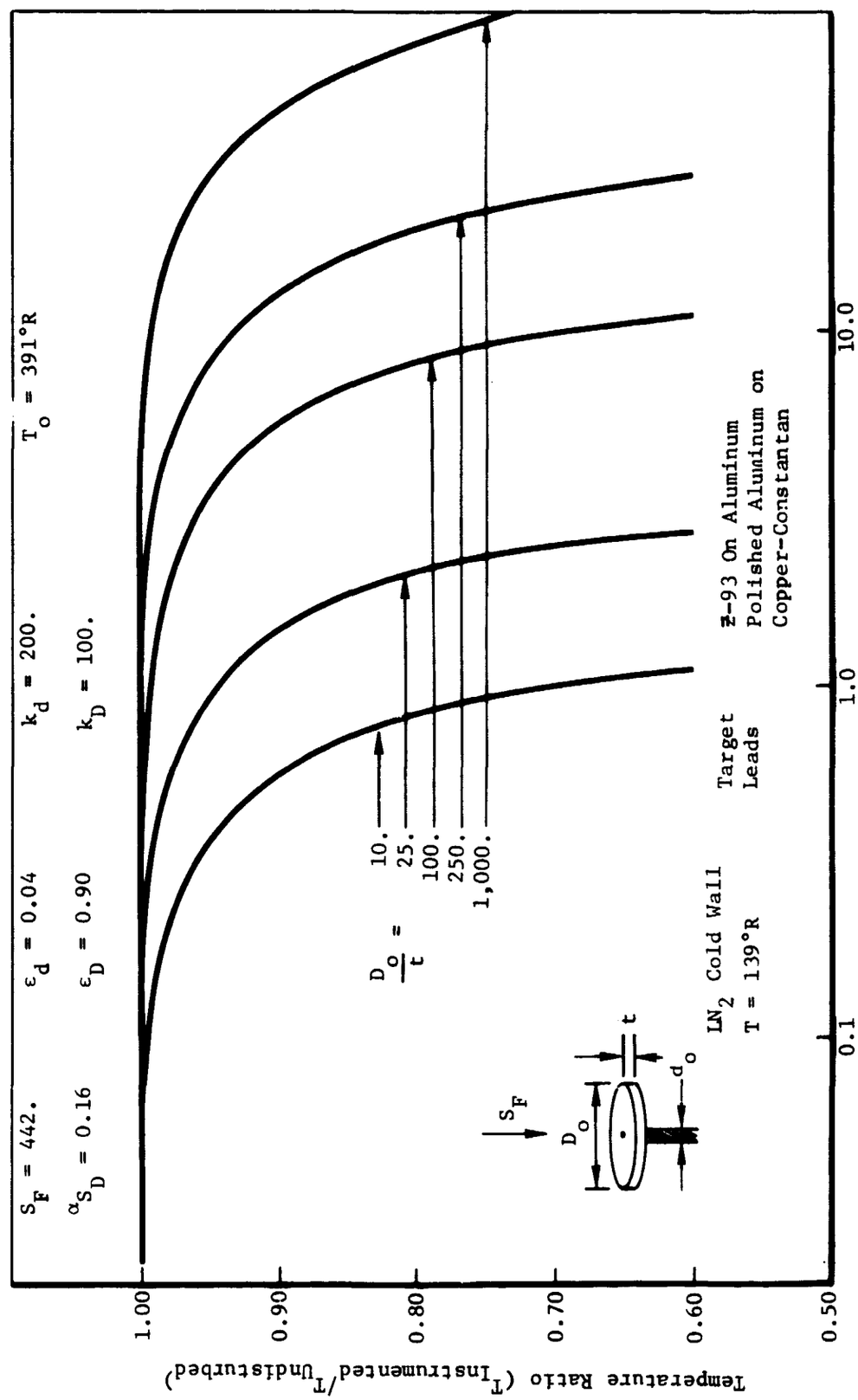

Figure 11: INSTRUMENTATION EFFECTS (EFFECT OF RELATIVE GEOMETRY)

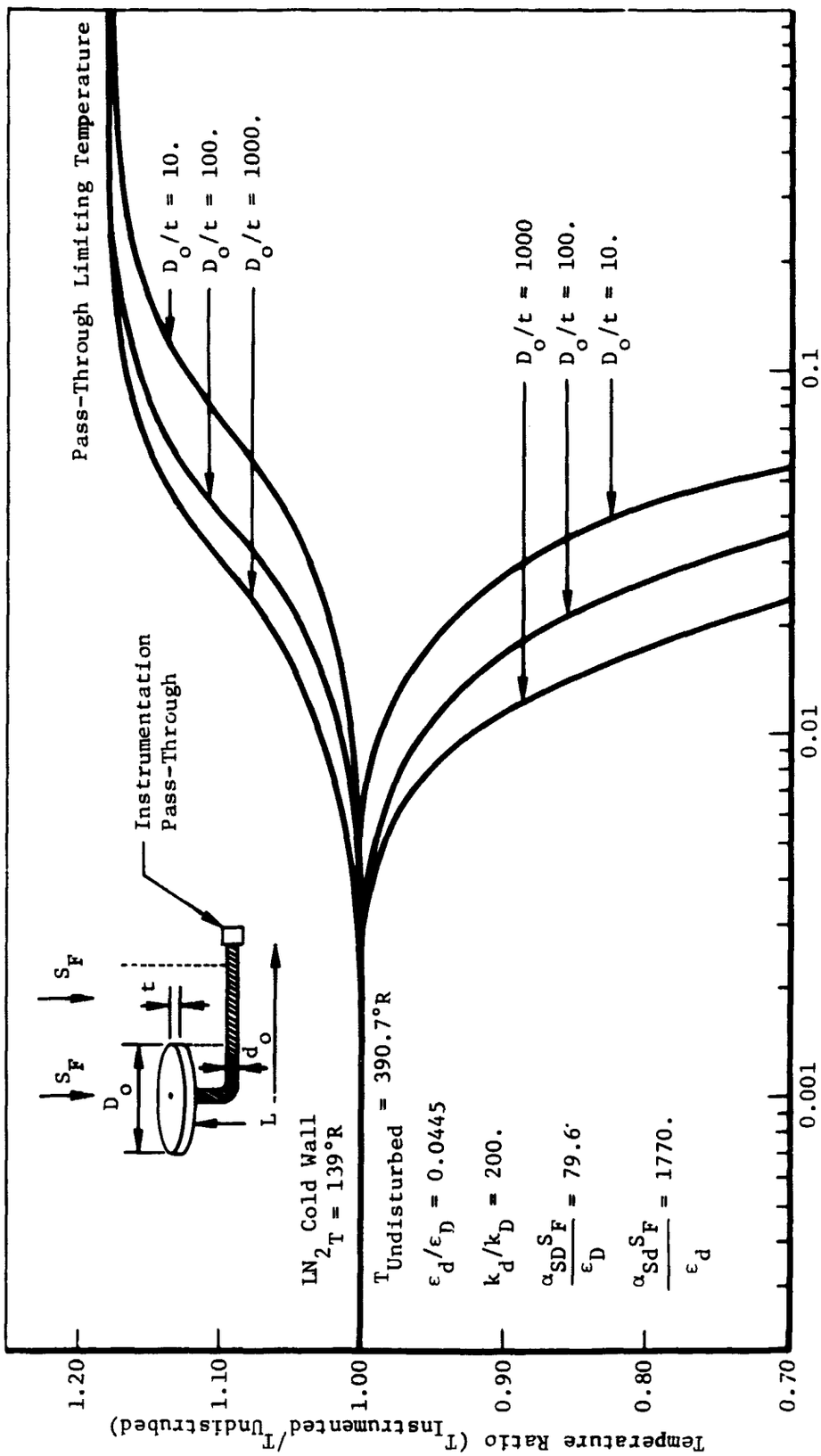

Figure 12: INSTRUMENTATION EFFECTS (EFFECT OF RELATIVE GEOMETRY)

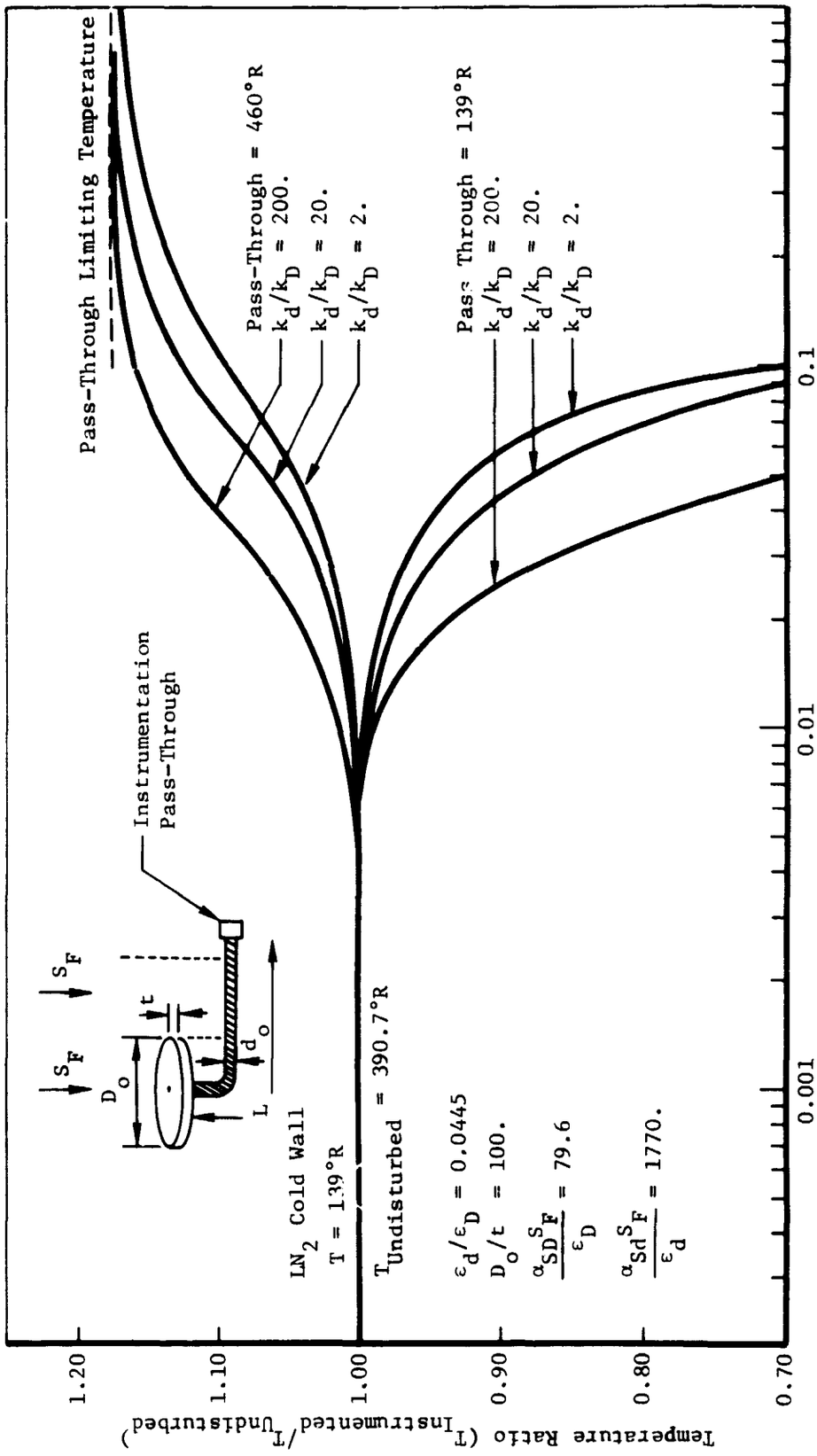

Figure 13: INSTRUMENTATION EFFECTS (EFFECT OF RELATIVE CONDUCTIVITY)

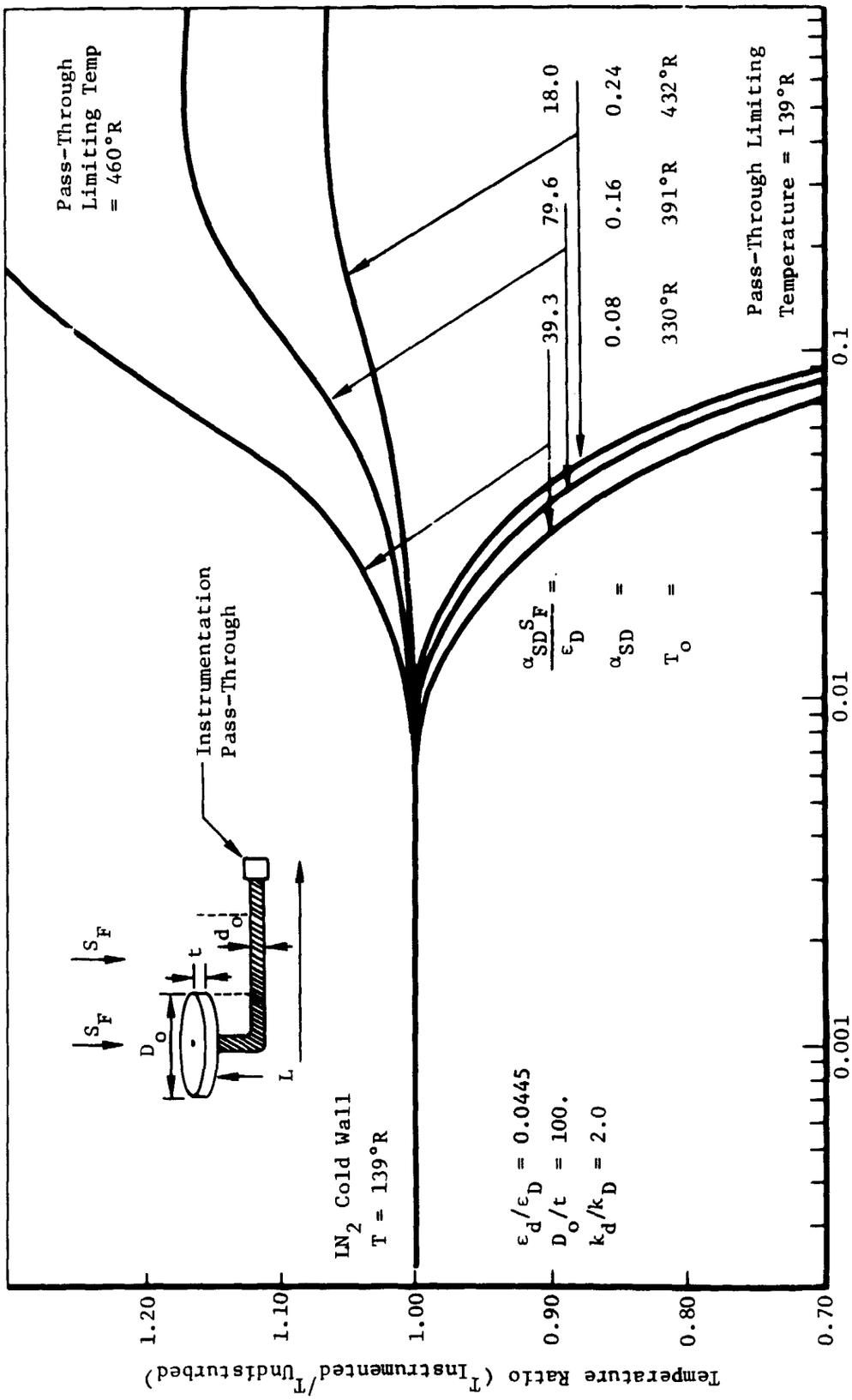

Figure 14: INSTRUMENTATION EFFECTS (EFFECT OF RADIATIVE PROPERTIES)

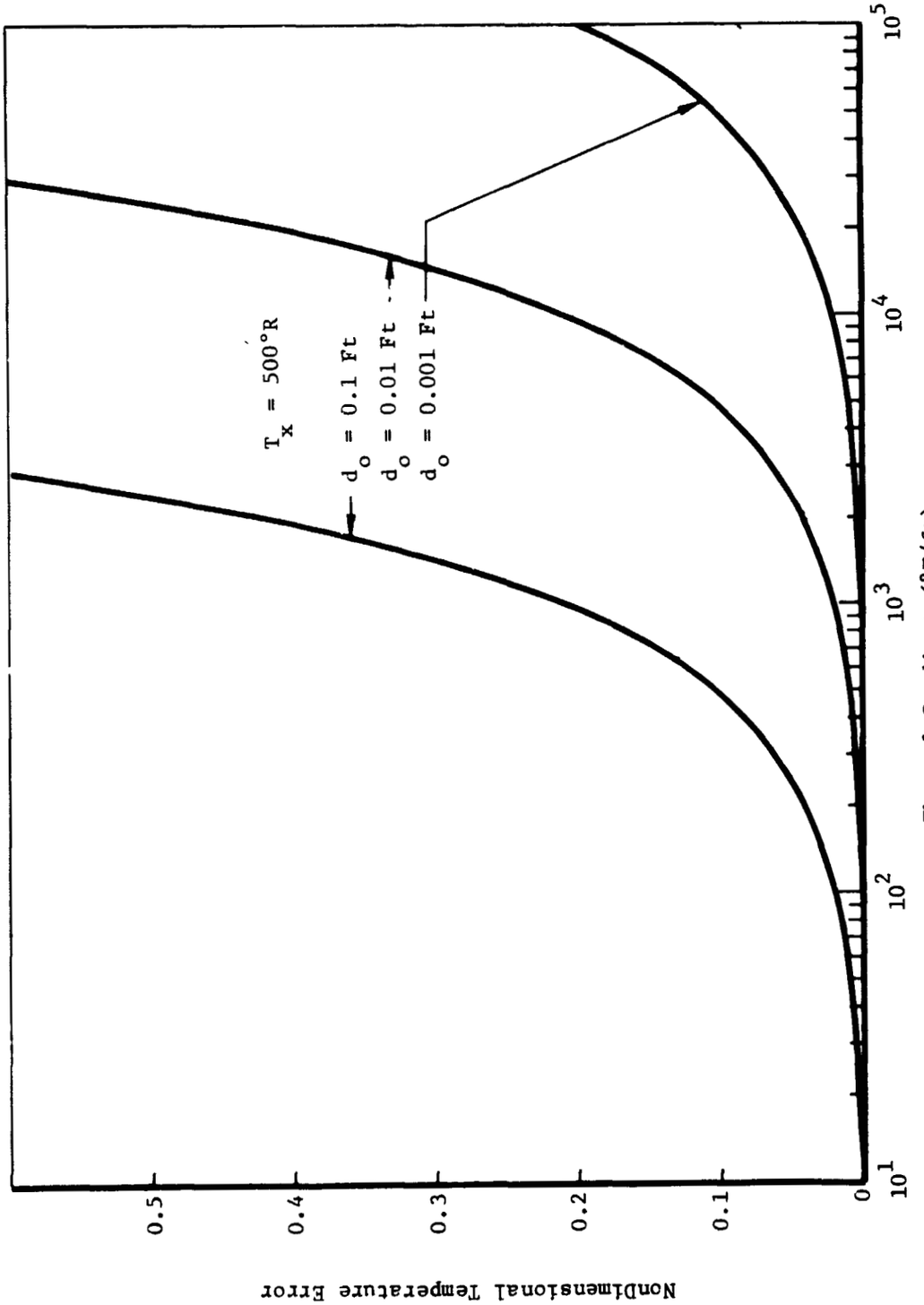

Figure 15: EFFECT OF LARGE THERMAL GRADIENTS (UNCERTAINTY IN LOCATION)

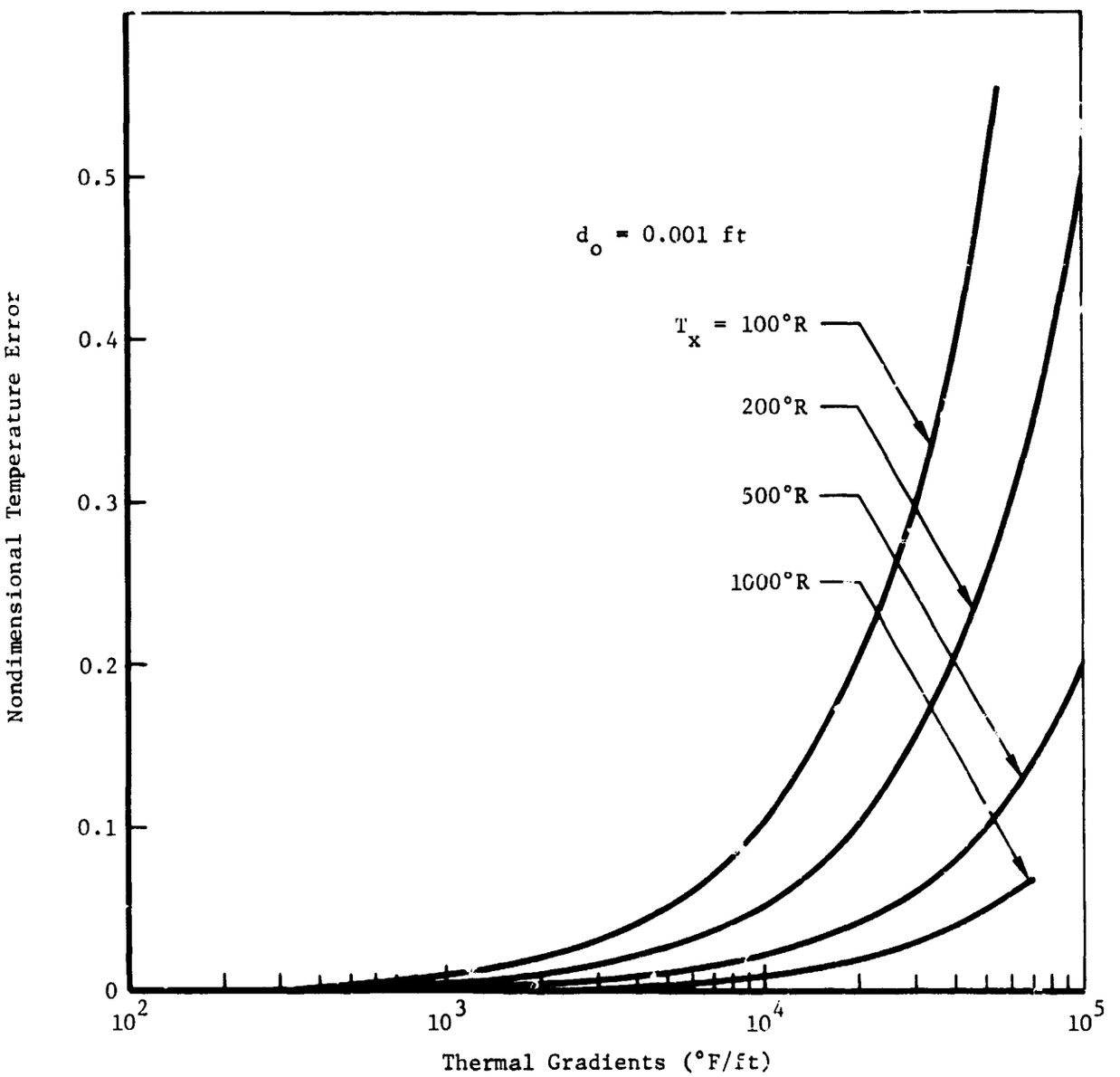

Figure 16: EFFECT OF LARGE THERMAL GRADIENTS (EFFECT OF MEAN TEMPERATURE)

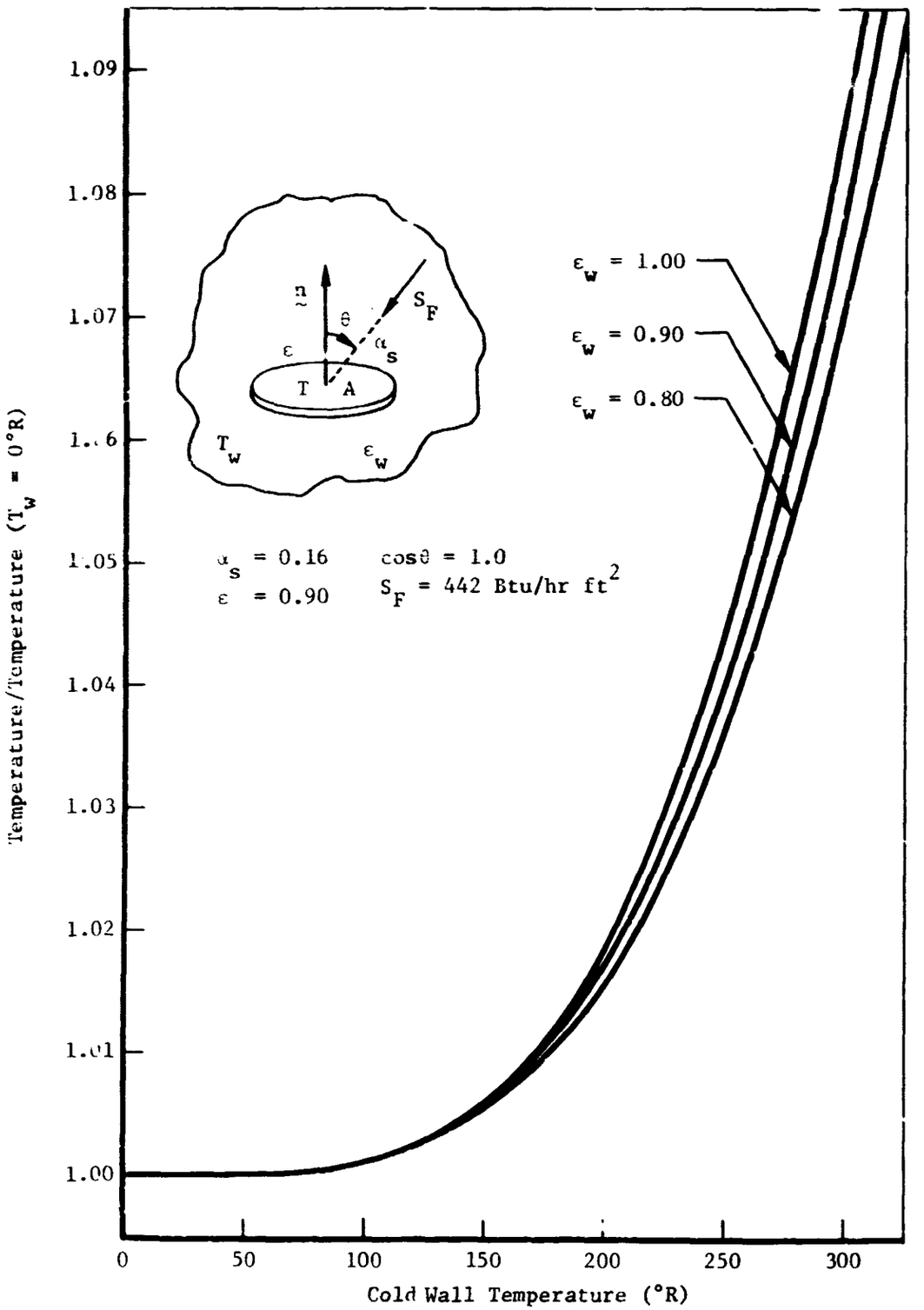

Figure 17: SPACE CHAMBER SHROUD EMISSIVITY AND TEMPERATURE EFFECT ON MODEL TEMPERATURES

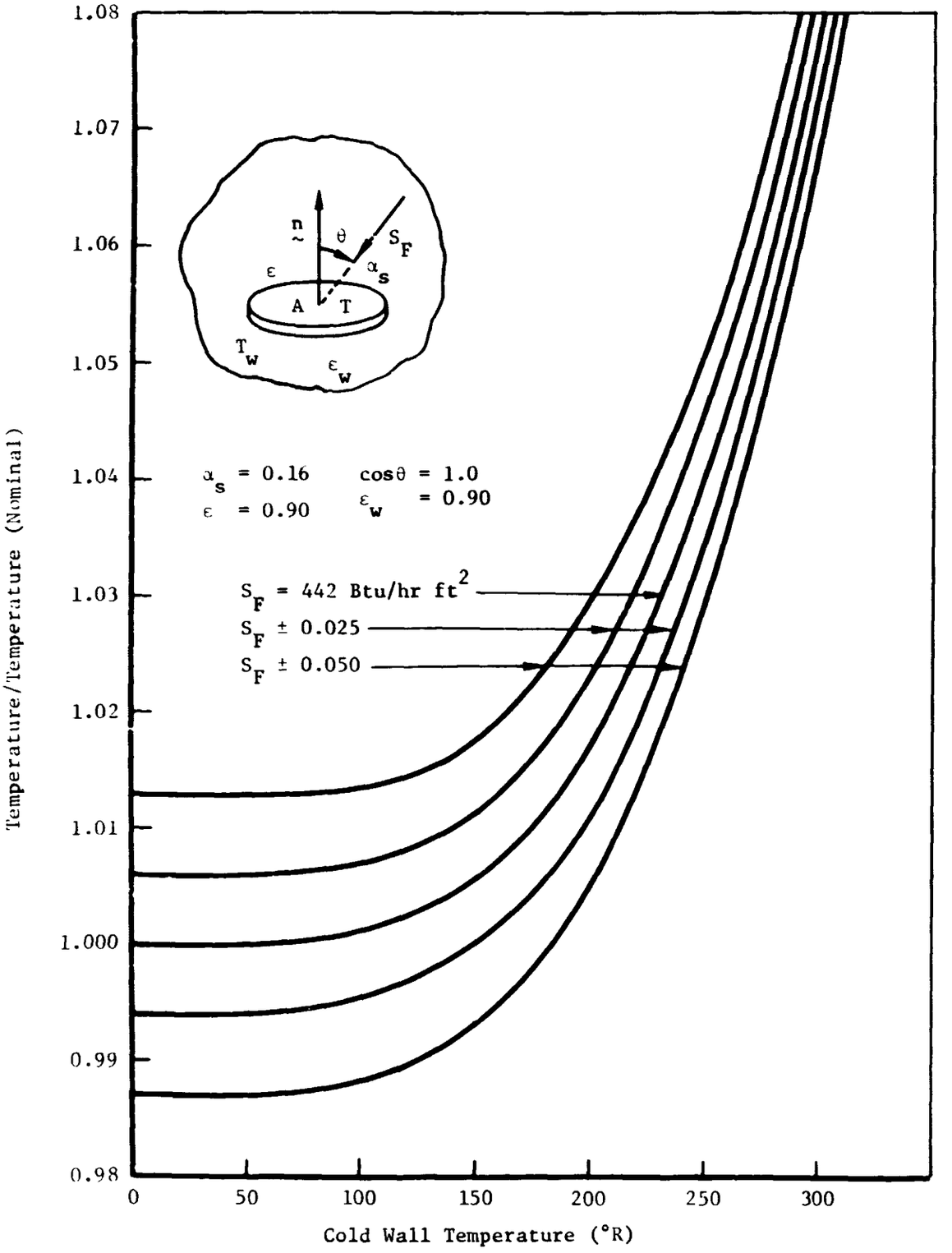

Figure 18: SOLAR SIMULATOR INTENSITY EFFECT ON MODEL TEMPERATURES

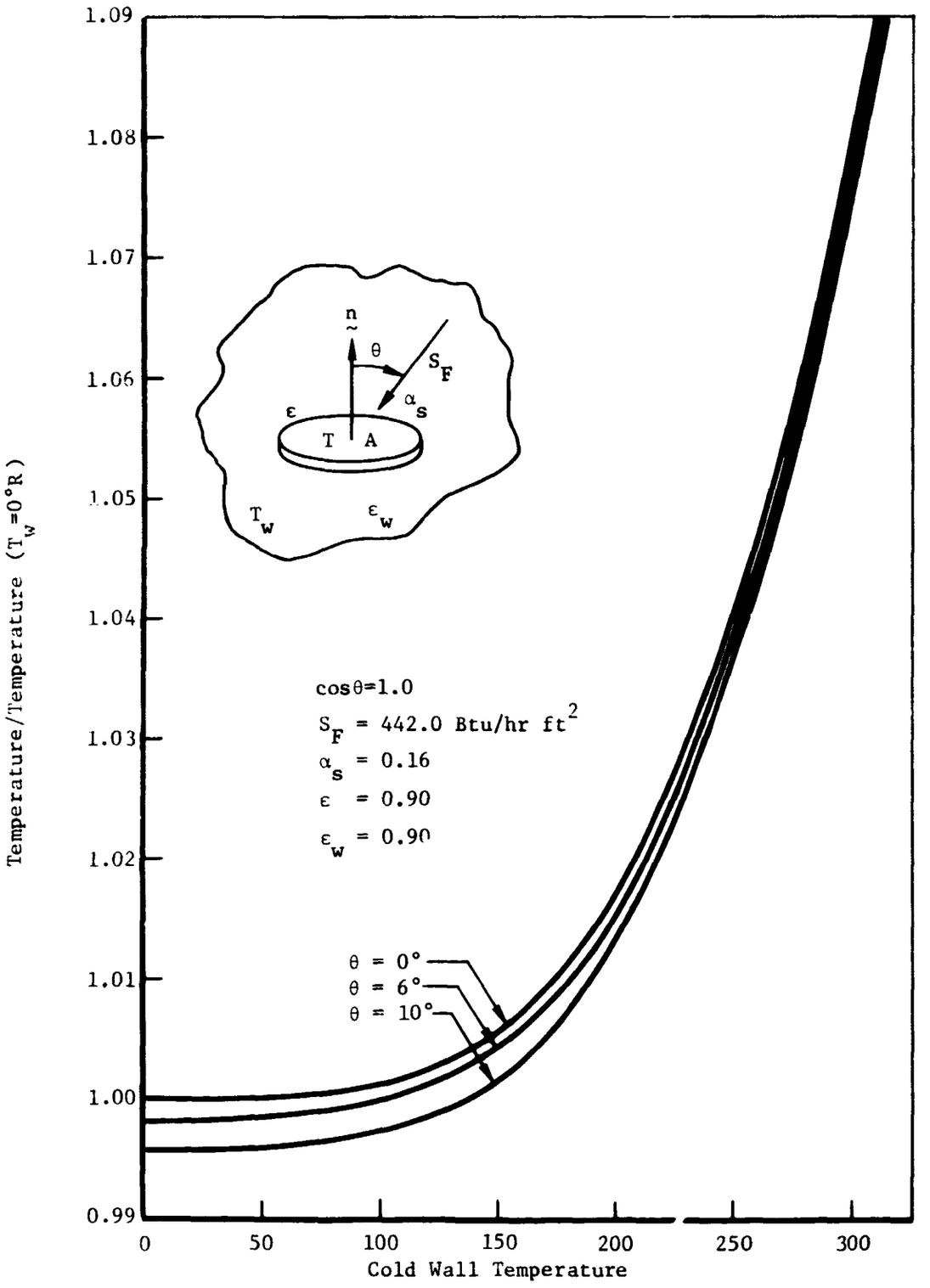

Figure 19: SOLAR SIMULATOR COLLIMATION EFFECT ON MODEL TEMPERATURES

5.0 EXPERIMENTAL STUDY

The purpose of the experimental work under this contract was to demonstrate that scale models could predict a prototype vehicle thermal performance within the error band resulting from the uncertainties described previously. This section will discuss details of the model design and instrumentation, the vacuum chamber and solar simulator operating characteristics, and the actual test conditions experienced by the models.

5.1 Model Design

The actual vehicle geometric configuration was arbitrarily selected with ease of manufacturing being a primary consideration. While the final design (Figure 20) did not resemble an actual spacecraft, it does incorporate the following characteristics typical of flight hardware:

1) lightweight exterior skin panels
2) a relatively heavy structural frame
3) an over extended base deck which results in solar reflections back onto exterior surfaces
4) energy sources interior to the spacecraft in discrete compartments to simulate electronics components.

Previous experience had indicated that the Boeing raw materials stores carried a large variety of 6061-T6 and 7075-T6 aluminum plate and structural shapes. It was thus decided to manufacture the prototype from 1/16 inch (0.1588 cm) 6061-T6 and 7075-T6 sheet stock with 6061-T6 being the dominant material.

The diameter of the simulated solar beam in the test chamber provided an upper limit on the prototype major dimensions of approximately 42 inches (106.8 cm).

The final configuration took the form of a 20 inch (50.8 cm) cube on a 30 inch (76.2 cm) square plate, with the basic fabrication materials being 1/16 inch (0.1588 cm) 6061-T6 and 7075-T6 sheet stock.

The Boeing raw materials catalog was searched to identify those materials which are carried in a wide range of gages and structural shapes. Those materials are identified in Tables 8 and 9 and their thermal conductivities at 535°R (297°K) are tabulated.

The two dimensional "geometric distortion" scaling criteria was used to calculate the gages required in each of these materials for nominal half and quarter scale models. The raw materials handbook was again searched and the available gages closest to the required gages were tabulated. The two dimensional scaling criteria was again used to calculate the corresponding nominal scale ratio for the available material gages.

It is quickly evident that as one goes to smaller scale ratios the materials and their available gages pose a severe limitation.

Examining the tabulated results indicates that for the nominal half scale model; 7075-T6 can be substituted for 6061-T6 at a scale ratio of 0.559 and 2024-0 can be substituted for 7075-T6 at a scale ratio of 0.496. This results in an acceptable temperature error on the order of -0.6 percent.

For the nominal quarter-scale model; Type 301 stainless steel could be substituted for both the 6061-T6 and 7075-T6 at scale ratios of 0.255 and 0.258, respectively. This would result in a temperature error on the order of +2.1 percent; however, changing to a 0.255 scale model ratio would result in an acceptable error.

Under this contract however, only the prototype and half scale models were fabricated and tested.

The overall vehicle configuration is shown in Figure 20. The pertinent dimensions and component design details are shown in Tables 10 through 12. The temperature dependent thermal properties of the materials are tabulated in Appendix A.

Table 10 indicates the gages of the structural elements which comprise the angle "iron" frame, the skin panels, and the equipment deck. As three heater elements were attached to the equipment deck it was made of a heavier gage to force stronger conductive coupling to the structural frame.

Table 11 indicates the dimensions and gages of the heater canister components. The heater itself consisted of #28 gage (#36 gage on the half scale model) nichrome wire in a helical wrap around the aluminum silicate heater core. Both ends of the nichrome wire were staked to the aluminum silicate where power leads (#24 gage wire) and voltage taps (#30 gage wire) were connected.

Table 12 indicates the dimensions and gages of the heater box components. The heater itself is identical in construction to those used in the heater canister, but with a greater overall length.

The "angle iron" frame was welded together and the skin panels and equipment deck were bolted to the frame. The bolts were sized and spaced such that the joint conductance was large compared to the conduction paths in the skin panels. A conducting silicone grease film along the joints also promoted conduction contact.

The heater canister and box assemblies are also bolted together in such a manner as to minimize the resistance across the joints.

The surface finishes used on the vehicles consisted of combinations of one of two thermal control coatings or bare polished metal. All exterior surfaces were coated with the Boeing developed B-1060 white thermal control coating. The single exception to this was the outer surface of the closure deck which was left as bare polished metal. All interior surfaces were coated with a Sherwin-Williams flat black thermal control coating. The one exception to this was the single side of the heater box which faced across the equipment deck enclosure to the two

heater canisters. This surface was also left as bare polished metal. The radiative properties of these surfaces are tabulated in Appendix A.

Multilayer insulation blankets were used to cover the five exposed faces of the cubical structure for three of the eight tests. The insulation blankets consisted of ten layers of radiation shields interspaced with ten layers of spacer material. The radiation shields were quarter mill sheets of mylar with a 270 Å aluminum film on both sides. The spacer material was a coarse mesh silk net (John Heathcote and Company, Style No. 5-6917).

The blanket layers were bonded together with a "skip bonding" technique which amounts to a random spacing of glue drops between layers. The blankets were attached to the spacecraft with Velcro hook and pile tape. Pile tabs were bonded to the spacecraft to mate with hook tabs bonded to the blankets.

Figure 21 shows the uninsulated half model beside the insulated prototype. The blanket joints were essentially open joints with occasional Teflon tape splicing to avoid excessive separation at the joints and curling of the mylar film.

Performance of this insulation system had been established by a separate set of tests (Reference 60). Radiative properties of the aluminized mylar and effective conductivity of the insulation systems are reported in Appendix A.

In Figure 21 a vent hole in the half scale model can be seen. This was necessary to allow adequate venting of the models during chamber pump down. The two small black disks in the photograph are reference thermocouples used to monitor the chamber conditions during testing.

5.2 Model Instrumentation

The circuit diagram for the model heaters is shown in Figure 22. Four regulated D.C. power supplies were connected to the spacecraft heaters. A decade box with fixed resistance was wired in series with each of the heaters. Voltage taps across both heater and decade resistances lead through a switch box to a Fluke digital voltmeter. The energy dissipated by each of the heaters is calculated from:

$$P_D = \frac{V_H V_D}{R_D} \tag{81}$$

where:

P_D = Power dissipated

V_H = Voltage drop across the heater

V_D = Voltage drop across the decade box

R_D = Decade box resistance

The voltage taps across the heaters remove the energy dissipation in the long lead wires from the calculation.

Twenty chromel-constantan thermocouples (paired wire with a double layer of stranded fiberglass insulation) were installed in each of the vehicles. Number 32 gage thermocouple wire was used in the prototype and number 36 gage wire was used in the half scale model. All the wires were taken from the same spool. The locations of the thermocouples are shown in Figure 20.

Two additional thermocouples were staked to small aluminum disks and used as reference thermocouples to monitor the chamber test conditions. One disk was tied into the chamber adjacent to and facing the shrouded cryo-wall. The other disk was supported in the vicinity of the model and faced up into the solar beam.

The twenty two thermocouples were calibrated relative to each other over a 250°R (139°K) temperature range. Over this range the maximum deviation between the twenty-two thermocouples was ± 0.0002 millivolts. This corresonds to a temperature range of ± 0.05°R (± 0.0278°K).

The relative calibration consisted of fixing the thermocouples for the models on a copper slug. The slug was then put in an insulated oven fixture and all the wires were checked against each other over the entire test temperature range. Other than the transferring of the test junctions from the copper slug to the model, all the thermocouple circuitry for the relative calibration was identical to that used during the tests. The oven and the thermocouple circuitry are shown in Figure 23.

An absolute calibration was conducted on samples of wire from the same spool at the Boeing Metrology Laboratory. This calibration has NBS traceability and claims an accuracy of ± 0.04°F (± 0.0222°K) for any particular calibration point. This calibration data is presented in Table 13.

TABLE 13. THERMOCOUPLE ABSOLUTE CALIBRATION

Temperature (°R)	Temperature (°F)	Thermocouple EMF (above ice point) True (m V)	Actual (m V)	Correction (μ V)
492	32	0	0	0
560	100	2.2753	2.2708	+ 4.5
660	200	5.8724	5.8598	+12.6
760	300	9.7112	9.6950	+16.2
860	400	13.7518	13.7378	+14.0

The digital computerized readout system utilized to obtain the test data, over the range of the test temperatures, has a digital least count of 0.6°R (0.334°K). As the digital least count far overshadowed the absolute calibration error and the spread of the thermocouple readings

observed in the relative calibration, the standard NBS thermocouple calibration curve was used to reduce the data.

5.3 Vacuum Chamber and Solar Simulator Description

The tests were conducted in Chamber B at the Boeing Space Environment Simulation Laboratory utilizing a 4-foot (1.22 meter) solar simulator. A basic description of space environment simulation techniques is presented in Reference 76 and the Boeing facilities are described in References 77 and 78. A brief description of the B chamber and 4-foot solar simulator system follows.

General Description.- The chamber is a vertical cylinder 10 feet (3.048 m) in diameter and 18 feet (5.49 m) high (Figures 24 and 25). The top head contains the ion and sublimation pumping systems and supports the top and cylindrical portions of the cold-wall shroud, the helium cryopumping array, and the 48-inch (122 cm) by 56-inch (142 cm) off-axis parabolic collimating mirror. View ports and instrumentation feedthroughs are contained in the chamber sidewall and bottom head. Test specimens are usually mounted on the bottom head and raised into the test zone by a hydraulic lift.

Environmental Simulation.- Vacuum pumping systems connected to the space simulator allow a variety of environmental conditions to be established from launch pressure profile to long-term ultra-high vacuum as low as 10^{-11} torr.

Top, sidewall and bottom cold-wall zones are cooled by 80 psia (5.51×10^5 n/m^2), subcooled, single-phase liquid nitrogen. The cold walls can absorb a maximum flux density of 3420 Btu/hr ft^2 (1076 watts/m^2) and a total of 6.83×10^5 Btu/hr (200 kilowatts) without exceeding 180°R (100°K) at the warmest point.

The solar system collimating mirror, which represents a deviation in the chamber cold wall, is constructed from a 4-inch (10.17 cm) thick slab of stabilized aluminum. The mirror is ground, Kannigen nickel plated, polished, vacuum aluminized, and then vacuum overcoated with SiOx to facilitate cleaning. Mirror temperature is controlled by painting the back and edges black, allowing heat flow to the 180°R (100°K) liquid nitrogen walls. The mirror is electrically heated from the back to keep it at a constant 432°R (240°K) during tests (with sun on or off). The same heating system raises mirror temperatures above ambient during the chamber warm up to prevent condensation.

Solar Simulator Performance.- Specific performance details of the 4-foot (1.22 m) solar simulator are expanded in the following paragraphs.

Solar Work Zone.- The solar beam is circular in cross section, measuring 42 inches (106.8 cm) or more across any diameter. The height of the work zone is 96 inches (244 cm), all in the zone of "cold black space." This means that the specimen cannot see its own reflection in the off-axis parabolic collimator from any position within the work zone.

Beam Uniformity.- The beam uniformity is $\pm$ 5 percent at the base and upper planes and $\pm$ 4 percent at the midpoint. Change in uniformity over the test volume is $\pm$ 1 percent. Beam uniformity in the system is controlled by the uniformity of the light from the nineteen 10-inch diameter (25.4 cm) "aconic" collectors and a seven-lenticule field and projection-lens system.

Solar Intensity.- Solar intensity is controlled by varying the lamp current and number of lamps in operation. Up to nineteen nominal 2500-watt Ozram XBO-2500 lamps can be employed. These lamps are operated at up to 95 amperes current by light servo-controlled, all solid state, 2 percent ripple power supplies. Light control servos are used to compensate for individual lamp degradation and use special solar cells in the feedback loop which look past the collector at each lamp.

Because light servos are used, the total source level is controlled immediately upon starting of the lamps. Arc stabilization occurs within five minutes as lamps warm up, and light ripple in the work zone is very low (± 2 percent), due to mixing of nineteen lamps and the low-ripple SCR power supplies used.

Absolute solar intensity is measured using specially calibrated total radiometers, Model DR-2 built by TRW Instruments. The output is measured on a digital millivoltmeter with a 10-microvolt resolution. Accuracy is ± 3 percent in air, and the vacuum calibration is determined by transfer measurements using a small xenon solar simulator and a small [30-inch by 30-inch (76.2 by 76.2 cm)] space chamber with liquid nitrogen cold walls. The DR-2 radiometer uses a half-bridge/thermister detector which is half silver and half black. The DR-2 radiometers do not require water cooling. Eight TRW radiometers and one Beckmann Spectroradiometer Model W139323 are used at Boeing as total and spectral irradiance measuring devices.

Collimation Angle.- The apparent sun, as viewed from the test zone subtends an average half angle of 1.8^{o}.

Spectral Match.- Table 14 represents the tabulated spectral match of the 4-foot solar simulator system. This reading was made with a Beckmann double-prism monochrometer using 1P28 and PbS detectors with 0.4 mm slit width. The data were integrated over selected bandwidths and compared with the NRL data in these bands. These data were referenced to a 200-watt NBS standard of spectral irradiance as viewed directly by the monochrometer.

Although less than 9 percent of the sun's energy falls below 4000 Angstroms, the ultraviolet match of any simulator is important in thermal balance testing. This is true since almost all useful coatings absorb strongly in this region but are often designed to reflect in the visible range. For example, the paints used on Mariner and Lunar Orbiter can

be considered. The deviation in spectral match of a solar simulator from true conditions between 0.25 to 0.40 microns would produce a greater error in energy absorbed than would twice the same deviation over the whole band from 0.45 to 1.0 microns.

5.4 Test Conditions

The planned test sequence and nominal heater power levels are shown in Table 15. The test sequence covered a variety of cases for both the uninsulated and insulated vehicles. The individual tests were conceived to allow a detailed examination of the behavior of the experimental vehicle as compared to the response of the numerical experiment.

Comparing the numerical and experimental results for test number 1 allows an evaluation of the interaction of the vehicle with the cold space environment and direct solar irradiation.

Comparing the numerical and experimental results for test number 3 allows an evaluation of the conduction-radiation dissipation from the heater and an evaluation of conduction paths internal to the vehicle.

Comparing the numerical and experimental results for test number 5 allows an evaluation of the conduction-radiation interchange in geometrically complex vehicle enclosure.

Comparing the results for tests number six and eight allows an indirect evaluation of the effective conductivity of the multilayer insulation system under sun-facing and space-facing conditions.

Comparing the experimental results of tests numbers 2, 4 and 7 allows an evaluation of thermal scale modeling of spacecraft under complex external and internal environments. The numerical and experimental comparison of results further substantiates the ability of numerical methods to model the spacecraft and their environments.

It was planned that this sequence of tests would allow an ordered updating of the numerical model as well as demonstrating the capabilities of thermal scale modeling over a wide range of test conditions. In actual practice the idealized test conditions can not be met as a result of practical considerations. However an understanding of the actual test conditions allows a correction of the resultant data to account for these deviations.

The power dissipated by the spacecraft heaters during the tests is tabulated in Table 16. The small deviations from the nominal test condition are a result of:

1) inability to adjust the power supplies with adequate resolution, and
2) the temperature dependent nature of the thermal resistance which allowed a drift in power dissipation over the transient portion of the test.

The non-uniformity of the solar beam results in a variation in actual power input to each of the external surfaces from that of an idealized one solar constant beam. Isointensity plots of the solar beam were taken prior to each test. The isointensity plots with a plan view of the spacecraft model overlaid are shown in Figures 26 through 28.

Figure 26 shows the prototype test condition for both insulated and uninsulated models. Figures 27 and 28 show the test conditions for the uninsulated and insulated half scale models, respectively. The large differences in intensity variation shown between these three plots are not due to a normal degradation of the beam. Between each of the test series represented by these three solar plots other test programs were conducted. These other programs had sufficient outgassing that mirror contamination resulted. Thus, the collimator mirror was removed and cleaned and each of the xenon lamps was adjusted prior to the next test.

The isointensity plots were integrated over each external surface node and the absorbed solar load at each node was calculated using the

surface area and solar absorptivity of each node. The resulting solar heating rates for each exterior node have been tabulated in Table 17.

The scale modeling relations require a preservation of radiative properties and a uniformity of solar intensity. Consequently, compromises of the scaling criteria have resulted. However, a five percent variation in the solar flux input only results in a one-two percent variation in the overall vehicle temperature.

In summary, it is felt that the scaling criteria compromise resulting from the internal heaters and the external solar source will produce a negligible effect when the measured temperatures are compared.

Figure 29 shows the prototype vehicle suspended in the chamber. The thermocouple and heater leads can be seen at the vehicle base. The chevroned liquid nitrogen wall is also visible.

Figure 30 is a view of the prototype in the chamber during the test with the sun on. Illumination, reflection, and shadowing of and by the bolt heads is easily visible. Shadowing of the chamber base by the model is also noticeable.

Figure 31 shows the half scale model suspended from a frame mounted on the chamber base. After the prototype tests it was decided to mount the half scale model from the base in order to simplify mounting in the chamber and to ease access to the model.

Figure 32 shows the half scale model in the chamber during testing. In the figure the solar reflection from the over extended base back onto the model structure is strongly evident. Solar illumination of the model support wires and thermocouple reference disk support wires is also noticeable.

The transient results for one of the tests were lost. During prototype test number four the helium shroud ruptured causing a shutdown in the test conditions until the leak was located and repaired. Rather than open the chamber, the helium shroud was back-pumped and the test continued. This, however, caused a two hour disruption of the transient results.

The transient and steady state results for these tests are presented in Section 7 of this report.

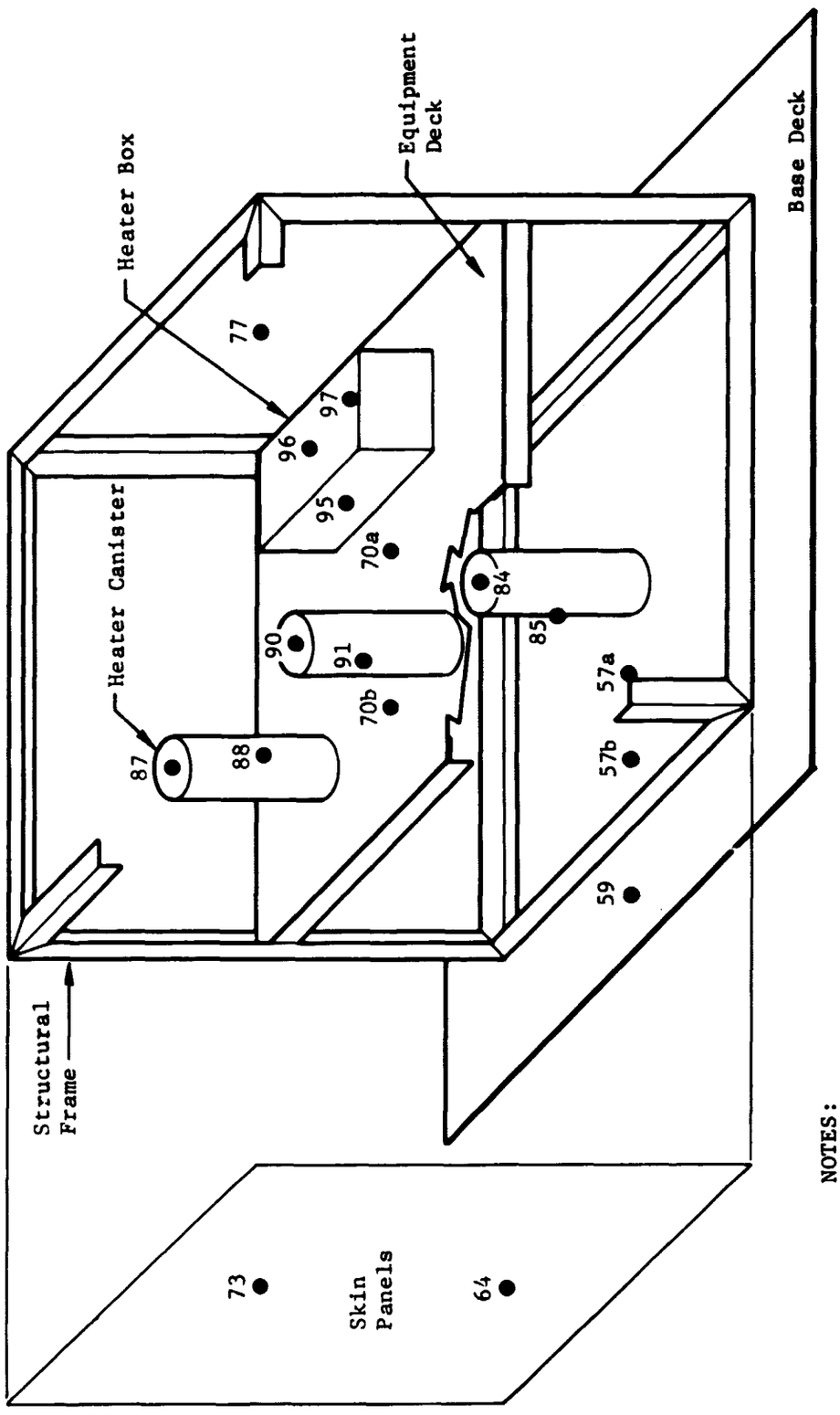

NOTES:
(1) ● Thermocouple Locations
(2) Thermocouples 91 and 97 Are Hidden From Direct View in Figure
(3) Closure Deck and Front Skin Panel Are Not Shown
(4) Thermocouples 79 and 81 Are On The Closure Deck
(5) Thermocouple 83 is Internal to The Base Deck Heater

Figure 20: SCHEMATIC OF THE EXPERIMENTAL CONFIGURATION

Table 10: STRUCTURAL ELEMENTS

STRUCTURAL FRAME

MODEL	MATERIAL	CONDUCTIVITY*	ANGLE	WEB
PROTOTYPE	6061-T6	96.6	1.0 X 1.0**	0.125
HALF SCALE	7075-T6	75.1	0.5 X 0.5	0.040

BASE DECK

CLOSURE DECK

SKIN PANELS

MODEL	MATERIAL	GAGE
PROTOTYPE	6061-T6	0.0625
HALF SCALE	7075-T6	0.020

EQUIPMENT DECK

MODEL	MATERIAL	GAGE
PROTOTYPE	6061-T6	0.125
HALF SCALE	7075-T6	0.040

* BTU/HR FT°R
** DIMENSIONS IN INCHES

Table 11: HEATER CANISTER ASSEMBLY

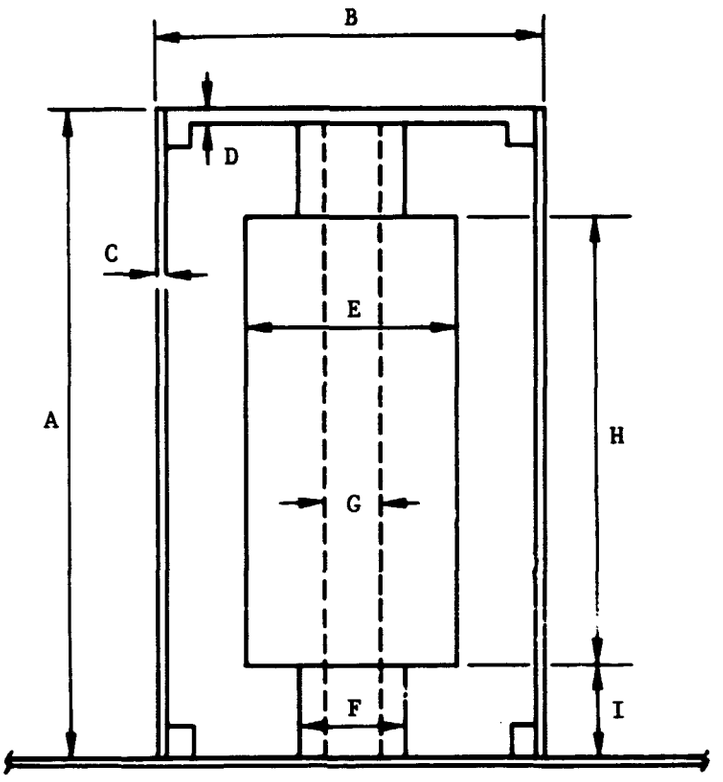

HEATER SHELL

MODEL	MATERIAL	A	B	C	D
PROTOTYPE	6061-T6	6.0	3.0	0.125	0.125
HALF SCALE	7075-T6	3.0	1.5	0.040	0.040

HEATER CORE

MODEL	MATERIAL	E	F	G	H	I
PROTOTYPE	ALUMINUM SILICATE	1.50	0.75	0.375	4.0	0.875
HALF SCALE	ALUMINUM SILICATE	0.75	0.375	0.1875	2.0	0.450

Table 12: HEATER BOX ASSEMBLY

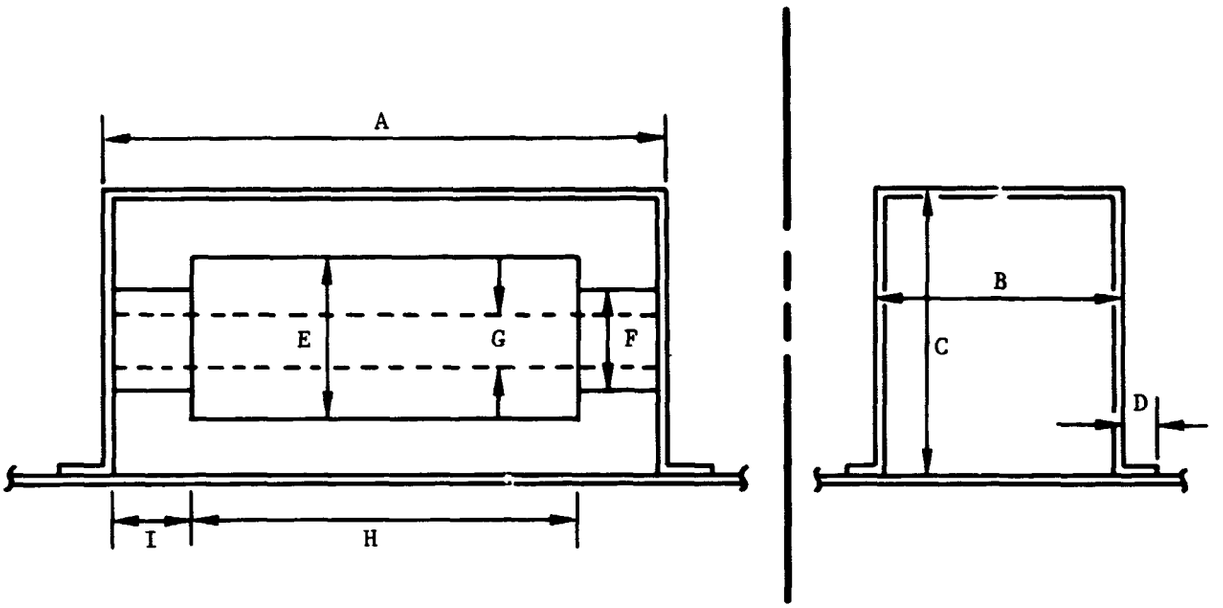

HEATER SHELL

Model	Material	Gage	A	B	C	D
Prototype	7075-T6	0.0625	8.0	4.0	3.0	0.75
Half Scale	2024-0	0.010	4.0	2.0	1.5	0.375

HEATER CORE

Model	Material	E	F	G	H	I
Prototype	Aluminum Silicate	1.50	0.75	0.375	6.0	0.875
Half Scale	Aluminum Silicate	0.75	0.375	0.1875	3.0	0.480

Figure 21: PROTOTYPE (INSULATED) AND HALF-SCALE VEHICLES

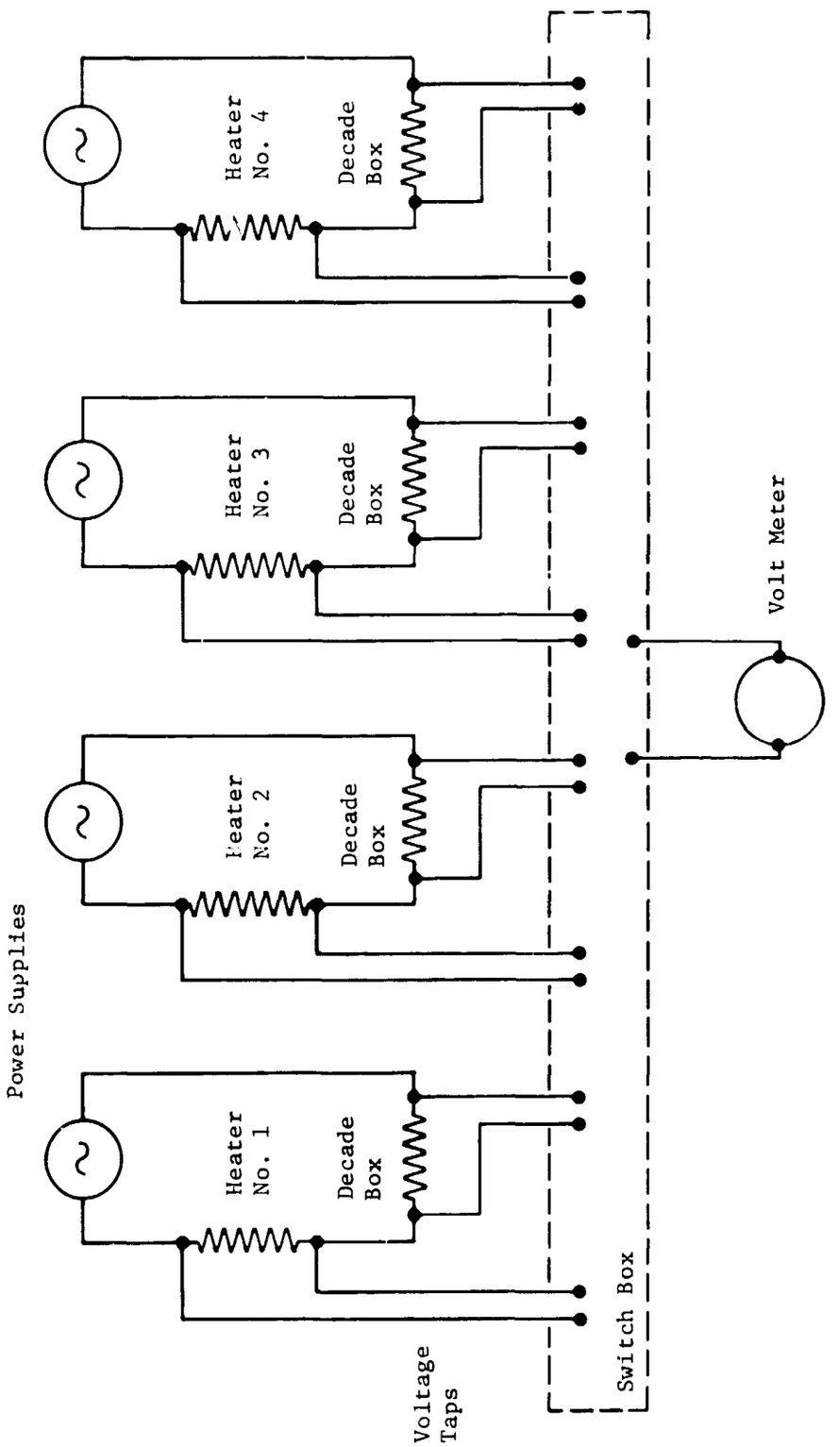

Figure 22: CIRCUIT DIAGRAM FOR SPACECRAFT HEATERS

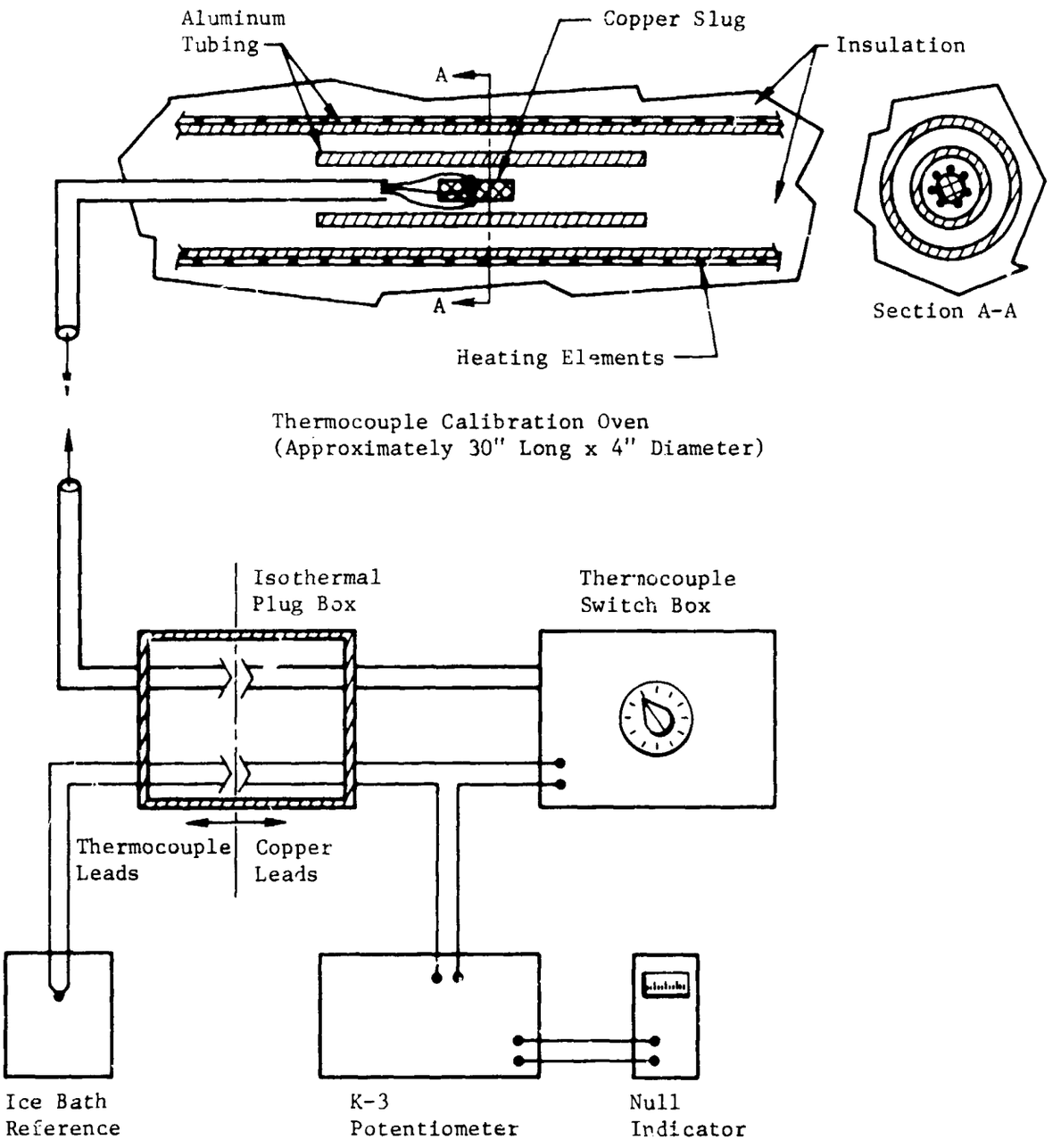

Figure 23: THERMOCOUPLE RELATIVE CALIBRATION CIRCUITRY

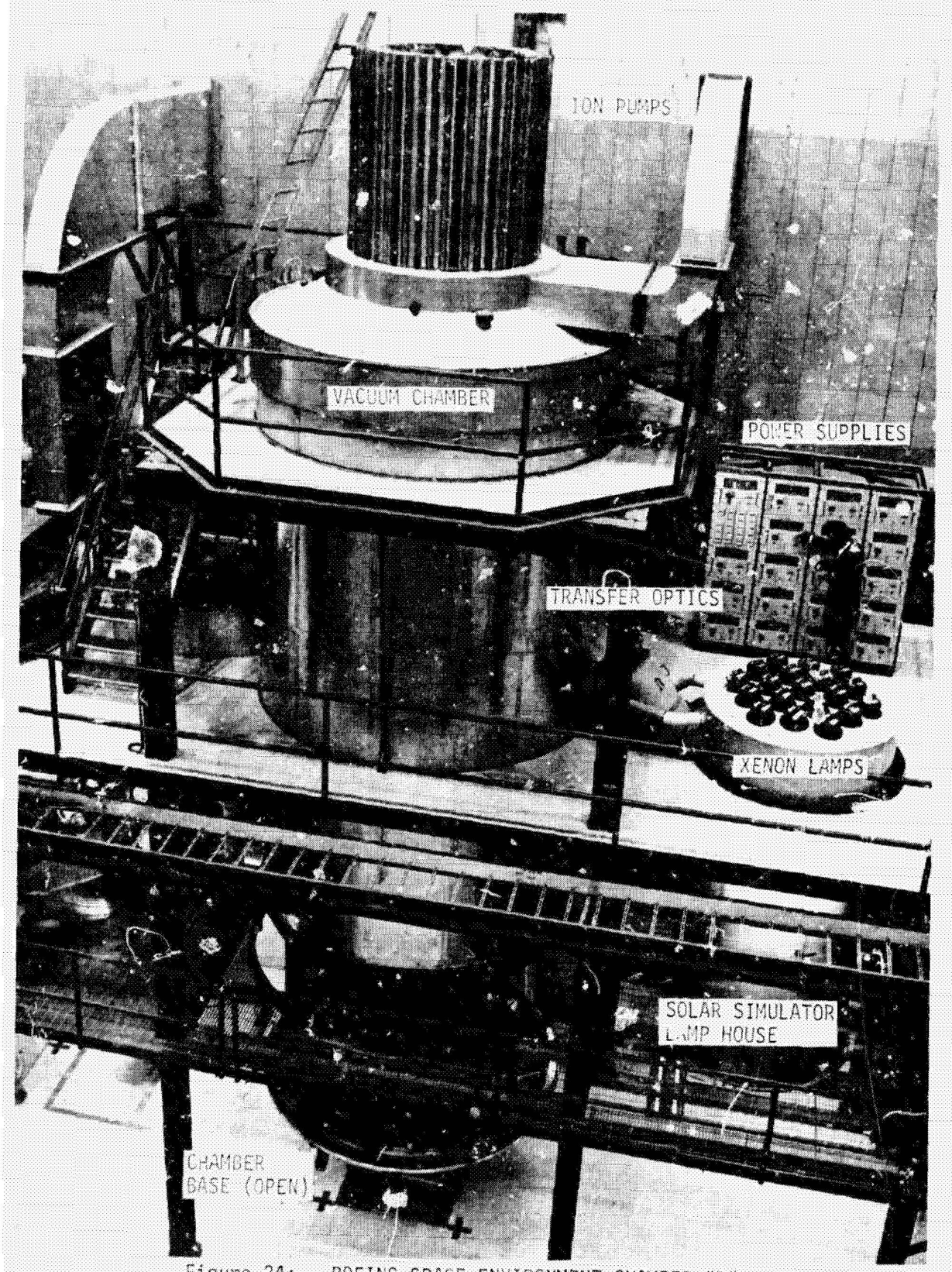

Figure 24: BOEING SPACE ENVIRONMENT CHAMBER "B"

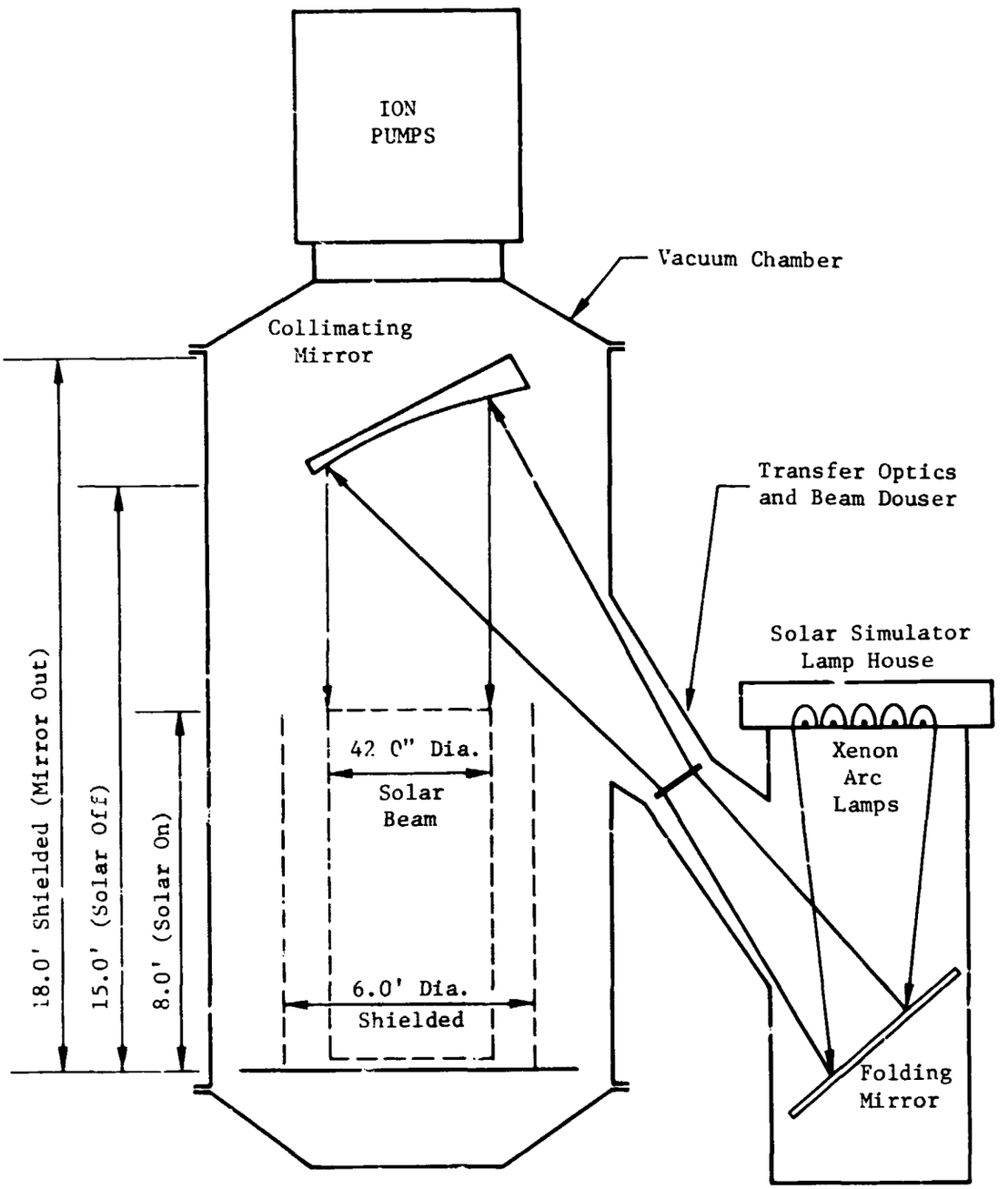

Figure 25: SCHEMATIC OF BOEING SPACE ENVIRONMENT CHAMBER "B" WITH SOLAR SIMULATOR

TABLE 14. SOLAR SIMULATOR SPECTRAL DISTRIBUTION

Bandwidth (microns)	Simulator Output (watts/m^2)	N.R.L. Solar Output (watts/m^2)	Percent Deviation From N.R.L.
0.25-0.35	39.50	62.82	-37.1
0.35-0.40	71.84	61.42	+17.0
0.40-0.45	74.48	95.90	-22.3
0.45-0.50	84.47	106.10	-20.4
0.50-0.60	168.87	191.25	-11.7
0.60-0.70	153.16	161.94	- 5.4
0.70-0.80	137.68	127.03	+ 8.4
0.80-0.90	97.57	100.52	- 2.9
0.90-1.00	86.52	80.96	+ 6.9
1.00-1.20	140.14	121.46	+15.4
1.20-1.50	131.67	111.68	+17.9
1.50-1.80	88.43	61.84	+43.0
1.80-2.20	53.66	44.25	+21.3
2.20-2.50	18.29	19.13	- 4.4

TABLE 15. TEST SEQUENCE

	Prototype	Half Scale
Uninsulated Vehicle		
Test #1		
Solar	On	On
Power	Off	Off
Test #2		
Solar	Off	On
Heater #1	120.0*	30.0
Test #3		
Solar	Off	Off
Heater #1	120.0	30.0
Test #4		
Solar	On	On
Heater #2	60.0	15.0
Heater #3	80.0	20.0
Heater #4	120.0	30.0
Test #5		
Solar	Off	Off
Heater #2	60.0	15.0
Heater #3	80.0	20.0
Heater #4	120.0	30.0
Insulated Vehicle		
Test #6		
Solar	On	On
Power	Off	Off
Test #7		
Solar	On	On
Heater #2	60.0	15.0
Heater #3	80.0	20.0
Heater #4	120.0	30.0
Test #8		
Solar	Off	Off
Heater #2	60.0	15.0
Heater #3	80.0	20.0
Heater #4	120.0	30.0

* Heater power levels (Btu/hr)

TABLE 16. EXPERIMENTAL HEATER POWER

Test	Vehicle*	Heater Power (Btu/hr)			
		One	Two	Three	Four
2	P	119.62	0	0	0
	H	30.14	0	0	0
3	P	119.84	0	0	0
	H	30.10	0	0	0
4	P	0	60.01	80.56	119.59
	H	0	15.01	20.13	30.11
5	P	0	60.25	80.81	119.84
	H	0	15.04	20.15	30.13
7	P	0	60.07	80.65	119.37
	H	0	15.19	20.20	30.02
8	P	0	60.29	80.93	119.57
	H	0	15.21	20.23	30.01

* P = Prototype Vehicle
H = Half Scale Vehicle

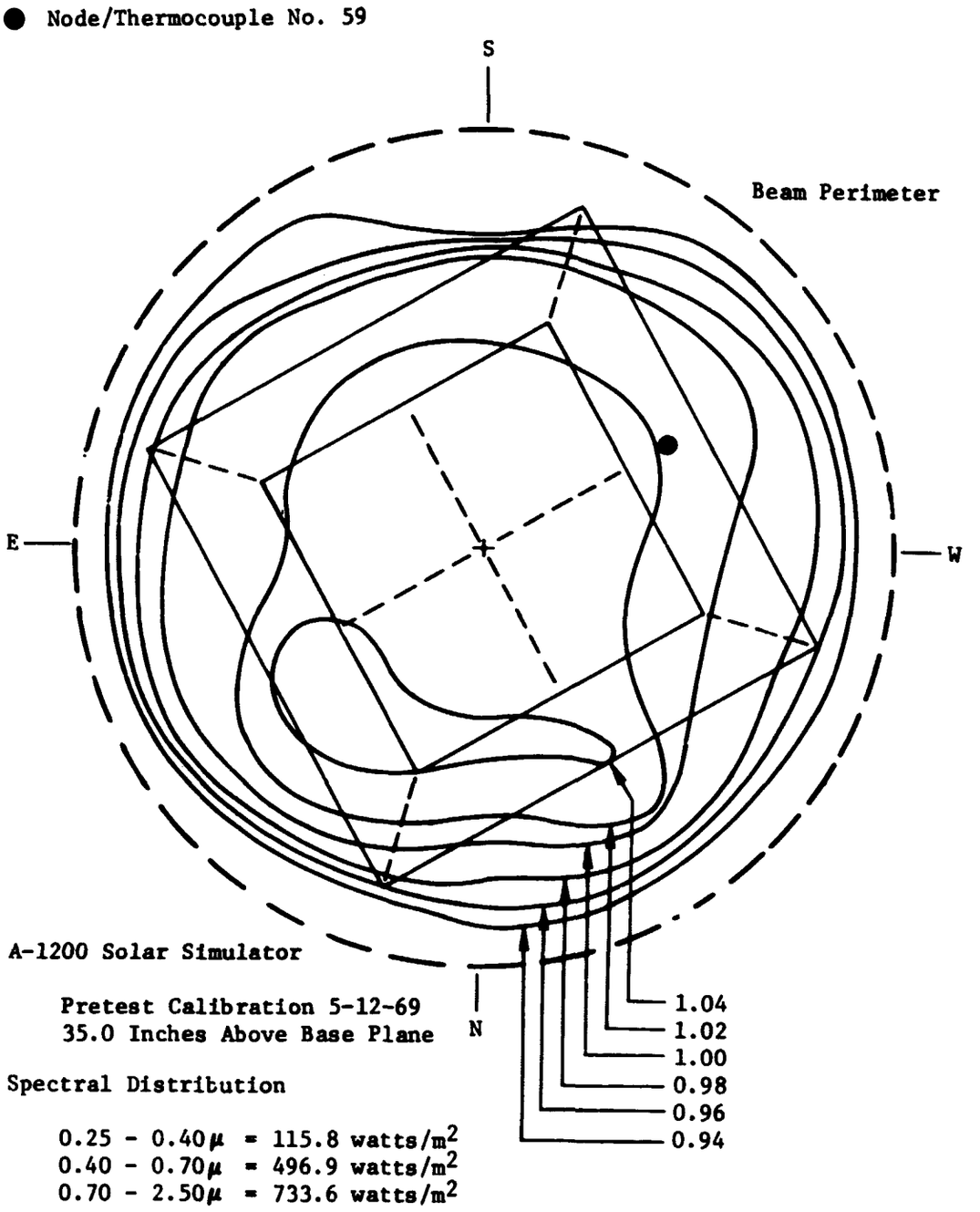

Figure 26: SOLAR SIMULATOR ISOINTENSITY PLOT OVERLAID BY PROTOTYPE PLAN VIEW

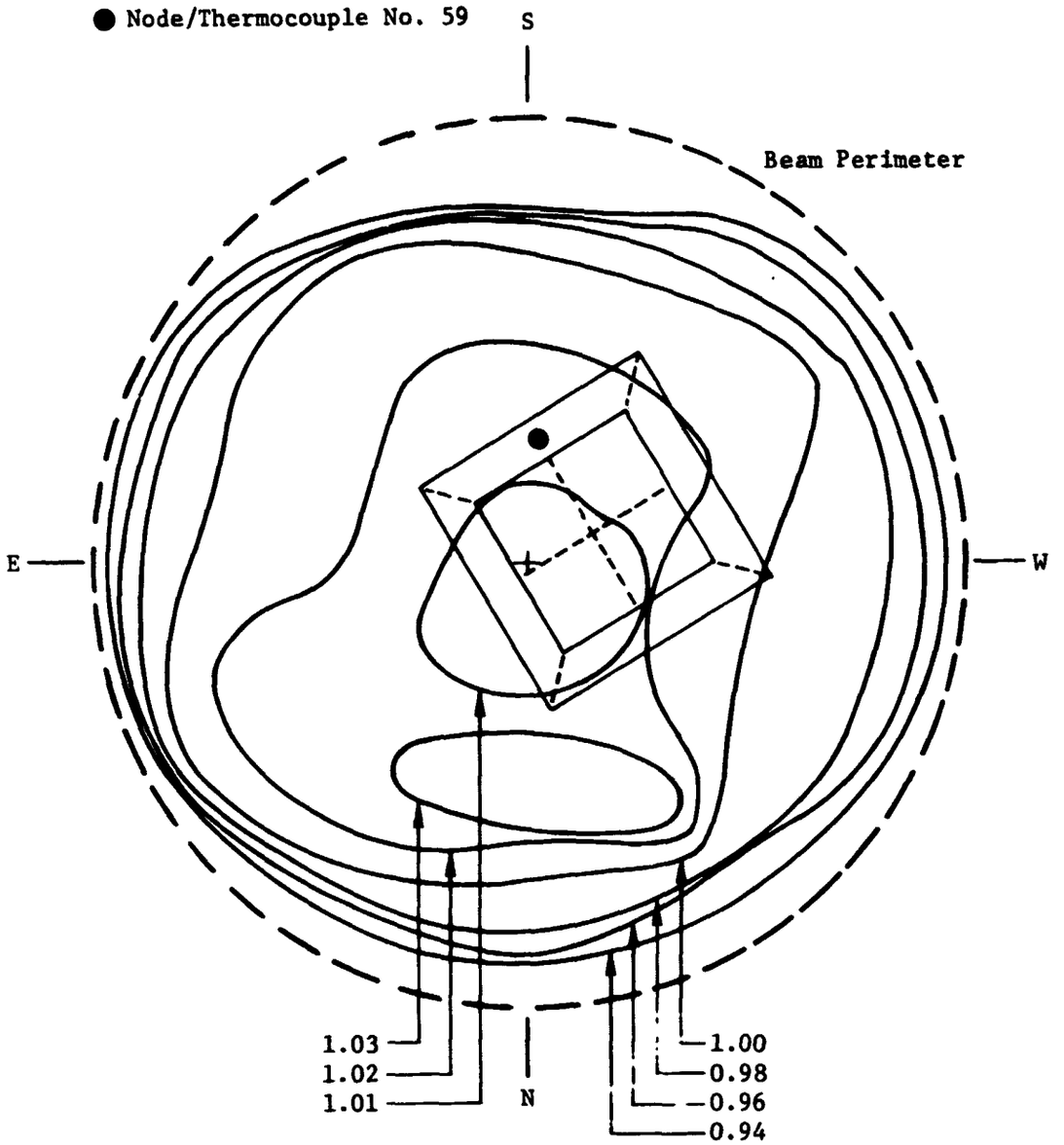

A-1200 Solar Simulator

Pretest Calibration 6-6-69
24.0 inches Above Base Plane

FIGURE 27: SOLAR SIMULATOR ISOINTENSITY PLOT OVERLAID BY HALF SCALE MODEL PLAN VIEW

● Node/Thermocouple No. 59

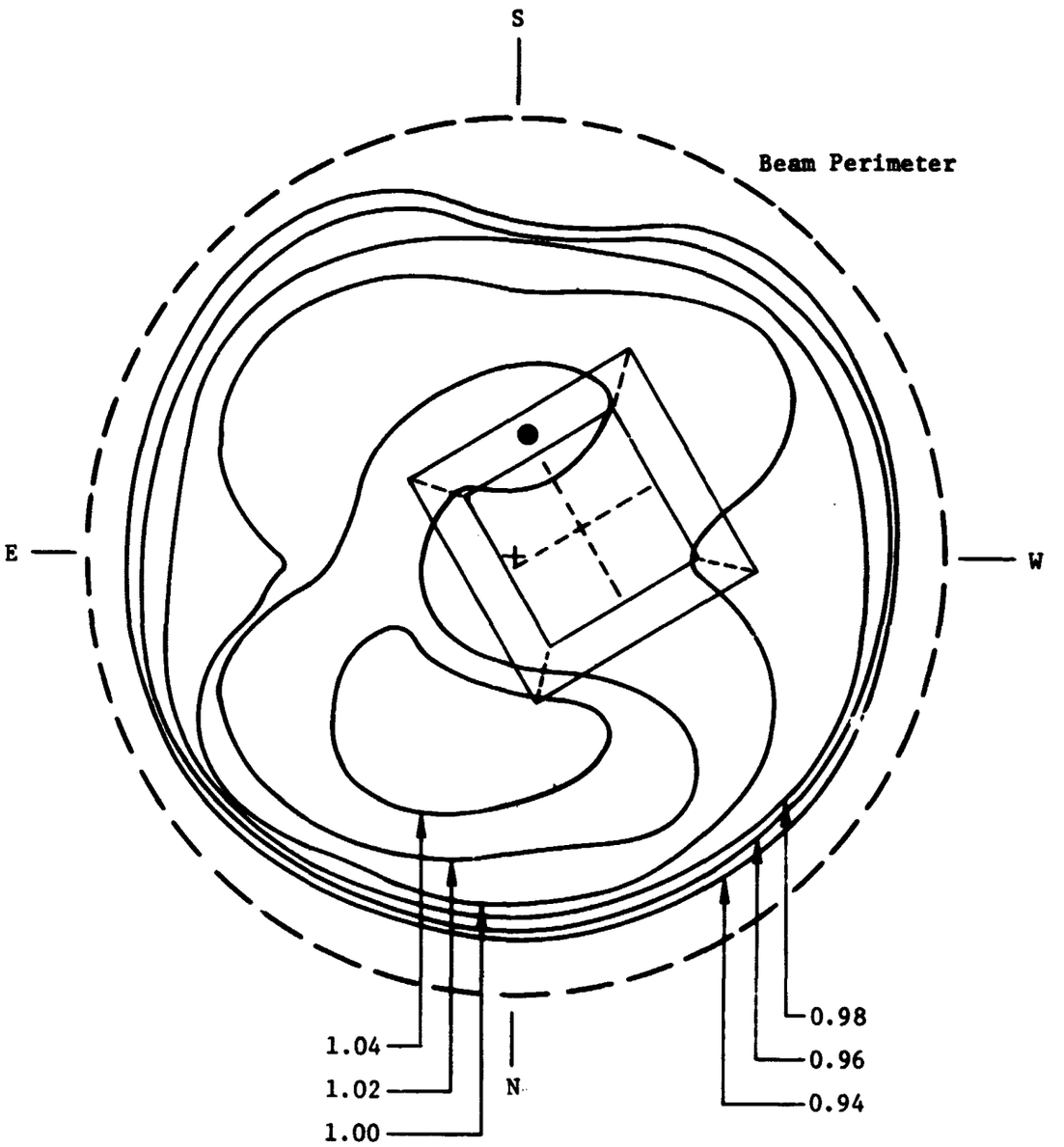

A-12 Solar Simulator

Pretest Calibration 6-26-69
24.0 Inches Above Base Plate

Figure 28: SOLAR SIMULATOR ISOINTENSITY PLOT OVERLAID BY INSULATED HALF SCALE MODEL PLAN VIEW

TABLE 17. EXPERIMENTAL SOLAR LOADS

Node	External Solar Loads (Btu/hr)			
	Prototype	Half Scale	Prototype Insulated	Half Scale Insulated
57	3.520	1.252	3.285	1.564
58	94.71	21.748	92.068	23.965
59	61.46	14.556	59.379	14.502
60	95.84	21.791	93.163	23.965
61	62.93	14.499	60.800	14.221
62	8.94	1.977	8.46	2.199
63	8.94	1.977	8.46	2.199
64	8.89	1.985	8.41	2.242
65	8.89	1.985	8.41	2.242
66	9.05	1.981	8.56	2.199
67	9.05	1.981	8.56	2.199
68	9.10	1.977	8.62	2.199
69	9.10	1.977	8.62	2.199
71	0.987	0.329	1.000	0.316
72	0.987	0.329	1.000	0.316
73	0.981	0.331	0.993	0.322
74	0.981	0.331	0.993	0.322
75	0.998	0.330	1.011	0.316
76	0.998	0.330	1.011	0.316
77	1.004	0.329	1.017	0.316
78	1.004	0.329	1.017	0.316
79	75.81	18.782	53.227	13.032
80	75.66	18.838	53.123	13.032
81	76.25	18.801	53.538	12.904
82	75.88	18.764	53.279	12.904
Total	701.96	167.509	598.004	150.307

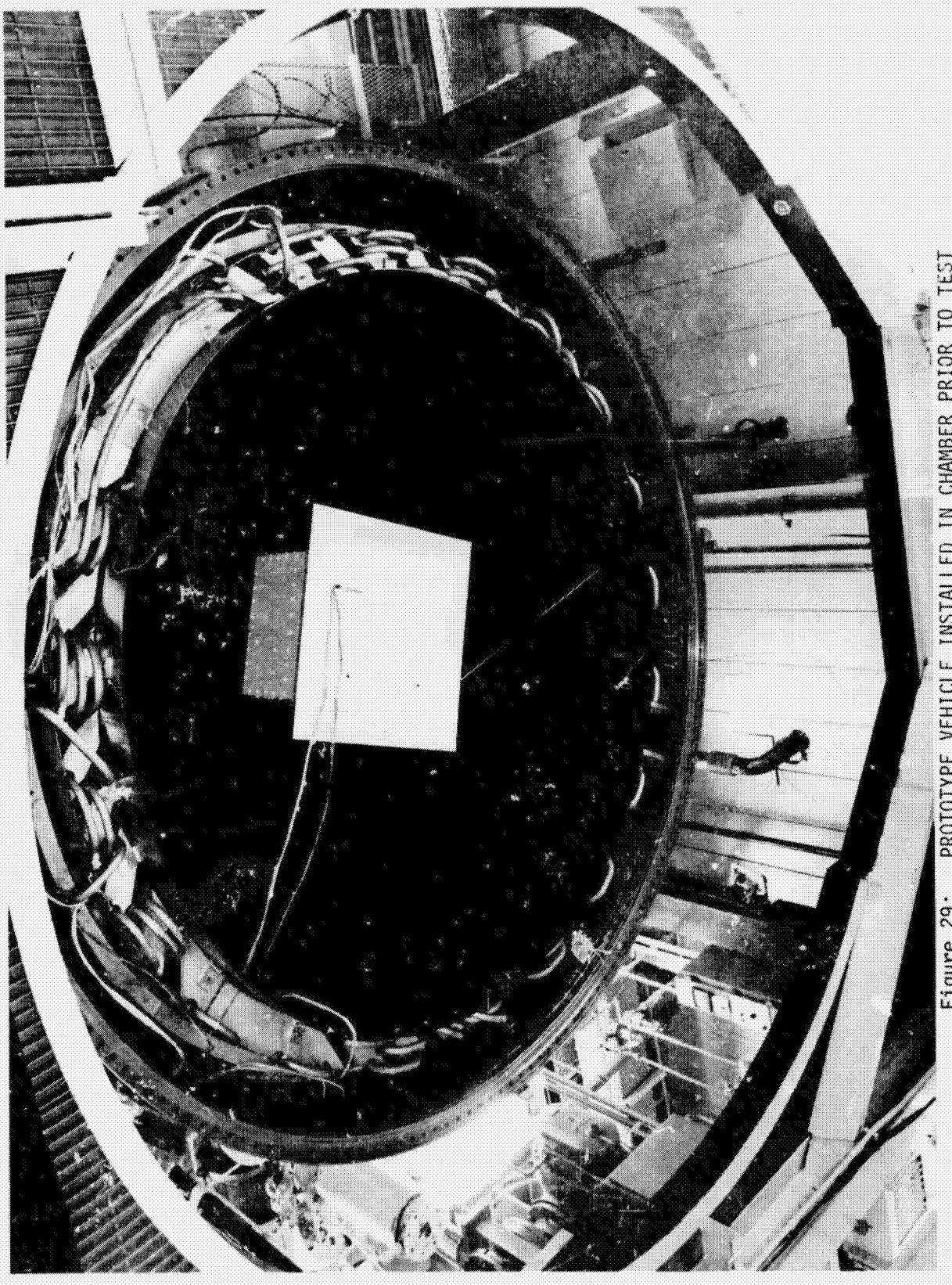

Figure 29: PROTOTYPE VEHICLE INSTALLED IN CHAMBER PRIOR TO TEST

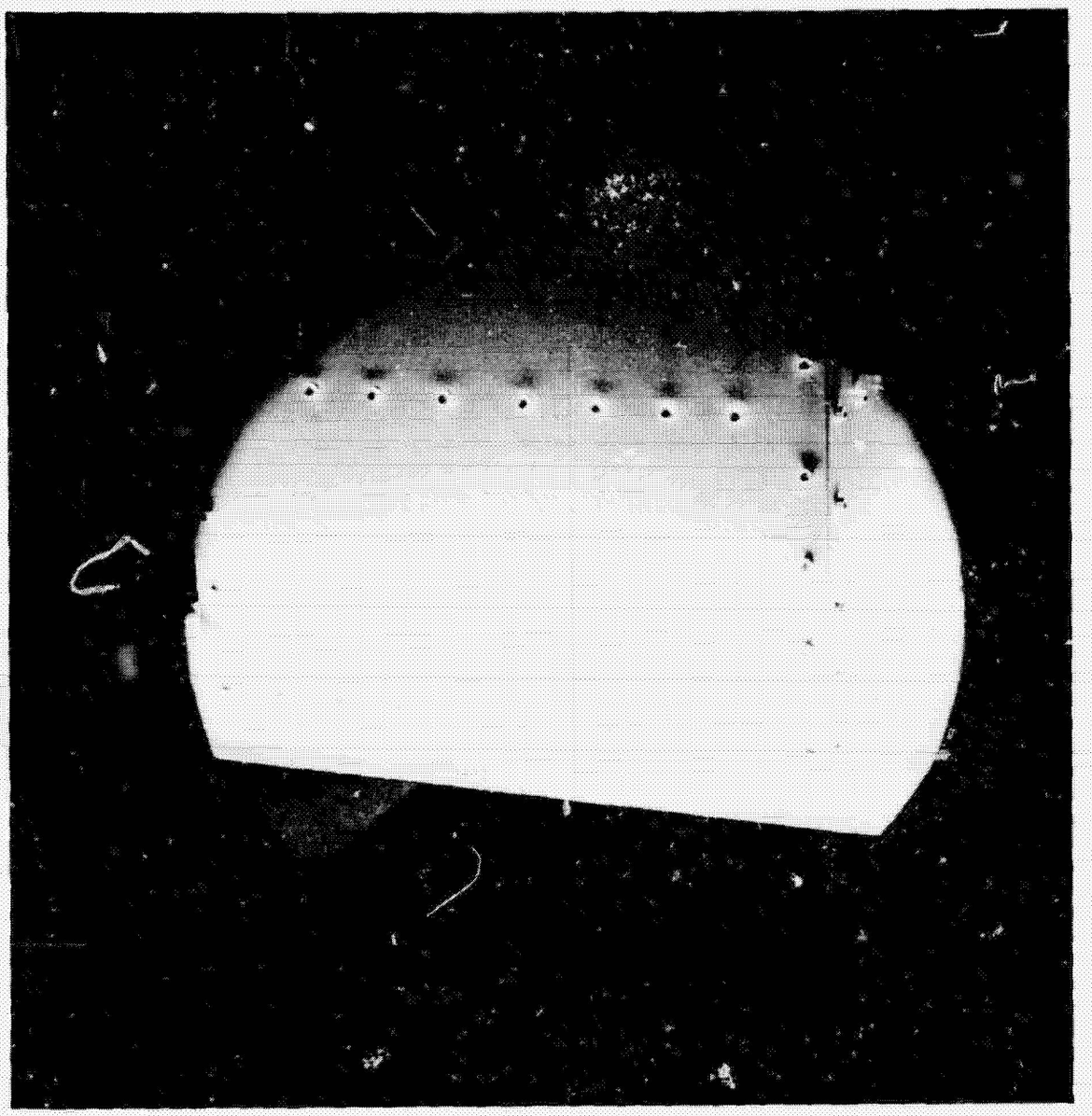

Figure 30: PROTOTYPE VEHICLE DURING TEST

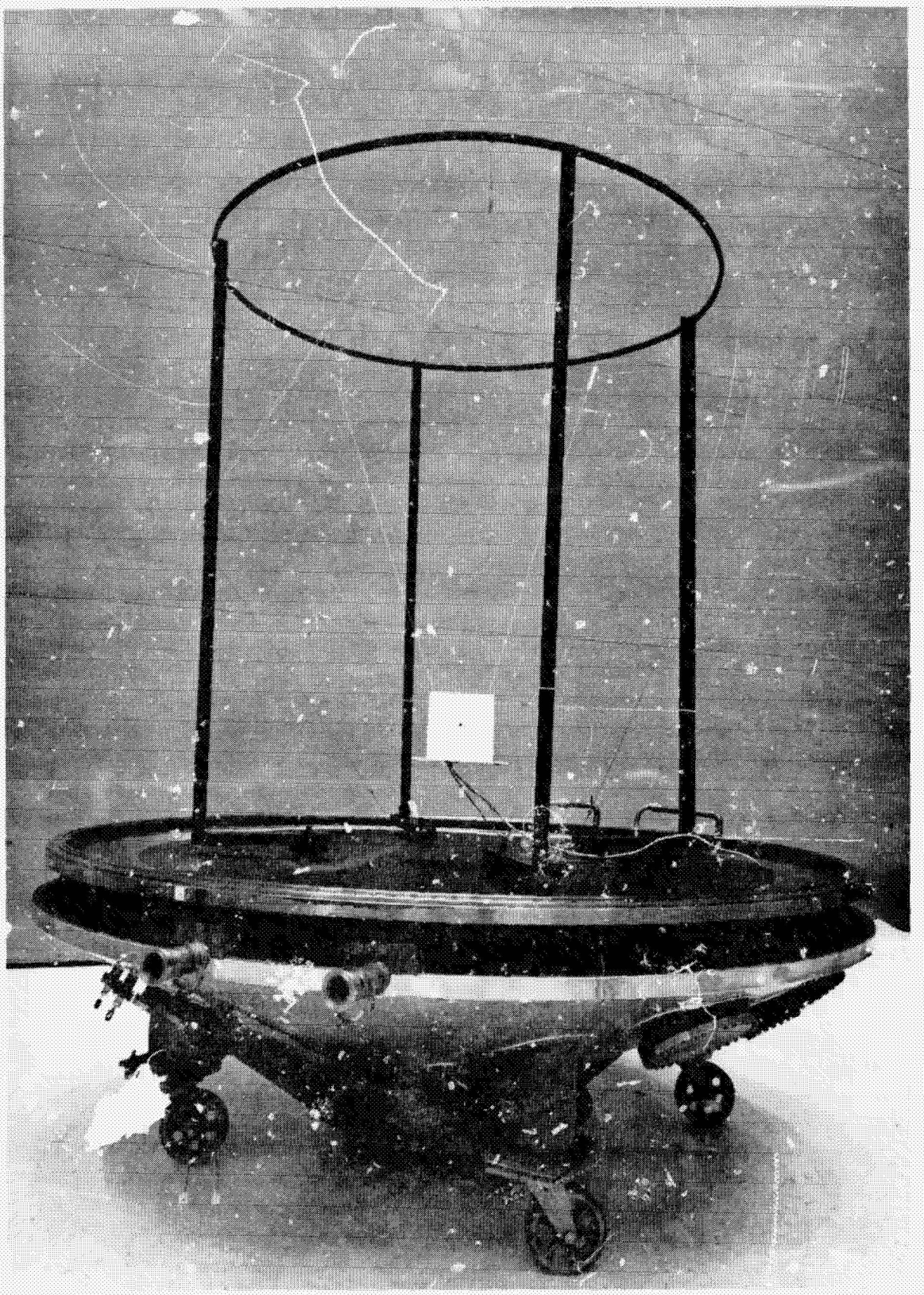

Figure 31: HALF-SCALE VEHICLE MOUNTED ON CHAMBER BASE PRIOR TO TEST

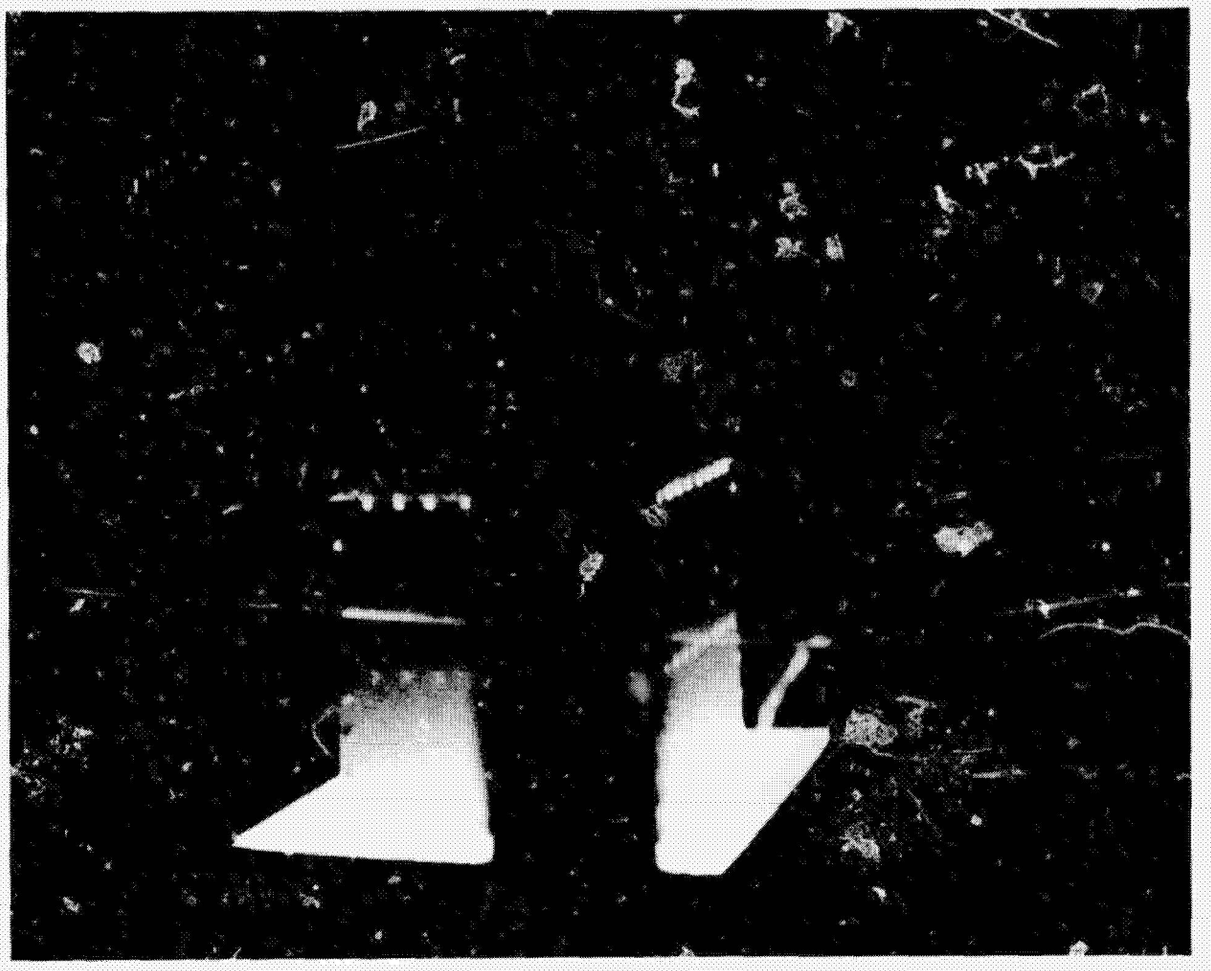

Figure 32: HALF-SCALE VEHICLE DURING TEST

PRECEDING PAGE BLANK NOT FILMED.

6.0 NUMERICAL ANALYSIS

There are several reasons for the substantial numerical analysis which has been performed for these vehicle configurations. First, a comparison of analysis and experiment allows a better understanding of the accuracy and limitations of numerical techniques. Second, the numerical model can be used to correct experimentally obtained temperatures for known compromises of the scaling criteria. Finally, a verified numerical model can be quickly "tested" for many environmental situations while actual chamber testing is expensive, time consuming, and is often unable to provide the desired external environmental heat loads.

This section will discuss the nodal network system of thermal analysis, the Boeing computer programs utilized to perform the calculations, and the nodal models established for the vehicles and the space simulation chamber.

6.1 Thermal Analysis

6.1.1 Network Thermal Analysis Technique.- Network thermal analysis (References 79-82) reduces to a node by node solution of the general energy equation as applied to each node and its interaction with adjacent nodes.

The energy equation for discrete nodal analysis can be written as:

$$C_i \frac{T_i^n - T_o^o}{\Delta t} = S_i + \sum_{j=1}^{n} K_{ij} (T_j - T_i) + \sum_{j=1}^{n} S_{ij} (T_j^4 - T_i^4) \quad (82)$$

Numerical values for the various terms are calculated as follows:

1) Node thermal capacitance for transient calculations is defined as

$$C_i = \rho_i V_i c_{pi} \quad (83)$$

where:

C_i = node thermal capacitance

ρ_i = temperature dependent density

V_i = nodal volume

c_{pi} = temperature dependent thermal capacity

2) Source terms (S_i) at the individual nodes are a result of either internally dissipated energy or energy absorbed by the exterior surfaces as a result of incident solar, albedo, or planet shine fluxes.

3) Conduction connectors between nodes i and j have a conductance defined as

$$K_{ij} = \frac{kA}{L_{ij}} \tag{84}$$

where:

K_{ij} = conductance

k = temperature dependent thermal conductivity of the material

A = cross-sectional area of the conduction path

L_{ij} = length of the conduction path

4) Radiation connectors between nodes i and j have a radiant exchange coefficient defined as

$$S_{ij} = \sigma A_i F_{ij} \tag{85}$$

where:

S_{ij} = radiation conductance

σ = Stefan-Boltzmann constant

A_i = nodal surface area

F_{ij} = radiation interchange factor

The energy equation for each node is evaluated numerically by a thermal analyzer program. The coefficients (either as constants or temperature and/or time dependent functionals) of Equation 82 must be provided to the program in order to obtain a solution for temperature distribution in the structure.

From the geometry and constituent materials of the structure the conductance and capacitance terms can be evaluated. A radiation interchange factor program utilizes the radiative properties of the materials and the configuration geometry to evaluate the radiation interchange factor. As the external environment for these tests consisted only of collimated solar energy, the radiation interchange factor program was also used to evaluate solar fluxes incident on the exterior nodes.

The following paragraphs briefly described pertinent features of the Boeing Radiative Interchange Factor Program and the Boeing Thermal Analyzer Program which were used to perform the numerical calculations reported in this study.

6.1.2 The Boeing Radiative Interchange Factor Program.- The Thermal Radiative Interchange Factor Program (References 84 and 85) is a Monte Carlo program for the calculation of radiant interchange factors among a set of surfaces in a vacuum (or a radiatively non-participating medium). This surface geometry is described in terms of primary surfaces and nodal or viewing surfaces. The primary surfaces are complete parallelograms, trapezoids, discs, spheres, skewed cylinders, and cones. The nodal surfaces are sectors of the primary surfaces definable in terms of their natural coordinates, as indicated schematically in Figure 22 (i.e. a nodal surface of a sphere is the domain between any two parallels and any two meridians; axial orientation of the sphere is arbitrary). A single nodal surface may comprise a complete primary surface. Alternatively, one or more nodal surfaces may completely or incompletely cover a primary surface.

The nodal surfaces are the physically meaningful surfaces treated in the analysis. The reasons for adopting this geometric definition system (i.e., nodal surfaces defined as segments of primary surfaces), as opposed to the completely independent definition of each nodal surface are three-fold.

First, this system of geometric definition reduces the amount of information necessary to describe system geometry and therefore eases storage requirements. Second, input effort and chances of input error are reduced. Third, machine time requirements are reduced. These advantages become very great when the average number of nodal surfaces per primary surface is large (as in a tankage enclosure where a small group of spheres and cylinders are subdivided into many nodes). When the average number nodal surfaces per primary surface approaches unity, the advantages vanish. However, even then the primary and nodal surface definition system incurs no disadvantage relative to alternative systems.

For whatever system of nodal surfaces is input, a matrix of interchange factors, F_{ij} or the equivalent, can be computed directly on the basis of Seban's specular-diffuse model. Alternatively, F_{ij} can be determined approximately from a matrix of exchange factors E_{ij} computed using this program. In the absence of non-black surfaces and specular reflection components, F_{ij} reduces to the geometric view factor matrix F_{ij}.

The underlying theory of these calculations has been covered in detail elsewhere (Reference 84) and will be only briefly discussed here.

Energy is emitted from a node as a discrete particle with a given energy level. Two random numbers are chosen to determine the point of emission on the nodal surface. The random numbers are chosen from a uniform distribution which eventually results in a uniform distribution of emission points on the nodal surface.

Two additional random numbers are chosen to determine the direction (azimuth and polar angle) of emission. A sufficient number of emitted particles will result in a Lambertion distribution of emitted energy from the surface.

The emitted particle is now followed in its path through the enclosure. As it strikes a surface in the enclosure a random number is generated and checked against the absorptivity, reflectivity and transmittance of each surface.

The tally scheme obeys the following rule:

$$\Delta V = \alpha \ V \qquad \text{if } V \geq \alpha \tag{86a}$$

$$\Delta V = V \qquad \text{if } V < \alpha \text{ and } R \leq \alpha \tag{86b}$$

$$\Delta V = 0 \qquad \text{if } V < \alpha \text{ and } R > \alpha \tag{86c}$$

where:

ΔV is the energy increment tallied on each surface struck

V is the energy remaining in the photon at each instant

R is a random number selected at each surface intersection

If partial absorption or no absorption occurs [cases (a) and (c)] at the surface then the random number is used to determine the mode of reflection (specular or diffuse) or transmission (straight through or diffuse).

The energy bundle is followed around the enclosure until its path is termined by:

1) total absorption of the remaining energy,
2) escape to space from the enclosure, or
3) arbitrary termination after sufficient partial absorptions that the energy remaining is a small fraction of the initially emitted energy level.

The radiative interchange factors are taken as the sum of the energy absorbed by each receiving node divided by the total energy radiated by the emitting node.

This tally scheme has zero systematic error (assuming a "perfect" set of uniformly distributed random numbers) and a random error which decreases as the number of energy bundles emitted increases.

Many special features have been incorporated into the Boeing Radiative Interchange Factor Program. These are described in detail in References 84 and 85 but those options utilized in this study will be noted below.

One subroutine causes a surface to emit uniform and collimated radiation. This allows any of the plane primary surfaces to be used as an emitter to simulate solar irradiation.

The program has the capability to handle calculations at two wavelengths. In general usage this allows simultaneous calculations at integrated solar and infrared wavelengths.

The collimated emission routine was used to simulated solar irradiation of the test vehicles. Adsorption at each of the external nodes was calculated as a heating rate and input to the thermal analyzer as a source term.

The radiative interchange factors are input to the thermal analyzer program as the coefficients for the radiation connectors between nodes.

6.1.3 The Boeing Thermal Analyzer Program.- Analysis of the thermal model started with the development of a discretized thermal network. All significant thermophysical properties and heat transfer modes have been represented. Isothermal areas are generally selected as nodes. Areas with uniform thermal properties and uniform interactions with the system boundary conditions (insulation or internal heat generation) were used.

The Boeing Engineering Thermal Analyzer program will be used to reduce the thermal analysis network and its time varying boundary conditions to a node by node temperature history of the model. This program is described in Reference 86.

The program uses relaxation techniques to compute equilibrium temperatures and forward differencing with refined time step control to compute transient temperatures. Pertinent capabilities of the program are:

1) Temperature dependent conductors may be used to represent material with variable conductivity.
2) Radiation conductors which vary with the temperature of emitting-receiving surfaces can be used.
3) Time or temperature dependent heat loads may be applied to any node.

The Boeing Thermal Analyzer is comparable to the NASA CINDA 3G Program in basic capability. The major difference is the large subroutine library available with CINDA which gives increased generality but results in a reduction in maximum problem size.

6.2 The Nodal Model

Numerical modeling of the experiment requires modeling not only of the vehicle but modeling of the space simulation chamber as well. The finite size of the chamber and its non-black character allow interactions which are not present under space conditions. Solar beam reflections and reflections of vehicle emitted energy back onto the vehicle force a consideration of the chamber in the numerical model.

Numerical modeling involves dividing the vehicle into a finite number of nodes. Each node being ideally an isothermal element of volume. The nodes are connected to each other by conduction and radiation paths. The presence of a gas introduces additional convection paths which were not

present in this study. The greater the number of nodes, the more acurately the numerical solution approaches an analytic solution to the governing differential equations.

In actual practice two nodal models are used. The detailed nodal model is used for thermal analysis while a simplified model is used to determine the coefficients for radiation interchange between surfaces. As conductivity is not a consideration in these latter calculations, only those nodes which have significant surface areas or high temperatures must be considered. Structural elements of high conductance but minimal surface area, for example, the structural frame used in this study, can be omitted from the radiation nodal network with a negligible effect on the final thermal analysis.

Figures 34 and 35 show the nodal subdivision of the model used to compute the radiation interchange factors. Figure 36 shows the nodal subdivision of the vacuum chamber and solar collimating mirror. The solar collimating mirror is approximated by a disk. One of the interchange factor program options allows emission normal to the emitter surface. This allows a disk to emit a collimated beam of energy to simulate a solar source.

The radiative properties of the spacecraft surfaces are presented in Appendix A. The radiative properties of the space chamber walls (both flat end surfaces and chevroned cylindrical shroud are presented in Table 18.

TABLE 18. CHAMBER RADIATIVE PROPERTIES

	Base	Shroud
α_s	0.94	0.98
ε	0.88	0.94

The matrix of radiation interchange factors for the uninsulated spacecraft is presented in Appendix B.

To simulate the insulated spacecraft configuration, other nodal surfaces are defined over the insulated surfaces. These surfaces have the radiative properties of aluminized mylar and represent the outer layer of insulation. The matrix of radiation interchange factors for the insulated spacecraft configuration is presented in Appendix C.

The radiation interchange factors presented in Appendices B and C are input to a network thermal analysis as the coefficients of radiant exchange between nodes. Figures 37 and 38 show the detailed nodal network established for thermal analysis. In addition to those nodes existing for the radiation interchange analysis, 56 nodes (numbers 1-56) have been defined over the structural frame.

The conduction connectors between these nodes have been detailed in Figures 39 through 45. Conductors in the structural frame and skin panels are shown in Figures 39 through 43. Conductors in the heater canisters and the heater box are shown in Figures 44 and 45, respectively.

In the cases where multilayer insulation blankets have been added to the vehicle structure, nodes representing the blanket have been added over the skin panel nodes covered by insulation. The radiation interchange factors for the insulated spacecraft are presented in Appendix C. Conductors have also been added between the skin nodes and the insulation nodes.

An energy balance on the insulation consists of an effective conductance through the insulation to the skin panels below and radiation to space based on the radiation properties of the outer layer of insulation The effective conductance was experimentally evaluated for similar blanket configurations and is presented in Appendix A.

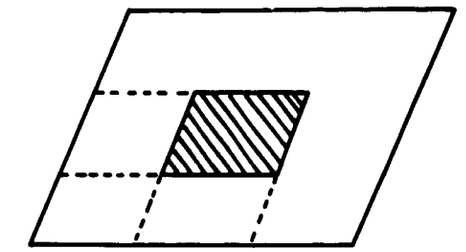

Segments of Parallelograms

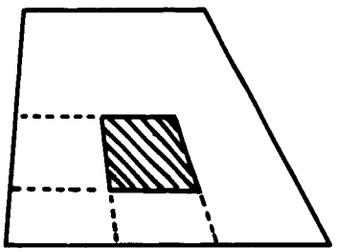

Segments of Trapezoids

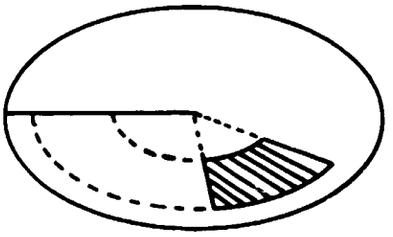

Segments of Discs

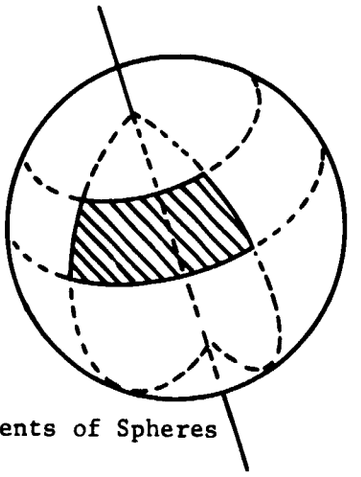

Segments of Spheres

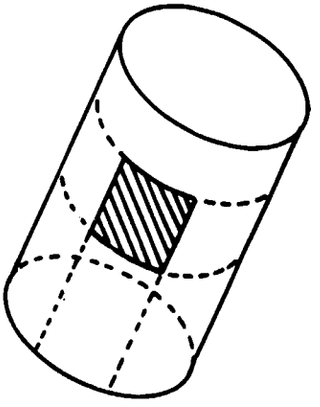

Segments of Cylinders

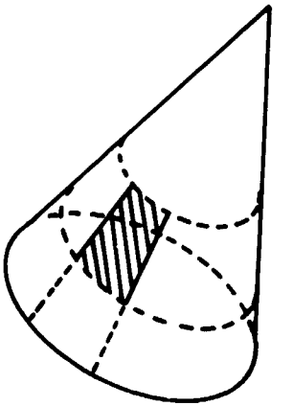

Segments of Cones

Figure 33: PRIMARY SURFACES AND TYPICAL NODAL SURFACES

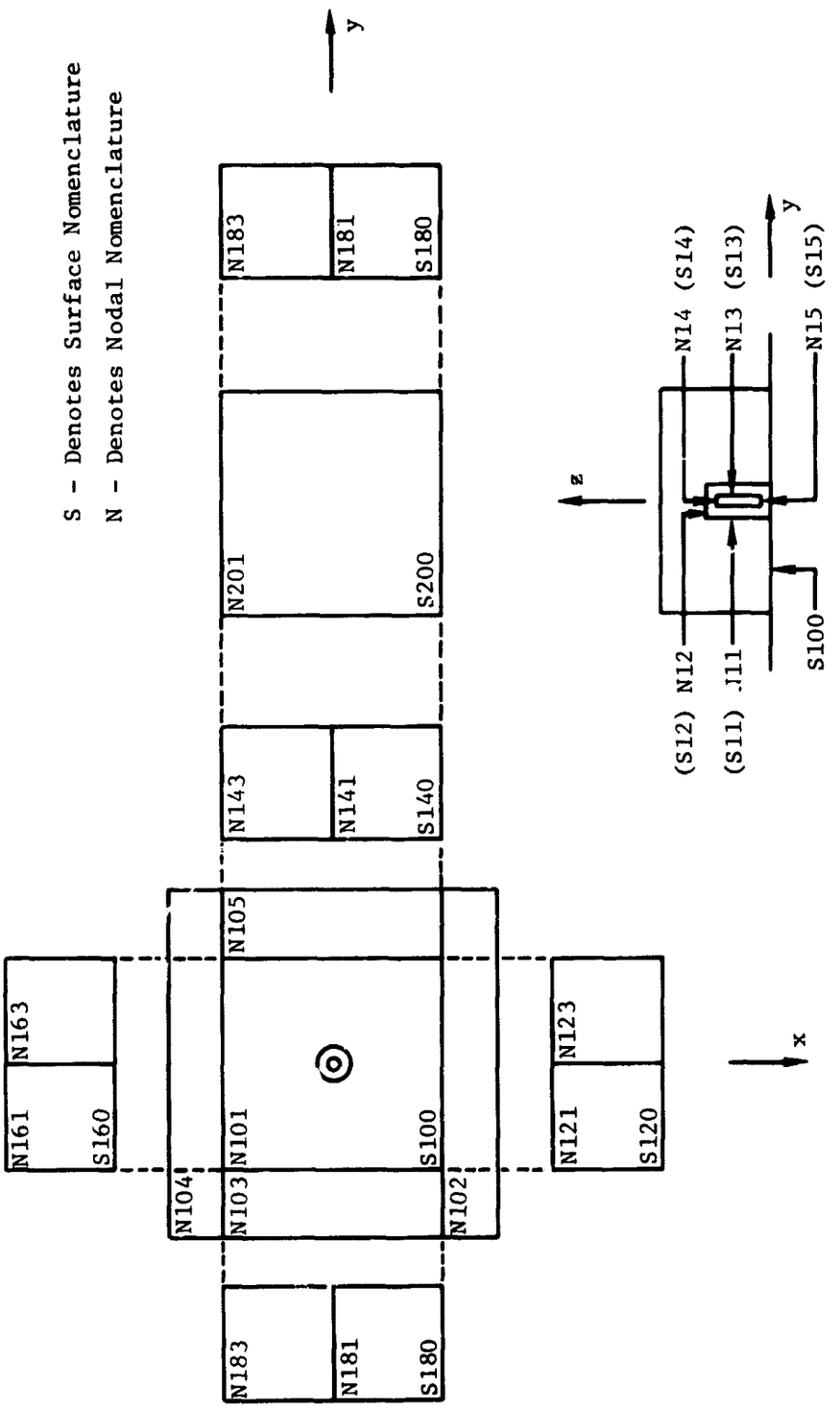

Figure 34: SURFACE AND NODE NOMENCLATURE---BASE DECK ENCLOSURE

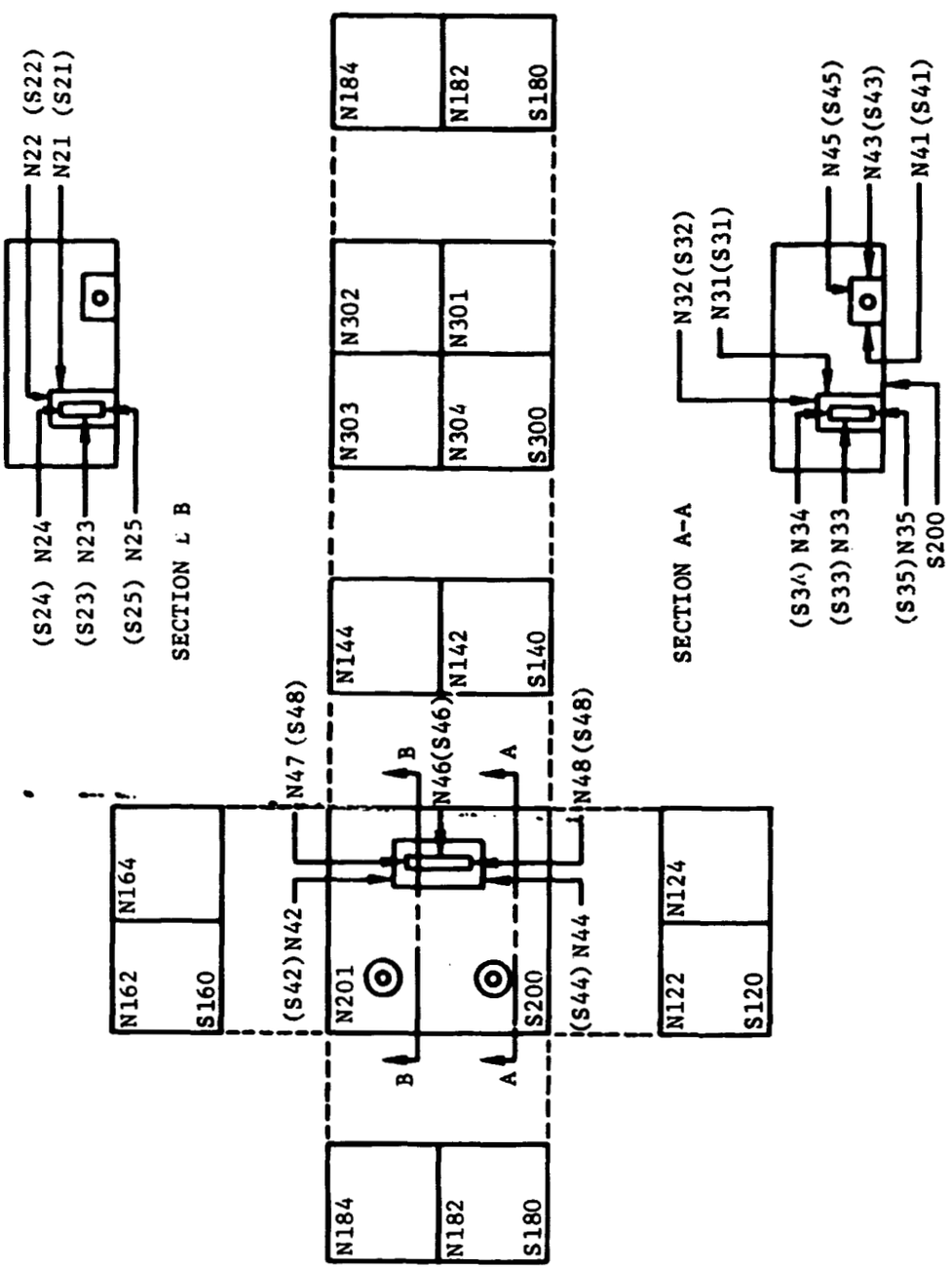

Figure 35: SURFACE AND NODE NOMENCLATURE---EQUIPMENT DECK ENCLOSURE

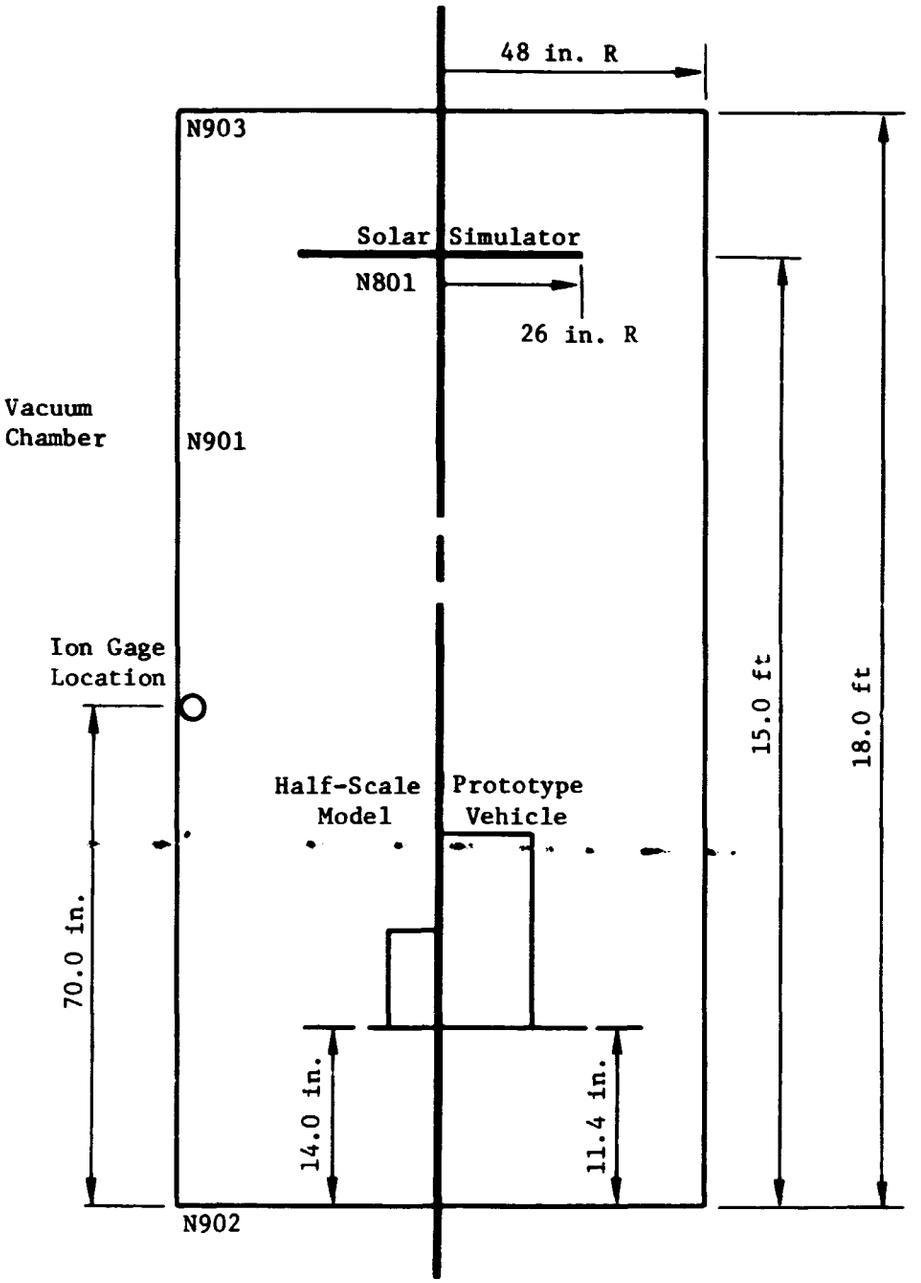

Figure 36: NODE NOMENCLATURE - VACUUM CHAMBER AND SOLAR SIMULATOR

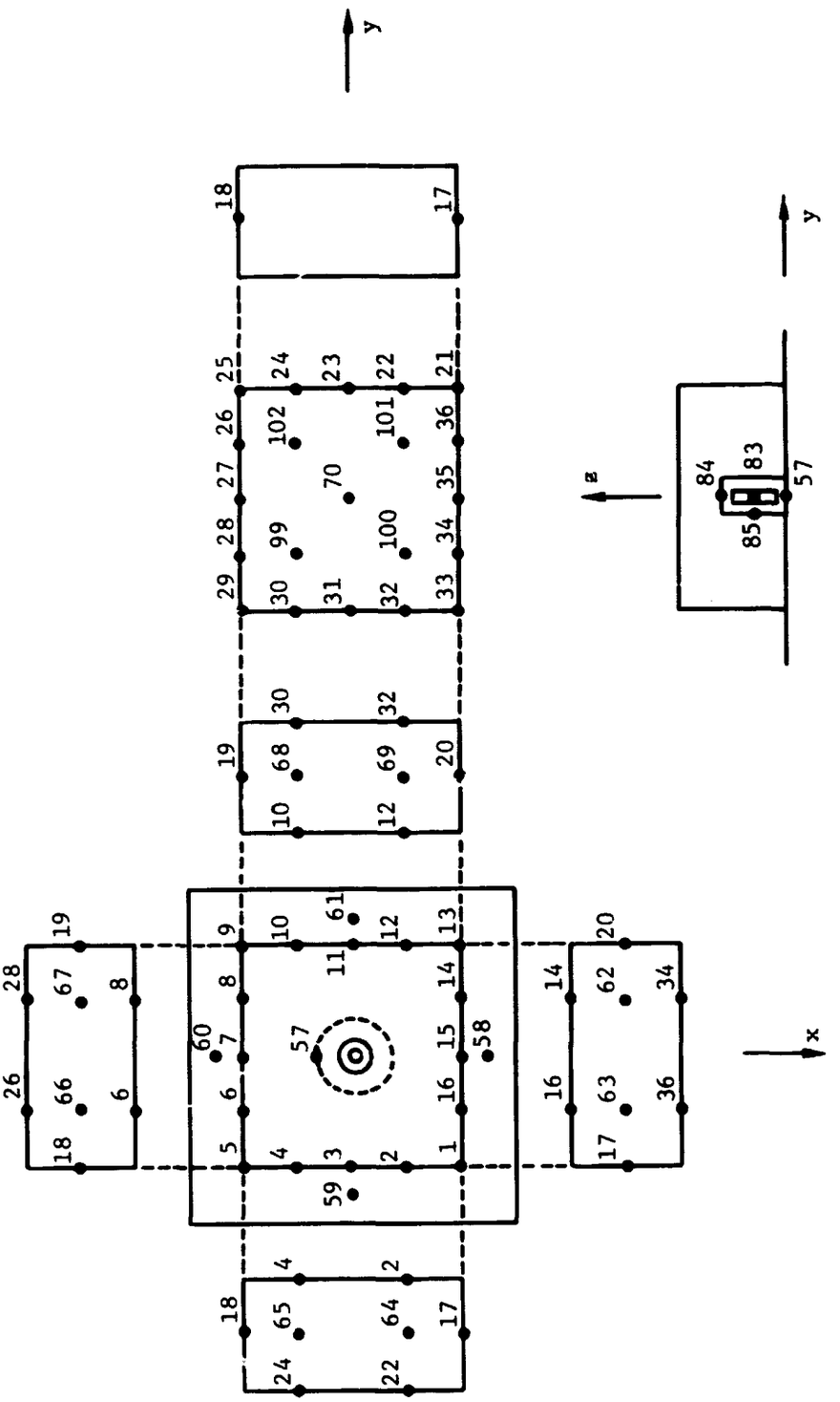

Figure 37: THERMAL ANALYZER NODE NOMENCLATURE---BASE DECK ENCLOSURE

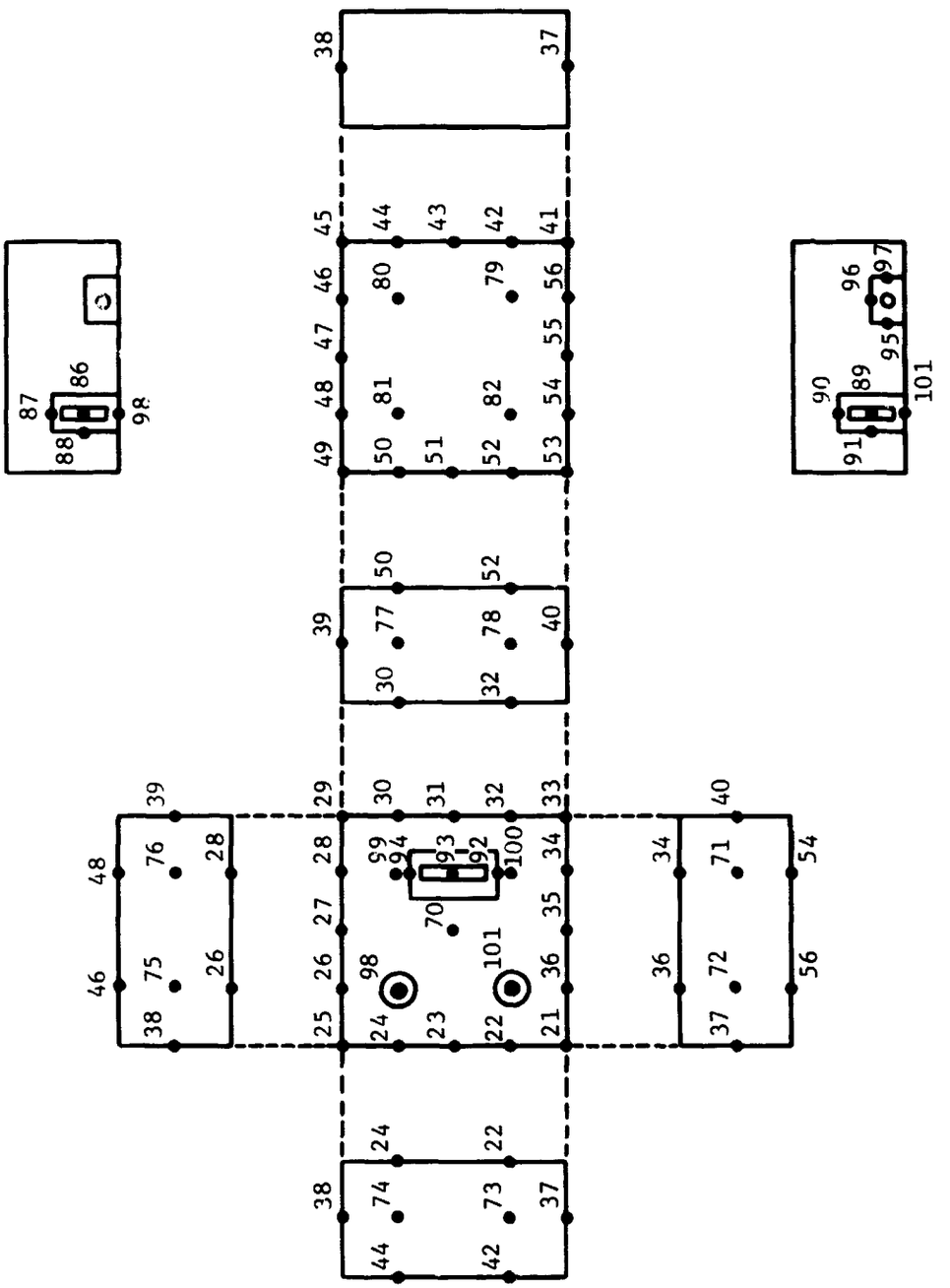

Figure 38: THERMAL ANALYZER NODE NOMENCLATURE---EQUIPMENT DECK ENCLOSURE

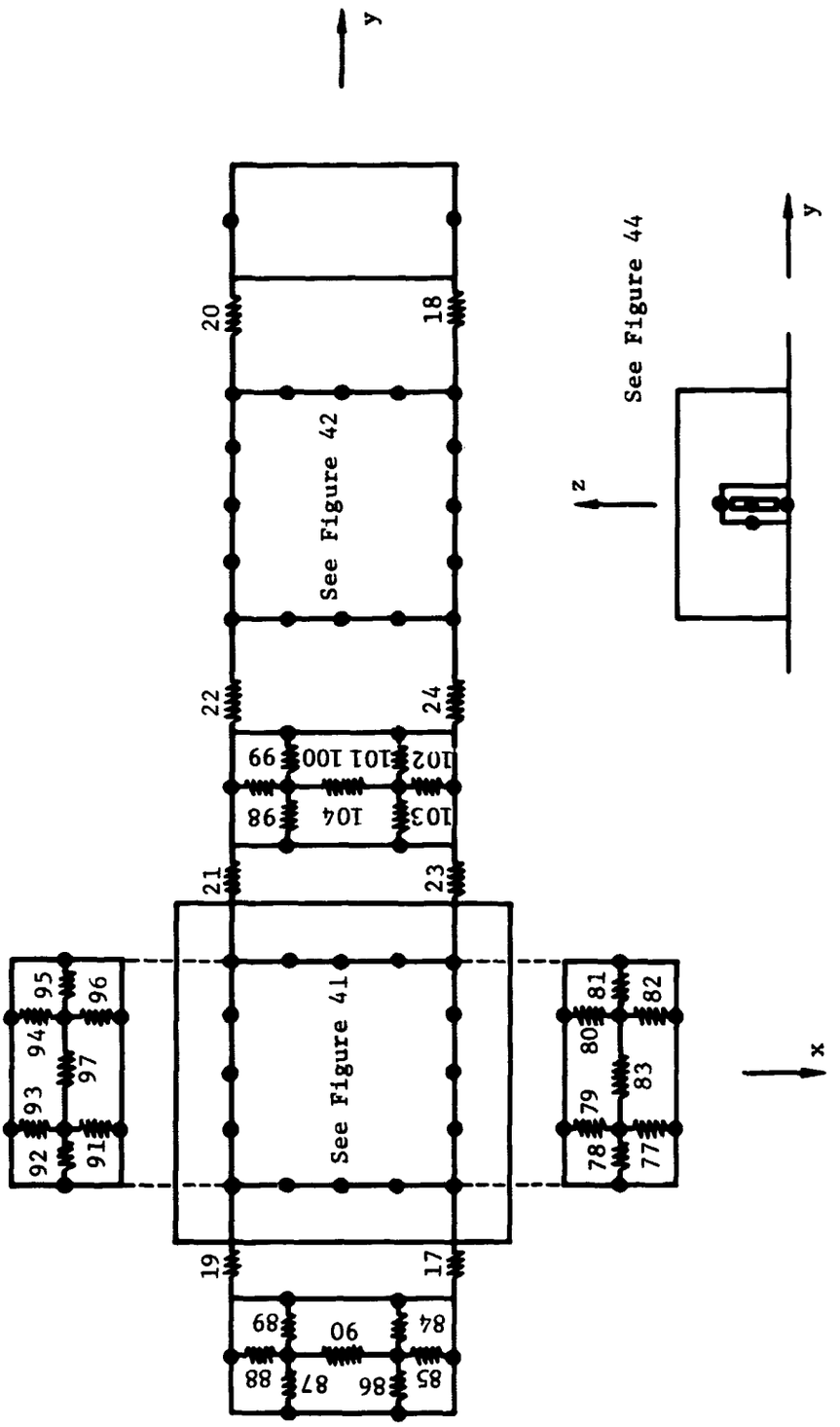

Figure 39: THERMAL ANALYZER CONDUCTOR NOMENCLATURE---BASE DECK ENCLOSURE

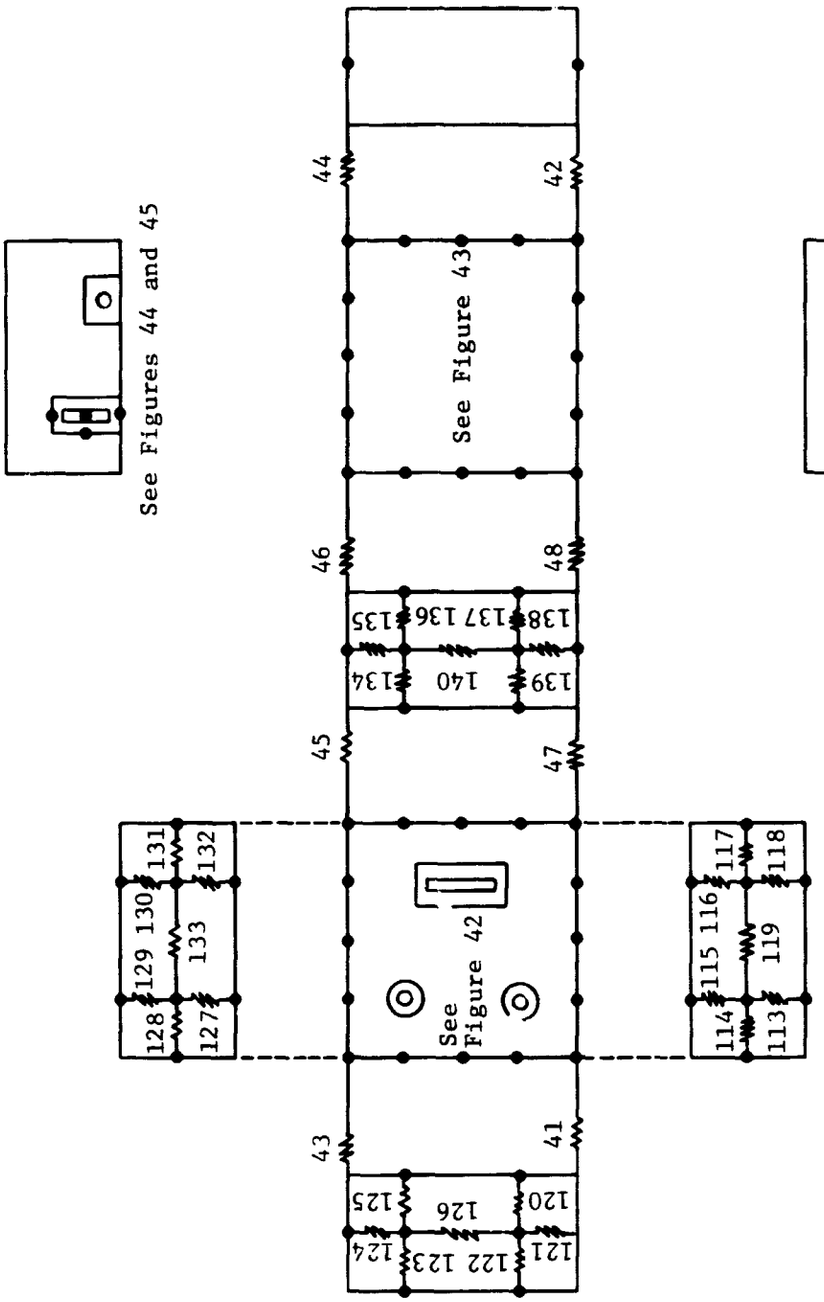

Figure 40: THERMAL ANALYZER CONDUCTOR NOMENCLATURE---EQUIPMENT DECK ENCLOSURE

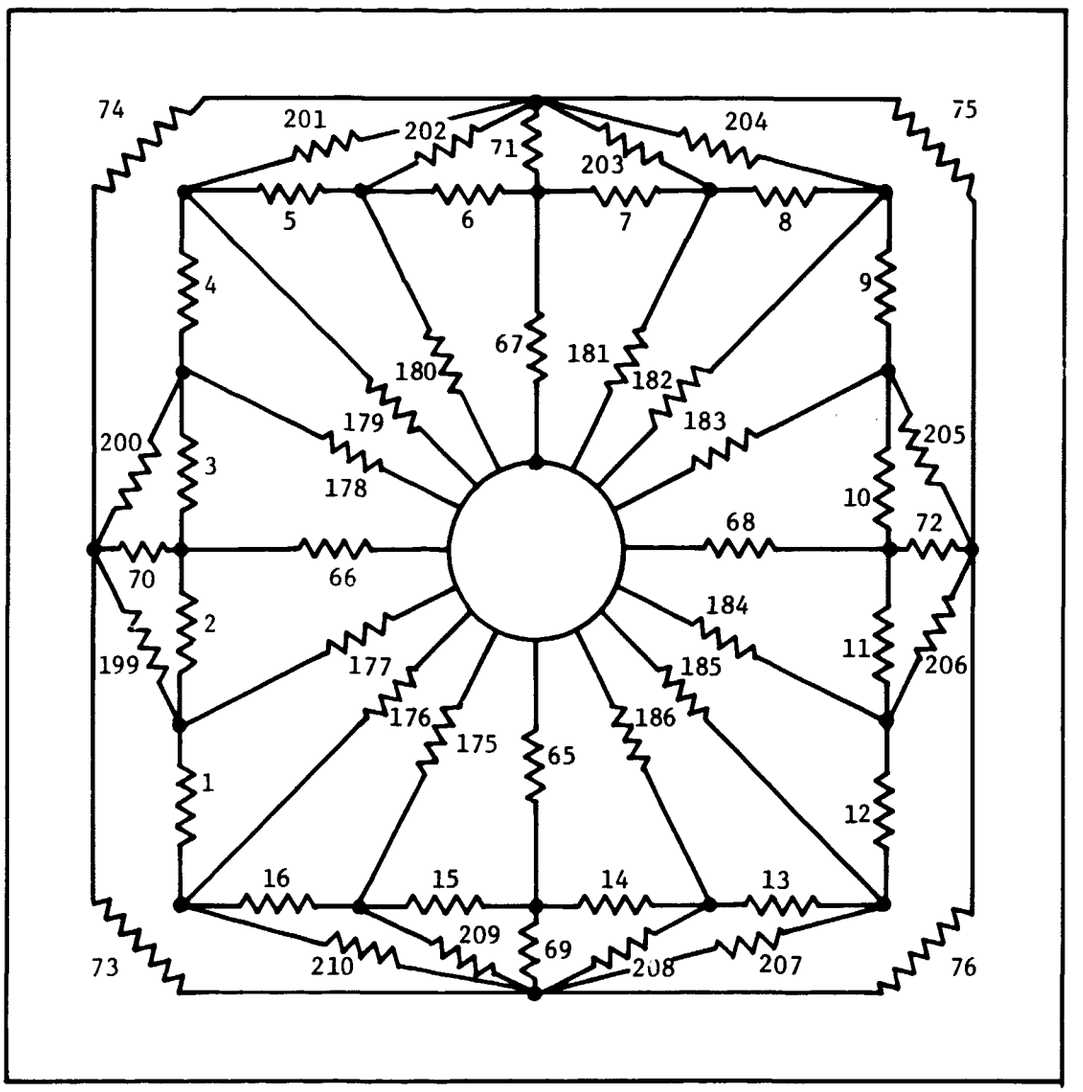

Figure 41: THERMAL ANALYZER CONDUCTOR NOMENCLATURE---BASE DECK

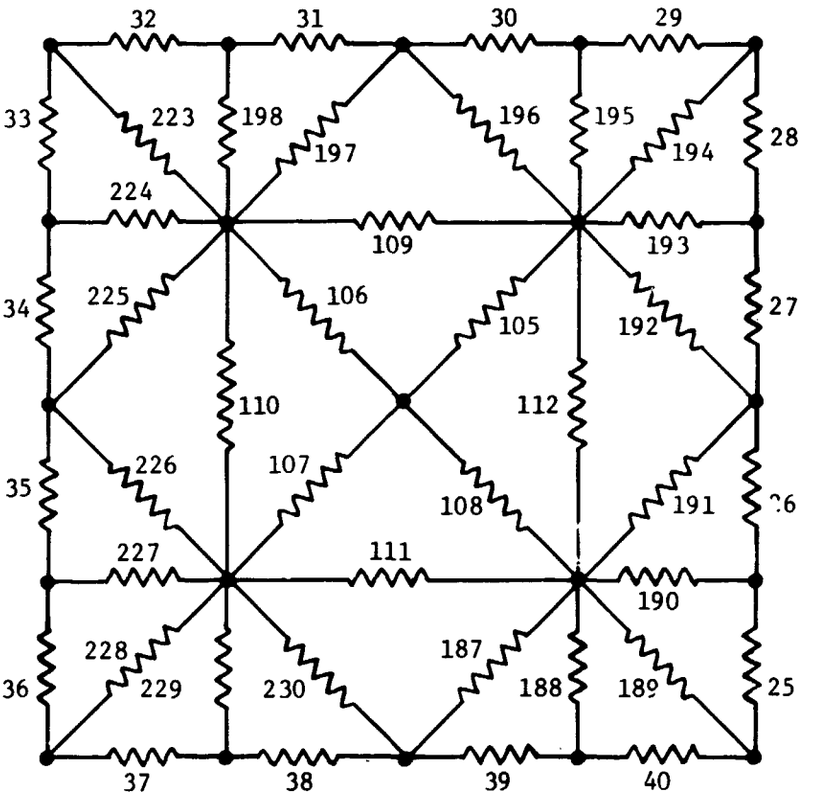

Figure 42: THERMAL ANALYZER CONDUCTOR NOMENCLATURE---EQUIPMENT DECK

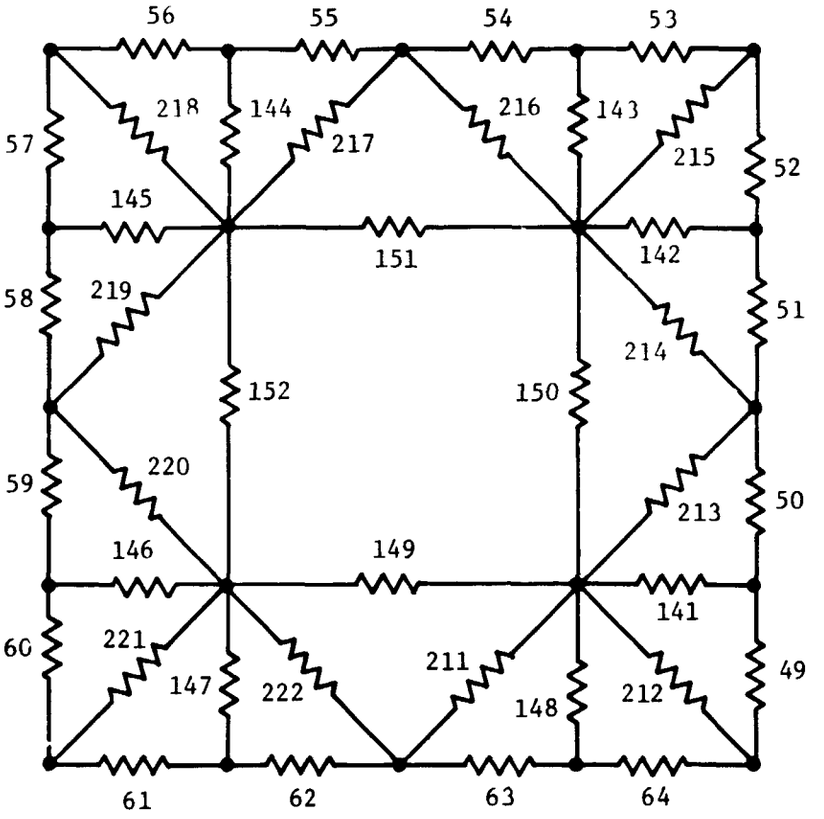

Figure 43: THERMAL ANALYZER CONDUCTOR NOMENCLATURE---CLOSURE DECK

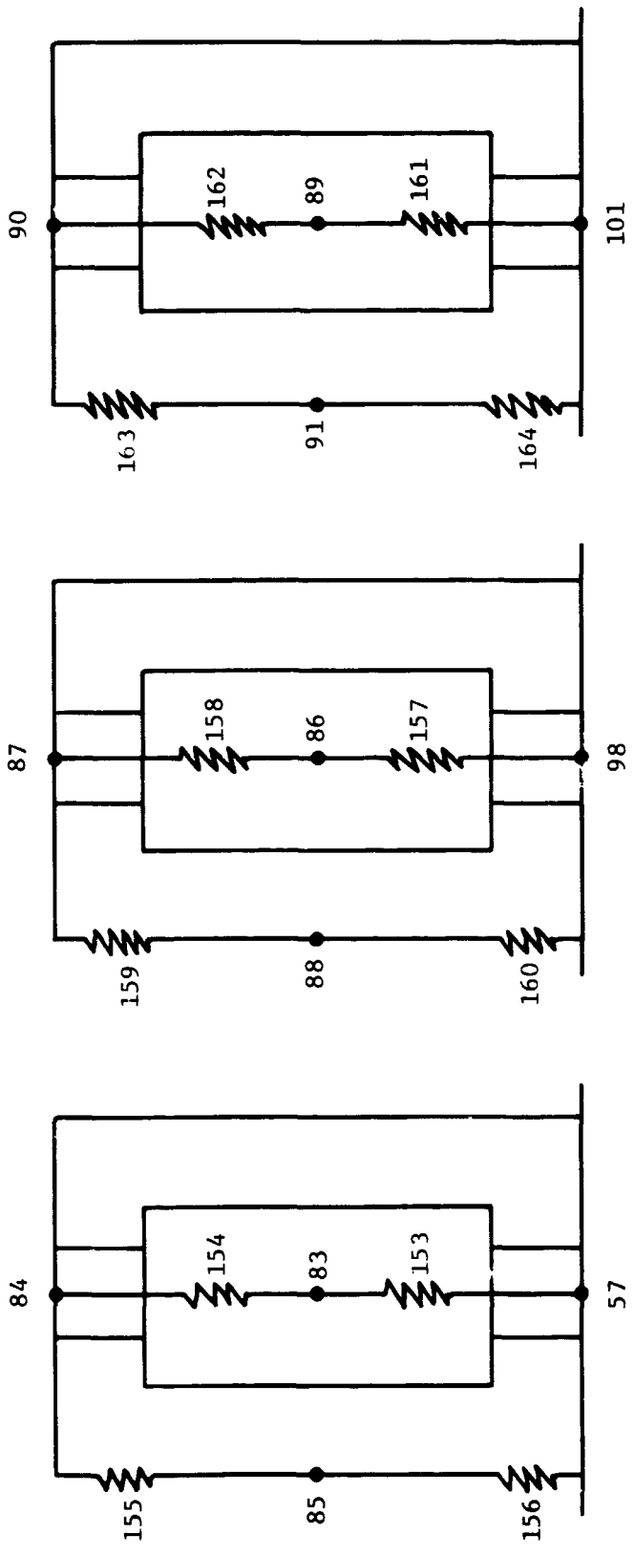

Figure 44: THERMAL ANALYZER CONDUCTOR NOMENCLATURE---HEATER CANISTERS

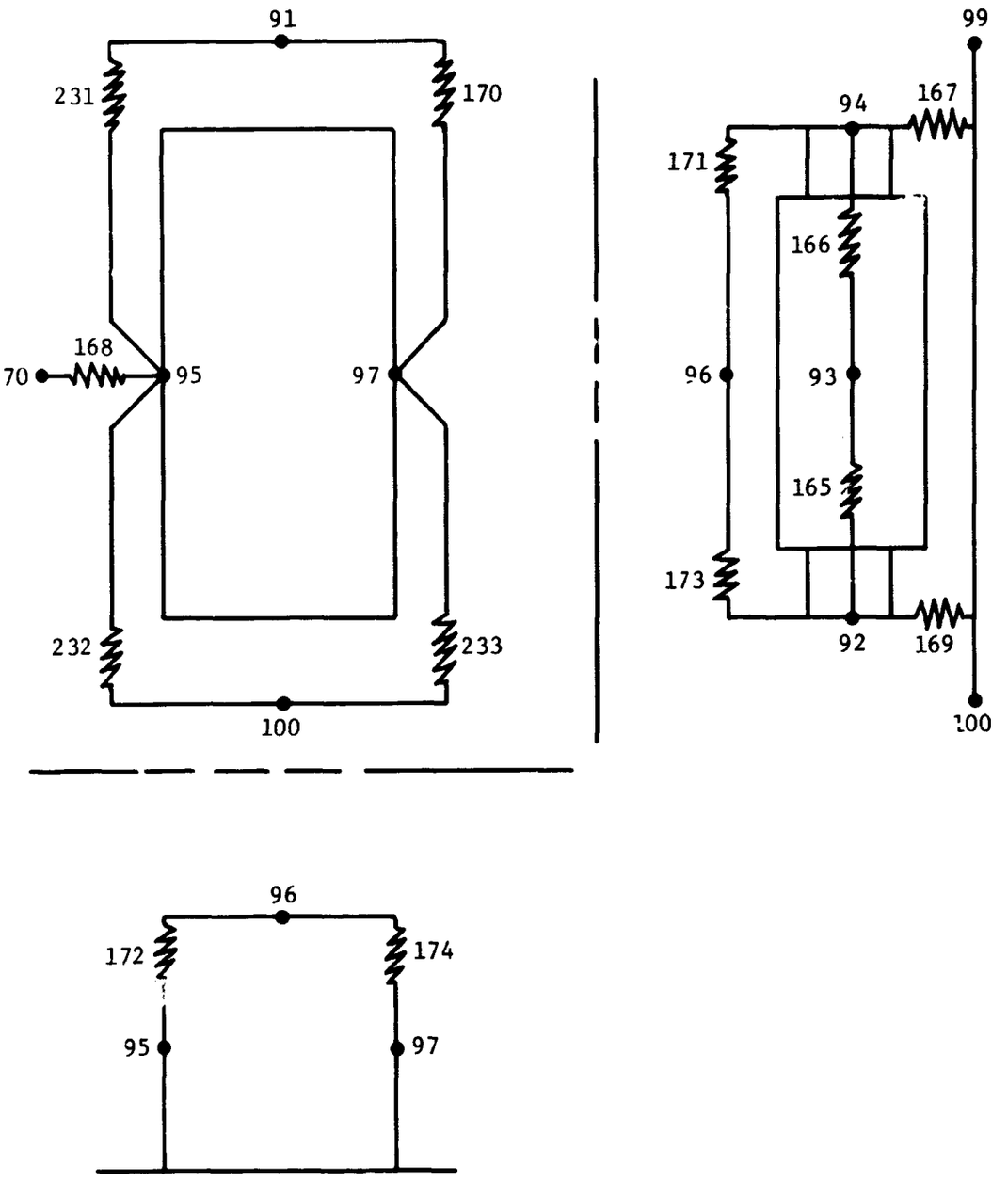

Figure 45: THERMAL ANALYZER CONDUCTOR NOMENCLATURE---HEATER BOX

7.0 DISCUSSION OF RESULTS

At the completion of this study, four sets of results were available for comparison; numerical and experimental data (steady state and transient) for both the prototype and half scale vehicles. The discussion of these results will be subdivided into two major sections; steady state and transient. The transient results will be presented briefly while considerably greater emphasis will be placed on the steady state results.

7.1 Steady State Results

The steady state results are compared and discussed in the following fashion. Steady state numerical and corresponding experimental results for each of the vehicle tests are compared to show the accuracy of numerical calculations. Steady state experimental results for both vehicles are compared to show the accuracy of scale modeling techniques. In addition, the half scale numerical results have been recomputed to account for known compromises of the scaling criteria in the half scale model. The resulting two sets of half scale numerical data are then used to adjust the half scale experimental data. This adjusted experimental data is compared with the prototype experiment to illustrate the advantage of using numerical techniques to correct experimental data.

7.1.1 Comparison of Numerical Experimental Results.- A tabulated comparison of the numerical and experimental results for the half scale and prototype test sequences are presented in Tables 19 through 34. Each table presents the results of a single test on the particular vehicle identified.

The first column identifies the node/thermocouple designation and gives a general idea of its location. The next two columns present the experimentally measured and numerically computed temperatures for each node. The final two columns tally the differential temperature between

analysis and experiment and the ratio of the experimental to analytic temperatures, respectively.

The ratios of experimental to analytic temperatures have been summarized in Figures 46 to 49. Here they are plotted in half percent increments and separated to show uninsulated and insulated, half scale and prototype results, respectively. Additionally, Figures 46 and 47 have the results of test number three separated from the remaining uninsulated test results.

The examination of the results in this fashion has lead to a number of observations which are significant in terms of achieving the goals of this study. A discussion of these points of interest follow on an item by item basis.

Examination of Figures 46 and 47 show that both the prototype and half scale model have a 5-1/2 percent systematic error for test number 3. Test number 3 was a prolonged cold soak with only a single heater operating. The mean steady state temperature was on the order of 270°R (150°K) in both cases. A reexamination of the emissivity of the B-1060 white thermal control coating indicated a strong temperature dependency at low temperatures. The emissivity was subsequently measured as 0.7 at this low temperature.

Examination of the temperature distributions across the base deck (Tables 19 through 34) indicates temperature differences as great as 45°R (25°K) in a region assumed isothermal and represented by a single node in the numerical analysis. The noding in the base deck should have been considerably more detailed.

Examination of the temperature distributions on the heater canisters and heater box when those heaters are operating (Tables 20 through 22 and 25 through 27) indicates that the heater temperatures are being poorly predicted.

The heater core is noded as a single lumped node as shown in the sketch below:

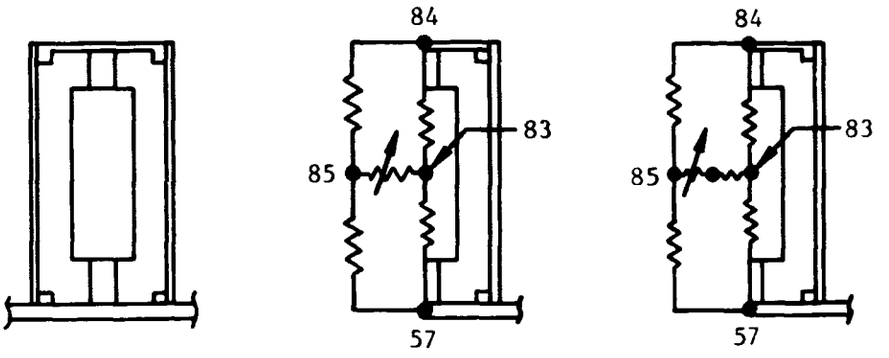

Heater Physical Model | Present Nodal Model | More Realistic Nodal Model

The problem appears to be one of obtaining the correct balance of radiation and conduction fluxes between the heater itself and the heater shell. The present nodal model operates at a lower average heater core temperature than the core surface which radiates predominately to the cylindrical portion of the surrounding shell. This nodal model thus forces more energy around the shell (nodal path 84-84-85-57) than occurs in the actual configuration. The more realistic nodal model shown would tend to correct this problem.

An examination of the results for nodes 79 and 81 on the external skin (on the sun facing upper closure) as shown in Tables 19 through 23 indicates relatively high temperatures predicted by analysis over the experimentally determined results. This is due to inaccuracies in the experimentally determined value of solar absorptivity for the bare aluminum surface.

These higher temperatures are not found in the prototype results (Tables 24 through 27) as the value of solar absorptivity used in that

analysis was back calculated from the analysis results as necessary to force agreement with the experiment.

Figures 48 and 49 show a comparison of data for the insulated half scale and prototype vehicles, respectively. The systematic error here appears due to inaccuracies in the value of effective conductivity utilized for the multilayer insulation in the calculations. The greater and more uniformly distributed range of differences is probably due to differences in effective conductivity particularly in the widely differing cases here of solar illumination of horizontal blankets and space facing vertical blankets.

In general, these problem areas located as a result of numerical and experimental comparisons can be rectified in the analysis. More experimental work in the form of component testing can be performed to:

1) determine temperature dependency of emissivity of thermal control coatings,
2) determine solar absorptivity of aluminum surfaces more accurately, and
3) determine effective conductivity of multilayer insulation blankets both under sun facing and space facing conditions.

The model can be noded in more detail particularly in the areas of:

1) selecting isothermal-nodes more carefully and
2) noding critical heater elements, so as to a allow a radiation/conduction balance which has a more accurate physical basis.

While it is felt that these modifications in the analytic scheme would greatly improve the results, time was lacking for this detailed a reconsideration of the analysis. However, the results are good for the uninsulated tests which show a standard deviation on the order of 2 percent. The insulated vehicle tests indicate a slightly greater standard deviation of 3 percent. Certainly an acceptable range of error for the level of detail to which the models were noded.

7.1.2 Comparison of the Experimental Results.- A tabulated comparison of the experimental results for the half scale and prototype vehicles are presented in Tables 35 through 42. Each table presents the results of a single test on both vehicles. The table format is arranged as in the previous section.

The ratios of the half scale/prototype temperatures have been summarized in Figures 50 and 51. Again they are plotted in half percent increments and separated to show uninsulated and insulated model results. From the figures it is evident that the correlation between the scale model and prototype uninsulated test results is better than the correlation between numerical and experimental results. This is mainly due to the inability of the numerical models to represent the physical reality of the experimental models which includes:

1) temperature dependence of thermal control coatings radiative properties and
2) an equivalent continuous model rather than the discrete nodal analysis model.

All of the half scale data points predict the prototype data within 2 percent except for the two nodes (numbers 79 and 81) on the bare aluminum sun facing upper closure surface. Here, differences on the order of 2 to 4 percent result from a lack of preservation of the radiative properties of the materials. The solar absorptivities of the two materials are tabulated in Appendix A. Differences between the models as a result of variable temperature dependence of thermal conductivity, and the use of aluminum silicate for the heater cores in both models have appeared to have a minor effect on the results.

The experimental data for the insulated vehicles does not compare as well as the uninsulated experiments. While the blanket systems were identical in design, the ratio of blanket surface area/blanket edge perimeter was different for the two configurations. This resulted in relatively greater edge losses for the half scale model.

The scatter in the data between the two has increased due to this edge loss effect on performance, and perhaps additionally due to inhomogeneities in blanket fabrication and attachment.

Uncertainty in multilayer insulation performance is seen to dominate the thermal scale modeling results. Greater effort will have to be placed on component testing to determine insulation performance and scale modeling techniques if scale modeling of insulated systems is to become a practical reality.

7.1.3 Numerical Adjustment of Experimental Data.- After the numerical analysis had been completed for the half scale model (as it had been built) in an effort to duplicate the experimental results, the nodal network was adjusted to predict the half scale model results as it should have been built.

That is, the following changes in the numerical analysis were made:

1) The thermal conductivity of the half scale model materials were given the same relative temperature dependence as the prototype materials.
2) The heater power dissipated in each of the heaters was scaled to that dissipated in the prototype tests.
3) The solar heating loads on each of the external nodes were scaled to those loads incident on the prototype.
4) The equipment deck on the half scale model was designed as a 0.040 (0.1016 cm) thickness. The shop fabricated the model with an 0.044 (0.1118 cm) plate and this thickness was used in the analysis. In the revised analysis the 0.040 (0.1016 cm) plate was treated.
5) The radiative properties of the prototype were substituted to comply with the scaling requirement for preservation of radiative properties.

The results of this study are tabulated in Tables 43 through 47 for the uninsulated tests. The first column identifies the node/thermocouple designation and its location. The next three columns tabulate the half scale experimental results, the correction factor derived from a comparison of the two numerical studies, and finally the adjusted half scale experimental data. The fourth column tabulates the prototype experimental data and the last column lists the ratio of corrected half scale/prototype experimental results. The ratios of corrected half scale/prototype experimental results are plotted in Figure 52.

While this correction scheme has shifted the distribution slightly no significant improvement has been made in the scatter of the data. This is felt due to a combination of causes. One being the poor noding of the base deck and heater elements which forces larger errors in the analysis than existing in the scaled experimental data. The other being the determination of the solar absorptivity of the prototype 6061-T6 aluminum surface as inferred from the prototype analysis. If this α_s had been experimentally determined with the same error as for the half scale material, then the temperature corrections could have resulted in substantial improvements for these nodes (79 and 81) rather than the minimal adjustments indicated.

This attempt to numerically adjust the experimental data has resulted in almost negligible improvement in the experimental correlations. This technique might have shown more promise if:

1) the numerical analysis had been redone to account for the previously noted deficiencies and
2) a smaller scale model (on the order of 1/4 - 1/6) had been tested with its resulting larger compromise induced deviations from the prototype results.

As a result, no attempt was made to numerically adjust the insulated test data due to their even larger error bands.

7.1.4 Summary of Steady State Results.- Table 48 has been prepared as a summary of the steady state results. Each of the comparisons previously discussed is entered in the table which indicates its systematic error, its range of error, and its standard deviation. In cases of experiment and numerical analysis, the analysis is compared to the experiment. In the experimental comparisons the half scale tests are compared to the prototype results.

A comparison of experiment and analysis for tests numbers 1, 2, 4 and 5 shows a negligible (0.1 percent) systematic error and a standard deviation of approximately 2 percent. It may seem surprising that the analysis predicted the half scale experiment with a smaller standard deviation than the prototype experiment. This is a chance occurrence due to:

1) The nodal model being developed and adjusted initially for the half scale vehicle. Thus, when noticeable disagreements occurred, the half scale model was carefully examined and several manufacturing errors were discovered and subsequently accounted for. This was not done for the prototype.

2) The distributions obtained are not ideally gaussian and other measures of error (i.e. a two sigma distribution) would show nearly identical results for the two vehicles. Note that the total range of error is 8.1 percent for the half scale and 8.2 percent for the prototype.

A comparison of test and analysis for test number three shows the 5.5 percent systematic error which was discussed previously as a result of the temperature dependency of the B-1060 thermal control coating. The standard deviation on the order of 1 percent is typical of the results of a single test as opposed to the group of tests reported previously.

A comparison of the two experiments, before and after correction of the half scale experimental data, shows a rather interesting effect. The raw data indicated a 0.5 percent systematic error and a 0.7 percent standard deviation. The adjusted experimental comparison shows a 0.1 percent systematic error and a 1.0 percent standard deviation. The improvement in systematic error is due to accounting for the non-similar temperature dependencies of the thermal conductivities of the materials. As both the standard deviation and the range of error increased slightly it is possible that utilizing the numerical model and its inaccuracies had a tendency to worsen the experimental comparison.

The $\pm$ 0.7 percent standard deviation reported for the comparison of the experimental results corresponds to a $\pm$ 0.47 percent probable error. An examination of the predicted probable error (Figure 3) for a half scale model as a result of inherent uncertainties indicates errors on the order of $\pm$ 1.2 percent for nodes which are not solar illuminated and $\pm$ 3.6 percent for solar illuminated nodes. It must be remembered that the probable error prediction forming the basis for Figure 3 was a maximum probable error based on alternative formulations of the scaling criteria. The corresponding minimum probable error was on the order of $\pm$ 3 percent for nodes which are not solar illuminated and $\pm$ 0.9 percent for solar illuminated nodes. The experimentally determined probable error of $\pm$ 0.47 percent falls within the predicted $\pm$ 0.3 to $\pm$ 0.9 percent range. An examination of Tables 35 through 39 shows that nodes 79 and 81 (the solar illuminated nodes) have larger errors as would be expected from the results of the statistical analysis.

The results of the insulated tests show greater systematic errors and standard deviations than the corresponding cases for the uninsulated tests. However, these tests showed a larger systematic error in the experiment than in the analysis. This perhaps results from the differences between the analysis (which handled heat transfer through the insulation in a one dimensional fashion) and experiment which had significantly different edge losses in the half scale insulation blanket than in the prototype.

Overall, however, good agreement has been shown both between the results of analysis and experiment, and in comparison of the experimental results themselves. Numerical correction of the experimental data has also assisted in reducing the systematic error in the half scale experiment.

7.2 Transient Results

This section will briefly present and comment on the transient results of these experiments.

The transient scaling criteria

$$\frac{t_m}{t_p} = \frac{d_m}{d_p} \frac{(\rho\, c_p)_m}{(\rho\, c_p)_p} \tag{87}$$

relates the model time scale to that of the prototype under the assumptions of temperature preservation and geometric distortion.

For the two vehicles tested, four characteristic pairs of materials and thicknesses were utilized as presented in Table 49. As a result, four unique characteristic time scales are associated with different elements of the vehicles. All of the structural elements, skin panels,

TABLE 49. RELATIVE TIME SCALES FOR MODEL MATERIALS

Prototype Material	Characteristic Thickness (in.)	$(\rho\, c_p)_p$ at 535°R (Btu/ft^3 °R)	Model Material	Characteristic Thickness (in.)	$(\rho\, c_p)_m$ at 535°R (Btu/ft^3 °R)	t_m/t_p
6061-T6	0.125	36.41	7075-T6	0.040	36.13	0.317
7075-T6	0.0625	36.13	2024-0	0.010	36.29	0.161
Aluminum Silicate	1.50	28.68	Aluminum Silicate	0.750	28.68	0.500
B-1060	0.010		B-1060	0.010		1.000

and heater canisters relate by a factor of 0.317. The heater box shell relates by a factor of 0.161 and the heater cores relate by a factor of 0.50. The thick white thermal control coating B-1060 applied over a major portion of the exterior of the vehicles has the same character istic time scale for both vehicles.

In advance of the experiments it was anticipated that the tests involving heater adjustments would be dominated by the time factor for the lava block heater cores. Additionally, it was thought that changes in the solar conditions would allow the time factor for the structural components (6061-T6 aluminum) to dominate the transient response.

Figures 53 through 56 present plots of the transient results for tests numbers two and three for selected nodes. The nodes selected were:

Node	Location
59	Extended base deck
85	Heater shell
70	Equipment deck
81	Sun facing upper closure

Consider Figure 53 which examines transient results for node 59 on the over extended base deck. In test number 1 the solar beam was turned on and the model was allowed to reach equilibrium. At the beginning of test number 2 the base deck heater was activated. After equilibrium was reached, test number 3 was initiated by turning off the solar beam. The transient sequences resulting from these latter two test conditions are shown.

Discounting the differences in temperature and examining only the relative transient effects, several observations are in order.

1) The numerical analysis predicts the prototype experimental response with a high degree of accuracy for most tests.

2) Test number two involved power dissipation from a heater mounted on the base deck. The half scale transient time has been scaled by a factor of two as the heater core dominated the transient results. With the factor of two scaling the characteristic times, the half scale and prototype experiments show good agreement for the transient results.

3) Test number three involved turning the solar beam off. As this event had its immediate effect on the exterior surface of the vehicle it was felt that the scaling time factor would be that of the 6061-T6 aluminum frame and skin panels. The half scale transient data is plotted with the time scale expanded both by a factor of 2.0 and 3.16. The scaling factor of 2.0 shows better agreement than the 3.16 factor for the skin elements. This is due to the white thermal control coating.

Consider the calculation of the volume and mass of the aluminum and coating materials at node 59 which is presented in Table 50.

TABLE 50. MASS OF VEHICLE SKIN COMPONENTS AT NODE 59

	Volume ($in.^3$)	Mass (lb_m)
Prototype		
Aluminum	7.81	0.781
B-1060	2.50	0.100
Half Scale		
Aluminum	0.625	0.0625
B-1060	0.625	0.025

While the B-1060 coating was only 1/8 of the mass of the prototype node, it represented 1/3 of the mass of the half scale node. This has resulted in an increase in the characteristic response time of nodes coated with B-1060. As the temperature

changes were substantial in these tests, the response times of the heater cores also contributed to the overall vehicle response. Thus, it is observed from Figure 53 that the characteristic response time lies between the two values plotted. The rest of the figures are plotted with a factor of two increase in the half scale experimental times for both tests.

No special emphasis was placed on scaling the transient response of the half scale model, as indicated in Section 4.1, as it was expected that numerical analysis would allow a correction of transient response data.

If it had been desired that the half scale model experimentally verify the full scale transient sequence, other scaling compromises would have been desirable. These compromises were discussed in Section 4.1 on Transient Response. In general, three choices are available to the designer:

1) the best selection of materials for steady state response,
2) the best selection of materials for transient response, or
3) optimization of selection for minimum errors in both steady and transient response.

In most cases "perfect" scale modeling is not possible and scaling compromises must be made. Ultimately numerical analysis of the "as built" model is used to demonstrate agreement with the experiment and then to adjust the experimental results from the "as built" model condition to the theoretical model condition.

TABLE 19. STEADY STATE TEMPERATURES

MODEL	Half Scale Model
TEST	1
CONDITIONS	Sun on Heater #1 off Heaters #2, 3, 4 off

NODE	EXPERIMENT (^{o}R)	ANALYSIS (^{o}R)	INCREMENT (^{o}R)	INCREMENT (Ratio)
Base Deck				
57a	381.5	365.4	-16.1	1.044
57b	384.3	365.4	-18.9	1.052
59	391.4	400.7	+ 9.3	0.977
Heater One				
83	375.1	366.7	- 8.4	1.023
84	380.1	367.7	-12.4	1.034
85	380.1	367.5	-12.6	1.034
Equipment Deck				
70a	398.5	398.8	+ 0.3	0.999
70b	398.5	398.8	+ 0.3	0.999
Heater Two				
87	397.8	399.0	+ 1.2	0.997
88	397.8	398.6	+ 0.8	0.998
Heater Three				
90	398.5	398.8	+ 0.3	0.999
91	397.8	398.4	+ 0.6	0.998
Heater Four				
95	398.5	398.8	+ 0.3	0.999
96	399.9	400.4	+ 0.5	0.999
97	397.1	398.7	+ 1.6	0.996
External Skin				
64	389.3	387.1	- 2.2	1.006
77	408.0	402.6	- 5.4	1.013
73	406.8	401.3	- 5.5	1.014
79	453.5	456.7	+ 3.2	0.993
81	451.6	457.4	+ 5.8	0.987

TABLE 20. STEADY STATE TEMPERATURES

MODEL Half Scale Model

TEST 2

CONDITIONS Sun on
Heater #1 on
Heaters #2, 3, 4 off

NODE	EXPERIMENT (^{o}R)	ANALYSIS (^{o}R)	INCREMENT (^{o}R)	INCREMENT (Ratio)
Base Deck				
57a	428.1	408.6	-19.5	1.048
57b	410.0	408.6	- 1.4	1.003
59	407.3	413.1	+ 5.8	0.986
Heater One				
83	709.9	719.1	+ 9.2	0.987
84	468.8	482.7	+13.9	0.971
85	483.9	469.4	-14.5	1.031
Equipment Deck				
70a	410.7	414.3	+ 3.6	0.991
70b	410.7	414.3	+ 3.6	0.991
Heater Two				
87	411.3	412.6	+ 1.3	0.997
88	411.3	412.2	+ 0.9	0.998
Heater Three				
90	411.3	412.4	+ 1.1	0.997
91	412.7	412.0	- 0.7	1.002
Heater Four				
95	411.3	413.0	+ 1.7	0.996
96	412.0	414.2	+ 2.2	0.995
97	409.3	412.4	+ 3.1	0.992
External Skin				
64	403.3	401.8	- 1.5	1.004
77	417.4	413.1	- 4.3	1.010
73	416.7	412.1	- 4.6	1.011
79	461.8	466.3	+ 4.5	0.990
81	459.3	466.9	+ 7.6	0.984

TABLE 21. STEADY STATE TEMPERATURES

MODEL Half Scale Model

TEST 3

CONDITIONS Sun off
Heater #1 on
Heaters #2, 3, 4 off

NODE	EXPERIMENT (^{o}R)	ANALYSIS (^{o}R)	INCREMENT (^{o}R)	(Ratio)
Base Deck				
57a	318.6	304.0	-14.6	1.048
57b	288.7	304.0	+15.3	0.950
59	275.0	253.9	-21.1	1.083
Heater One				
83	686.2	664.7	-21.5	1.032
84	385.8	388.7	+ 2.9	0.992
85	384.3	371.9	-12.4	1.033
Equipment Deck				
70a	268.0	254.6	-13.4	1.053
70b	268.0	254.6	-13.4	1.053
Heater Two				
87	267.2	252.3	-14.9	1.059
88	267.2	252.3	-14.9	1.059
Heater Three				
90	267.2	252.4	-14.8	1.059
91	268.0	252.4	-15.4	1.062
Heater Four				
95	267.2	252.9	-14.3	1.056
96	267.2	252.5	-14.7	1.058
97	267.2	252.4	-14.8	1.059
External Skin				
64	271.5	254.6	-16.9	1.066
77	264.6	247.6	-17.0	1.069
73	264.6	248.1	-16.5	1.066
79	263.7	248.0	-15.7	1.063
81	263.7	247.8	-15.9	1.064

TABLE 22. STEADY STATE TEMPERATURES

MODEL	Half Scale Model
TEST	4
CONDITIONS	Sun on Heater #1 off Heaters #2, 3, 4 on

NODE	EXPERIMENT (^{o}R)	ANALYSIS (^{o}R)	INCREMENT (^{o}R)	INCREMENT (Ratio)
Base Deck				
57a	408.0	396.0	-12.0	1.030
57b	412.7	396.0	-16.7	1.042
59	414.7	423.6	+ 8.9	0.979
Heater One				
83	401.3	398.7	- 2.6	1.006
84	408.7	400.6	- 8.1	1.020
85	408.0	400.2	- 7.8	1.019
Equipment Deck				
70a	458.6	459.4	+ 0.8	0.998
70b	455.5	459.4	+ 3.9	0.992
Heater Two				
87	477.1	483.9	+ 6.8	0.986
88	472.0	475.9	+ 3.9	0.992
Heater Three				
90	488.8	493.6	+ 4.8	0.990
91	482.1	483.7	+ 1.6	0.997
Heater Four				
95	478.4	471.9	- 6.5	1.014
96	488.8	481.2	- 7.6	1.016
97	472.0	471.7	- 0.3	1.001
External Skin				
74	422.7	425.1	+ 2.4	0.994
77	445.3	443.3	- 2.0	1.004
73	444.0	443.5	- 0.5	1.001
79	487.0	495.7	+ 8.7	0.982
81	484.5	495.8	+11.3	0.977

TABLE 23. STEADY STATE TEMPERATURES

MODEL	Half Scale Model
TEST	5
CONDITION	Sun off Heater #1 off Heaters #2, 3, 4 on

NODE	EXPERIMENT (^{o}R)	ANALYSIS (^{o}R)	INCREMENT (^{o}R)	(Ratio)
Base Deck				
57a	310.6	299.3	-11.3	1.038
57b	313.0	299.3	-13.7	1.046
59	308.2	297.8	-10.4	1.035
Heater One				
83	305.7	300.4	- 5.3	1.018
84	309.0	301.3	- 7.7	1.026
85	309.8	301.1	- 8.7	1.029
Equipment Deck				
70a	358.9	355.3	- 3.6	1.010
70b	354.4	355.3	+ 0.9	0.997
Heater Two				
87	379.4	380.7	+ 1.3	0.996
88	373.7	370.7	- 3.0	1.008
Heater Three				
90	393.6	392.3	- 1.3	1.003
91	385.8	379.8	- 6.0	1.016
Heater Four				
95	380.1	367.2	-12.9	1.035
96	391.4	377.0	-14.4	1.038
97	373.7	366.8	- 6.9	1.019
External Skin				
64	321.7	320.4	- 1.3	1.004
77	326.2	327.7	+ 1.5	0.995
73	328.4	329.2	+ 0.8	0.998
79	327.6	330.9	+ 3.3	0.990
81	326.9	330.4	+ 3.5	0.989

TABLE 24. STEADY STATE TEMPERATURES

MODEL	Prototype Vehicle
TEST	1
CONDITIONS	Sun on Heater #1 off Heaters #2, 3, 4 off

NODE	EXPERIMENT (^{o}R)	ANALYSIS (^{o}R)	INCREMENT (^{o}R)	INCREMENT (Ratio)
Base Deck				
57a	382.5	371.2	-11.3	1.030
57b	387.4	371.2	-16.2	1.043
59	398.1	405.2	+ 7.1	0.982
Heater One				
83	-*	372.4	-	-
84	382.5	373.2	-10.3	1.025
85	382.5	373.1	-10.4	1.025
Equipment Deck				
70a	400.2	403.0	+ 2.8	0.993
70b	400.8	403.0	+ 2.2	0.994
Heater Two				
87	404.2	402.6	- 1.6	1.004
88	401.5	402.2	+ 0.7	0.998
Heater Three				
90	403.5	402.7	- 0.8	1.002
91	401.5	402.2	+ 0.7	0.998
Heater Four				
95	402.9	403.6	+ 0.7	0.998
96	402.9	405.4	+ 2.5	0.994
97	400.8	403.4	+ 2.6	0.994
External Skin				
64	390.3	392.5	+ 2.2	0.994
77	412.3	403.8	- 8.5	1.021
73	410.9	403.0	- 7.9	1.020
79	467.1	467.9	+ 0.8	0.998
81	468.5	468.5	+ 0.1	1.000

* Thermocouple out

TABLE 25. STEADY STATE TEMPERATURES

MODEL Prototype Vehicle

TEST 2

CONDITIONS Sun on
Heater #1 on
Heaters #2, 3, 4 off

NODE	EXPERIMENT (^{o}R)	ANALYSIS (^{o}R)	INCREMENT (^{o}R)	INCREMENT (Ratio)
Base Deck				
57a	429.7	411.0	-18.7	1.045
57b	408.9	411.0	+ 2.1	0.995
59	410.9	417.5	+ 6.6	0.984
Heater One				
83	-*	779.9	-	-
84	497.6	484.4	-13.2	1.027
85	487.8	475.8	-12.0	1.025
Equipment Deck				
70a	411.6	418.1	+ 6.5	0.984
70b	410.9	418.1	+ 7.2	0.983
Heater Two				
87	413.6	415.9	+ 2.3	0.994
88	412.3	415.4	+ 3.1	0.992
Heater Three				
90	413.6	415.9	+ 2.3	0.994
91	413.6	415.5	+ 1.9	0.995
Heater Four				
95	412.9	417.2	+ 4.3	0.990
96	413.6	418.8	+ 5.2	0.988
97	410.9	416.7	+ 5.8	0.986
External Skin				
64	403.5	406.5	+ 3.0	0.993
77	419.6	414.2	- 5.4	1.013
73	419.0	413.6	- 5.4	1.013
79	472.9	477.4	+ 4.5	0.991
81	473.5	478.0	+ 4.5	0.991

* Thermocouple out

TABLE 26. STEADY STATE TEMPERATURES

MODEL	Prototype Vehicle
TEST	3
CONDITIONS	Sun off Heater #1 on Heaters #2, 3, 4 off

NODE	EXPERIMENT (^{o}R)	ANALYSIS (^{o}R)	INCREMENT (^{o}R)	INCREMENT (Ratio)
Base Deck				
57a	321.2	296.6	-24.6	1.083
57b	285.6	296.6	+11.0	0.963
59	276.9	250.3	-26.6	1.106
Heater One				
83	-*	742.2	-	-
84	402.9	376.2	-26.7	1.071
85	392.4	365.6	-26.8	1.073
Equipment Deck				
70a	266.6	255.0	-11.6	1.045
70b	268.3	255.0	-13.3	1.052
Heater Two				
87	266.6	253.5	-13.1	1.052
88	266.6	253.5	-13.1	1.052
Heater Three				
90	267.5	253.4	-14.1	1.056
91	266.6	253.4	-13.2	1.052
Heater Four				
95	267.5	253.8	-13.7	1.054
96	266.6	253.6	-13.0	1.051
97	266.6	253.5	-13.1	1.052
External Skin				
64	271.8	255.1	-16.7	1.065
77	263.1	250.0	-13.1	1.052
73	264.0	250.2	-13.8	1.055
79	263.1	250.2	-12.9	1.052
81	263.1	250.1	-13.0	1.052

* Thermocouple out

TABLE 27. STEADY STATE TEMPERATURES

MODEL	Prototype Vehicle
TEST	4
CONDITIONS	Sun on Heater #1 off Heaters #2, 3, 4 on

NODE	EXPERIMENT (^{o}R)	ANALYSIS (^{o}R)	INCREMENT (^{o}R)	(Ratio)
Base Deck				
57a	406.2	400.8	- 5.4	1.013
57b	410.2	400.8	- 9.4	1.023
59	416.3	427.8	+11.5	0.973
Heater One				
83	- *	403.6	-	-
84	409.6	405.2	- 4.4	1.011
85	407.6	404.8	- 2.8	1.007
Equipment Deck				
70a	459.5	466.1	+ 6.6	0.986
70b	456.3	466.1	+ 9.8	0.979
Heater Two				
87	482.9	481.9	- 1.0	1.002
88	478.6	476.3	- 2.3	1.005
Heater Three				
90	490.2	491.4	+ 1.2	0.998
91	485.4	484.5	- 0.9	1.002
Heater Four				
95	480.5	493.9	+13.4	0.973
96	490.2	505.3	+15.1	0.970
97	476.7	491.3	+13.6	0.970
External Skin				
64	422.3	428.1	+ 5.8	0.986
77	447.3	443.7	- 3.7	1.008
73	446.8	443.8	- 3.0	1.007
79	496.9	506.3	+ 9.4	0.981
81	497.6	506.9	+ 9.3	0.982

* Thermocouple out

TABLE 28. STEADY STATE TEMPERATURES

MODEL Prototype Vehicle

TEST 5

CONDITIONS Sun off
Heater #1 off
Heaters #2, 3, 4 on

NODE	EXPERIMENT ($^{\circ}$R)	ANALYSIS ($^{\circ}$R)	INCREMENT ($^{\circ}$R)	INCREMENT (Ratio)
Base Deck				
57a	310.0	303.1	- 6.9	1.023
57b	310.0	303.1	- 6.9	1.023
59	307.6	300.9	- 6.7	1.022
Heater One				
83	- *	304.0	-	-
84	312.5	304.7	- 7.8	1.026
85	310.8	304.6	- 6.2	1.020
Equipment Deck				
70a	361.2	359.4	- 1.6	1.005
70b	358.2	359.4	+ 1.2	0.997
Heater Two				
87	386.0	371.1	-14.9	1.040
88	383.2	364.4	-15.8	1.052
Heater Three				
90	394.5	381.5	-13.0	1.034
91	388.8	373.4	-15.4	1.041
Heater Four				
95	382.5	388.5	+ 6.0	0.984
96	393.8	402.1	+ 8.3	0.979
97	378.2	386.0	+ 7.8	0.980
External Skin				
64	324.2	319.0	- 5.2	1.016
77	331.8	326.7	- 5.1	1.016
73	332.5	327.4	- 5.1	1.016
79	330.3	329.5	- 0.8	1.002
81	329.5	329.5	0	1.000

* Thermocouple out

TABLE 29. STEADY STATE TEMPERATURES

MODEL Half Scale Model with Insulation

TEST 6

CONDITIONS Sun on
Heater #1 off
Heaters #2, 3, 4 off

NODE	EXPERIMENT (°R)	ANALYSIS (°R)	INCREMENT (°R)	(Ratio)
Base Deck				
57a	368.9	360.3	- 8.6	1.024
57b	371.0	360.3	- 9.7	1.030
59	378.1	394.6	+16.5	0.958
Heater One				
83	367.4	361.4	- 6.0	1.017
84	362.5	362.2	- 0.3	1.001
85	367.4	362.1	- 5.3	1.015
Equipment Deck				
70a	376.6	381.5	+ 4.9	0.987
70b	376.6	381.5	+ 4.9	0.987
Heater Two				
87	375.9	382.7	+ 6.8	0.982
88	375.2	382.7	+ 7.5	0.980
Heater Three				
90	375.9	382.7	+ 6.8	0.982
91	375.9	382.7	+ 6.8	0.982
Heater Four				
95	375.9	382.3	+ 6.4	0.983
96	375.9	382.5	+ 6.6	0.983
97	375.9	382.5	+ 6.6	0.983
External Skin				
64	375.9	383.7	+ 7.8	0.980
77	377.4	382.9	+ 5.5	0.986
73	376.6	383.1	+ 6.5	0.983
79	378.1	382.9	+ 4.8	0.987
81	378.1	382.9	+ 4.8	0.987

TABLE 30. STEADY STATE TEMPERATURES

MODEL Half Scale Model with Insulation

TEST 7

CONDITIONS Sun on
Heater #1 off
Heaters #2, 3, 4 on

NODE	EXPERIMENT (^{o}R)	ANALYSIS (^{o}R)	INCREMENT (^{o}R)	(Ratio)
Base Deck				
57a	439.6	438.5	- 1.1	1.002
57b	442.2	438.5	- 3.7	1.008
59	440.9	448.5	+ 7.6	0.983
Heater One				
83	442.2	443.7	+ 1.5	0.997
84	433.6	447.1	+13.5	0.970
85	441.5	446.4	+ 4.9	0.989
Equipment Deck				
70a	499.3	511.4	+12.1	0.976
70b	496.8	511.4	+14.6	0.971
Heater Two				
87	517.4	538.4	+21.0	0.961
88	513.2	531.8	+18.6	0.965
Heater Three				
90	528.1	547.0	+18.9	0.965
91	522.8	538.8	+16.0	0.970
Heater Four				
95	517.4	526.2	+ 8.8	0.983
96	526.9	533.9	+ 7.0	0.987
97	513.8	526.9	+13.1	0.975
External Skin				
64	467.7	487.6	+19.9	0.959
77	487.7	509.2	+21.5	0.958
73	487.7	509.5	+21.8	0.958
79	489.5	510.7	+21.2	0.958
81	488.9	510.9	+22.0	0.957

TABLE 31. STEADY STATE TEMPERATURES

MODEL Half Scale Model with Insulation

TEST 8

CONDITIONS Sun off
Heater #1 off
Heaters #2, 3, 4 on

NODE	EXPERIMENT (^{o}R)	ANALYSIS (^{o}R)	INCREMENT (^{o}R)	(Ratio)
Base Deck				
57a	380.2	376.0	- 4.2	1.011
57b	380.9	376.0	- 4.9	1.013
59	373.1	361.8	-11.3	1.031
Heater One				
83	380.9	379.3	- 1.6	1.004
84	373.8	381.8	+ 8.0	0.979
85	380.9	381.3	+ 0.4	0.999
Equipment Deck				
70a	442.8	449.8	+ 7.0	0.984
70b	439.6	449.8	+10.2	0.977
Heater Two				
87	461.9	476.9	+15.0	0.968
88	456.8	469.1	+12.3	0.974
Heater Three				
90	473.4	486.4	+13.0	0.973
91	467.7	476.7	+ 9.0	0.981
Heater Four				
95	461.9	463.9	+ 2.0	0.996
96	472.1	472.4	+ 0.3	0.999
97	457.5	464.3	+ 6.8	0.985
External Skin				
64	406.7	418.1	+11.4	0.973
77	426.9	443.3	+16.4	0.963
73	426.9	443.3	+16.4	0.963
79	428.2	444.9	+16.7	0.962
81	427.5	445.2	+17.7	0.960

TABLE 32. STEADY STATE TEMPERATURES

MODEL Prototype Vehicle with Insulation

TEST 6

CONDITIONS Sun on
Heater #1 off
Heaters #2, 3, 4 off

NODE	EXPERIMENT (^{o}R)	ANALYSIS (^{o}R)	INCREMENT (^{o}R)	(Ratio)
Base Deck				
57a	382.5	382.2	- 0.3	1.001
57b	389.5	382.2	- 7.3	1.019
59	401.5	411.1	+ 9.6	0.977
Heater One				
83	378.9	383.8	+ 4.9	0.987
84	381.7	384.8	+ 3.1	0.992
85	381.0	384.7	+ 3.7	0.990
Equipment Deck				
70a	393.1	412.4	+19.3	0.953
70b	393.1	412.4	+19.3	0.953
Heater Two				
87	393.1	414.0	+20.9	0.950
88	393.1	414.0	+20.9	0.950
Heater Three				
90	393.1	414.0	+20.9	0.950
91	392.4	414.0	+21.6	0.948
Heater Four				
95	393.1	413.8	+20.7	0.950
96	393.1	414.2	+21.1	0.949
97	393.1	414.0	+20.9	0.950
External Skin				
64	391.7	411.9	+20.0	0.951
77	395.2	416.6	+21.4	0.949
73	394.5	416.3	+21.8	0.948
79	396.6	424.1	+27.5	0.935
81	398.1	424.3	+26.2	0.938

TABLE 33. STEADY STATE TEMPERATURES

MODEL Prototype Vehicle with Insulation

TEST 7

CONDITIONS Sun on
Heater #1 off
Heaters #2, 3, 4 on

NODE	EXPERIMENT (^{o}R)	ANALYSIS (^{o}R)	INCREMENT (^{o}R)	INCREMENT (Ratio)
Base Deck				
57a	451.9	449.2	- 2.7	1.006
57b	457.6	449.2	- 8.4	1.019
59	460.1	458.7	- 1.4	1.003
Heater One				
83	451.9	455.0	+ 3.1	0.993
84	456.3	458.0	+ 1.7	0.996
85	454.4	457.2	+ 2.8	0.994
Equipment Deck				
70a	515.7	527.0	+11.3	0.978
70b	513.9	527.0	+13.1	0.975
Heater Two				
87	536.0	548.2	+12.2	0.978
88	535.0	543.7	+10.7	0.980
Heater Three				
90	544.3	557.1	+12.8	0.977
91	540.2	551.5	+11.3	0.980
Heater Four				
95	535.7	555.9	+20.2	0.964
96	544.3	564.5	+20.2	0.964
97	533.0	554.2	+21.2	0.962
External Skin				
64	483.5	499.6	+16.1	0.968
77	507.3	523.0	+15.7	0.970
73	506.7	523.2	+16.9	0.968
79	509.1	530.3	+21.2	0.960
81	509.8	530.6	+20.8	0.961

TABLE 34. STEADY STATE TEMPERATURES

MODEL Prototype Vehicle with Insulation

TEST 8

CONDITIONS Sun off
Heater #1 off
Heaters #2, 3, 4 on

NODE	EXPERIMENT ($^{\circ}$R)	ANALYSIS ($^{\circ}$R)	INCREMENT ($^{\circ}$R)	(Ratio)
Base Deck				
57a	381.0	370.3	-10.7	1.029
57b	382.5	370.3	-12.2	1.033
59	373.9	361.2	-12.7	1.035
Heater One				
83	381.0	373.1	- 7.9	1.021
84	384.6	374.9	- 9.7	1.027
85	382.5	374.4	- 8.1	1.022
Equipment Deck				
70a	446.8	442.8	- 4.0	1.009
70b	446.1	442.8	- 3.3	1.007
Heater Two				
87	469.1	460.1	- 9.0	1.020
88	467.1	454.7	-12.4	1.027
Heater Three				
90	478.0	470.0	- 8.0	1.017
91	474.2	463.2	-11.0	1.024
Heater Four				
95	472.9	472.0	- 0.9	1.002
96	477.3	482.8	+ 5.5	0.989
97	464.6	470.0	+ 5.4	0.988
External Skin				
64	410.2	407.1	- 3.1	1.008
77	434.4	428.6	- 5.8	1.014
73	435.1	428.9	- 6.2	1.014
79	435.7	430.4	- 5.3	1.012
81	435.1	430.7	- 4.4	1.010

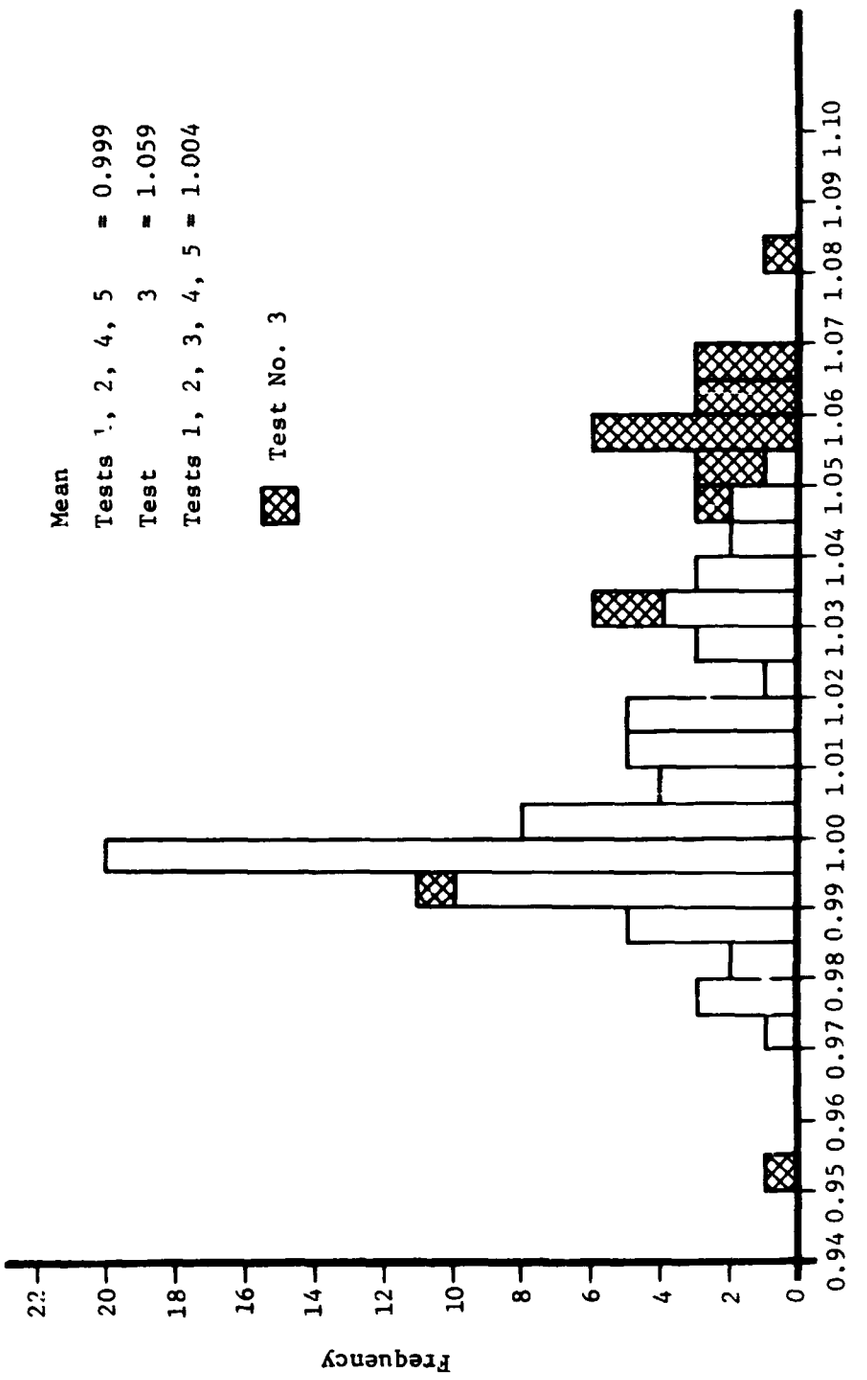

Figure 46: DISTRIBUTION OF DEVIATIONS BETWEEN HALF SCALE EXPERIMENT AND ANALYSIS (TESTS NUMBER 1-5)

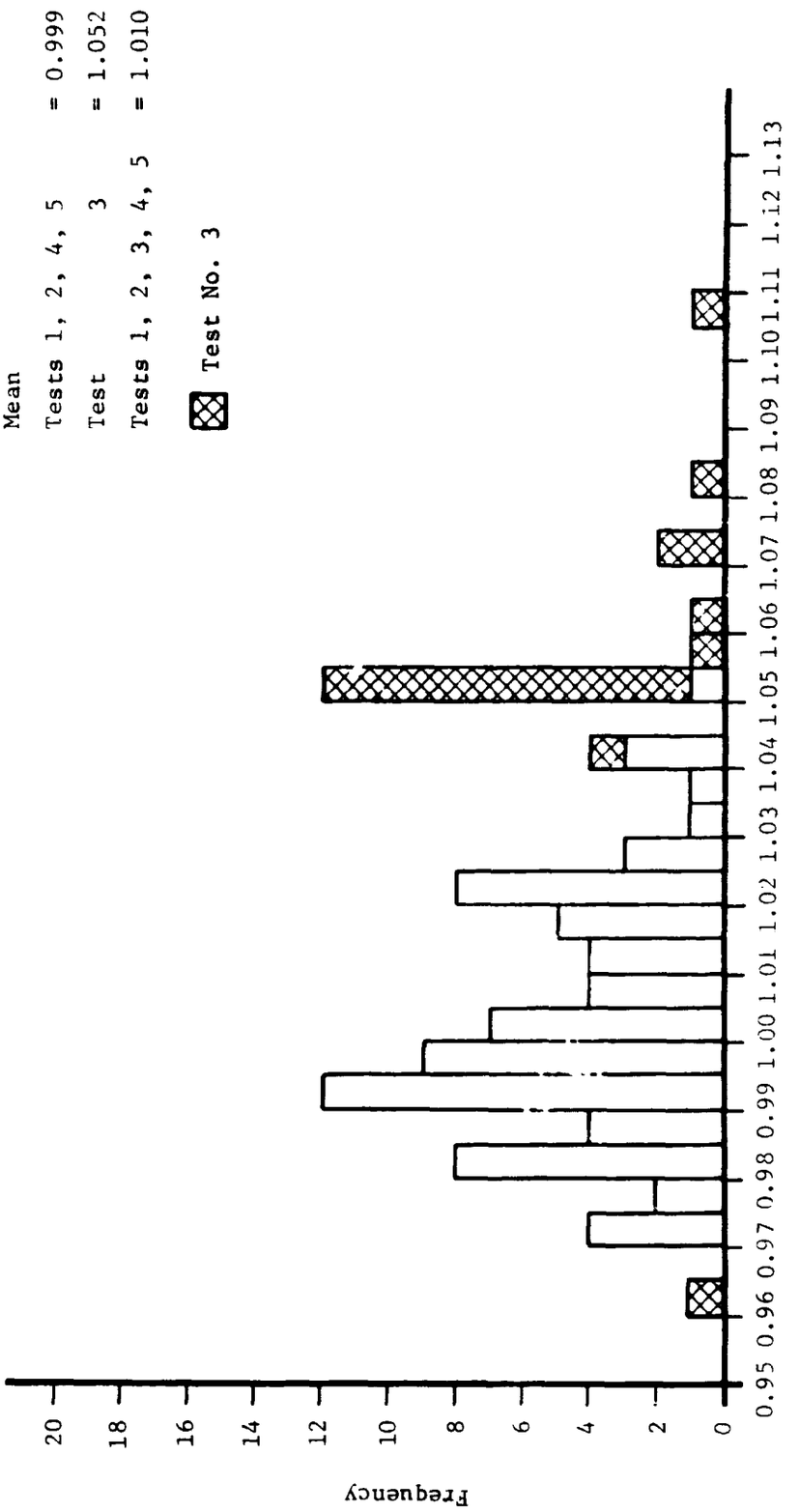

Figure 47: DISTRIBUTION OF DEVIATIONS BETWEEN PROTOTYPE EXPERIMENT AND ANALYSIS (TESTS NUMBER 1-5)

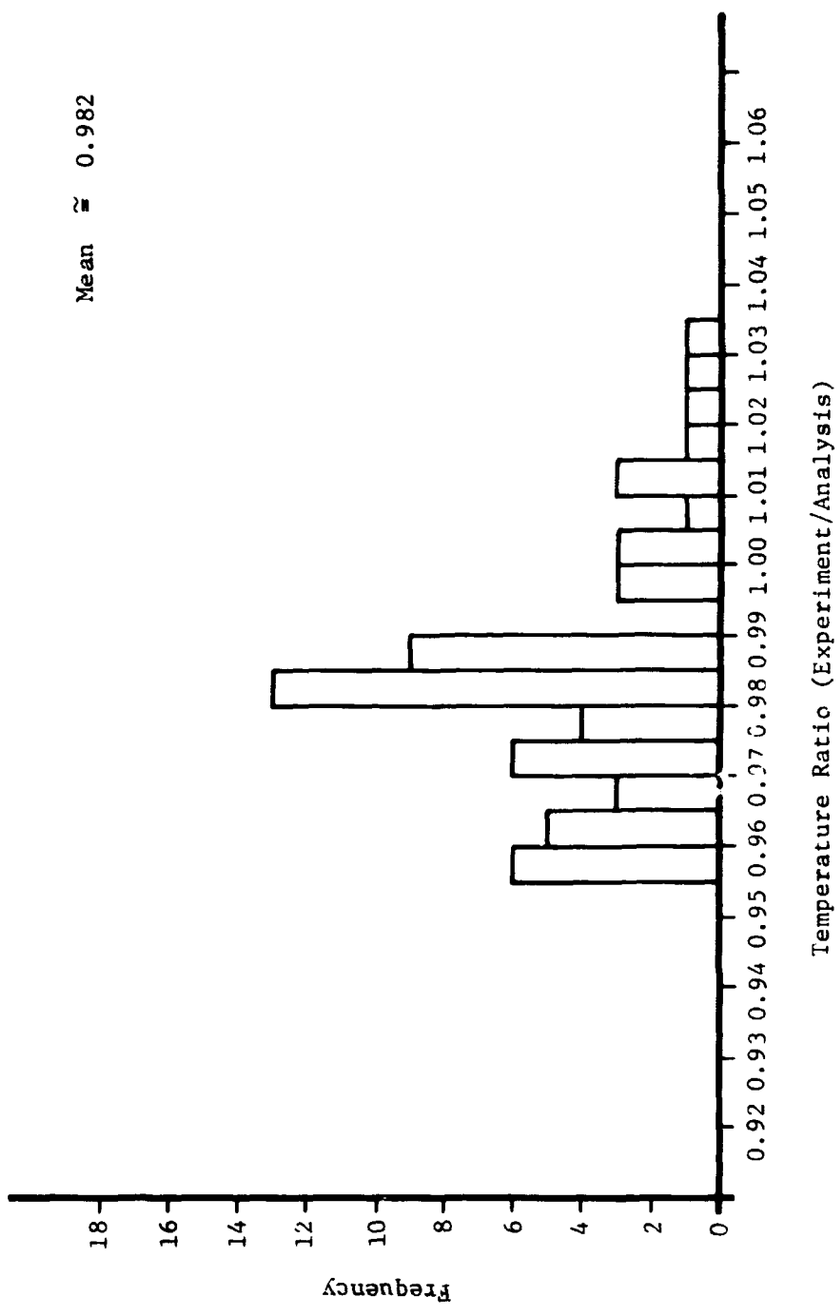

Figure 48: DISTRIBUTION OF DEVIATIONS BETWEEN HALF SCALE EXPERIMENT AND ANALYSIS (TESTS NUMBER 6-8)

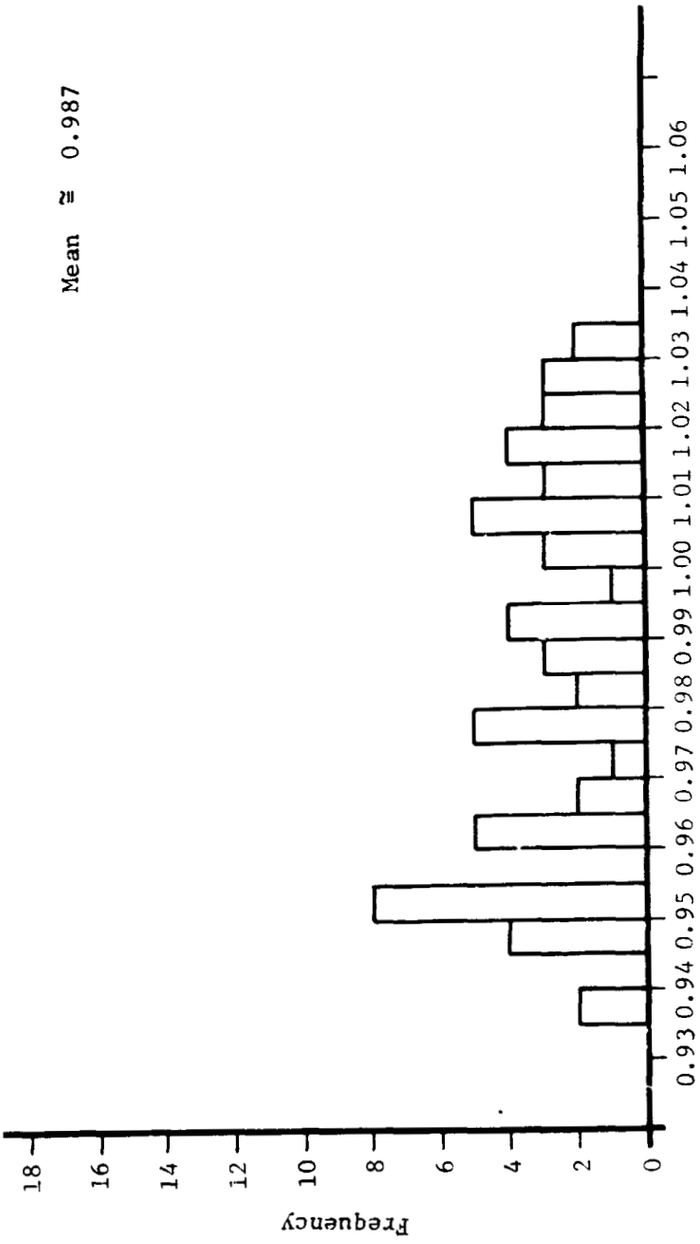

Figure 49: DISTRIBUTION OF DEVIATIONS BETWEEN PROTOTYPE EXPERIMENT AND ANALYSIS (TESTS NUMBER 6-8)

TABLE 5. STEADY STATE EXPERIMENTAL TEMPERATURES

TEST 1

CONDITIONS Sun on
Heater #1 off
Heaters #2, 3, 4 off

NODE	HALF SCALE	PROTOTYPE	INCREMENT	
	(°R)	(°R)	(°R)	(Ratio)
Base Deck				
57a	381.5	382.5	- 1.0	0.997
57b	384.3	387.4	- 3.1	0.992
59	391.4	398.1	- 6.7	0.983
Heater One				
83	375.1	- *	-	-
84	380.1**	382.5	-	-
85	380.1	382.5	- 2.4	0.994
Equipment Deck				
70a	398.5	400.2	- 1.7	0.996
70b	398.5	400.8	- 2.3	0.994
Heater Two				
87	397.8	404.2	- 6.4	0.984
88	397.8	401.5	- 3.7	0.991
Heater Three				
90	398.5	403.5	- 5.0	0.988
91	397.8	401.5	- 3.7	0.991
Heater Four				
95	398.5	402.9	- 4.4	0.989
96	399.9	402.9	- 3.0	0.992
97	397.1	400.8	- 3.7	0.991
External Skin				
64	389.3	390.3	- 1.0	0.997
77	408.3	412.3	- 4.3	0.990
73	406.8	410.9	- 4.1	0.990
79	453.5	467.1	-13.6	0.971
81	451.6	468.4	-16.8	0.964

* Inoperative thermocouple
** Apparently erroneous thermocouple reading

TABLE 36. STEADY STATE EXPERIMENTAL TEMPERATURES

TEST 2

CONDITION Sun on
Heaters #1 on
Heaters #2, 3, 4 off

NODE	HALF SCALE (°R)	PROTOTYPE (°R)	INCREMENT (°R)	INCREMENT (Ratio)
Base Deck				
57a	428.1	429.7	- 1.6	0.996
57b	410.0	408.9	+ 1.1	1.003
59	407.3	410.9	- 3.6	0.991
Heater One				
83	709.9	-*	-	-
84	468.8**	497.6	-	-
85	483.9	487.8	- 3.9	0.992
Equipment Deck				
70a	410.7	411.6	- 0.9	0.998
70b	410.7	410.9	- 0.2	1.000
Heater Two				
87	411.3	413.6	- 2.3	0.994
88	411.3	412.3	- 1.0	0.998
Heater Three				
90	411.3	413.6	- 2.3	0.994
91	412.7	413.6	- 0.9	0.998
Heater Four				
95	411.3	412.9	- 1.6	0.996
96	412.0	413.6	- 1.6	0.996
97	409.3	410.9	- 1.6	0.996
External Skin				
64	403.3	403.5	- 0.2	1.000
77	417.4	419.6	- 2.2	0.995
73	416.7	419.0	- 2.3	0.994
79	461.8	472.9	-11.1	0.976
81	459.3	473.5	-14.2	0.970

* Inoperative thermocouple
** Apparently erroneous thermocouple reading

TABLE 37. STEADY STATE EXPERIMENTAL TEMPERATURES

TEST 3

CONDITIONS Sun off
Heater #1 on
Heaters #2, 3, 4 off

NODE	HALF SCALE	PROTOTYPE	INCREMENT	
	(°R)	(°R)	(°R)	(Ratio)
Base Deck				
57a	318.6	321.2	- 2.6	0.992
57b	288.7	285.6	+ 3.1	1.011
59	275.0	276.9	- 1.9	0.993
Heater One				
83	686.2	- *	-	-
84	385.8**	402.9	-	-
85	384.3	392.4	- 8.1	0.979
Equipment Deck				
70a	268.0	266.6	+ 1.4	1.005
70b	268.0	268.3	- 0.3	0.999
Heater Two				
87	267.2	266.6	+ 0.6	1.002
88	267.2	266.6	+ 0.6	1.002
Heater Three				
90	267.2	267.5	- 0.3	0.999
91	268.0	266.6	+ 1.4	1.005
Heater Four				
95	267.2	267.5	- 0.3	0.999
96	267.2	266.6	+ 0.6	1.002
97	267.2	266.6	+ 0.6	1.002
External Skin				
64	271.5	271.8	- 0.3	0.999
77	264.6	263.1	+ 1.5	1.006
73	264.6	264.0	+ 0.6	1.002
79	263.7	263.1	+ 0.6	1.002
81	263.7	263.1	+ 0.6	1.002

* Inoperative thermocouple
** Apparently erroneous thermocouple reading

TABLE 38. STEADY STATE EXPERIMENTAL TEMPERATURES

TEST 4

CONDITIONS Sun on
Heater #1 off
Heaters #2, 3, 4 on

NODE	HALF SCALE (^{o}R)	PROTOTYPE (^{o}R)	INCREMENT (^{o}R)	(Ratio)
Base Deck				
57a	408.0	406.2	+ 1.8	1.004
57b	412.7	410.2	+ 2.5	1.006
59	414.7	416.3	- 1.6	0.996
Heater One				
83	401.3	- *	-	-
84	408.7**	409.6	-	-
85	408.0	407.6	+ 0.4	1.001
Equipment Deck				
70a	458.6	459.5	- 0.9	0.998
70b	455.5	456.3	- 0.8	0.998
Heater Two				
87	477.1	482.9	- 5.8	0.988
88	472.0	478.6	- 6.6	0.986
Heater Three				
90	488.8	490.2	- 1.4	0.997
91	482.1	485.4	- 3.3	0.993
Heater Four				
95	478.4	480.5	- 2.1	0.996
96	488.8	490.2	- 1.4	0.997
97	472.0	476.7	- 4.7	0.990
External Skin				
64	422.7	422.3	+ 0.4	1.001
77	445.3	447.4	- 2.1	0.995
78	444.0	446.8	- 2.8	0.994
79	487.0	496.9	- 9.9	0.980
81	484.5	497.6	-13.1	0.974

* Inoperative thermocouple
** Apparently erroneous thermocouple reading

TABLE 39. STEADY STATE EXPERIMENTAL TEMPERATURES

TEST 5

CONDITIONS Sun off
Heater #1 off
Heaters #2, 3, 4 on

NODE	HALF SCALE (°R)	PROTOTYPE (°R)	INCREMENT (°R)	(Ratio)
Base Deck				
57a	310.6	310.0	+ 0.6	1.002
57b	313.0	310.0	+ 3.0	1.010
59	308.2	307.6	+ 0.6	1.002
Heater One				
83	306.7	- *	-	-
84	309.0**	312.5	-	-
85	309.8	310.8	- 1.0	0.997
Equipment Deck				
70a	358.9	361.2	- 2.3	0.994
70b	354.4	358.2	- 3.8	0.989
Heater Two				
87	379.4	386.0	- 6.6	0.983
88	373.7	383.2	- 9.5	0.975
Heater Three				
90	393.6	394.5	- 0.9	0.998
91	385.8	388.8	- 3.0	0.992
Heater Four				
95	380.1	382.5	- 2.4	0.994
96	391.4	393.8	- 2.4	0.994
97	373.7	378.2	- 4.5	0.988
External Skin				
64	321.7	324.2	- 2.5	0.992
77	326.2	331.8	- 5.6	0.983
73	328.4	332.5	- 4.1	0.988
79	327.6	330.3	- 2.7	0.992
81	326.9	329.5	- 2.6	0.992

* Inoperative thermocouple
** Apparently erroneous thermocouple reading

TABLE 40. STEADY STATE EXPERIMENTAL TEMPERATURES

TEST 6

CONDITICNS Sun on
Heater #1 off
Heaters #2, 3, 4 off

NODE	HALF SCALE (^{o}R)	PROTOTYPE (^{o}R)	INCREMENT (^{o}R)	(Ratio)
Base Deck				
57a	368.9	382.5	-13.6	0.964
57b	371.0	389.5	-18.5	0.952
59	378.1	401.5	-23.4	0.942
Heater One				
83	367.4	378.9	-11.5	0.970
84	362.5**	381.7	-	-
85	367.4	381.0	-13.6	0.964
Equipment Deck				
70a	376.6	393.1	-16.5	0.958
70b	376.6	393.1	-16.5	0.958
Heater Two				
87	375.9	393.1	-17.2	0.956
88	375.2	393.1	-17.9	0.955
Heater Three				
90	375.9	393.1	-17.2	0.956
91	375.9	392.4	-16.5	0.958
Heater Four				
95	375.9	393.1	-17.2	0.956
96	375.9	393.1	-17.2	0.956
97	375.9	393.1	-17.2	0.956
External Skin				
64	375.9	391.7	-15.8	0.960
77	377.4	395.2	-17.8	0.955
73	376.6	394.5	-17.9	0.955
79	378.1	396.6	-18.5	0.953
81	378.1	398.1	-20.0	0.950

** Apparently erroneous thermocouple reading

TABLE 41. STEADY STATE EXPERIMENTAL TEMPERATURES

TEST 7

CONDITIONS Sun on
Heater #1 off
Heaters #2, 3, 4 on

NODE	HALF SCALE	PROTOTYPE	INCREMENT	
	(^{o}R)	(^{o}R)	(^{o}R)	(Ratio)
Base Deck				
57a	439.6	451.9	-12.3	0.973
57b	442.2	457.6	-15.4	0.966
59	440.9	460.1	-19.2	0.958
Heater One				
83	442.2	451.9	- 9.7	0.978
84	433.6**	456.3	-	-
85	441.5	454.4	-12.9	0.972
Equipment Deck				
70a	499.3	515.7	-16.4	0.968
70b	496.8	513.9	-17.1	0.967
Heater Two				
87	517.4	536.0	-18.6	0.965
88	513.2	533.0	-19.8	0.963
Heater Three				
90	528.1	544.3	-16.2	0.970
91	522.8	540.2	-17.4	0.968
Heater Four				
95	517.4	535.7	-18.3	0.966
96	526.9	544.3	-17.4	0.968
97	513.8	533.0	-19.2	0.964
External Skin				
64	467.7	483.5	-15.8	0.967
77	487.7	507.3	-19.6	0.961
73	587.7	506.7	-19.0	0.962
79	489.5	509.1	-19.6	0.962
81	488.9	509.8	-20.9	0.959

** Apparently erroneous thermocouple reading

TABLE 42. STEADY STATE EXPERIMENTAL TEMPERATURES

TEST 8

CONDITIONS Sun off
Heater #1 off
Heater #2, 3, 4 on

NODE	HALF SCALE	PROTOTYPE	INCREMENT	
	(^{o}R)	(^{o}R)	(^{o}R)	(Ratio)
Base Deck				
57a	380.2	381.0	- 0.8	0.998
57b	380.9	382.5	- 1.6	0.996
59	373.1	373.9	- 0.8	0.998
Heater One				
83	380.9	381.0	- 0.1	1.000
84	373.8**	384.6	-	-
85	380.9	382.5	- 1.6	0.996
Equipment Deck				
70a	442.8	446.8	- 4.0	0.991
70b	439.6	446.1	- 6.5	0.985
Heater Two				
87	461.9	469.1	- 7.2	0.985
88	456.8	467.1	-10.3	0.978
Heater Three				
90	473.4	478.0	- 4.6	0.990
91	467.7	474.2	- 6.5	0.986
Heater Four				
95	461.9	472.9	-11.0	0.977
96	472.1	477.2	- 5.1	0.989
97	457.5	464.6	- 7.1	0.985
External Skin				
64	406.7	410.2	- 3.5	0.991
77	426.9	434.4	- 7.5	0.983
73	426.9	435.1	- 8.2	0.981
79	428.2	435.7	- 7.5	0.983
81	427.5	435.1	- 7.6	0.983

** Apparently erroneous thermocouple reading

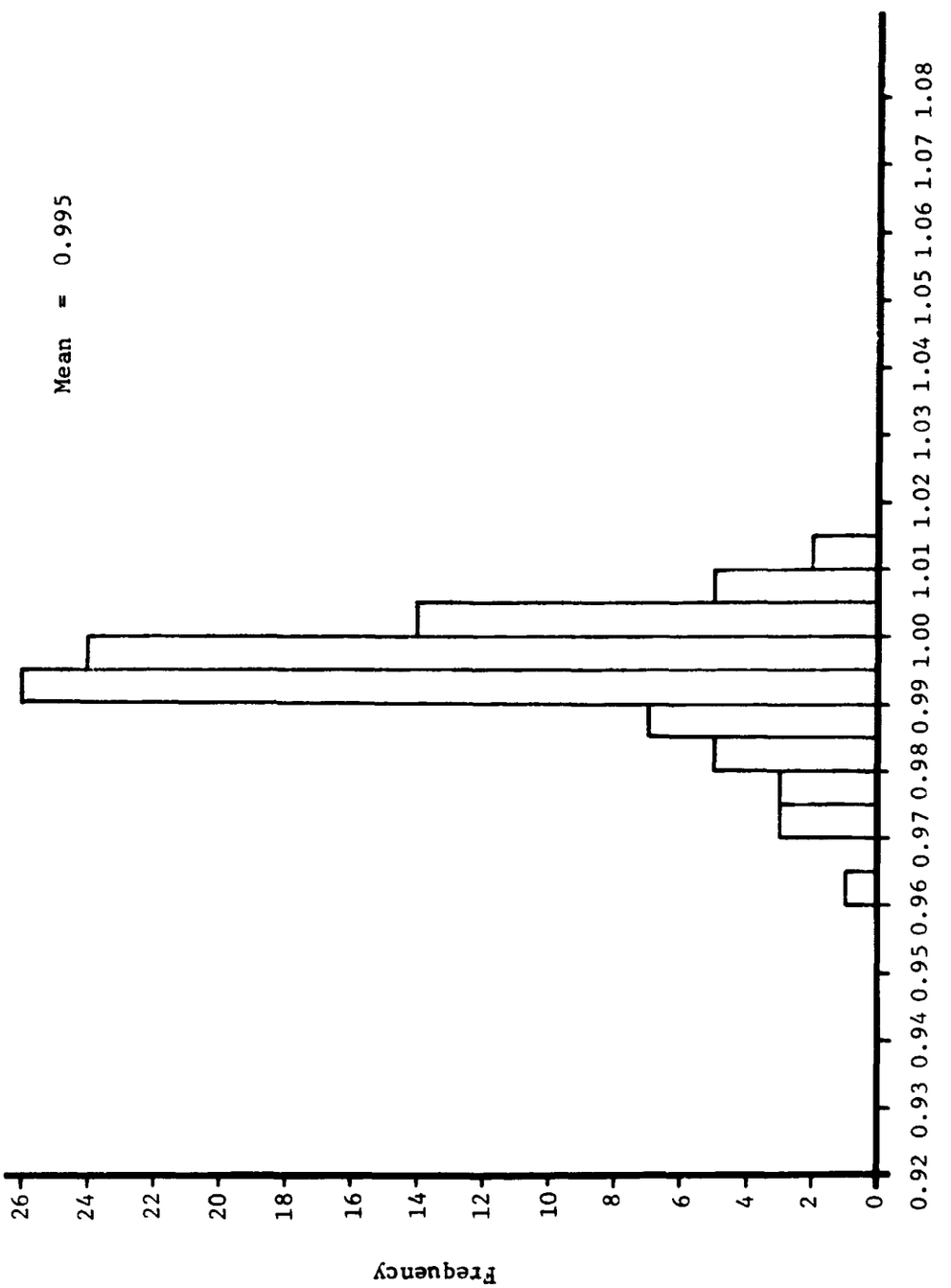

Figure 50: DISTRIBUTION OF DEVIATIONS BETWEEN HALF SCALE AND PROTOTYPE EXPERIMENTAL DATA (TESTS NUMBER 1-5)

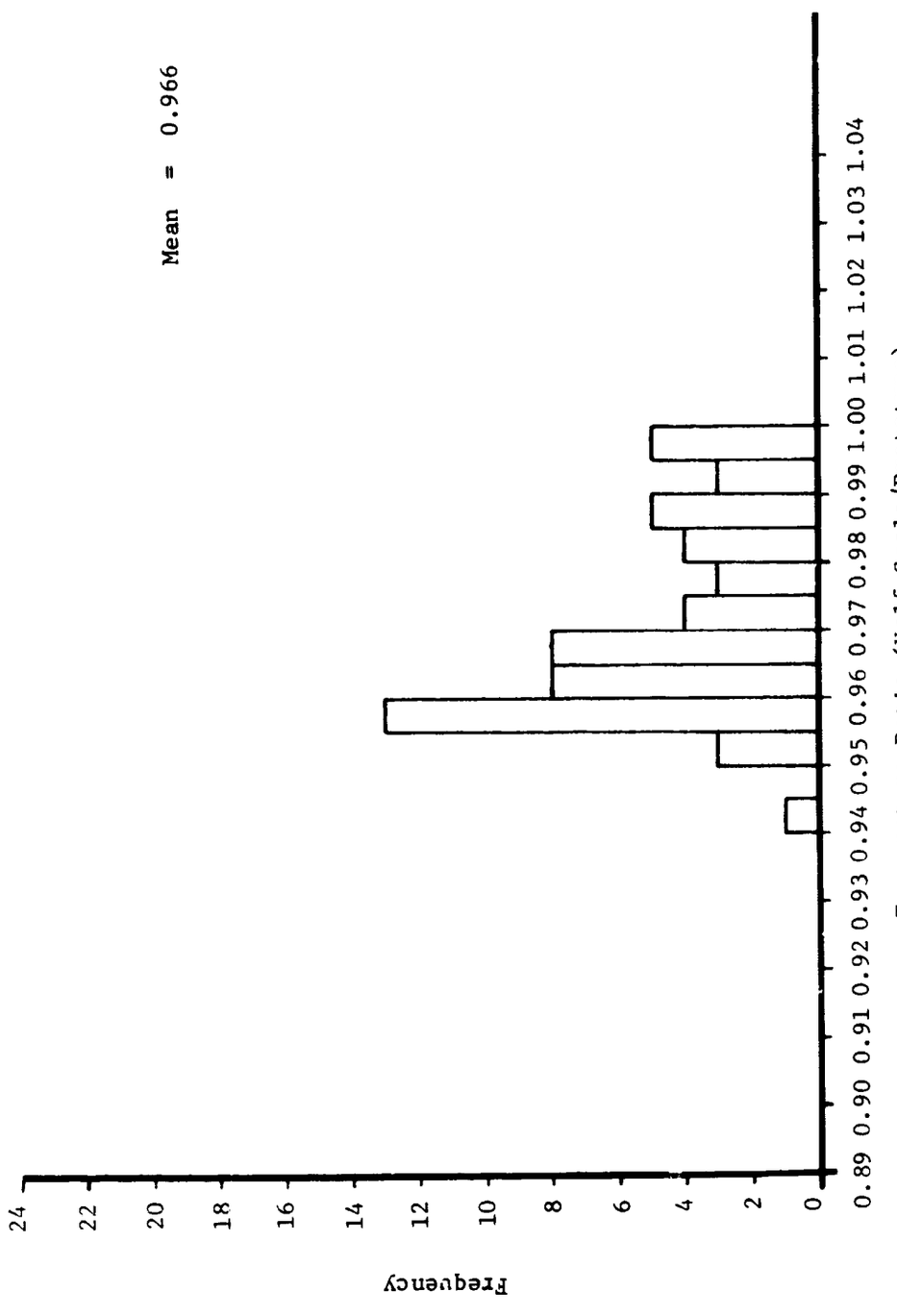

Figure 51: DISTRIBUTION OF DEVIATIONS BETWEEN HALF SCALE AND PROTOTYPE EXPERIMENTAL DATA WITH MULTILAYER INSULATION (TESTS NUMBER 6-8)

TABLE 43. NUMERICAL CORRECTION OF HALF SCALE EXPERIMENT

TEST 1

NODE	HALF SCALE EXPERIMENTAL DATA (°R)	NUMERICAL CORRECTION FACTOR (°R)	HALF SCALE CORRECTED DATA (°R)	PROTOTYPE EXPERIMENTAL DATA (°R)	CORRECTED TEMPERATURE RATIO
Base Deck					
57a	381.5	+ 5.6	387.1	382.5	1.012
57b	384.3	+ 5.6	389.9	387.4	1.006
59	391.4	+ 4.7	396.1	398.1	0.995
Heater One					
83	375.1	+ 5.6	380.7	- *	-
84	380.1**	+ 5.4	385.5	382.5	-
85	380.1	+ 5.4	385.5	382.5	1.008
Equipment Deck					
70a	398.5	+ 3.3	401.8	400.2	1.004
70b	398.5	+ 3.3	401.8	400.8	1.002
Heater Two					
87	397.8	+ 3.2	401.0	404.2	0.992
88	397.8	+ 3.3	401.1	401.5	0.999
Heater Three					
90	398.5	+ 3.2	401.7	403.5	0.996
91	397.8	+ 3.3	401.1	401.5	0.999
Heater Four					
95	398.5	+ 3.3	401.8	402.9	0.997
96	399.9	+ 3.1	403.0	402.9	1.000
97	397.1	+ 3.3	400.3	400.8	0.999
External Skin					
64	389.3	+ 5.0	394.3	390.3	1.010
77	408.3	+ 2.7	411.0	412.3	0.997
73	406.8	+ 2.7	409.5	410.9	0.996
79	453.5	- 1.0	452.5	467.1	0.969
81	451.6	- 0.9	450.7	468.4	0.962

* Inoperative thermocouple

** Apparently erroneous thermocouple reading

TABLE 44. NUMERICAL CORRECTION OF HALF SCALE EXPERIMENT

TEST 2

NODE	HALF SCALE EXPERIMENTAL DATA (°R)	NUMERICAL CORRECTION FACTOR (°R)	HALF SCALE CORRECTED DATA (°R)	PROTOTYPE EXPERIMENTAL DATA (°R)	CORRECTED TEMPERATURE RATIO
Base Deck					
57a	428.1	+ 2.4	430.5	429.7	1.002
57b	410.0	+ 2.4	412.4	408.9	1.008
59	407.3	+ 4.5	411.8	410.9	1.002
Heater One					
83	709.9	+60.3	770.2	- *	-
84	468.8**	+ 1.9	470.7	497.6	-
85	483.9	+ 6.4	490.3	487.8	1.005
Equipment Deck					
70a	410.7	+ 2.9	413.6	411.6	1.005
70b	410.7	+ 2.9	413.6	410.9	1.006
Heater Two					
87	411.3	+ 2.9	414.2	413.6	1.001
88	411.3	+ 2.9	414.2	412.3	1.005
Heater Three					
90	411.3	+ 2.9	414.2	413.6	1.001
91	412.7	+ 3.0	415.7	413.6	1.005
Heater Four					
95	411.3	+ 2.9	414.2	412.9	1.003
96	412.0	+ 2.7	414.7	413.6	1.003
97	409.3	+ 3.0	412.3	410.9	1.006
External Skin					
64	403.3	+ 4.4	407.7	403.5	1.010
77	417.4	+ 2.5	419.9	419.6	1.001
73	416.7	+ 2.5	419.2	419.0	1.000
79	461.8	- 0.7	461.1	472.9	0.975
81	459.3	- 0.7	458.6	473.5	0.968

* Inoperative thermocouple

** Apparently erroneous thermocouple reading

TABLE 45. NUMERICAL CORRECTION OF HALF SCALE EXPERIMENT

TEST 3

NODE	HALF SCALE EXPERIMENTAL DATA (°R)	NUMERICAL CORRECTION FACTOR (°R)	HALF SCALE CORRECTED DATA (°R)	PROTOTYPE EXPERIMENTAL DATA (°R)	CORRECTED TEMPERATURE RATIO
Base Deck					
57a	318.6	- 7.1	311.5	321.2	0.970
57b	288.7	- 7.1	281.6	285.6	0.986
59	275.0	+ 1.7	276.7	276.9	0.999
Heater One					
83	686.2	+76.9	763.1	*	-
84	385.8**	-12.0	373.8	402.9	-
85	384.3	- 5.9	378.4	392.4	0.964
Equipment Deck					
70a	268.0	+ 0.5	268.5	266.6	1.007
70b	268.0	+ 0.5	268.5	268.3	1.001
Heater Two					
87	267.2	+ 1.3	268.5	266.6	1.007
88	267.2	+ 1.3	268.5	266.6	1.007
Heater Three					
90	267.2	+ 1.3	268.5	267.5	1.004
91	268.0	+ 1.3	269.3	266.6	1.010
Heater Four					
95	267.2	+ 1.1	268.3	267.5	1.003
96	267.2	+ 1.2	268.4	266.6	1.007
97	267.2	+ 1.0	268.2	266.6	1.006
External Skin					
64	271.5	+ 0.9	272.4	271.8	1.002
77	264.6	+ 2.4	267.0	263.1	1.015
73	264.6	+ 2.3	266.9	264.0	1.011
79	263.7	+ 2.3	266.0	263.1	1.011
81	263.7	+ 2.3	266.0	263.1	1.011

* Inoperative thermocouple

** Apparently erroneous thermocouple reading

TABLE 46. NUMERICAL CORRECTION OF HALF SCALE EXPERIMENT

TEST 4

NODE	HALF SCALE EXPERIMENTAL DATA (°R)	NUMERICAL CORRECTION FACTOR (°R)	HALF SCALE CORRECTED DATA (°R)	PROTOTYPE EXPERIMENTAL DATA (°R)	CORRECTED TEMPERATURE RATIO
Base Deck					
57a	408.0	+ 4.2	412.2	406.2	1.015
57b	412.7	+ 4.2	416.9	410.2	1.016
59	414.7	+ 3.5	418.2	416.3	1.004
Heater One					
83	401.3	+ 4.2	405.5	- *	-
84	408.7**	+ 4.0	412.7	409.6	-
85	408.0	+ 3.9	411.9	407.6	1.011
Equipment Deck					
70a	458.6	+ 2.3	460.9	459.5	1.003
70b	455.5	+ 2.3	457.8	456.3	1.003
Heater Two					
87	477.1	- 0.3	476.8	482.9	0.987
88	472.0	+ 2.2	474.2	478.6	0.991
Heater Three					
90	488.8	- 0.6	488.2	490.2	0.996
91	482.1	+ 2.5	484.6	485.4	0.998
Heater Four					
95	478.4	+ 2.4	480.8	480.5	1.001
96	488.4	+ 2.3	490.1	490.2	1.000
97	472.0	+ 2.1	474.1	476.7	0.994
External Skin					
64	422.7	+ 3.5	426.2	422.3	1.009
77	445.3	+ 1.3	446.6	447.4	0.998
73	444.0	+ 1.4	445.4	446.8	0.997
79	487.0	- 0.7	486.3	496.9	0.979
81	484.5	- 0.6	483.9	497.6	0.972

* Inoperative [illegible]ocouples

** Apparently [illegible]s thermocouple reading

TABLE 47. NUMERICAL CORRECTION OF HALF SCALE EXPERIMENT

TEST 5

NODE	HALF SCALE EXPERIMENTAL DATA (°R)	NUMERICAL CORRECTION FACTOR (°R)	HALF SCALE CORRECTED DATA (°R)	PROTOTYPE EXPERIMENTAL DATA (°R)	CORRECTED TEMPERATURE RATIO
Base Deck					
57a	310.6	+ 1.4	312.0	310.0	1.006
57b	313.0	+ 1.4	314.4	310.0	1.014
59	308.2	+ 2.6	310.8	307.6	1.010
Heater One					
83	306.7	+ 1.2	307.9	- *	-
84	30 .0**	+ 0.9	309.9	312.5	-
85	309.8	+ 1.0	310.8	310.8	1.000
Equipment Deck					
70a	358.9	- 2.8	356.1	361.2	0.986
70b	354.4	- 2.8	351.6	358.2	0.982
Heater Two					
87	379.4	- 8.0	371.4	386.0	0.962
88	373.7	- 4.6	369.1	383.2	0.963
Heater Three					
90	393.6	- 9.0	384.6	394.5	0.975
91	385.8	- 4.7	381.1	388.8	0.980
Heater Four					
95	380.1	- 3.5	376.6	382.5	0.984
96	391.4	- 4.0	387.4	393.8	0.984
97	373.7	- 4.0	369.7	378.2	0.978
External Skin					
64	321.7	- 1.0	320.7	324.2	0.989
77	326.2	- 2.1	324.1	331.8	0.977
73	328.4	- 2.2	326.2	332.5	0.981
79	327.6	- 2.6	325.0	330.3	0.984
81	326.9	- 2.8	324.1	329.5	0.984

* Inoperative thermocouples

** Apparently erroneous thermocouple reading

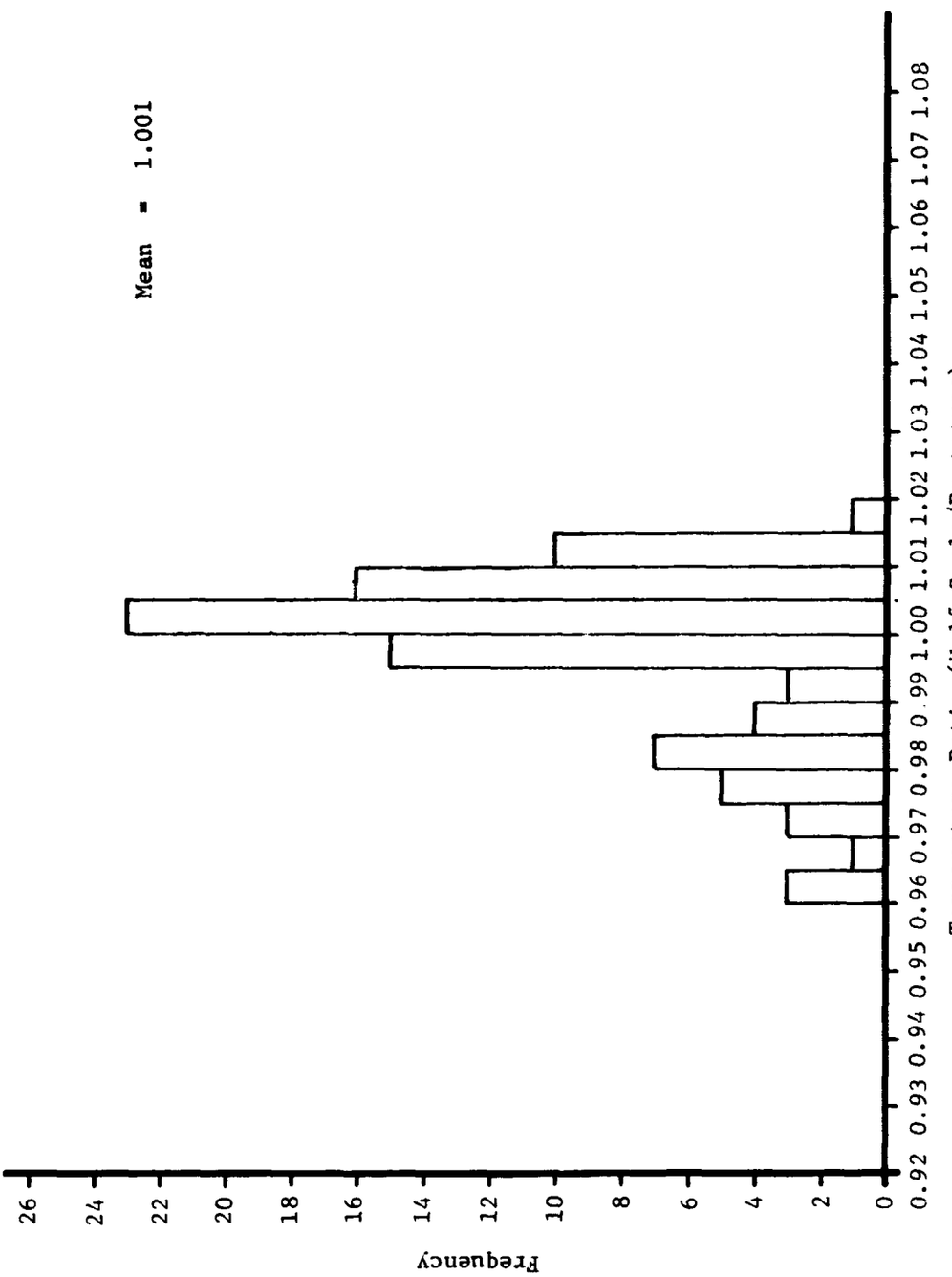

Figure 52: DISTRIBUTION OF DEVIATIONS BETWEEN CORRECTED HALF SCALE AND PROTOTYPE EXPERIMENTAL DATA (TESTS NUMBER 1-5)

TABLE 48. SUMMARY OF ERRORS

Comparison	Systematic* Error (%)	Maximum** Error (%)		Standard*** Deviation (%)
Tests 1, 2, 4, 5				
Experiment and Analysis				
Half Scale	- 0.1	+ 5.3	- 2.8	± 1.5
Prototype	- 0.1	+ 5.3	- 2.9	± 2.2
Test 3				
Experiment and Analysis				
Half Scale	+ 5.9	+ 2.4	-10.9	± 1.0
Prototype	+ 5.2	+ 5.4	- 8.9	± 0.7
Tests 1-5				
Experiment	- 0.5	+ 1.8	- 3.1	± 0.7
Adjusted Experiment	+ 0.1	+ 1.5	- 4.0	± 1.0
Tests 6-8 (insulated)				
Experiment and Analysis				
Half Scale	- 1.8	+ 4.9	- 2.5	± 2.2
Prototype	- 1.3	+ 4.8	- 5.2	± 3.5
Experiment	- 3.4	+ 3.4	- 2.4	± 1.5

* Displacement of mean from 1.0
** Total range of deviations about mean
*** Range of deviations about mean which encompass 68 percent of the data points shown

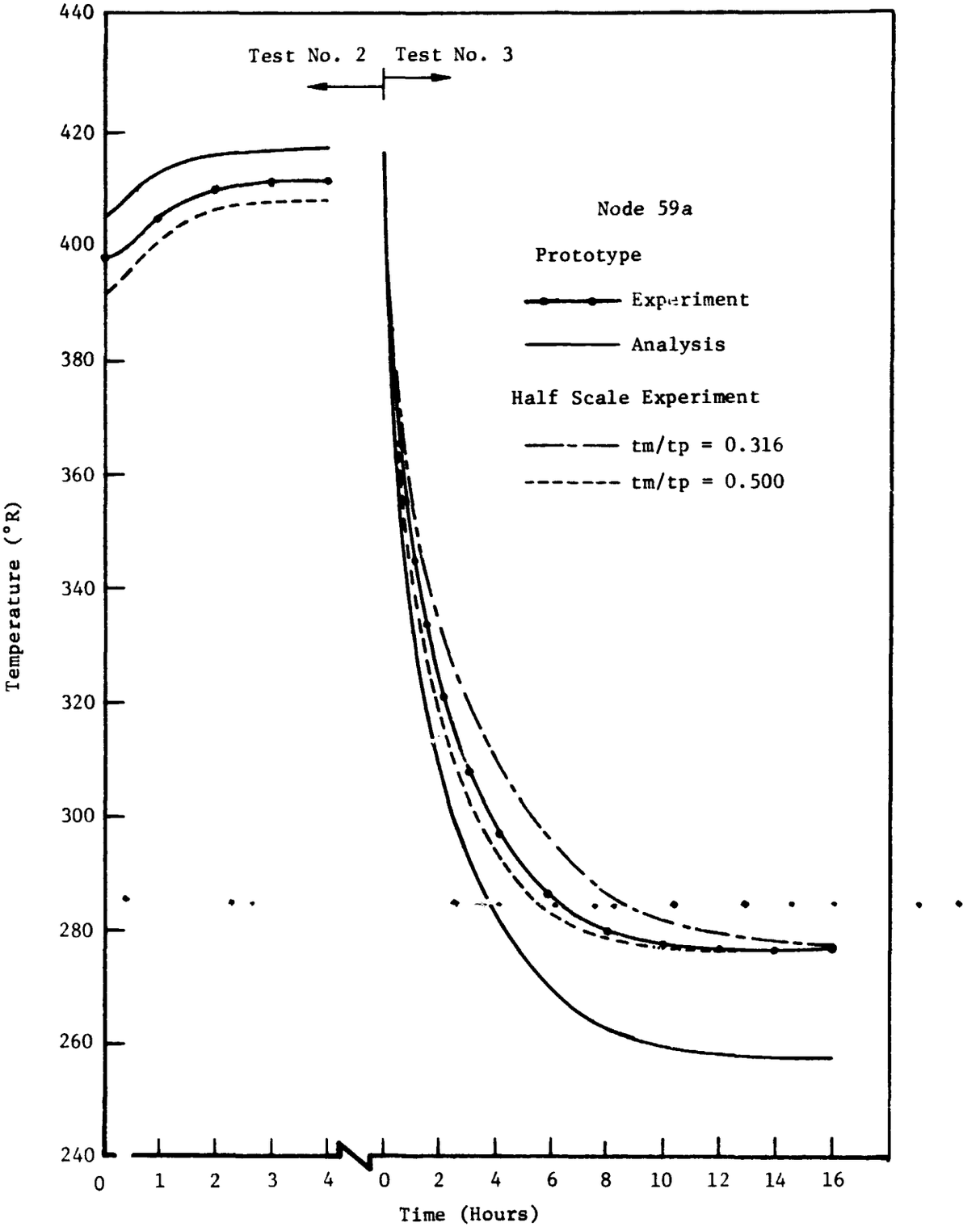

Figure 53: TRANSIENT RESULTS FOR NODE 59a

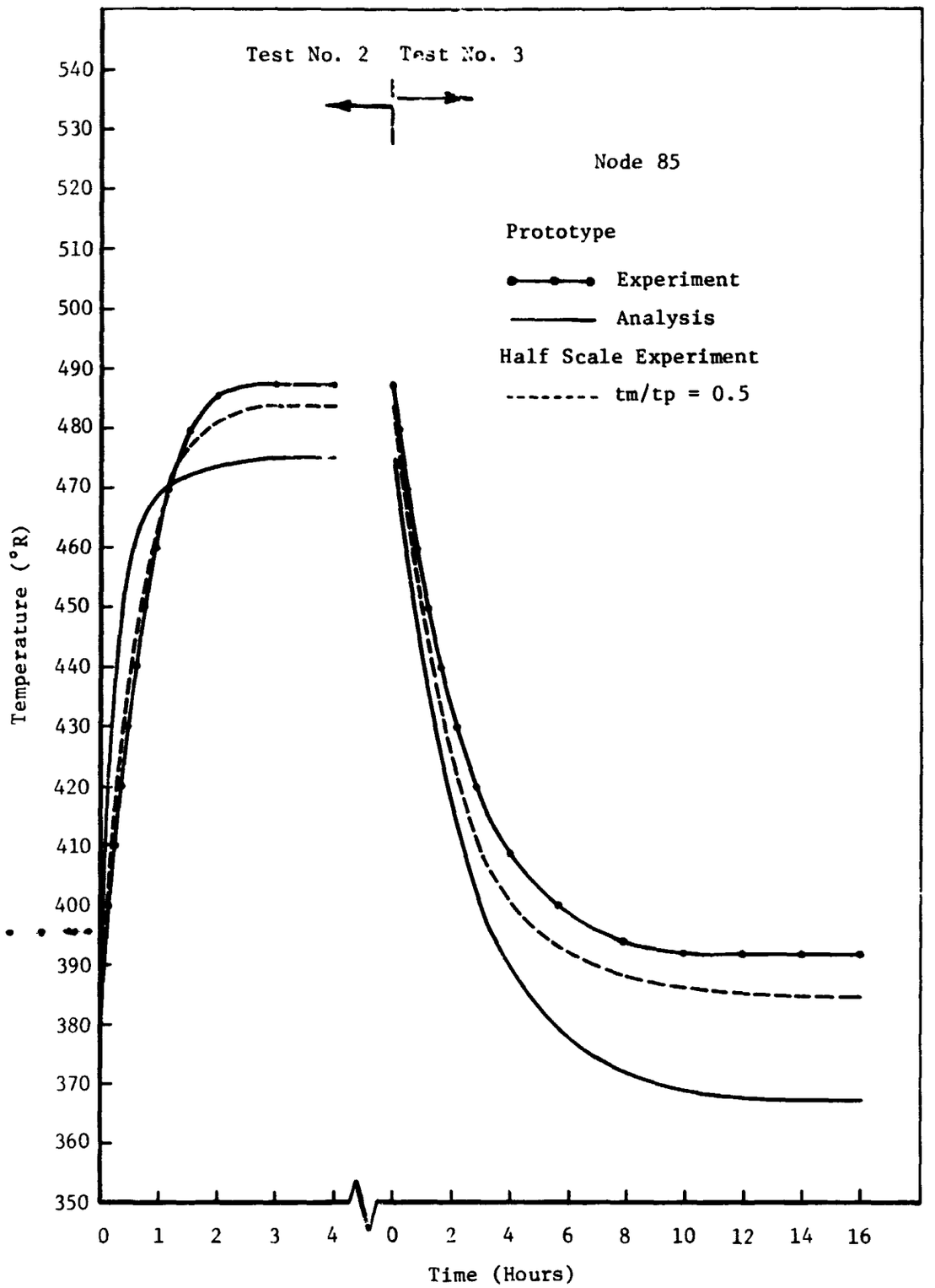

Figure 54: TRANSIENT RESULTS FOR NODE 85

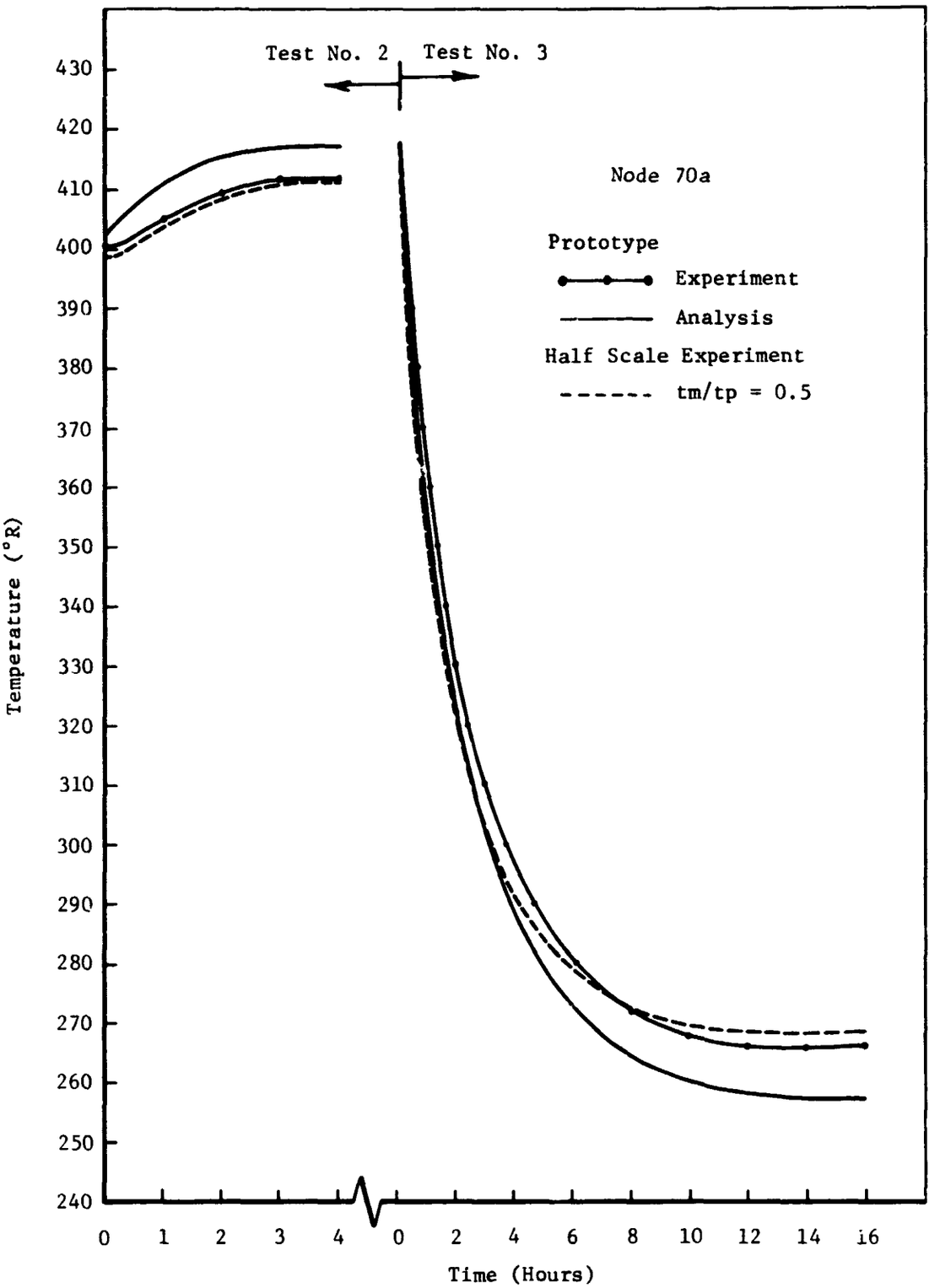

Figure 55: TRANSIENT RESULTS FOR NODE 70a

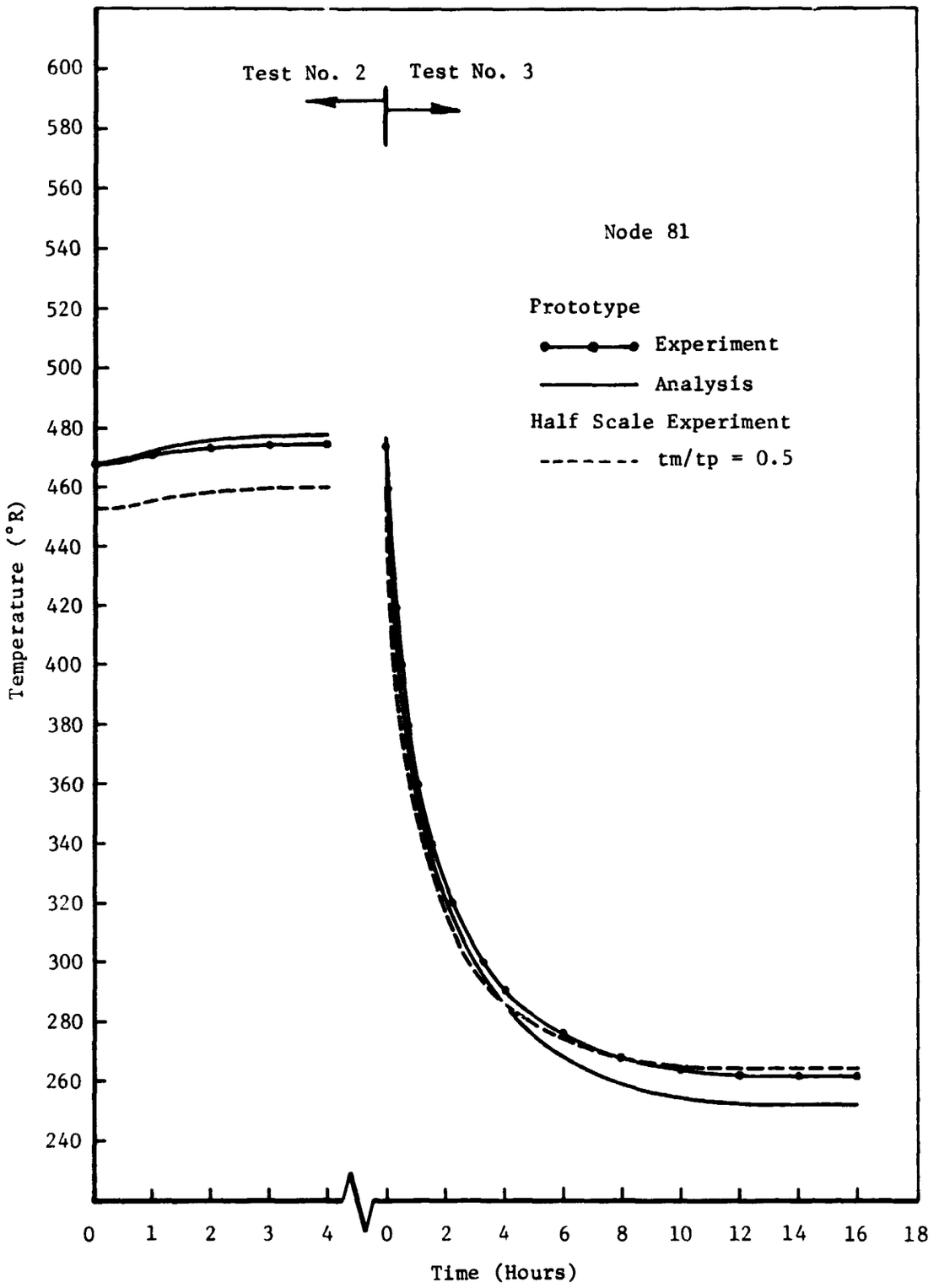

Figure 56: TRANSIENT RESULTS FOR NODE 81

8.0 CONCLUDING REMARKS

This concluding section is devoted to a series of remarks on the questions of numerical modeling versus scale modeling approaches to thermal design verification, limitations in both thermal scale modeling and numerical modeling, and recommendations for additional work required to extend the usefulness of scale modeling techniques and further validate the conclusions of this study.

The sheer size of the spacecraft currently being envisioned for the future decade (the space shuttle, the Mars '75, and Grand Tour missions) will eventually require either modifications of existing thermal verification testing procedures or significantly larger space simulation facilities. Several techniques are available beyond full size thermal testing. These alternates include numerical analysis, thermal scale modeling, and component testing. Most likely a combination of these techniques will ultimately be utilized.

This study has shown that thermal scale modeling can successfully verify the thermal design of a spacecraft with complex conductive/radiative interchange. Scale modeling is limited, as are all experimental approaches, by the time and cost requirements of vacuum chamber testing. Scale modeling is also limited by the difficulty of producing complex external environments in existing vacuum chamber facilities.

This study has also shown that numerical analysis can accurately predict the performance of a complex spacecraft. The major difficulty with a numerical model is that it requires a complete understanding of the spacecraft, its material properties and their temperature dependence.

A combination of the experimental and numerical methods, which utilizes the advantages of each method, appears to be the best approach to thermal design verification. A small scale model could be tested and used to aid the development of an accurate mathematical model. The upgraded mathematical

model could then be used to predict the performance of a full size vehicle over a much large range of simulated flight conditions than could be achieved in the space simulator.

A possible alternate would be the use of the combined numerical/ scale modeling study to define spacecraft surface temperatures and gross structural interior temperatures. Component testing could then be accomplished with the space vehicle exterior boundary temperatures being simulated rather than by direct simulation of the space thermal environment.

However, as always, the preferred approach depends upon the particular problem being investigated. This requires an understanding of the limitations of each approach.

As we have seen in this study the major limitations on numerical analysis are not related to the size of the problem being studied, but rather the completeness of our understanding of the problem.

In addition to understanding the problem there is a limitation as a result of the ability of our computer programs to simulate the problem, particularly in the areas of defining external environment and the calculation of radiation interchange factors between surfaces. The programs presently operating appear adequate for most problems studied to date.

The area of least understanding appears in the area of multilayer insulation performance. This is a difficult problem due to the near impossibility of uniform manufacturing and the complex anisotropic nature of heat transfer within the insulation.

The only "size" limitations involved with numerical analysis are a result of a computer storage capability and not really pertinent to the question at hand.

On the other hand the limitations on thermal scale modeling are manifold. Several are mentioned in the paragraphs below:

1) Limitations as a result of uncertainties in material thermal properties, model dimensions, instrumentation effects, and environment simulation.
2) Limitations as a result of existing materials and the range of available gages makes design for both steady state and transient results difficult.
3) Limitations as a result of inadequate or incomplete understanding in the areas of multilayer insulation, joint conductance, and convective heat transfer in manned cabins.

These limitations combine to indicate a realistic lower limit on scale modeling of 1/5 to 1/7 scale. An absolute lower limit on the order of 1/10 scale seems appropriate. The lower the scale ratio the more difficult, time consuming and expensive will be the resulting model. These limitations appear reasonable based on the assumptions of this study but the reader is reminded that the lower limit on scaling is strongly a function of original model size and the manufacturing tolerances that the modeler is willing to pay for.

In cases such as the present study where the prototype itself is a small vehicle (smaller than one would normally consider a candidate for scale modeling), an additional lower limit on model size is imposed by the sheer miniaturization required. For example, a one-tenth scale model would be a two inch (5.08 cm) cube mounted on a three inch (7.62 cm) square plate. The 6 inch (15.25 cm) heater canisters would be 0.6 inch (1.525 cm) by 0.3 inch (0.761 cm) diameter cylinders with the nichrome wound heater cores. This level of miniaturization would require an exceptionally intricate level of workmanship and a probable large increase in model fabrication cost.

Additional work could extend and strengthen the conclusions reached in this study.

The analyses performed could be redone based upon the observations of this study to obtain a more accurate mathematical model. This would allow more accurate mathematical modeling of the experimental results and improved experimental correlations where the half scale results are mathematically adjusted to account for scaling compromises.

An additional smaller scale model in the 1/4 to 1/6 scale range could be built and tested to show additional verification of the probable error analysis developed in Section 3.0 as a function of scale ratio. This model should have additional emphasis on scaling the transient results, perhaps even to the extent of accepting steady state temperature errors in order to obtain an accurate transient sequence of events.

The range of usefulness of thermal scale modeling could also be improved by detailed studies in the areas of:

1) Multilayer insulation. Both performance studies and scaling technique studies would be useful to applications of scale modeling of real spacecraft.
2) Joint conductance. In actual spacecraft, joint conductance could be a limiting factor which would require consideration in scale modeling.
3) Cabin convective flows. Manned spacecraft will have environmental control systems to replenish oxygen content of the cabin atmosphere. This will result in convective interaction with the cabin walls and could be the dominant interior heat transfer mechanism.

It is felt, however, that a study of multilayer insulation scaling techniques would be applicable to virtually all spacecraft studies whether manned or not. The final recommendations of this study would be:

1) a detailed study of multilayer insulation scaling techniques and
2) an extension of the present study to experimentally verify the effects of uncertainties in scale modeling at lower scale model ratios.

9.0 REFERENCES

1. L. G. Clark and K. A. Laband, "Orbital Station Temperature Control," Astronautics, Vol. 7, No. 9, pp. 40-43, 1962.

2. F. Gabron and A. A. Fowle, "Thermal Modeling of a Simulated JPL Spacecraft, Phase I Results," Contract NAS7-100, September 1962.

3. A. J. Katz, "Thermal Testing," Space/Aeronautics (Aerospace Test Engineering - Part 2), pp. 30-34, October 1962.

4. J.M.F. Vickers, "Thermal Scale Modeling: Basic Considerations," Jet Propulsion Laboratory Space Programs Summary IV, No. 37-18, pp. 80-83, December 1962.

5. S. Katzoff, "Similitude in Thermal Models of Spacecraft," NASA TN D-1631, April 1963.

6. A. A. Fowle, F. Gabron and R. W. Johnson, "Thermal Scale Modeling of Spacecraft: An Experimental Investigation," A. D. Little, Inc., JPL Contract #950252, NASA-CR-56624, June 28, 1963.

7. J.M.F. Vickers, "Space Programs Summary," Vol. IV:

   No. 37-19, pp. 89-90, February 1963.
   No. 37-21, pp. 48-50, June 1963.
   No. 37-24, pp. 57-59, December 1963.

8. J. B. Wainwright, L. R. Kelley and T. H. Keesee, "Modeling Criteria and Testing Techniques for the Simulation of Space Environments," Fourth Annual Symposium on Space Environment Simulation, Los Angeles, California, pp. 1-4, May 1963.

9. A. A. Fowle, F. Gabron, and J.M.F. Vickers "Thermal Scale Modeling of Spacecraft: An Experimental Investigation," AIAA Space Simulation and Testing Conference, New York, 1964, pp. 240-246; also J. Spacecraft, Vol. 3, pp. 577-581, 1966.

10. B. P. Jones, "Similitude Research in Space Vehicle Thermal Problems," Proceedings of Conference on Thermal Scale Modeling, NASA/OART, pp. 17-35, February 1964.

11. B. P. Jones, "Thermal Similitude Studies, J. Spacecraft, Vol. 1, pp. 364-369, 1964.

12. J.M.F. Vickers, "A Study of Thermal Modeling Techniques," Proceedings of Symposium on Aeroelastic and Dynamic Modeling Technology, USAF RTD-TDR-63-4197 (Part 1), pp. 97-126, March 1964.

13. J.M.F. Vickers, "Space Programs Summary," Vol. IV:

No. 37-27, pp. 38-39, June 1964.
No. 37-30, pp. 75-77, December 1964.

14. D. L. Adkins, "Scaling of Transient Temperature Distributions of Simple Bodies in a Space Chamber," AIAA Paper 65-660, September 1965; also AIAA Progress in Astronautics and Aeronautics: Thermophysics and Temperature Control of Spacecraft and Entry Vehicles, edited by G. B. Heller (Academic Press, Inc., 1966) Vol. 18, pp. 661-674.

15. B. T. Chao and G. L. Wedekind, "Similarity Criteria for Thermal Modeling of Spacecraft," J. Spacecraft, Vol. 2, pp. 146-152, 1965.

16. N. R. Folkman, F. L. Baldwin and J. B. Wainwright, "Tests on a Thermally Scaled Model Space Station in a Simulated Solar Environment," AIAA Paper 65-658, September 1965; also AIAA Progress in Astronautics and Aeronautics: Thermophysics and Temperature Control of Spacecraft and Entry Vehicles, edited by G. B. Heller (Academic Press Inc., 1966), Vol. 18, pp. 607-626.

17. F. Gabron, R. W. Johnson and J.M.F. Vickers, "Thermal Scale Modeling of a Modified Prototype of the Mariner Mars 1964 Spacecraft," AIAA Paper 65-386, July 1965; also, "Thermal Scale Modeling of a Modified Prototype of the Mariner Spacecraft," J. Spacecraft, Vol. 3, pp. 1123-1126, 1966.

18. F. Gabron and R. W. Johnson, "Thermal Scale Modeling of the Mariner IV Spacecraft," A. D. Little, Inc., Contract NAS7-100, No. C-66326, August 1965.

19. B. P. Jones and J. K. Harrison, "A Set of Experiments in Thermal Similitude," NASA TMX-53346, October 1965.

20. R. E. Rolling, "Results of Transient Thermal Modeling in a Simulated Space Environment," AIAA Paper 65-659, September 1965; also, AIAA Progress in Astronautics and Aeronautics: Thermophysics and Temperature Control of Spacecraft and Entry Vehicles; edited by G. B. Heller (Academic Press Inc., 1966), Vol. 18, pp. 627-659.

21. J.M.F. Vickers, "Space Program Summaries," Vol. IV:

No. 37-31, pp. 111-112, February 1965.
No. 37-34, pp. 89-91, August 1965.

22. J.M.F. Vickers, "Thermal Scale Modeling," Astronautics and Aeronautics, Vol. 3, pp. 34-39, May 1965.

23. D. L. Adkins, "Scaling of Isothermal Simple-Shaped Bodies in a Transient Temperature Environment," Arnold Engineering Development Center, AEDC-TR-66-21, April 1966.

24. N. R. Folkman, "Tests or a Thermally Scaled Model Space Station in a Simulated Solar Environment," Douglas Aircraft Company, SM-47916, June 1966.

25. F. Gabron, R. W. Johnson, J.M.F. Vickers, and J. W. Lucas, Thermal Scale Modeling of the Mariner IV Spacecraft," AIAA Paper 66-23, January 1966; also AIAA Progress in Astronautics and Aeronautics: Thermophysics and Temperature Control of Spacecraft and Entry Vehicles, edited by G. B. Heller; (Academic Press, Inc., 1966), Vol. 18, pp. 675-695.

26. F. Gabron, "Thermal Scale Modeling Techniques for Voyager-Type Spacecraft," A. D. Little, Inc., Contract NAS7-100, C-66326-02, June 15, 1966.

27. F. Gabron, R. W. Johnson and J.M.F. Vickers, "Thermal Scale Modeling of a Modified Prototype of the Mariner Spacecraft," J. Spacecraft, pp. 1123-1126, July 1966.

28. F. Gabron and A. A. Fowle, "Thermal and Structural Scale-Modeling of Optical Systems," AIAA/IES/ASTM Solar Simulation Conference, September 1966.

29. B. P. Jones, "Theory of Thermal Similitude with Applications to Spacecraft - A Survey," Astronautics Acta, Vol. 12, No. 4, 1966.

30. P. L. Miller, Jr., "Thermal Modeling in a Simulated Space Environment," PhD Thesis, Oklahoma State University, July 1966.

31. R. E. Rolling, "Thermal Scale Modeling in a Simulated Space Environment," Lockheed Research Laboratory, N-05-66-1, June 1966.

32. R. E. Rolling, "Thermal Modeling of a Truncated Cone in a Simulated Space Environment," AIAA/IES/ASTM Space Simulation Conference, Houston, Texas, September 1966.

33. R. K. Thompson, "Thermal Scale Modeling Research - Phase I," The Boeing Company, D2-113009-1, 1966.

34. R. K. Thompson, V. G. Klockzien and G. E. Dufoe, "Analysis and Tests of Full Size and Scaled Spacecraft Models in a Simulated Space Environment," AIAA/IES/ASTM Space Simulation Conference, Houston, Texas, September 1966.

35. R. L. Young and R. V. Shanklin, III, "Thermal Similarity Study of a Typical Space Vehicle Element in a Conducting and Radiating Mode" Arnold Engineering Development Center, AEDC-TR-66-22, May 1966.

36. R. L. Young and R. V. Shanklin, III, "Thermal Similarity Study of a Typical Space Vehicle Element," AIAA Paper 66-460, AIAA 4th Aerospace Sciences Meeting, June 27-30, 1966.

37. Jochen Doenecke, "Thermal Scale Modeling Without Similitude," International J. of Heat and Mass Transfer, Vol. 10, July-December 1967, pp. 1894-1899.

38. Han M. Hsia, "Internal Convection Effects in Thermal Models of Space Vehicles," Arnold Engineering Development Center, AEDC TR-66-257, February 1967.

39. P. L. Miller and J. A. Wiebelt, "Thermal Modeling in a Simulated Space Environment," AIAA No. 67-305, AIAA Thermophysics Specialists Conference, April 17-20, 1967.

40. R. K. Thompson, "Thermal Scale Modeling of Insulated Spacecraft - Research Program - Phase II." The Boeing Company, D2-114109-1, 1967.

41. C. Shih, "Thermal Similitude of Manned Spacecraft," Paper 68-22 presented at AIAA 3rd Aerospace Sciences Meeting.

42. R. E. Rolling, K. N. Marshall and D. O. Murray, "Thermal and Structural Modeling of a Large Aperture Space Telescope," Lockheed Report N-05-68-1, November 1968.

43. R. L. Shannon, "A Thermal Scale Modeling Study for Apollo and Apollo Applications," The Boeing Company, D2-114152-1, February 1968.

44. R. L. Shannon, "A Thermal Scale Modeling Study for Apollo and Apollo Applications," Quarterly Report No. 1, Contract NAS9-8332, October 1968.

45. R. L. Shannon, "A Thermal Scale Modeling Study for Apollo and Apollo Applications," Quarterly Report No. 2, Contract NAS9-8332, October through December 1968.

46. R. L. Shannon, W. J. Sauerbrey, and W. G. Foster, "A Thermal Scale Modeling Study for Apollo and Apollo Applications," Quarterly Report No. 3, Contract NAS9-8332, January through March 1969.

47. R. L. Shannon, W. J. Sauerbrey and W. G. Foster, "A Thermal Scale Modeling Study for Apollo and Apollo Applications," Quarterly Report No. 4, Contract NAS9-8332, April through June 1969.

48. R. L. Shannon, R. C. Zentner, and W. J. Sauerbrey, "A Thermal Scale Modeling Study for Apollo and Apollo Applications," Quarterly Report No. 5, Contract NAS9-8332, July through September 1969.

49. D. W. Lewis, "Thermal Scale Modeling - Why and Why Not?" AIAA Paper 69-1010, AIAA/ASTM/IES 4th Space Simulation Conference, September 1969.

50. R. E. Rolling, "Limitations in Thermal Modeling," Lockheed Report LMSC 61-78-69-41, December 1969.

51. Yardley Beers, "Introduction to the Theory of Error," Addison-Wesley Publ. Co., Inc., Reading Mass., 1953.

52. T. Ishimoto and J. T. Bevans, "Temperature Variance in Spacecraft Thermal Analysis," AIAA Paper 68-62, 6th Aerospace Sciences Meeting, January 1968.

53. S. J. Kline and F. A. McClintock, "Describing Uncertainties in Single-Sample Experiments," Mechanical Engineering, pp. 3-8, January 1953.

54. A. G. Worthing and J. Geffner, Treatment of Experimental Data, John Wiley and Sons, Inc., New York, 1943.

55. R. P. Caren and G. R. Cunnington, "Heat Transfer in Multilayer Insulation Systems," Advances in Cryogenic Heat Transfer, Chemical Engineering Progress Symposium Series, Vol. 64, No. 87, pp.67-81, 1968.

56. R. M. Costen and G. C. Vliet, "Thermal Energy Transport Along the Laminations of Multilayer Insulations," AIAA Paper 67-295, Thermophysics Specialists Conference, April 1967.

57. G. R. Cunnington and C. L. Tien, "A Study of Heat Transfer Processes in Multilayer Insulation," AIAA Paper No. 69-07, June 1969.

58. A. G. Emslie, "Radiative Heat Transfer Through Seams and Penetrations in Panels of Multilayer Metal-Foil Insulation," ADL-63270-04, April 1962.

59. R. K. MacGregor, J. T. Pogson and D. J. Russell, "Radiation Interchange Interior to Multilayer Insulation Blankets," accepted for publication, J. of Spacecraft.

60. R. K. MacGregor, J. T. Pogson, D. J. Russell and T. M. Gilpin, "Thermal Scale Modeling of Multilayer Insulation," The Boeing Company, D2-121307-1, to be released.

61. J. T. Pogson and R. K. MacGregor, "A Calorimetric Method of Establishing the Performance of Multilayer Insulation Systems," presented AIAA 4th Thermophysics Conference, Open Forum Session, June 1969.

62. J. T. Pogson and R. K. MacGregor, "A Method of Increasing the Lateral Thermal Resistance of Multilayer Insulation Blankets," presented AIAA 8th Aerospace Sciences Meeting, January 1970.

63. J. T. Pogson and R. K. MacGregor, "The Calculation of the Effective Parallel Conductance Interior to Multilayer Insulation Blankets," presented Open Forum on Current Heat Transfer Research, 90th Winter Annual ASME Meeting, Los Angeles, California, November 1969.

64. E. R. Streed, G. R. Cunnington and C. A. Zierman, "Performance of Multilayer Insulation Systems for the 300° to 800°K Temperature Range," AIAA Paper 65-663, Thermophysics Specialists Conference, September 1965.

65. C. B. Barnes, Jr. and C. B. Hood, Jr., "Vehicle Temperature Error in Space Simulators," Institute of Environmental Sciences 1964 Proceedings, pp. 555-559.

66. P. Hrycak and B. A. Unger, "General Criteria for Solar Simulation and Model Testing," Institute of Environmental Sciences 1964 Proceedings, pp. 257-263, 1964.

67. K. N. Newhouse, "Thermocouple Conduction Errors in a Vacuum Cold Wall Environment," ASME Paper 67-HT-57, ASME-AIChE Heat Transfer Conference, June 1967.

68. K. W. Nutt and J. A. van der Bliek, "Some Aspects of Thermal Model Testing in Space Chambers," Arnold Engineering Development Center, AEDC-TR-67-38, April 1967 (also AIAA Paper 67-306, Thermophysics Specialists Conference, April 1967).

69. M. J. Rosenberg, "Theoretical Error Analysis as Applied to Space Chamber Environmental Thermal Anomalies," Institute of Environmental Sciences 1965 Proceedings, pp. 545-561, 1965.

70. G. Belleman, "Thermophysical Properties of Materials; The Boeing Company, D-16103-1, March 1961.

71. E. Fitzer, "Thermophysical Properties of Materials," NATO, AGARD Advisory Report No. 12, March 1967.

72. C. G. Goetzel, J. B. Rittenhouse and J. B. Singletary, Editors, "Space Materials Handbook, Second Edition, Lockheed Missiles and Space Company, ML-TDR-64-40, January 1965.

73. J. B. Rittenhouse and J. B. Singletary, "Space Materials Handbook," Supplement 1 to the Second Edition - Space Materials Experience, Lockheed Missiles and Space Company, NASA SP-3025, 1966.

74. J. B. Rittenhouse and J. B. Singletary, "Space Materials Handbook," Supplement 2 to the Second Edition - Space Materials Experience, Lockheed Missiles and Space Company, AFML-TR-64-40, Supplement 2, 1968.

75. J. G. Sessler, Editor, "Materials Data Handbook, Aluminum Alloy 6061," Marshall Space Flight Center, PB 183 426, 1969.

76. J. S. Griffith, Editor, "Handbook of Solar Simulation for Thermal Vacuum Testing," Institute of Environmental Sciences, 1968.

77. M. L. Lerner, "Space Environment Simulation Laboratory Equipment and Capabilities," The Boeing Company, D2-20419-1, 1964.

78. A. R. Lunde, "Solar Simulation and Support Equipment - Description and Capabilities," The Boeing Company, D2-114156-1, 1968.

79. A. K. Oppenheim, "Radiation Analysis by the Network Method," TASME, Vol. 78, 1954.

80. H. C. Hottel, "Radiant Heat Transmission," Chapter 4 of Heat Transmission, 3rd Edition, W. H. McAdams, McGraw-Hill Book Company, Inc., New York, 1954.

81. B. Gebhart, "Unified Treatment for Thermal Radiation Processes - Grey Diffuse Radiators and Absorbers," ASME paper 57-A-34, 1957.

82. E. M. Sparrow, "On the Calculation of Radiant Interchange Between Surfaces," Modern Developments in Heat Transfer, W. Ibele, Ed., Academic Press, New York, 1963.

83. M. Toussaint, "Verification of the Thermal Mathematical Model for Artificial Satellites: A New Test Philosophy," AIAA Paper 67-302, Thermophysics Specialists Conference, 1967.

84. R. C. Corlett, "Direct Monte Carlo Calculation of Thermal Radiation in Vacuum, Journal of Heat Transfer, TASME, Vol. 88, Series C, pp. 376-382, 1966.

85. R. K. MacGregor, R. L. Drake and A. B. Lester, "Thermal Radiative Interchange Factor Program (An Engineer's Guide to AS 2814)," The Boeing Company, D2-114470-1, January 1969.

86. J. C. Almond, "Thermal Analyzer II," The Boeing Company, AS 1917, June 1966.

APPENDICES

APPENDIX A

THERMOPHYSICAL PROPERTIES OF MATERIALS

The following tables present the thermophysical properties used in the calculations for the prototype and half scale model components.

TABLE A1. ALUMINUM SILICATE - GRADE A

Density	0.083 lb/in^3
Specific Heat	0.20 Btu/lbm ^oR
Thermal Conductivity	1.21 Btu/hr ft ^oR

TABLE A2. 6061-T6 ALUMINUM (ρ = 169.34 lb/ft^3)

Temperature (^oR)	k (Btu/hr ft ^oF)	c_p (Btu/lb ^oF)	ρc_p (Btu/ft^3 ^oF)
160		0.094	14.918
492	94.1		
535	96.6	0.215	36.408
660	99.4		
760	99.4	0.231	39.118
860	101.6		
960	101.6	0.243	41.150
1060	104.1		
1160	104.1	0.255	43.182
1260	104.1		

Reference: D-16103-1, Thermophysical Properties of Materials, G. Belleman, March 1961.

TABLE A3. 7075-T6 ALUMINUM (ρ = 174.53 lb/ft^3)

Temperature (^oR)	k (Btu/hr ft ^oF)	c_p (Btu/lb ^oF)	ρc_p (Btu/ft^3 ^oF)
40		0.004	0.698
160	43.2	0.092	16.06
360	62.2		
460	68.2		
535	72.6	0.207	36.13
660	77.8		
760	81.2	0.222	38.74
860	84.2		
960	86.8	0.234	40.84
1060	89.0		
1160	91.1	0.245	42.76
1260	92.4		

Reference: D-16103-1, Thermophysical Properties of Materials, G. Belleman, March 1961.

TABLE A4. 2024-0 ALUMINUM (ρ = 172.8 lb/ft^3)

Temperature (^oR)	k (Btu/hr ft ^oF)	c_p (Btu/lb ^oF)	ρc_p (Btu/ft^3 ^oF)
160	53.57	0.08	13.82
535	111.46	0.21	36.29
660	111.46		
760	111.46	0.225	38.88
860	111.46		
960	111.46	0.240	41.47
1060	111.4		
1160	111.46	0.250	43.20
1260	111.46		

Reference: D-16103-1, Thermophysical Properties of Materials, G. Belleman, March 1961.

TABLE A5. MULTILAYER INSULATION BLANKETS

Substrate Temperature (^{o}R)	Effective Conductance (Btu/hr ft^2 ^{o}R)
437	1.073×10^{-3}
478	1.312×10^{-3}
512	1.562×10^{-3}
560	1.993×10^{-3}

10 layers Aluminized Mylar
1/4 mill mylar
270 Å aluminum film
aluminized both sides

10 layers silk net

skip bonding fabrication

velcro hook and pile attachment

TABLE A6. RADIATIVE PROPERTIES

Surface	Predicted Properties α_s	Predicted Properties ε	Measured Properties α_s	Measured Properties ρ_s^s	Measured Properties ρ_s^d	Measured Properties ε_{RT}
Flat Black	0.96	0.88				
on 2024-0			0.962	-	0.038	0.841
6061-T6			0.967	-	0.033	0.843
7075-T6			0.967	-	0.033	0.875
B-1060	0.193	0.896				
on 2024-0			0.184	0.014	0.802	0.894
6061-T6			0.184	0.015	0.801	0.892
7075-T6			0.181	0.012	0.807	0.905
Aluminum						
Chem Cleaned	0.160	0.060				
2024-0			0.308	0.220	0.472	0.055
6061-T6			0.349	0.182	0.469	0.052
			0.241*			
7074-T6			0.229	0.431	0.340	0.040
Aluminized						
Mylar	0.160	0.060				
I			0.215	0.703	0.082	0.048
II			0.174	0.761	0.065	0.041

* Value inferred as a result of the prototype test results

APPENDIX B

RADIATION INTERCHANGE FACTOR MATRIX

This appendix presents the radiation interchange factors calculated for the prototype vehicle without multilayer insulation.

The first column of the table indicates the nodal designation used in the Radiative Interchange Factor Program while the next column indicates designations corresponding to nodal locations in the Thermal Analyzer Program. The third column indicates nodal surface area in square inches.

Only half of the total matrix is presented due to symmetry which allows a calculation of the other elements from

$$F_{ji} = \frac{A_i}{A_j} F_{ij}$$

Radiation connectors are required for the thermal analyzer program only for the non-diagonal, non-zero, elements of the half matrix shown.

As radiative properties and relative geometry were preserved, this same matrix of interchange factors was used for the half scale model. The only adjustment required for the half scale was in the emissivity of the sun facing polished aluminum upper closure. This required changing the view factors to space (node 200) from nodes 79, 80, 81 and 82.

RADIATION INTERCHANGE FACTORS - PROTOTYPE SPACECRAFT
NO MULTILAYER INSULATION

			85	84		83		88	87		86	
NODE	NODE	AREA	N11	N12	N13	N14	N15	N21	N22	N23	N24	N25
N11	85	56.549	0.3920	0.0769	0.2970	0.0115	0.0156	0	0	0	0	0
N12	84	7.069		0.0315	0.0502	0.0005	0.1428	0	0	0	0	0
N13		18.850			0.0657	0.0012	0.0012	0	0	0	0	0
N14	83	1.767				0.0263	0	0	0	0	0	0
N15		1.767					0.0245	0	0	0	0	0
N21	88	56.549						0.3920	0.0769	0.2970	0.0115	0.0156
N22	87	7.069							0.0315	0.0502	0.0005	0.1428
N23		18.850								0.0657	0.0012	0.0012
N24	86	1.767									0.0263	0
N25		1.767										0.0245
N31	91	56.549										
N32	90	7.069										
N33		18.850										
N34	89	1.767										
N35		1.767										
N41	95	24.0										
N42	94	12.0										
N43	97	24.0										
N44	92	12.0										
N45	96	32.0										

RADIATION INTERCHANGE FACTORS - PROTOTYPE SPACECRAFT
NO MULTILAYER INSULATION

NODE	NODE	91 N31	90 N32	N33	89 N34	N35	95 N41	94 N42	97 N43	92 N44	96 N45
N11	85	0	0	0	0	0	0	0	0	0	0
N12	84	0	0	0	0	0	0	0	0	0	0
N13		0	0	0	0	0	0	0	0	0	0
N14	83	0	0	0	0	0	0	0	0	0	0
N15		0	0	0	0	0	0	0	0	0	0
N21	88	0.0172	0.0005	0	0	0	0.0007	0.0012	0.0006	0.0002	0.0029
N22	87	0.0030	0.0006	0	0	0	0.0001	0.0003	0.0002	0.0001	0.0034
N23		0	0	0	0	0	0	0	0	0	0
N24	86	0	0	0	0	0	0	0	0	0	0
N25		0	0	0	0	0	0	0	0	0	0
N31	91	0.3920	0.0769	0.2970	0.0115	0.0156	0.0009	0.0003	0.0004	0.0012	0.0038
N32	90		0.0315	0.0502	0.0005	0.1428	0.0001	0.0001	0.0001	0.0005	0.0027
N33				0.0657	0.0012	0.0012	0	0	0	0	0
N34	89				0.0263	0	0	0	0	0	0
N35						0.0245	0	0	0	0	0
N41	95						0.0241	0.0726	0.0701	0.0722	0.2215
N42	94							0.0326	0.1578	0.0198	0.1974
N43	97								0.0487	0.0684	0.2191
N44	92									0.0346	0.1934
N45	96										0.0315

RADIATION INTERCHANGE FACTORS - PROTOTYPE SPACECRAFT
NO MULTILAYER INSULATION

NODE	NODE	93 N46	N47	N48	57 N101	58 N102	59 N103	60 N104	61 N105
N11	85	0	0	0	0.3406	0	0	0	0
N12	84	0	0	0	0.0588	0	0	0	0
N13		0	0	0	0.0180	0	0	0	0
N14	83	0	0	0	0.5645	0	0	0	0
N15		0	0	0	0.0019	0	0	0	0
N21	88	0	0	0	0	0	0	0	0
N22	87	0	0	0	0	0	0	0	0
N23		0	0	0	0	0	0	0	0
N24	86	0	0	0	0	0	0	0	0
N25		0	0	0	0	0	0	0	0
N31	91	0	0	0	0	0	0	0	0
N32	90	0	0	0	0	0	0	0	0
N33		0	0	0	0	0	0	0	0
N34	89	0	0	0	0	0	0	0	0
N35		0	0	0	0	0	0	0	0
N41	95	0.2112	0.0035	0.0038	0	0	0	0	0
N42	94	0.0631	0.0002	0.0997	0	0	0	0	0
N43	97	0.2177	0.0042	0.0040	0	0	0	0	0
N44	92	0.0539	0.0967	0.0003	0	0	0	0	0
N45	96	0.2336	0.0043	0.0059	0	0	0	0	0

RADIATION INTERCHANGE FACTORS - PROTOTYPE SPACECRAFT
NO MULTILAYER INSULATION

NODE	NODE	63 N121	72 N122	62 N123	71 N124	69 N141	N142	68 N143	77 N144
N11	85	0.0539	0	0.0535	0	0.0503	0	0.0517	0
N12	84	0.0215	0	0.0192	0	0.0146	0	0.0161	0
N13		0	0	0	0	0	0	0	0
N14	83	0	0	0	0	0	0	0	0
N15		0	0	0	0	0	0	0	0
N21	88	0	0.0244	0	0.0226	0	0.0192	0	0.0303
N22	87	0	0.0106	0	0.0068	0	0.0052	0	0.0086
N23		0	0	0	0	0	0	0	0
N24	86	0	0	0	0	0	0	0	0
N25		0	0	0	0	0	0	0	0
N31	91	0	0.1543	0	0.0326	0	0.0274	0	0.0155
N32	90	0	0.0859	0	0.0139	0	0.0080	0	0.0052
N33		0	0	0	0	0	0	0	0
N34	89	0	0	0	0	0	0	0	0
N35		0	0	0	0	0	0	0	0
N41	95	0	0.0028	0	0.0008	0	0.0002	0	0.0002
N42	94	0	0.0028	0	0.0036	0	0.0023	0	0.1006
N43	97	0	0.0031	0	0.0220	0	0.2595	0	0.2532
N44	92	0	0.0544	0	0.2892	0	0.0971	0	0.0023
N45	96	0	0.0194	0	0.0553	0	0.0837	0	0.0774

RADIATION INTERCHANGE FACTORS - PROTOTYPE SPACECRAFT
NO MULTILAYER INSULATION

NODE	NODE	66 N161	75 N162	67 N163	76 N164	64 N181	73 N182	65 N183	74 N184
N11	85	0.0545	0	0.0551	0	0.0515	0	0.0510	0
N12	84	0.0185	0	0.0179	0	0.0153	0	0.0166	0
N13		0	0	0	0	0	0	0	0
N14	83	0	0	0	0	0	0	0	0
N15		0	0	0	0	0	0	0	0
N21	88	0	0.1456	0	0.0374	0	0.0362	0	0.1429
N22	87	0	0.0814	0	0.0137	0	0.0156	0	0.0755
N23		0	0	0	0	0	0	0	0
N24	86	0	0	0	0	0	0	0	0
N25		0	0	0	0	0	0	0	0
N31	91	0	0.0230	0	0.0225	0	0.1492	0	0.0325
N32	90	0	0.0075	0	0.0068	0	0.0728	0	0.0145
N33		0	0	0	0	0	0	0	0
N34	89	0	0	0	0	0	0	0	0
N35		0	0	0	0	0	0	0	0
N41	95	0	0.0027	0	0.0006	0	0.0030	0	0.0027
N42	94	0	0.0585	0	0.2990	0	0.0028	0	0.0088
N43	97	0	0.0025	0	0.0169	0	0.0024	0	0.0022
N44	92	0	0.0023	0	0.0040	0	0.0091	0	0.0028
N45	96	0	0.0179	0	0.0495	0	0.0127	0	0.0110

RADIATION INTERCHANGE FACTORS - PROTOTYPE SPACECRAFT
NO MULTILAYER INSULATION

NODE	NODE	70 N201	79 N301	80 N302	81 N303	82 N304	200 N901
N11	85	0.1506	0	0	0	0	0
N12	84	0.6481	0	0	0	0	0
N13		0	0	0	0	0	0
N14	83	0	0	0	0	0	0
N15		0	0	0	0	0	0
N21	88	0.2997	0.0326	0.0447	0.0349	0.0182	0
N22	87	0.0510	0.0477	0.4720	0.0456	0.0097	0
N23		0.0180	0	0	0	0	0
N24	86	0.5680	0	0	0	0	0
N25		0.0015	0	0	0	0	0
N31	91	0.3021	0.0468	0.0280	0.0189	0.0318	0
N32	90	0.0486	0.4819	0.0419	0.0104	0.0424	0
N33		0.0190	0	0	0	0	0
N34	89	0.5714	0	0	0	0	0
N35		0.0020	0	0	0	0	0
N41	95	0.2112	0.0031	0.0029	0.0008	0.0007	0
N42	94	0.4612	0.0027	0.0190	0.0601	0.0040	0
N43	97	0.4351	0.0025	0.0033	0.0204	0.0184	0
N44	92	0.4848	0.0209	0.0030	0.0037	0.0571	0
N45	96	0.1729	0.0578	0.0511	0.1943	0.1893	0

RADIATION INTERCHANGE FACTORS - PROTOTYPE SPACECRAFT
NO MULTILAYER INSULATION

NODE	NODE	AREA	N46	93 N47	N48	57 N101	58 N102	59 N103	60 N104	61 N105
N46		28.274	0.0424	0.0003	0.0006	0	0	0	0	0
N47	93	1.767		0.0188	0	0	0	0	0	0
N48		1.767			0.0200	0	0	0	0	0
N101	57	400.0				0.0578	0.0043	0.0035	0.0046	0.0032
N102	58	150.0					0.0130	0.0028	0.0017	0.0034
N103	59	100.0						0.0128	0.0036	0.0014
N104	60	150.0							0.0124	0.0025
N105	61	100.0								0.0123
N121	63	100.0								
N122	72	100.0								
N123	62	100.0								
N124	71	100.0								
N141	69	100.0								
N142	78	100.0								
N143	68	100.0								
N144	77	100.0								

RADIATION INTERCHANGE FACTORS - PROTOTYPE SPACECRAFT
NO MULTILAYER INSULATION

NODE	NODE	63 N121	72 N122	62 N123	71 N124	69 N141	78 N142	68 N143	77 N144
N46		0	0	0	0	0	0	0	0
N47	93	0	0	0	0	0	0	0	0
N48		0	0	0	0	0	0	0	0
N101	57	0.0587	0	0.0588	0	0.0571	0	0.0544	0
N102	58	0.0980	0.0098	0.0948	0.0129	0.0119	0.0021	0.0010	0.0003
N103	59	0.0001	0.0002	0	0.0001	0	0	0.0001	0
N104	60	0	0	0	0	0.0012	0.0013	0.0100	0.0025
N105	61	0.0001	0.0001	0	0.0002	0.1346	0.0163	0.1253	0.0144
N121	63	0.0267	0.0006	0.0083	0.0008	0.0295	0	0.0264	0
N122	72		0.0286	0.0004	0.0070	0.0001	0.0283	0	0.0199
N123	62			0.0269	0.0008	0.1503	0	0.0308	0
N124	71				0.0231	0.0001	0.1509	0.0001	0.0284
N141	69					0.0261	0.0006	0.0077	0.0006
N142	78						0.0251	0.0005	0.0073
N143	68							0.0254	0.0006
N144	77								0.0234

RADIATION INTERCHANGE FACTORS - PROTOTYPE SPACECRAFT
NO MULTILAYER INSULATION

NODE	NODE	66 N161	75 N162	67 N163	76 N164	64 N181	73 N182	65 N183	74 N184
N46		0	0	0	0	0	0	0	0
N47	93	0	0	0	0	0	0	0	0
N48		0	0	0	0	0	0	0	0
N101	57	0.0525	0	0.0562	0	0.0570	0	0.0549	0
N102	58	0	0	0	0	0.0071	0.0018	0.0009	0.0008
N103	59	0.0002	0.0001	0	0.0001	0.1271	0.0143	0.1398	0.0119
N104	60	0.0966	0.0127	0.0989	0.0114	0.0013	0.0003	0.0111	0.0032
N105	61	0	0.0003	0	0.0002	0	0	0	0
N121	63	0.0548	0	0.0271	0	0.1548	0	0.0304	0
N122	72	0	0.0388	0	0.0269	0.0002	0.1508	0	0.0190
N123	62	0.0287	0	0.0558	0	0.0261	0	0.0273	0
N124	71	0	0.0293	0	0.0491	0.0002	0.0168	0	0.0237
N141	69	0.0270	0	0.0277	0	0.0555	0	0.0235	0
N142	78	0	0.0203	0.0001	0.0226	0.0001	0.0381	0	0.0234
N143	68	0.0331	0	0.1523	0.0002	0.0254	0	0.0559	0
N144	77	0	0.0274	0.0001	0.1516	0	0.0254	0	0.0374

RADIATION INTERCHANGE FACTORS - PROTOTYPE SPACECRAFT
NO MULTILAYER INSULATION

NODE	NODE	70 N201	79 N301	80 N302	81 N303	82 N304	200 N901
N46	93	0.2613	0	0	0	0	0
N47	93	0.1027	0	0	0	0	0
N48	93	0.1080	0	0	0	0	0
N101	57	0.2978	0	0	0	0	0.8596
N102	58	0	0	0	0	0	1.5065
N103	59	0	0	0	0	0	1.4562
N104	60	0	0	0	0	0	1.5065
N105	61	0	0	0	0	0	1.4562
N121	63	0.2431	0	0	0	0	0.7408
N122	72	0.1880	0.1561	0.0196	0.0180	0.0324	0.8694
N123	62	0.2440	0	0	0	0	0.7408
N124	71	0.1917	0.0357	0.0158	0.0262	0.1609	0.8694
N141	69	0.2322	0	0	0	0	0.7408
N142	78	0.1631	0.0296	0.0142	0.0313	0.1464	0.8694
N143	68	0.2351	0	0	0	0	0.7408
N144	77	0.1680	0.0156	0.0291	0.1503	0.0341	0.8694

RADIATION INTERCHANGE FACTORS - PROTOTYPE SPACECRAFT
NO MULTILAYER INSULATION

			66	75	67	76	64	73	65	74
NODE	NODE	AREA	N161	N162	N163	N164	N181	N182	N183	N184
N161	66	100.0	0.0268	0.0010	0.0086	0.0006	0.0290	0	0.1533	0.0001
N162	75	100.0		0.0277	0.0007	0.0075	0	0.0172	0	0.1501
N163	67	100.0			0.0267	0.0068	0.0294	0.0001	0.0257	0.0001
N164	76	100.0				0.0229	0	0.0227	0.0001	0.0165
N181	64	100.0					0.0262	0.0007	0.0079	0.0007
N182	73	100.0						0.0267	0.0005	0.0090
N183	65	100.0							0.0279	0.0007
N184	74	100.0								0.0281
N201	70	400.0								
N301	79	100.0								
N302	80	100.0								
N303	81	100.0								
N304	82	100.0								

RADIATION INTERCHANGE FACTORS - PROTOTYPE SPACECRAFT
NO MULTILAYER INSULATION

NODE	NODE	70 N201	79 N301	80 N302	81 N303	82 N304	200 N901
N161	66	0.2348	0	0	0	0	0.7408
N162	75	0.1904	0.0274	0.1623	0.0299	0.0145	0.8694
N163	67	0.2370	0	0	0	0	0.7408
N164	76	0.1973	0.0188	0.0337	0.1578	0.0300	0.8694
N181	64	0.2414	0	0	0	0	0.7408
N182	73	0.1925	0.1480	0.0342	0.0160	0.0211	0.8694
N183	65	0.2427	0	0	0	0	0.7408
N184	74	0.1947	0.0355	0.1463	0.0226	0.0172	0.8694
N201	70	0.0837	0.0598	0.0605	0.0606	0.0559	0
N301	79		0.0234	0.0082	0.0052	0.0078	0.0519
N302	80			0.0229	0.0072	0.0051	0.0519
N303	81				0.0210	0.0077	0.0519
N304	82					0.0220	0.0519

APPENDIX C

RADIATION INTERCHANGE FACTOR MATRIX
(with multilayer insulation)

This appendix presents the radiation interchange factors calculated for the prototype vehicle with multilayer insulation.

For those exterior surface nodes covered by insulation, the covering insulation node has been designated by adding one hundred to the surface node designation. Hence, surface nodes 62-69 and 71-82 are covered by insulation nodes 162-169 and 171-182.

As radiative properties and relative geometry were preserved, this same matrix of interchange factors was used for the insulated half scale model.

RADIATION INTERCHANGE FACTORS - PROTOTYPE SPACECRAFT
WITH MULTILAYER INSULATION

			85	84		83		88	87		86	
NODE	NODE	AREA	N11	N12	N13	N14	N15	N21	N22	N23	N24	N25
N11	85	56.549	0.3920	0.0769	0.2970	0.0115	0.0156	0	0	0	0	0
N12	84	7.069		0.0315	0.0502	0.0005	0.1428	0	0	0	0	0
N13		18.850			0.0657	0.0012	0.0012	0	0	0	0	0
N14	83	1.767				0.0263	0	0	0	0	0	0
N15		1.767					0.0245	0	0	0	0	0
N21	88	56.549						0.3920	0.0769	0.2970	0.0115	0.0156
N22	87	7.069							0.0315	0.0502	0.0005	0.1428
N23		18.850								0.0657	0.0012	0.0012
N24	86	1.767									0.0263	0
N25		1.767										0.0245
N31	91	56.549										
N32	90	7.069										
N33		18.850										
N34	89	1.767										
N35		1.767										
N41	95	24.0										
N42	94	12.0										
N43	97	24.0										
N44	92	12.0										
N45	96	32.0										

RADIATION INTERCHANGE FACTORS - PROTOTYPE SPACECRAFT
WITH MULTILAYER INSULATION

NODE	NODE	91 N31	90 N32	N33	89 N34	N35	95 N41	94 N42	97 N43	92 N44	96 N45
N11	85	0	0	0	0	0	0	0	0	0	0
N12	84	0	0	0	0	0	0	0	0	0	0
N13		0	0	0	0	0	0	0	0	0	0
N14	83	0	0	0	0	0	0	0	0	0	0
N15		0	0	0	0	0	0	0	0	0	0
N21	88	0.0172	0.0005	0	0	0	0.0007	0.0012	0.0006	0.0002	0.0029
N22	87	0.0030	0.0006	0	0	0	0.0001	0.0003	0.0002	0.0001	0.0034
N23		0	0	0	0	0	0	0	0	0	0
N24	86	0	0	0	0	0	0	0	0	0	0
N25		0	0	0	0	0	0	0	0	0	0
N31	91	0.3920	0.0769	0.2970	0.0115	0.0156	0.0009	0.0003	0.0004	0.0012	0.0038
N32	90		0.0315	0.0502	0.0005	0.1428	0.0001	0.0001	0.0001	0.0005	0.0027
N33				0.0657	0.0012	0.0012	0	0	0	0	0
N34	89				0.0263	0	0	0	0	0	0
N35						0.0245	0	0	0	0	0
N41	95						0.0241	0.0726	0.0701	0.0722	0.2215
N42	94							0.0326	0.1578	0.0198	0.1974
N43	97								0.0487	0.0684	0.2191
N44	92									0.0346	0.1934
N45	96										0.0315

RADIATION INTERCHANGE FACTORS - PROTOTYPE SPACECRAFT
WITH MULTILAYER INSULATION

NODE	NODE	93 N46	93 N47	93 N48	57 N101	58 N102	59 N103	60 N104	61 N105
N11	85	0	0	0	0.3406	0	0	0	0
N12	84	0	0	0	0.0588	0	0	0	0
N13		0	0	0	0.0180	0	0	0	0
N14	83	0	0	0	0.5645	0	0	0	0
N15		0	0	0	0.0019	0	0	0	0
N21	88	0	0	0	0	0	0	0	0
N22	87	0	0	0	0	0	0	0	0
N23		0	0	0	0	0	0	0	0
N24	86	0	0	0	0	0	0	0	0
N25		0	0	0	0	0	0	0	0
N31	91	0	0	0	0	0	0	0	0
N32	90	0	0	0	0	0	0	0	0
N33		0	0	0	0	0	0	0	0
N34	89	0	0	0	0	0	0	0	0
N35		0	0	0	0	0	0	0	0
N41	95	0.2112	0.0035	0.0038	0	0	0	0	0
N42	94	0.0631	0.0002	0.0997	0	0	0	0	0
N43	97	0.2177	0.0042	0.0040	0	0	0	0	0
N44	92	0.0599	0.0967	0.0003	0	0	0	0	0
N45	96	0.2336	0.0043	0.0059	0	0	0	0	0

RADIATION INTERCHANGE FACTORS - PROTOTYPE SPACECRAFT
WITH MULTILAYER INSULATION

NODE	NODE	63 N121	72 N122	62 N123	71 N124	69 N141	78 N142	68 N143	77 N144
N11	85	0.0539	0	0.0535	0	0.0503	0	0.0517	0
N12	84	0.0215	0	0.0192	0	0.0147	0	0.0161	0
N13	83	0	0	0	0	0	0	0	0
N14		0	0	0	0	0	0	0	0
N15		0	0	0	0	0	0	0	0
N21	88	0	0.0244	0	0.0226	0	0.0192	0	0.0303
N22	87	0	0.0106	0	0.0068	0	0.0052	0	0.0086
N23	86	0	0	0	0	0	0	0	0
N24		0	0	0	0	0	0	0	0
N25		0	0	0	0	0	0	0	0
N31	91	0	0.1543	0	0.0326	0	0.0274	0	0.0155
N32	90	0	0.0859	0	0.0139	0	0.0080	0	0.0052
N33	89	0	0	0	0	0	0	0	0
N34		0	0	0	0	0	0	0	0
N35		0	0	0	0	0	0	0	0
N41	95	0	0.0028	0	0.0008	0	0.0002	0	0.0002
N42	94	0	0.0028	0	0.0036	0	0.0023	0	0.1006
N43	97	0	0.0031	0	0.0220	0	0.2595	0	0.2532
N44	92	0	0.0544	0	0.2892	0	0.0971	0	0.0023
N45	96	0	0.0194	0	0.0553	0	0.0837	0	0.0774

RADIATION INTERCHANGE FACTORS - PROTOTYPE SPACECRAFT
WITH MULTILAYER INSULATION

NODE	NODE	66 N161	75 N162	67 N163	76 N164	64 N181	73 N182	65 N183	74 N184
N11	85	0.0545	0	0.0551	0	0.0515	0	0.0510	0
N12	84	0.0185	0	0.0179	0	0.0153	0	0.0166	0
N13		0	0	0	0	0	0	0	0
N14	83	0	0	0	0	0	0	0	0
N15		0	0	0	0	0	0	0	0
N21	88	0	0.1456	0	0.0374	0	0.0362	0	0.1429
N22	87	0	0.0814	0	0.0137	0	0.0156	0	0.0755
N23		0	0	0	0	0	0	0	0
N24	86	0	0	0	0	0	0	0	0
N25		0	0	0	0	0	0	0	0
N31	91	0	0.0230	0	0.0225	0	0.1492	0	0.0325
N32	90	0	0.0075	0	0.0068	0	0.0728	0	0.0145
N33		0	0	0	0	0	0	0	0
N34	89	0	0	0	0	0	0	0	0
N35		0	0	0	0	0	0	0	0
N41	95	0	0.0027	0	0.0006	0	0.0030	0	0.0027
N42	94	0	0.0585	0	0.2990	0	0.0028	0	0.0088
N43	97	0	0.0025	0	0.0169	0	0.0024	0	0.0022
N44	92	0	0.0023	0	0.0040	0	0.0091	0	0.0028
N45	96	0	0.0179	0	0.0495	0	0.0127	0	0.0110

RADIATION INTERCHANGE FACTORS - PROTOTYPE SPACECRAFT
WITH MULTILAYER INSULATION

NODE	NODE	70 N201	79 N301	80 N302	81 N303	82 N304	200 N901
N11	85	0.1506	0	0	0	0	0
N12	84	0.6481	0	0	0	0	0
N13		0	0	0	0	0	0
N14	83	0	0	0	0	0	0
N15		0	0	0	0	0	0
N21	88	0.2997	0.0326	0.0447	0.0349	0.0182	0
N22	87	0.0510	0.0477	0.4720	0.0456	0.0097	0
N23		0.0180	0	0	0	0	0
N24	86	0.5680	0	0	0	0	0
N25		0.0015	0	0	0	0	0
N31	91	0.3021	0.0468	0.0280	0.0189	0.0318	0
N32	90	0.0486	0.4819	0.0419	0.0104	0.0424	0
N33		0.0190	0	0	0	0	0
N34	89	0.5714	0	0	0	0	0
N35		0.0020	0	0	0	0	0
N41	95	0.2112	0.0031	0.0029	0.0008	0.0007	0
N42	94	0.4612	0.0027	0.0190	0.0601	0.0040	0
N43	97	0.4351	0.0025	0.0033	0.0204	0.0184	0
N44	92	0.4848	0.0209	0.0030	0.0037	0.0571	0
N45	96	0.1729	0.0578	0.0511	0.1943	0.1893	0

RADIATION INTERCHANGE FACTORS - PROTOTYPE SPACECRAFT
WITH MULTILAYER INSULATION

				93		57	58	59	60	61
NODE	NODE	AREA	N46	N47	N48	N101	N102	N103	N104	N105
N46	93	28.274	0.0424	0.0003	0.0006	0	0	0	0	0
N47		1.767		0.0188	0	0	0	0	0	0
N48		1.767			0.0200	0	0	0	0	0
N101	57	400.0				0.0612	0.0042	0.0033	0.0045	0.0033
N102	58	150.0					0.0613	0.0052	0.0014	0.0041
N103	59	100.0						0.0773	0.0048	0.0014
N104	60	150.0							0.0576	0.0050
N105	61	100.0								0.0711
N121	63	100.0								
N122	72	100.0								
N123	62	100.0								
N124	71	100.0								
N141	69	100.0								
N142	78	100.0								
N143	68	100.0								
N144	77	100.0								

RADIATION INTERCHANGE FACTORS - PROTOTYPE SPACECRAFT
WITH MULTILAYER INSULATION

NODE	NODE	63 N121	72 N122	62 N123	71 N124	69 N141	78 N142	68 N143	77 N144
N46		0	0	0	0	0	0	0	0
N47	93	0	0	0	0	0	0	0	0
N48		0	0	0	0	0	0	0	0
N101	57	0.0587	0	0.0588	0	0.0571	0	0.0544	0
N102	58	0	0	0	0	0	0	0	0
N103	59	0	0	0	0	0	0	0	0
N104	60	0	0	0	0	0	0	0	0
N105	61	0	0	0	0	0	0	0	0
N121	63	0.0218	0	0.0069	0	0.0295	0	0.0264	0
N122	72		0.0278	0	0.0064	0	0.0283	0	0.0199
N123	62			0.0221	0	0.1501	0	0.0308	0
N124	71				0.0226	0	0.1507	0	0.0284
N141	69					0.0211	0	0.0064	0
N142	78						0.0245	0	0.0067
N143	68							0.0205	0
N144	77								0.0228

RADIATION INTERCHANGE FACTORS - PROTOTYPE SPACECRAFT
WITH MULTILAYER INSULATION

NODE	NODE	66 N161	75 N162	67 N163	76 N164	64 N181	73 N182	65 N183	74 N184
N46	93	0	0	0	0	0	0	0	0
N47		0	0	0	0	0	0	0	0
N48		0	0	0	0	0	0	0	0
N101	57	0.0525	0	0.0562	0	0.0570	0	0.0549	0
N102	58	0	0	0	0	0	0	0	0
N103	59	0	0	0	0	0	0	0	0
N104	60	0	0	0	0	0	0	0	0
N105	61	0	0	0	0	0	0	0	0
N121	63	0.0548	0	0.0271	0	0.1546	0	0.0304	0
N122	72	0	0.0388	0	0.0269	0	0.1508	0	0.0190
N123	62	0.0287	0	0.0558	0	0.0261	0	0.0273	0
N124	71	0	0.0293	0	0.0491	0	0.0167	0	0.0236
N141	69	0.0270	0	0.0277	0	0.0555	0	0.0235	0
N142	78	0	0.0202	0	0.0225	0	0.0381	0	0.0234
N143	68	0.0282	0	0.1521	0	0.0254	0	0.0559	0
N144	77	0	0.0274	0	0.1514	0	0.0254	0	0.0374

RADIATION INTERCHANGE FACTORS - PROTOTYPE SPACECRAFT
WITH MULTILAYER INSULATION

NODE	NODE	70 N201	79 N301	80 N302	81 N303	82 N304	200 N901
N46		0.2613	0	0	0	0	0
N47	93	0.1027	0	0	0	0	0
N48		0.1080	0	0	0	0	0
N101	57	0.2978	0	0	0	0	0.8596
N102	58	0	0	0	0	0	0
N103	59	0	0	0	0	0	0
N104	60	0	0	0	0	0	0
N105	61	0	0	0	0	0	0
N121	63	0.2431	0	0	0	0	0
N122	72	0.1880	0.1561	0.0195	0.0180	0.0324	0
N123	62	0.2440	0	0	0	0	0
N124	71	0.1917	0.0357	0.0158	0.0262	0.1609	0
N141	69	0.2322	0	0	0	0	0
N142	78	0.1631	0.0296	0.0142	0.0313	0.1464	0
N143	68	0.2351	0	0	0	0	0
N144	77	0.1680	0.0156	0.0291	0.1503	0.0341	0

RADIATION INTERCHANGE FACTORS - PROTOTYPE SPACECRAFT
WITH MULTILAYER INSULATION

NODE	NODE	AREA	66 N161	75 N162	67 N163	76 N164	64 N181	73 N182	65 N183	74 N184
N161	66	100.0	0.0227	0	0.0074	0	0.0290	0	0.1532	0
N162	75	100.0		0.0269	0	0.0070	0	0.0172	0	0.1499
N163	67	100.0			0.0223	0	0.0293	0	0.0256	0
N164	76	100.1				0.0223	0	0.0226	0	0.0164
N181	64	100.1					0.0212	0	0.0065	0
N182	73	100.0						0.0261	0	0.0083
N183	65	100.0							0.0223	0
N184	74	100.0								0.0276
N[illegible]1	78	400.0								
N301	79	100.0								
N302	80	100.0								
N303	81	100.0								
N304	82	100.0								

RADIATION INTERCHANGE FACTORS - PROTOTYPE SPACECRAFT
WITH MULTILAYER INSULATION

NODE	NODE	70 N201	79 N301	80 N302	81 N303	82 N304	200 N901
N161	66	0.2348	0	0	0	0	0
N162	75	0.1904	0.0274	0.1623	0.0299	0.0145	0
N163	67	0.2370	0	0	0	0	0
N164	76	0.1973	0.0188	0.0337	0.1578	0.0080	0
N181	64	0.2414	0	0	0	0	0
N182	73	0.1925	0.1480	0.0342	0.0160	0.0211	0
N183	65	0.2427	0	0	0	0	0
N184	74	0.1947	0.0355	0.1463	0.0226	0.0172	0
N201	70	0.0837	0.0598	0.0605	0.0606	0.0559	0
N301	79		0.0234	0.0082	0.0052	0.0078	0
N302	80			0.0229	0.0072	0.0051	0
N303	81				0.0210	0.0077	0
N304	82					0.0220	0

RADIATION INTERCHANGE FACTORS - PROTOTYPE SPACECRAFT
WITH MULTILAYER INSULATION

NODE	NODE	AREA	162 N123	163 N121	164 N181	165 N183	166 N161	167 N163	168 N143	169 N141
N102	58	150.	0.0051	0.0047	0.0004	0	0	0	0	0.0004
N103	59	100.	0	0	0.0070	0.0067	0	0	0	0
N104	60	150.	0	0	0	0.0005	0.0043	0.0050	0.0006	0
N105	61	100.	0	0	0	0	0	0	0.0069	0.0065
N123	162	100.	0	0	0	0	0	0	0	0
N121	163	100.		0	0	0	0	0	0	0
N181	164	100.			0	0	0	0	0	0
N183	165	100.				0	0	0	0	0
N161	166	100.					0	0	0	0
N163	167	100.						0	0	0
N143	168	100.								0
N141	169	100.								
N124	171	100.								
N122	172	100.								
N182	173	100.								
N184	174	100.								

RADIATION INTERCHANGE FACTORS - PROTOTYPE SPACECRAFT
WITH MULTILAYER INSULATION

NODE	NODE	171 N124	172 N122	173 N182	174 N184	175 N162	176 N164	177 N144	178 N142
N102	58	0.0006	0.0006	0.0001	0.0001	0	0	0.0001	0.0001
N103	59	0	0	0.0006	0.0006	0	0	0	0
N104	60	0	0	0	0.0002	0.0006	0.0006	0.0001	0
N105	61	0	0	0	0	0	0	0.0008	0.0008
N123	162	0	0	0	0	0	0	0	0
N121	163	0	0	0	0	0	0	0	0
N181	164	0	0	0	0	0	0	0	0
N183	165	0	0	0	0	0	0	0	0
N161	166	0	0	0	0	0	0	0	0
N163	167	0	0	0	0	0	0	0	0
N143	168	0	0	0	0	0	0	0	0
N141	169	0	0	0	0	0	0	0	0
N124	171	0	0	0	0	0	0	0	0
N122	172		0	0	0	0	0	0	0
N182	173			0	0	0	0	0	0
N184	174				0	0	0	0	0

RADIATION INTERCHANGE FACTORS - PROTOTYPE SPACECRAFT
WITH MULTILAYER INSULATION

NODE	NODE	179 N301	180 N302	181 N303	182 N304	200 N901
N102	58	0	0	0	0	1.6905
N103	59	0	0	0	0	1.6686
N104	60	0	0	0	0	1.6905
N105	61	0	0	0	0	1.6686
N123	162	0	0	0	0	0.0365
N121	163	0	0	0	0	0.0365
N181	164	0	0	0	0	0.0365
N183	165	0	0	0	0	0.0365
N161	166	0	0	0	0	0.0365
N163	167	0	0	0	0	0.0365
N143	168	0	0	0	0	0.0365
N141	169	0	0	0	0	0.0365
N124	171	0	0	0	0	0.0430
N122	172	0	0	0	0	0.0430
N182	173	0	0	0	0	0.0430
N184	174	0	0	0	0	0.0430

RADIATION INTERCHANGE FACTORS - PROTOTYPE SPACECRAFT
WITH MULTILAYER INSULATION

NODE	NODE	AREA	162 N123	163 N121	164 N181	165 N183	166 N161	167 N163	168 N143	169 N141
N162	175	100	0	0	0	0	0	0	0	0
N164	176	100	0	0	0	0	0	0	0	0
N144	177	100	0	0	0	0	0	0	0	0
N142	178	100	0	0	0	0	0	0	0	0
N301	179	100	0	0	0	0	0	0	0	0
N302	180	100	0	0	0	0	0	0	0	0
N303	181	100	0	0	0	0	0	0	0	0
N304	182	100	0	0	0	0	0	0	0	0

RADIATION INTERCHANGE FACTORS - PROTOTYPE SPACECRAFT
WITH MULTILAYER INSULATION

NODE	NODE	171 N124	172 N122	173 N182	174 N184	175 N162	176 N164	177 N144	178 N142
N162	175					0	0	0	0
N164	176						0	0	0
N144	177							0	0
N142	178								0
N301	179								
N302	180								
N303	181								
N304	182								

RADIATION INTERCHANGE FACTORS - PROTOTYPE SPACECRAFT
WITH MULTILAYER INSULATION

NODE	NODE	179 N301	180 N302	181 N303	182 N304	200 N901
N16[illegible]	175	0	0	0	0	0.0430
N164	176	0	0	0	0	0.0430
N144	177	0	0	0	0	0.0430
N142	178	0	0	0	0	0.0430
N301	179	0	0	0	0	0.0440
N302	180		0	0	0	0.0440
N303	181			0	0	0.0440
N304	182				0	0.0440

APPENDIX D

CONVERSION FACTORS
INTERNATIONAL SYSTEM OF UNITS

Quantity	English	International
Length	1 inch	2.54 cm
	1 foot	0.3048 m
Angle	1 degree	0.0174 radians
Mass	1 lb_m	0.4536 Kg
Temperature	1 R^o	0.555 K^o
Density	1 lb_m/ft^3	0.0160 gm/cm^3
	1 lb_m/ft^3	16.018 Kg/m^3
Pressure	1 lb_f/in^2	6894.7 n/m^2
Specific Heat	1 $Btu/lb_m\ ^oR$	4.184 Joules/gm ^oK
Thermal Conductivity	1 Btu/hr ft ^oR	0.0173 Watts/cm ^oK
	1 Btu-in/ft^2 sec ^oR	518.87 Joules/m sec ^oK
Power	1 Btu/sec	1054.35 Watts
Energy Flux	1 Btu/hr ft^2	0.3152 Watts/m^2